SOLID SOLUTION STRENGTHENING OF MAGNESIUM

by

AINUL AKHTAR

B.Sc. (Hons), Utkal University, India, 1962
B.E., Indian Institute of Science, India, 1964

A THESIS SUBMITTED IN PARTIAL FULFILMENT OF
THE REQUIREMENTS FOR THE DEGREE OF
DOCTOR OF PHILOSOPHY

in the Department

of

METALLURGY

We accept this thesis as conforming to the
required standard

THE UNIVERSITY OF BRITISH COLUMBIA

July, 1968

In presenting this thesis in partial fulfilment of the requirements for an advanced degree at the University of British Columbia, I agree that the Library shall make it freely available for reference and Study. I further agree that permission for extensive copying of this thesis for scholarly purposes may be granted by the Head of my Department or by his representatives. It is understood that copying or publication of this thesis for financial gain shall not be allowed without my written permission.

Department of **Metallurgy**

The University of British Columbia
Vancouver 8, Canada

Date **September 18, 1968**

ABSTRACT

Solid solution strengthening in magnesium polycrystals containing Zn, Al, Cd, In and Pb as solute has been investigated over the temperatures between 78° and 513°K with particular emphasis on the dilute alloys. The variation of yield stress with concentration occurs in either two or three stages. In stage I, the yield stress increases rapidly and linearly with concentration; in stage II, the rate of increase of yield stress is very much less than in stage I; in stage III, the yield stress decreases with solute additions. The solution hardening rates and the transition concentrations from stage I to stage II (C_T) depend on the size-difference between Mg and the solutes. The results are discussed in terms of the variation with concentration of the CRSS for both basal and prismatic slip. It is proposed that at concentrations less than C_T, the increase in CRSS for prismatic slip is the dominant factor; beyond C_T, yield is governed by a balance between basal hardening and prismatic softening. The effect of solute on the ductility of magnesium at elevated temperatures is discussed in terms of a stress induced polygonization process and the ductility maxima observed in the Mg-Al alloys are explained.

Single crystals of Mg-Zn alloys oriented for basal slip have been deformed in tension over the temperature range from 78°K to 423°K.

The variation of the basal dislocation density caused by the addition of solute has been studied using transmission electron microscopy of thin foils. The increase in dislocation density which was found to be proportional to the square root of the solute concentration, cannot account for the observed increase in the athermal stress.

A dislocation etch pit technique has been developed and used to measure the variation in the forest dislocation density with solute

concentration. The forest density increases linearly and rapidly up to a certain minimum solute concentration, beyond which it remains almost constant. The results are in good agreement with the observed thermally activated flow stress for low solute concentrations.

The observed variation in the athermal component of CRSS has been discussed in the light of an increased friction stress arising due to a random distribution of solute.

Using rate theory, it has been shown that the forest intersection remains the rate controlling mechanism up to a certain low concentration of solute beyond which the single solute atom pinning of dislocations becomes the rate determining process.

The solute dependence of the work hardening parameters are also reported and examined in the light of the existing theories of work hardening.

Single crystals of Mg - Zn and Mg- Al alloys have also been deformed so as to suppress basal slip and $\{10\bar{1}2\}$ twinning and to induce prismatic slip. The results have been explained in terms of an increasing athermal stress and a decreasing Peierls stress with the addition of solute. Peierls stress has been shown to be the rate controlling mechanism below room temperature. The observed variation of CRSS for prism slip with solute concentration accounts adequately for the concentration dependence of yield stress in the polycrystalline aggregate. The results also suggest that the decrease in Peierls stress with solute addition is not necessarily associated with a decreasing c/a ratio and the monovalent nature of the solute.

ACKNOWLEDGEMENT

The author gratefully acknowledges the advice and encouragement given by his research director, Professor E. Teghtsoonian. Thanks are also extended to other members of the faculty and the graduate students for helpful discussions. Financial assistance in the form of Lead-Zinc research fellowship and the National Research Council studentship is gratefully acknowledged.

TABLE OF CONTENTS

		Page
1. Solution Strengthening in Polycrystals		1
1.1. Introduction and Objectives		1
1.2. Experimental Procedure		4
1.2.1. Materials and alloy preparation		4
1.2.2. Preparation of polycrystalline specimens		4
1.2.3. The growth of single crystals		5
1.2.4. Standard sections used		7
1.2.5. Spark erosion damage		8
1.2.6. Preparation of single crystal specimens for tensile tests		9
1.2.7. Testing procedure		10
1.3. Deformation characteristics of polycrystalline aggregates		12
1.3.1. Nature of the stress-strain curves		12
1.3.2. The yield stress		
	1.3.2.1. The temperature dependence of yield	18
	1.3.2.2. The concentration dependence of yield	21
	1.3.2.3. Solution strengthening in stage I	24
	1.3.2.4. Strengthening above C_T	28
	1.3.2.5. The temperature dependence of the solution strengthening parameters	28
1.3.3. The critical transition concentration		31
1.3.4. The maximum stress variation with temperature and alloying		35
1.3.5. Flow stress in relation to temperature and alloying		38
1.3.6. Ductility		44
	1.3.6.1. Alloying effect	44
	1.3.6.2. The temperature dependence of ductility	44
1.4. Discussions		49
1.4.1. Deformation modes in Magnesium		49
	1.4.1.1. Crystallographic slip	50

		Page
1.4.1.2.	Plastic deformation by twinning	54
1.4.1.3.	Grain boundary deformation	57
1.4.1.4.	Cell formation	58
1.4.2.	Fracture of Magnesium polycrystals	59
1.4.3.	Solution hardening	60
1.4.3.1.	The variation of σ_{YP} and ductility with solute concentration	64
1.4.3.2.	The solution hardening rate $(\frac{d\sigma}{dc})$	64
1.4.3.3.	Hardening beyond C_T	66
1.4.3.4.	The transition concentration C_T	67
1.4.3.5.	The flow stress	68
1.4.4.	The effect of temperature on ductility	69
1.4.4.1.	The ductility maxima	70
1.4.5.	Strengthening effects in multicomponent solid solutions	72
2.	Solution hardening in alloy single crystals	75
2.1.	Introduction and Objectives	75
2.2.	Stress-Strain Relationships in Basal Slip	76
2.2.1.	The stress-strain curves	76
2.2.2.	The effect of substructure on work hardening	78
2.2.3.	The stress-strain curves of the Mg-Zn alloys	80
2.2.4.	Yield points	84
2.2.5.	The critical resolved shear stress	88
2.2.6.	The rate of solution hardening	91
2.2.6.1.	The temperature dependence of S_I	91
2.2.6.2.	The variation of S_{II} with temperature	93
2.2.7.	Work hardening	93
2.2.7.1.	The work hardening rate in Stage A, θ_A	93
2.2.7.2.	The extent of easy glide	96
2.2.7.3.	Stress at the onset of Stage B, τ_B	100
2.2.7.4.	The work hardening rate in stage B, θ_B	100
2.2.7.5.	Deformation in stage C	103
2.3.	The effect of solute on the dislocation densities	103
2.3.1.	The basal dislocation density	105
2.3.1.1.	Foil preparation	106
2.3.1.2.	Observations	107

Page

2.3.1.3. The technique of dislocation dislocation density measurement and its limitations 108
2.3.1.4. The effect of solute on the basal dislocation density 112

2.3.2. The forest dislocation density 114

2.3.2.1. Crystal orientation and the pit characteristics 114
2.3.2.2. The study of spark erosion damage in Mg using the dislocation etch pit method 115
2.3.2.3. Variation of the etch pit density with alloying 118

2.4. Discussions 119

2.4.1. The critical resolved shear stress 119

2.4.2. Solution strengthening in the athermal region 121

2.4.2.1. The basal dislocation density 122
2.4.2.2. Elastic interaction 125
2.4.2.3. Chemical interaction 126
2.4.2.4. Short range order 128
2.4.2.5. Strengthening due to a random distribution of the solute 130
2.4.2.6. Strengthening at low solute concentrations 133
2.4.2.7. Valency effect 135
2.4.2.8. Other hardening mechanisms 135

2.4.3. Solution strengthening at low temperatures 136

2.4.3.1. Thermally activated deformation 140
2.4.3.2. The effect of solute on the apparent activation parameters 143
2.4.3.3. The activation volume at yield 145
2.4.3.4. Solution effect on the apparent activation energy 148
2.4.3.5. Zinc alloying and the thermally activated flow 149

2.4.3.5.1. Cross slip 151
2.4.3.5.2 Peierls, Pseudo Peierls and Recombination mechanisms 152
2.4.3.5.3. The intersection model 153
a) intersection model at low solute concentration 155
2.4.3.5.4. Dislocation pinning by the solute atoms 156

Table of Contents (Cont)

	Page
2.4.3.6. Strengthening mechanisms in dilute alloys	159
2.4.3.6.1. Deviations from square array	163
2.4.4. Work hardening of Mg solid solutions	164
2.4.4.1.1. The easy glide in Mg	165
2.4.4.1.2. Easy glide in alloy cyrstal	167
2.4.4.2. The temperature dependence of θ_A in alloy crystals	168
2.4.4.3. The extent of easy glide	169
2.4.4.4. Work hardening in stage B	171
2.4.4.5. The stage 'C' of deformation	172
2.4.5. The Effect of solute on the ease of prismatic slip	173
2.4.5.1. Introduction and objectives	173
2.4.5.2. Experimental results	174
2.4.5.2.1. The stress-strain curves	174
2.4.5.2.2. Ductility	181
2.4.5.2.3. The CRSS for prismatic slip	181
2.4.5.2.4. The CRSS of Mg-Zn alloys	183
2.4.5.2.5. The effect of solute on the flow stress	187
2.4.5.3. Discussions	189
2.4.5.3.1. The dislocation mechanism for prismatic slip	189
2.4.5.3.2. The effect of solute	190
2.4.5.3.3. The results of the present work	192
2.4.5.3.4. The Origin of τ_G and τ^*	195
2.4.5.3.4.1. The athermal stress	195
2.4.5.3.4.2. The variation of τ^* with alloying	196
3. Summary of Conclusions	198
4. Suggestions for Future Work	201
5. Appendices	202
A. Determination of solute concentration in the alloys	202
B. The Preferential nature of the solute-dislocation interaction	206
C. The determination of $\Delta\tau^*$ from strain rate change tests	209
Bibliography	211

LIST OF FIGURES

No.		Page
1.	Standard sections for obtaining tensile specimens from the as-grown crystal	6
2.	Gripping arrangement for basal slip specimens	11
3.	Stress-strain curves for Mg-Zn alloys tested at 295°K .	13
4.	Stress-strain curves for Mg-Al alloys tested at 295°K .	14
5.	Stress-strain curves for 65μ grain size Mg	15
6.	Stress-strain curves for Mg + 0.055 at.% Al alloy . . .	16
7.	Stress-strain curves for Mg + 0.53 at.% Al alloy	17
8.	Yield stress-temperature relationships for Mg-Al alloys	19
9.	Yield stress-temperature relationships for Mg-Cd alloys	20
10.	The composition dependence of Tt in Mg-Al and Mg-Cd alloys	22
11.	Yield stress-concentration plot for Mg-Zn alloys	23
12.	Yield stress-concentration plot for Mg-Cd alloys	23
13.	Stage I solution hardening at 295°K for various alloys .	26
14.	Stage I slope vs size misfit parameter	27
15.	Stage II slope vs size misfit parameter	27
16.	The effect of temperature on the solution hardening curve for Mg-Al alloys	29
17.	The effect of temperature on the solution hardening curve for Mg-Cd alloys	30
18.	Critical transition concentration, C_T, from stage I to stage II vs temperature for Cd solute	32
19.	C_T vs temperature for Al solute	32
20.a)	Stage I slope vs temperature for Mg-Cd alloys	33
b)	Stage II slope vs temperature for Mg-Cd alloys	33
21.	Stage I slope vs temperature for Al solute	34

List of Figures (Cont)

No.		Page
22.	Critical transition concentration, C_T from stage I to stage II vs size misfit parameter	34
23.	Maximum stress vs. temperature for Mg-Al alloys	36
24.	Fracture stress vs. composition for Mg-Cd alloys tested at 295°K	37
25.	Flow stress vs. temperature for 65μ Mg	39
26.	Flow stress vs. temperature for Mg + 0.055 at.% Al alloy	40
27.	Flow stress vs. temperature for Mg + 0.53 at.% Al alloy	41
28.	Transition temperature from stage I to stage II in the flow stress-temperature curves of Mg + 0.055 at.% Al alloy vs. strain	42
29.	Flow stress vs. composition for Mg-Zn alloy	43
30.	Ductility vs. concentration for various solutes	45
31.	True strain to fracture vs. temperature for Mg-Al alloys	46
32.	True strain to maximum stress vs. temperature for Mg-Al alloys	48
33.	True strain associated with negative work hardening vs. temperature for Mg-Al alloys	48
34.	CRSS for basal slip vs. concentration (After Levine et al(74)).	63
35.	Revised curves drawn for data from ref. 74.	63
36.	Solution hardening curve for Mg-Zn-In, ternary alloys tested at 295°K with Zn concentration fixed at 0.004 at.%.	74
37.	Solution hardening curve for Mg-Zn-In ternary alloys tested at 295°K with Zn concentration fixed at 0.007 at.%.	74
38.	Resolved shear stress-shear strain curves for Mg single crystals oriented for basal slip	77
39.	Schematic resolved shear stress-shear strain curve	79

List of Figures (Cont)

No.		Page
40.	Sub-boundary running parallel to the tensile-axis in a Mg + 0.054 at.% Zn alloy crystal deformed in easy glide at room temperature	79
41.	Resolved shear stress-shear strain curves for Mg single crystals deformed by various workers at room temperature	81
42.	Resolved shear stress vs. shear strain curves for Mg + 0.019 at.% Zn alloy single crystals	82
43.	Resolved shear stress vs. shear strain curves for Mg + 0.019 at.% Zn alloy single crystals	83
44.	Resolved shear stress vs. shear strain curves for Mg-Zn single crystals deformed at 373°K	85
45.	Resolved shear stress vs. shear strain curves for Mg-Zn alloy single crystals deformed at 295°K.	86
46.	Resolved shear stress vs. shear strain curves for Mg-Zn alloy single crystals deformed at 195°K	87
47.	CRSS for basal slip vs. temperature for Mg-Zn single crystals	89
48.	Solution strengthening in basal slip vs. concentration for Mg-Zn alloys	90
49.	Solution strengthening in basal slip vs. square root of the solute concentration	90
50.	The variation of the solution strengthening parameter S_I with temperature	92
51.	The variation of the solution strengthening parameter S_{II} with temperature	92
52.	The work hardening rate in stage A vs. temperature for Mg-Zn single crystals	94
53.	The temperature dependence of the work hardening rate in the easy glide of Magnesium as reported by various workers	95
54.	The increase in work hardening rate in easy glide vs. Zn concentration	97

List of Figures (Cont)

No.		Page
55.	The increase in work hardening rate in easy glide vs. square root of the Zn concentration	98
56.	The extent of easy glide as a function of temperature for Mg-Zn single crystals	99
57.	The decrease in the extent of easy glide as a function of the solute concentration	99
58.	The effect of temperature and solute concentration on the stress at the onset of stage B	101
59.	The effect of temperature on the work hardening rate of Mg-Zn crystals in stage B	102
60.	The increase in the work hardening rate in stage B vs. Zn concentration	102
61.	The stress at the onset of stage C vs. Zn concentration	104
62.	Typical dislocation structure in as grown Mg crystal. .	107
63.	Electron micrograph showing dislocations surrounding a particle.	109
64.	Typical dislocation structure in an undeformed Mg + 0.18 at. % Al alloy single crystal	110
65.	Typical dislocation structure in an undeformed Mg + 0.38 at. % Al alloy single crystal	111
66.	Basal dislocation density vs. square root of solute concentration for Mg-Al alloys	113
67.a)	Hexagonal shape of the etch pits	116
b)	Distribution of etch pits in a Mg + 0.019 at.%. Zn alloy crystal	116
68.	Dislocation etch pits on the {0001} plane of Mg single crystal	117
69.	Etch pit density vs. Zn concentration	117
70.	The temperature dependence of yield in terms of the stress components	120
71.	Comparison of the observed solution strenthening with that expected from the increase in the basal dislocation density	124

List of Figures (Cont)

No.		Page
72.	The increase in CRSS of Mg vs. (Li concentration)$^{1/2}$ in Mg-Li alloy single crystals	124
73.	τ_G vs. concentration for Ag solid solutions	134
74.	The effect of solute on the τ-T curve (schematic) . .	136
75.	τ^* vs. temperature for Mg-Zn single crystals	138
76.	$(\frac{d\tau^*}{dT})_{\gamma/\gamma_o}$ vs. solute concentration for Mg-Zn single crystals	138
77.	Activation volume vs. shear strain for Mg-Zn single crystals	144
78.	Activation volume at yield vs. Zn concentration . . .	146
79.	Activation volume at yield vs. temperature for Mg and Mg + 0.045 at.% Zn alloy single crystals	146
80.	Activation volume at yield vs. τ^* for Mg and Mg + 0.45 at.% Zn alloy single crystals	147
81.	Apparent activation energy vs. Zn concentration . . .	150
82.	Dislocation pinning by solute atoms giving rise to low temperature friction stress (schematic)	156
83.	Comparison of the experimental results with the composition dependence of activation volume as predicted by Friedel's model	158
84.	Concentration dependence of CRSS extrapolated to 0°K for Ag-In and Ag-Al single crystals	158
85.	Resolved shear stress vs. shear strain curves for Mg single crystals oriented for prismatic slip	175
86.	Resolved shear stress vs. shear strain for Mg + 0.019 at.% Zn alloy single crystals oriented for prismatic slip	176
87.	Resolved shear stress vs. shear strain curves for Mg + 0.258 at.% Zn alloy single crystals oriented for prismatic slip	177

List of Figures (Cont)

No.		Page
88.	Resolved shear stress vs. shear strain curves for Mg + 0.45 at.% Zn alloy single crystals oriented for prismatic slip	178
89.	Resolved shear stress vs. shear strain curves for Mg-Zn single crystals deformed at 423°K in prism slip orientation	179
90.	Resolved shear stress vs. shear strain curves for Mg-Zn single crystals deformed at 78°K in prism slip orientation	180
91.	Shear strain to fracture vs. temperature for Mg-Zn single crystals oriented for prismatic slip	182
92.	CRSS for prismatic slip vs. temperature for Mg-Zn single crystals	184
93.	CRSS for prismatic slip vs. Zn concentration	185
94.	CRSS for prismatic slip vs. temperature for Mg-Al single crystals	186
95.	Flow stress for prismatic slip vs. concentration for Mg-Zn single crystals tested at 78°K	188
96.	Flow stress vs. concentration for Mg-Zn single crystals tested at 423°K	188
97.	Activation volume at yield vs. temperature for Mg-Zn single crystals deformed in prism slip orientation	191
98.	CRSS for prismatic slip vs. temperature for Mg-Li alloy single crystals	193
99.	Schematic representation of the effect of solute on the various components of flow stress in prismatic slip	194
100.	Absorbance vs. Zn concentration	205
101.	Solution hardening curves for Mg-Zn and Mg-In binary systems	207
102.	The nature of the flow stress observed during strain rate change tests in Mg-Zn single crystals. (Oriented for basal slip).	210

LIST OF TABLES

		Page
I	Solution hardening parameters for polycrystals tested at 295°K	25
II	Slip systems in hexagonal metals	54
III	Comparison of solution hardening rates	65
IV	Strengthening due to increased forest density	162

PART I

1. Solution Strengthening in Polycrystals

1.1. INTRODUCTION & OBJECTIVES:

The systematic study of solid solution strengthening mechanisms has lagged considerably behind its applications. This is especially the case for materials with hcp structure. Solid solutions with fcc structure have been considered in some detail during the past decade[1,2]. However, the limited understanding of the deformation characteristics of hcp pure metals has inhibited investigations of solution strengthening in this class of material.

Of all hexagonal metals, titanium and magnesium have been studied in the greatest detail because of their favourable strength to weight ratio. The pure metal magnesium is not used in many technological applications, mainly due to its embrittlement during cold working. Therefore, the problem of determining the deformation mechanisms which control flow in magnesium has been a subject of considerable interest[3-13].

As in the engineering of other metals alloying of magnesium has been used to obtain strength, ductility, workability, corrosion resistance, low density and castability. In relation to deformation behaviour much of the solid solution work in magnesium and in hexagonal structures in general has been confined to the Mg-Li alloys[14,15,16]. Interest in this system of alloys was aroused mainly because these alloys showed an unusual lowering of the critical resolved shear stress for prismatic slip with increasing solute addition. This anomalous solid solution effect was attributed to the decrease of c/a ratio in these alloys, compared to that of pure magnesium. It was concluded that only those

alloying elements which decrease the c/a ratio of magnesium can lower the CRSS for prismatic slip.

One of the objectives of the present investigation was to evaluate the significance of the c/a ratio in the ease of prismatic slip and also to evaluate the effect of relative valence of the solute on the properties examined. For this purpose the solutes chosen were Zn, Cd, Al, In and Pb. Of these Zn and Cd belong to the same valency group as Mg and have the same crystal structure as well, but differ in the atomic size. Zn has little effect on the c/a ratio, whereas Cd increases it[17]. Al, In and Pb belong to higher valency groups, and all three increase the c/a ratio. These elements cover a wide range of size differences with respect to magnesium.

A second objective of the work presented in this thesis was to examine the effects of alloying at low concentrations. Work by Hardie and Parkins[18] using hardness measurements had indicated the possibility of a very high strengthening effect at low concentrations in Mg base alloys containing a wide variety of solutes.

Many of the previous solid solution strengthening studies have been carried out on polycrystals. It is possible to derive quantitative information concerning the dislocation-solute interaction in face centred cubic alloys. However, in the case of hexagonal solid solutions such studies may at best be considered to provide a qualitative understanding of the subject. The difference in the two groups of close packed structures arises mainly due to the different ways in which their polycrystalline aggregate undergoes plastic deformation.

A necessary condition for a polycrystal to deform plastically and yet retain continuity is that the number of independent deformation systems be five[19-22,60]. In the face centred cubic structures the primary single slip mode, is capable of giving rise to five independent slip systems. Since the slip systems are crystallographically equivalent, they are affected equally by the addition of solute. In contrast, no single slip mode is capable of giving rise to five independent slip systems in hexagonal metals. (The second order $\{11\bar{2}2\}$ $\langle 11\bar{2}3\rangle$ pyramidal slip is capable of giving rise to five independent modes, but it operates as a secondary system at high temperatures in the case of Cd, Zn and Ti. This system, however, does not operate in magnesium).

The plastic deformation of polycrystalline magnesium involves more than two sets of crystallographically nonequivalent slip systems[14]. The solute dislocation interaction, therefore, on the two sets of planes cannot be expected to be identical.

In view of this limitation of the polycrystal study, the investigation has been extended to include the effect of solute on single crystals as well.

The first part of this thesis is concerned with the effect of solute on the deformation behaviour of the polycrystalline aggregates. The second part deals with studies on single crystals in making quantitative estimates of the dislocation solute interaction for various slip systems.

1.2. EXPERIMENTAL PROCEDURE:

1.2.1. Materials and Alloy Preparation:

High purity Mg (99.995), obtained from the United Minerals and Chemicals Corporation, N.Y., in the vapour deposited form, and alloying elements having an impurity level below 0.005% were used in the present investigation. Melting was carried out at 680°C in a cylindrical graphite mould, housed inside a vertical resistance heated furnace. Alloying additions were made in the form of pre-weighed pure metals for compositions greater than 0.2 at.%. However, master alloys were used for lower concentrations. After stirring, the melt was solidified in the melting pot by sharp unidirectional cooling in order to avoid pipe formation. For alloys containing high vapour pressure solutes (at the melting temperature) like Zn and Cd, the graphite pot along with a tapered graphite plug was enclosed in a stainless steel bomb. This procedure minimized the loss of the more volatile component from the melt. The compositions of the alloys were checked and found to be close to the nominal values. Details of the chemical analyses are described in appendix (A).

1.2.2. Preparation of Polycrystalline Specimens:

The castings approximately $1\frac{1}{8}$" in diameter and 5" long were homogenized and subsequently hot rolled at 430°C to 0.032" thickness. Reductions of 10 - 15% per pass were made in the beginning to break down the cast structure, followed by 20 - 25% reduction per pass, which controlled the final grain size of the material. The material was given intermittent annealing for 5 minutes at 430°C before every pass. The rolled sheet was sheared into 3" long by 0.75" wide

strips, which in turn were punched into tensile test specimens having a reduced gauge length of 0.8" with a width of 0.2". The tensile axis of the specimen was kept parallel to the rolling direction. Edges were removed by 3/0 emergy paper and the specimens were given 20 mins. anneal at 430°C. The last annealing operation removed all residual stresses due to punching, and gave a consistently uniform grainsize of 60 - 65μ.

The test pieces were pickled in 20% HNO_3 which removed the oxide layer from the surface and also gave slight grain boundary grooving, which helped examining the microstructure subsequently.

1.2.3. The Growth of Single Crystals:

Single crystals were grown from the melt using a modified Bridgeman technique. Alloys were made following the procedure described earlier. The polycrystalline rod approximately 1⅛" in diameter, and 5" long was cleaned and kept in a graphite mould, which was covered with a tight fitting tapered graphite plug, as shown in fig. (1). The mould was then lowered in a vertical tube resistance furnace at the rate of 0.4"/hr. This procedure gave consistently good quality single crystals. A shallow temperature gradient was used in order to minimize the solute segregation in the alloy crystals. For a constant degree of supercooling and temperature gradient, the apex angle of the nucleation tip was found to influence the orientation of the crystal with respect to the direction of growth. The orientation of the crystals grown in this manner could be controlled without seeding. All crystals used in the present work were grown such that the basal plane remained inclined at nearly 45° to the growth direction. This procedure was

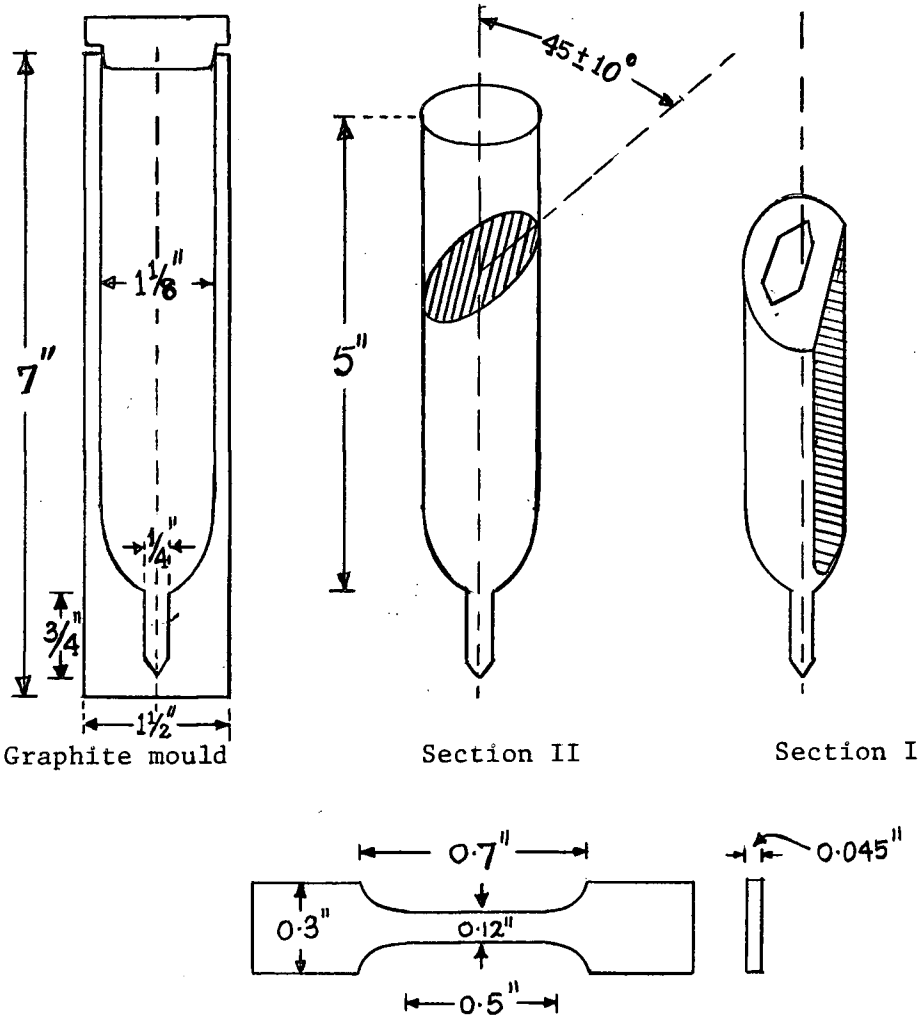

Fig. 1. Standard sections for obtaining tensile specimens from the as grown crystal.

found to be most convenient in obtaining large sections having the desired orientation. Subsequent chemical analyses on samples taken from the two ends of the relatively short length of the as grown crystal did not show a detectable variation in composition.

For each solute concentration investigated, only one crystal was grown from which all the tensile test specimens as well as samples for dislocation density evaluation could be obtained.

1.2.4. Standard Sections Used:

The orientation of the as grown crystal was determined using X-ray back reflection Laue technique. The crystal was mounted on a "V" block which in turn was clamped on to the base plate of a spark erosion machine. Using a goniometer, the crystal was rotated with respect to its growth axis and the spark erosion tool - a flat copper strip - was adjusted such that the desired section could be obtained on subsequent spark erosion. Two sets of slices having a thickness of 0.1" each were used in the present investigation.

Section I:

These slices were cut parallel to the direction of growth, keeping the {0001} plane perpendicular to the flat face. Tensile test specimens oriented for basal slip were obtained from this section.

Section II:

The surface of this series of slices was kept parallel to the basal {0001} plane within 2 degrees. Samples for dislocation density evaluations as well as tensile test pieces to induce prismatic slip were obtained from this section.

1.2.5. Spark Erosion Damage:

In recent years spark erosion has become a more attractive alternative to the acid machining methods, in the shaping of suitable test specimens from larger single crystals. The main reasons for the preference of spark erosion over the acid machining methods are the relatively faster cutting rate and the flatter surfaces obtainable by the former technique. However, the uncertainty in the depth of the plastically deformed layer, due to spark erosion, has been a drawback.

Lately interest has been shown in determining the depth and distribution of spark damage. Much of this work has been based on the revealing of dislocations by suitable etching techniques. Samuels[23] has shown that the depth of damage in polycrystalline 70-30 brass is limited to 45μ below the surface. The work of Šesták and Libovický[24] on Fe-4%Si alloy, of Steeds[25] on copper and of Platnik[26] on the (111) plane of Sb and Bi and {0001} plane of Zn have demonstrated that with a spark energy of the order of 10^3 ergs the damage is limited to a depth of 150 μ from the surface. Hazzledine[27] working with Cu-Al alloys concluded that the damage was 300 μ deep for similar spark energy. More recently Turner et al[28] have evaluated the effect of plastic anisotropy on spark damage in Zn single crystals.

Spark energies of the order of 10^3 ergs have been used in the present work. Using similar spark energies and transmission electron microscopy for revealing dislocations, Hirsch and Lally[29] have found that the basal dislocation density remains unaffected if slices thicker than 1 mm are cut. However, an accurate check on the depth of damage could not be made by these authors because of the non-availability of a

suitable etchant to reveal dislocations in magnesium. In the course of the present investigation, an etchant has been developed to reveal the non basal dislocations in Mg and its dilute alloys. The details of the method will be described in a later chapter. Using this method of etching it was found that the depth of spark damage was limited to a surface layer 300μ thick. It is important to note that the present etch pitting technique reveals the effect of spark erosion on the nonbasal edge dislocation density alone.

The effect of spark erosion at and below a depth of 300μ on the basal dislocations was checked as follows. Two tensile test specimens were taken from the same slice. One was chemically polished to a depth of 300μ and the other to 500μ . The initialflow stresses and the initial work hardening rates of the two specimens were found to be equal within experimental error, indicating that the spark damage on the basal planes was insignificant below a depth of 300μ .

1.2.6. Preparation of Single Crystal Specimens for Tensile Tests:

A copper tool was used to spark erode test pieces whose final shape and dimensions after chemical polishing are shown in fig. (1). The material used for obtaining the test pieces was in the form of slices cut from the as grown crystal. After shaping the specimens were chemically polished in 10-20% HNO_3 to remove the damaged layer. The orientation of each specimen was checked by the back reflection Laue method. No asterism was observed, indicating that the crystals were strain free.

The orientation of the slip plane with respect to the tensile axis is shown in fig. (1) for basal and prismatic slip respectively.

In the case of specimens oriented for basal slip the basal plane made an angle of $45 \pm 8°$ with the tensile axis whereas those oriented for prismatic slip had the basal plane parallel to the tensile axis within 2 degrees. In the latter case one of the 1st. order prism planes of the form $\{10\bar{1}0\}$ was kept at an angle close to 45° to the tensile axis, so as to have the maximum shear stress acting on this plane. The alignment of the basal plane with the wider face of the test piece facilitated the identification of the prism slip markings on the narrow face.

All specimens were given a 2 hr. anneal at 450°C in order to remove any straining caused during handling. The specimens were chemically polished again in order to remove the surface layer for easier examination of the deformation markings.

1.2.7. Testing Procedure:

All specimens were deformed on a Floor Model Instron. The polycrystalline specimens were tested at a strain rate of $2 \times \bar{10}^{3}$ sec^{-1}; whereas the single crystals were deformed at 1.66×10^{-4} sec^{-1} except when otherwise stated. Testing media included

Liquid Nitrogen	78°K
Petroleum ether + Dry ice	195°K
Petroleum ether cooled with liquid nitrogen	133°K to 295°K
Air	295°K
Silicone Oil	295°K to 513°K

In each case the temperature was controlled to ± 2°. For polycrystalline specimens wedge grips were used which provided a rigid testing apparatus. Single crystals oriented for prismatic slip were much stronger than the polycrystalline specimens. Hence the split jaw grips were used in this case with increased precaution in the alignment

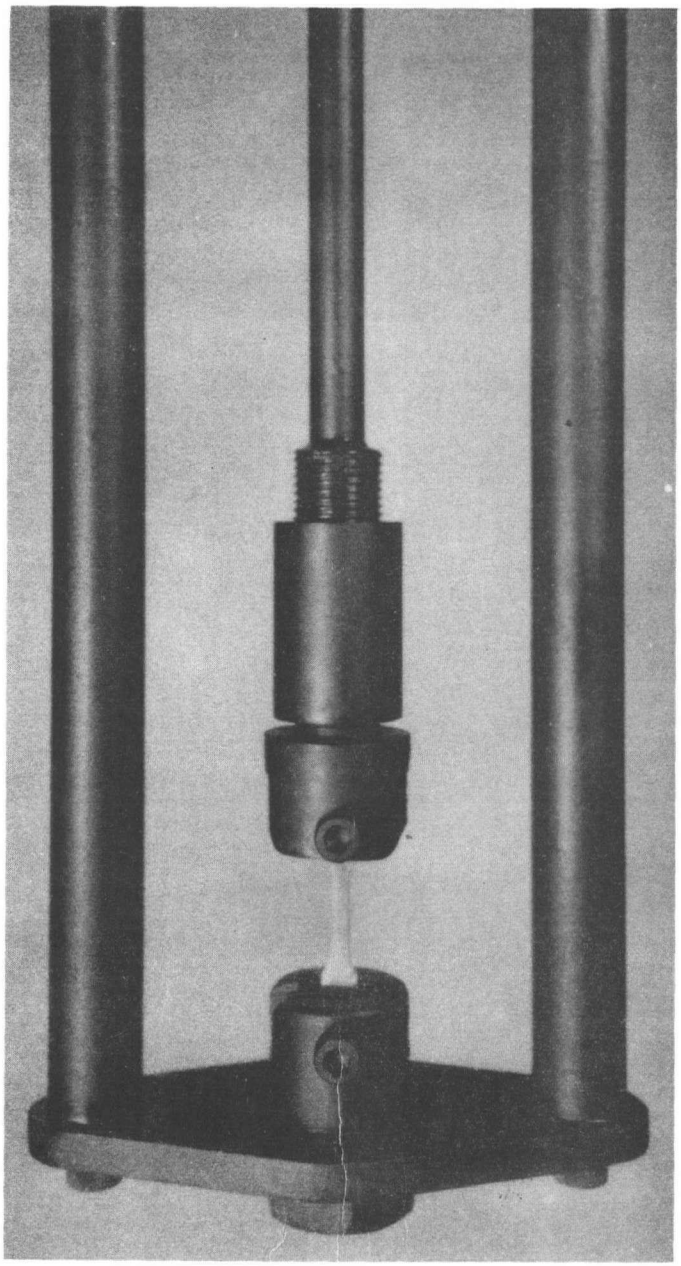

Fig. 2. Gripping arrangement for basal slip specimens.

procedure. For single crystal specimens oriented for basal slip a separate set of grips was used as shown in fig. (2). In all cases cycle control was used in order to prevent overloading of specimens during gripping.

The data on mechanical properties of the polycrystals are expressed in FPS units, while those for single crystals are given in CGS units. This is done in order to facilitate comparison with previous work.

1.3. DEFORMATION CHARACTERISTICS OF POLYCRYSTALLINE AGGREGATES:

1.3.1. Nature of the Stress Strain Curves:

The true stress vs true strain curves for pure magnesium and representative sets of Mg-Zn and Mg-Al alloys deformed at room temperature are shown in figs. (3) and (4). It is readily observed that at low solute concentrations the stress-strain curves for the alloys lie above that for pure magnesium. At higher concentrations of solute, however, a knee appears and the stress strain curves fall below those of the alloys containing lower amounts of solute. Similar results were obtained for Mg-Cd, Mg-Pb and Mg-In alloys. These results are consistent with the observations of Yoshinaga and Horiuchi[16] and of Hauser et al[14] on Mg-Li alloys. The lowest concentration of lithium studied by Yoshinaga was 0.4 at%.

The effect of temperature on the stress-strain curves of magnesium is shown in fig. (5), and for two of the Mg-Al alloys in figs. (6) and (7). It is observed that in the early stages of straining the work hardening curve is parabolic at high effective temperatures, however, the rate of initial work hardening increases more rapidly with strain at lower temperatures. Reference to figs. (5), (6) and (7) indicates a large amount of strain beyond the point of maximum stress

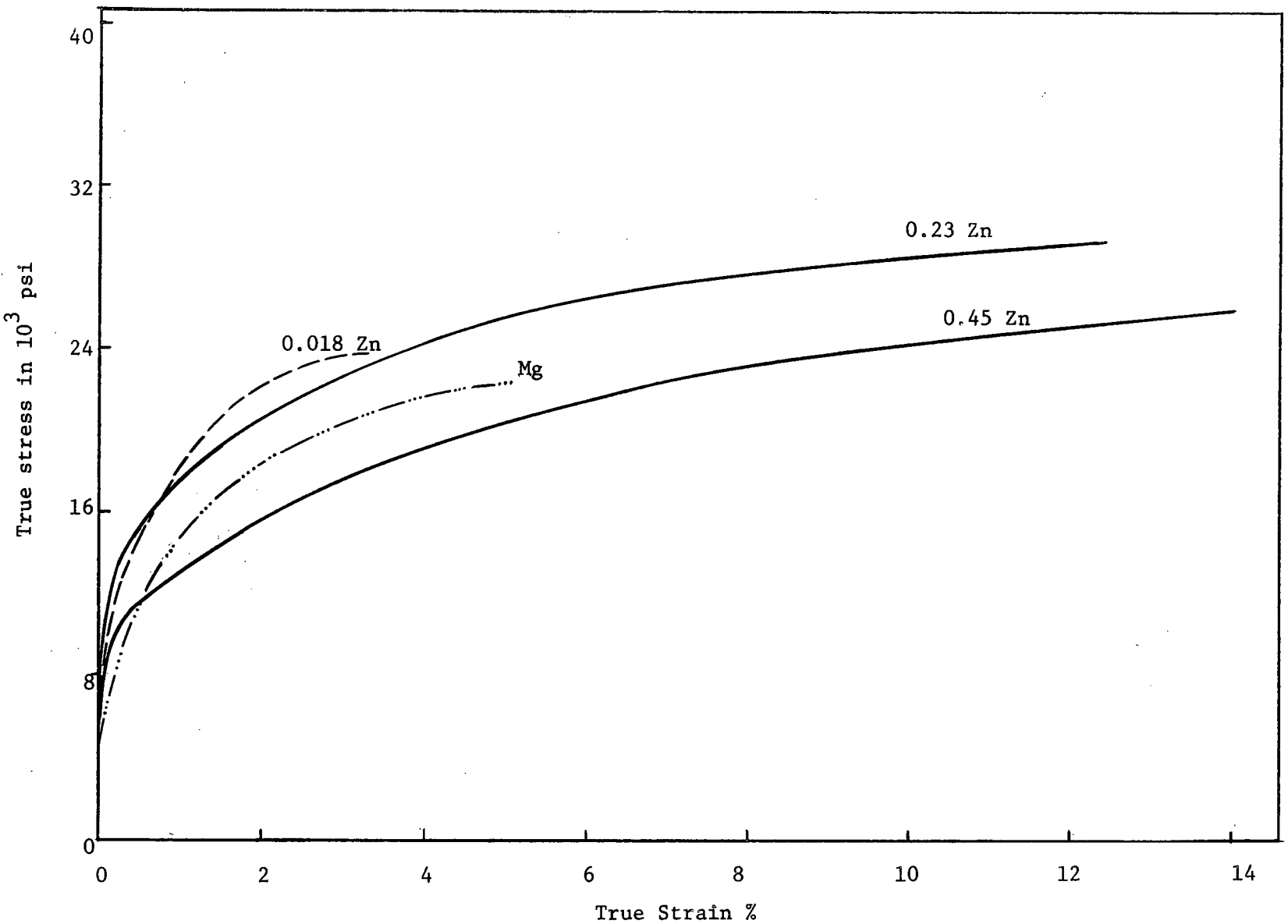

Fig. 3. Stress-strain curves for Mg-Zn alloys tested at 295°K.

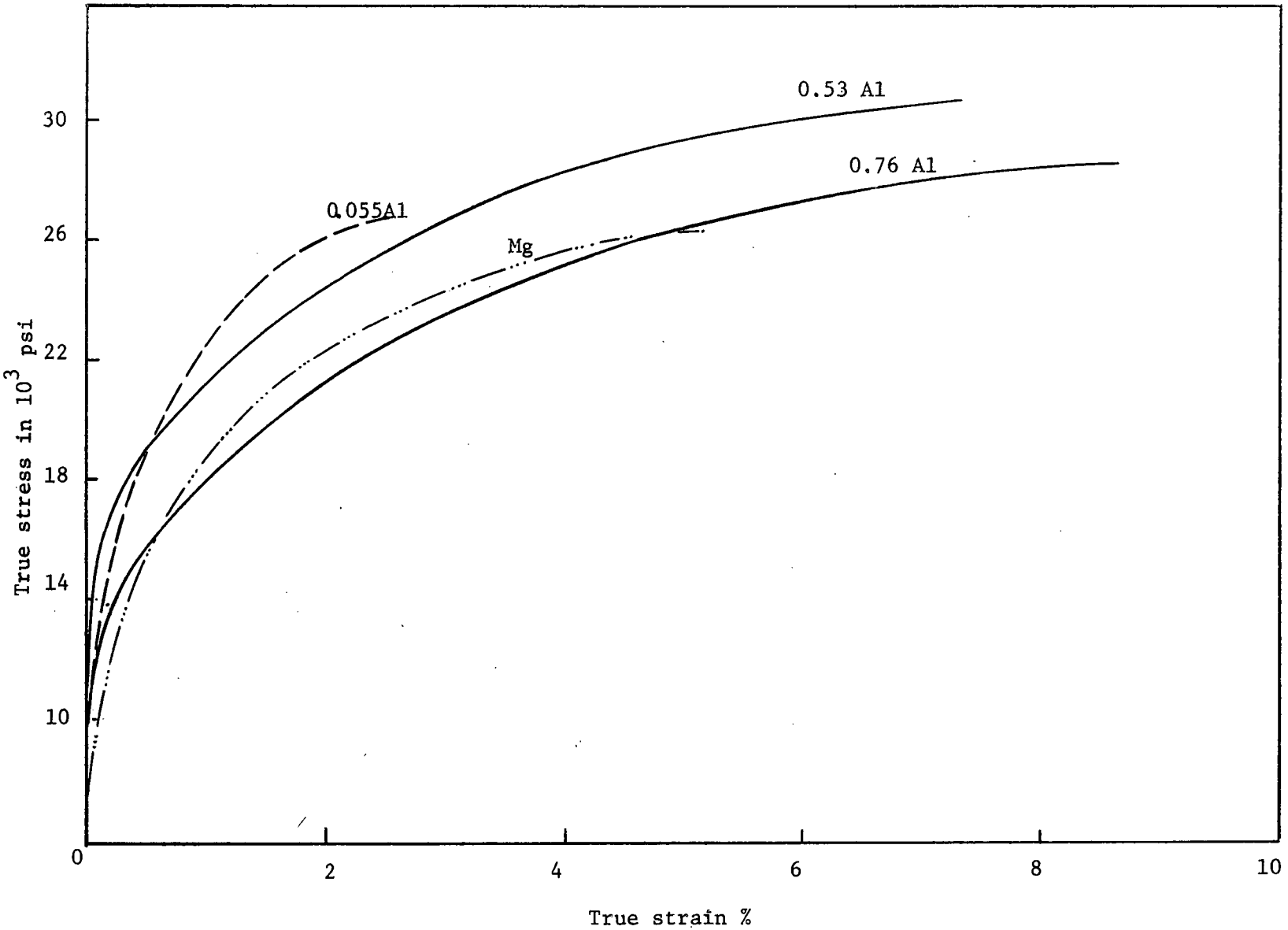

Fig. 4. Stress-strain curves for Mg-Al alloys tested at 295°K.

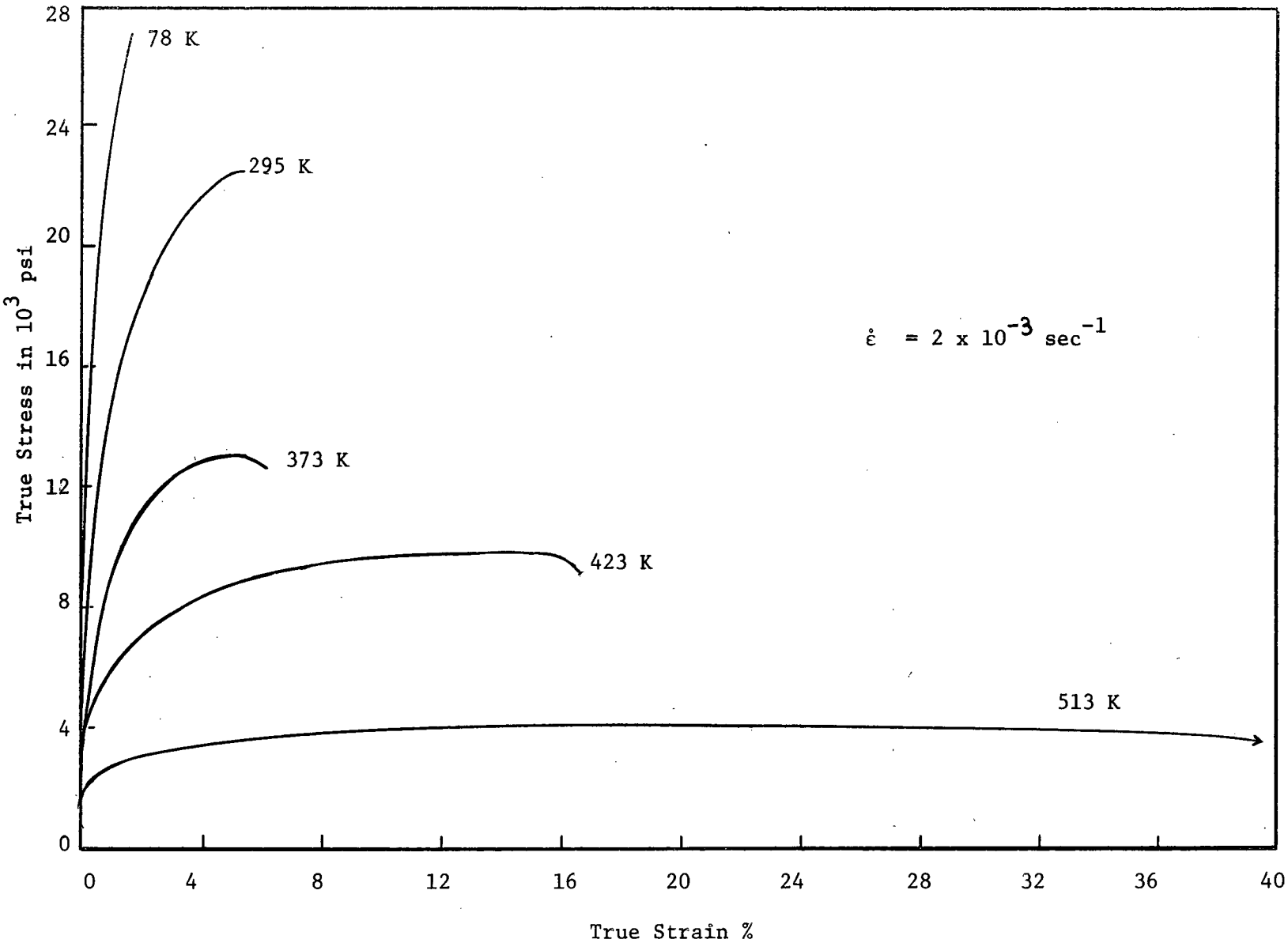

Fig. 5. Stress-strain curves for 65μ grain size Mg.

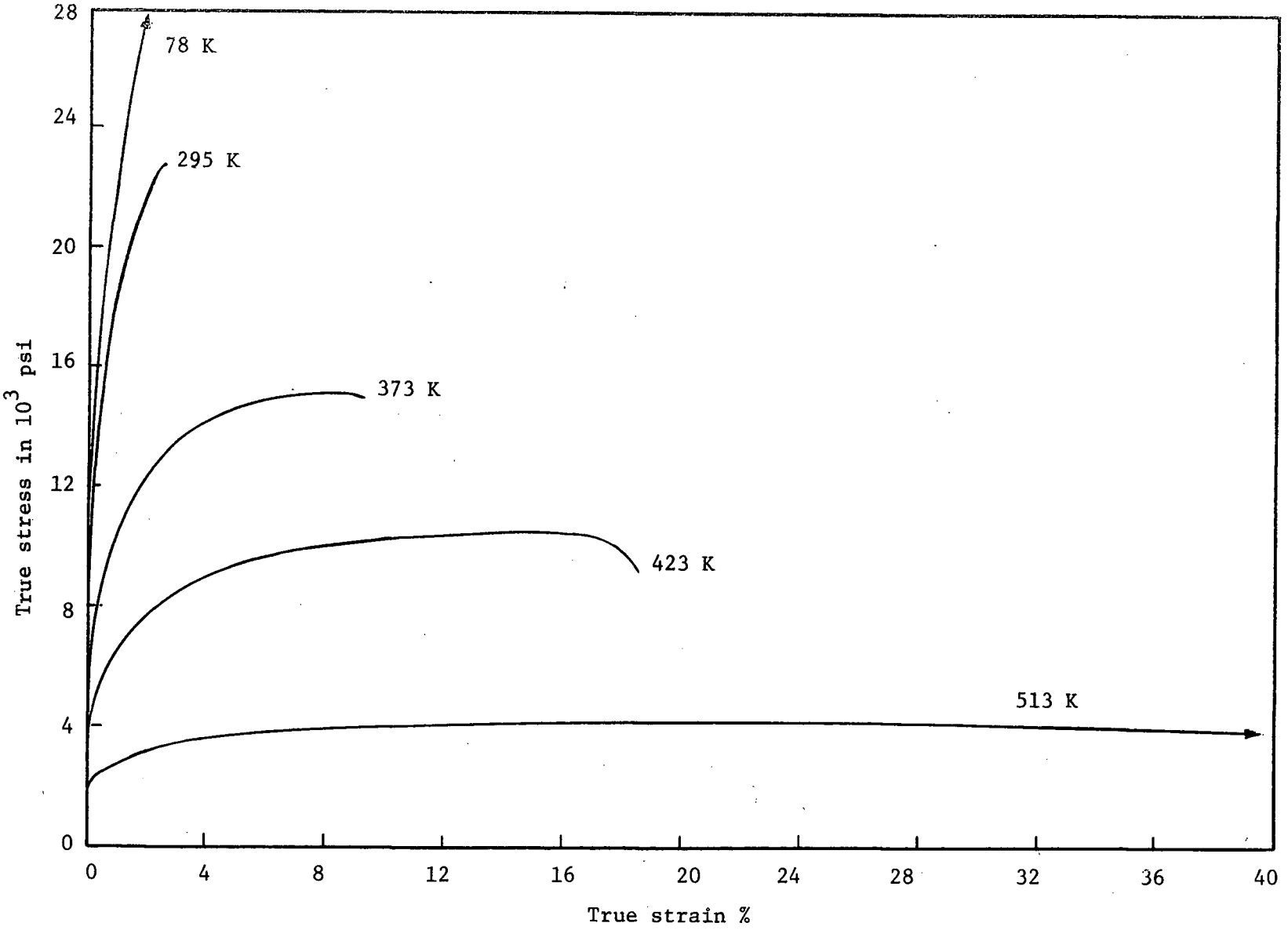

Fig. 6. Stress-strain curves for Mg + 0.055 at. % Al alloy.

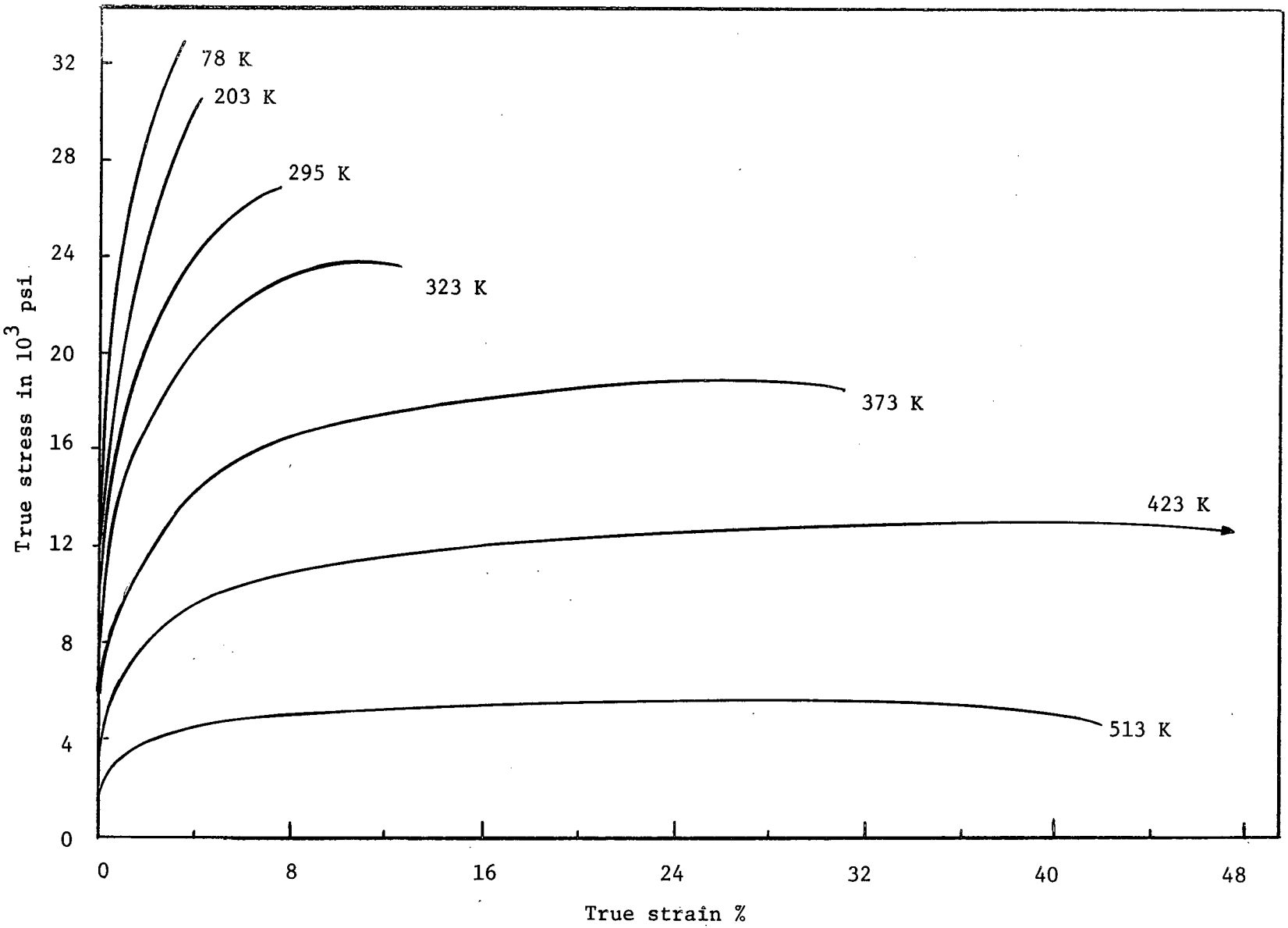

Fig. 7. Stress-strain curves for Mg + 0.53 at. % Al alloy.

in specimens tested above 373°K. The Mg-Cd alloys also exhibited a similar behaviour. This behaviour was observed not to be associated with necking.

1.3.2. The Yield Stress:

The definition of a yield stress in polycrystalline magnesium is difficult because of the gradual nature of the yield process. Therefore, in the present work the stress at 0.2% offset strain will be called the yield stress σ_{YP}.

1.3.2.1. The Temperature Dependence of Yield:

The temperature dependence of the yield stress for various alloys is shown in figs. (8) and (9) for both aluminum and cadmium solutes. The curves may be divided conveniently into three stages. At low temperatures there exists a region of moderate and linear decrease in σ_{YP} with increasing temperature (stage I), followed by stage II, in which the yield stress decreases more rapidly with temperature. Stage II ends at approximately 400°K [fig. (8)] and a third linear stage follows where the rate of decrease of σ_{YP} with temperature is similar to that in stage I. Yield stress-temperature relationships have been obtained by Hauser, Landon and Dorn[30], for polycrystalline pure Mg of varying grain sizes; however, their study was not sufficiently extensive as to establish the various stages shown in fig. (8).

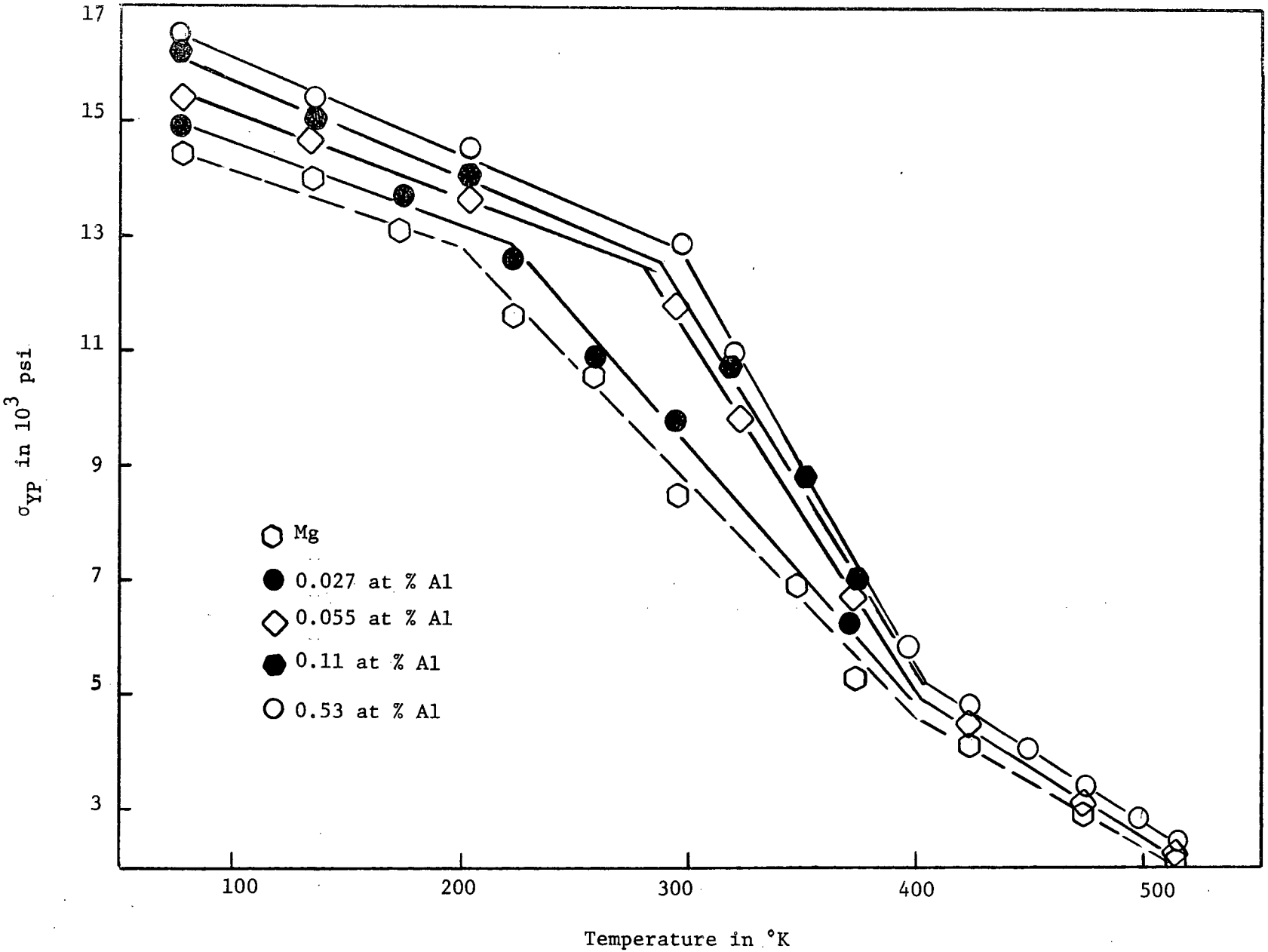

Fig. 8. Yield stress-temperature relationships for Mg-Al alloys.

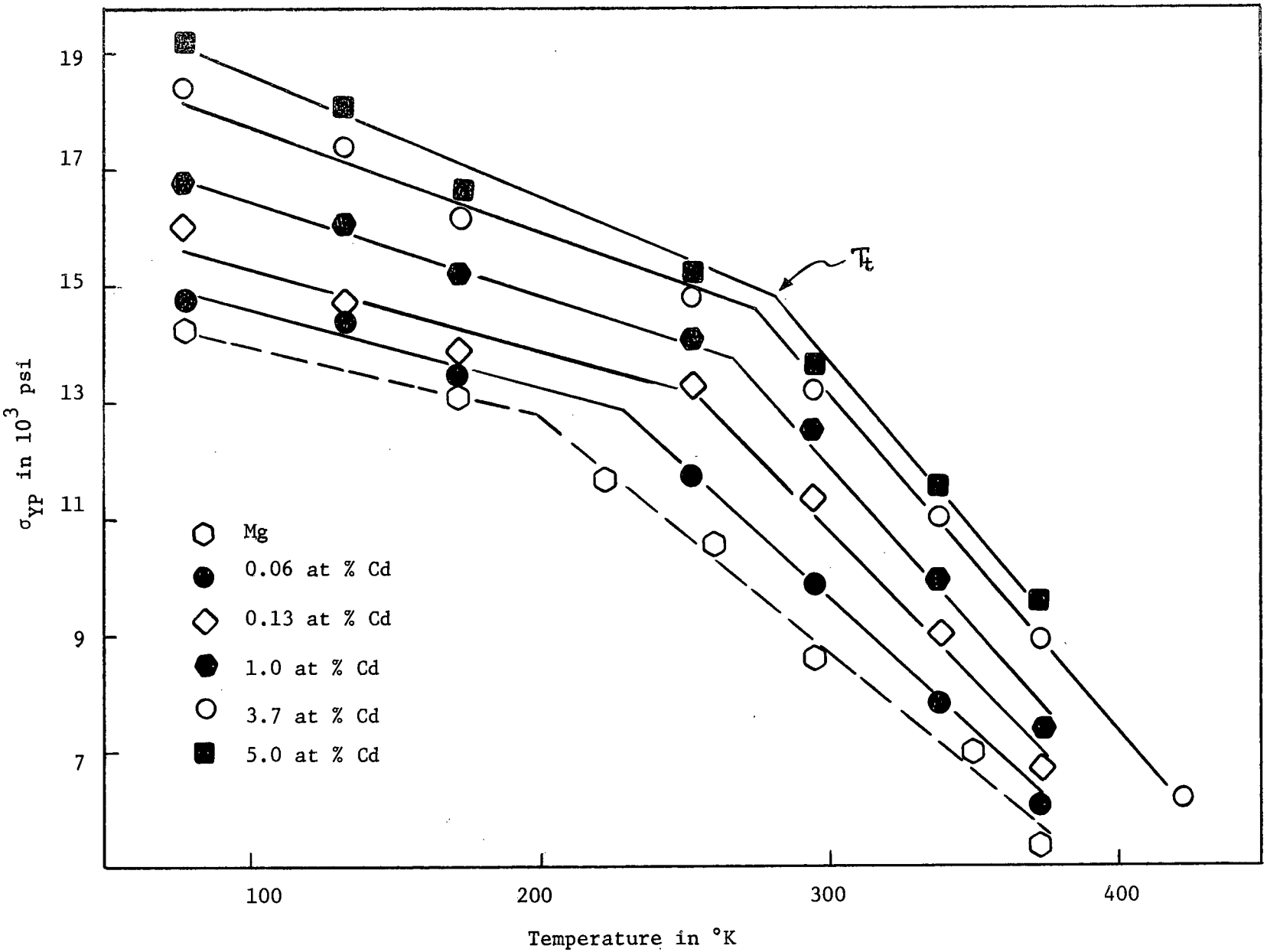

Fig. 9. Yield stress-temperature relationships for Mg-Cd alloys.

It is also interesting to note that the temperature at which transition from stage I to stage II occurs (T_t) is a sensitive function of the solute concentration in the low alloys. However, beyond a certain minimum concentration of solute, which we will designate C_c, the transition temperature increases only slightly with increasing solute content. This is shown in fig. (10), where T_t is plotted against the solute concentration for both aluminum and cadmium solutes. The numerical values of C_c are 0.17 and 0.054 at % for Mg-Cd and Mg-Al alloys respectively.

1.3.2.2. The Concentration Dependence of Yield:

The yield stress at room temperature is plotted against solute concentration for both Zn and Cd solutes as shown in figs. (11) and (12). The curves may be divided into three stages. Stage I at the lowest solute concentrations is a region of rapid and linear increase in yield stress with increasing solute. At a concentration C_T the stage I ends and the stage II strengthening begins, which is also approximately linear but has a slope approximately an order of magnitude lower than that in stage I. Stage II ends with a gradual decrease in τ_{YP} with further increase in solute concentration during stage III.

This type of multistage solution strengthening has also been observed with Al, Pb, Cd and In solutes, although, the stage III region has not been observed in all cases.

Earlier work by Hardie and Parkins [18] using hardness measurements had indicated the possibility of a high strengthening effect at low solute concentrations followed by a less rapid increase in hardness at higher concentrations, in alloys of Magnesium containing a variety of solutes. Work by Hauser, Landon and Dorn[14], had indicated a three

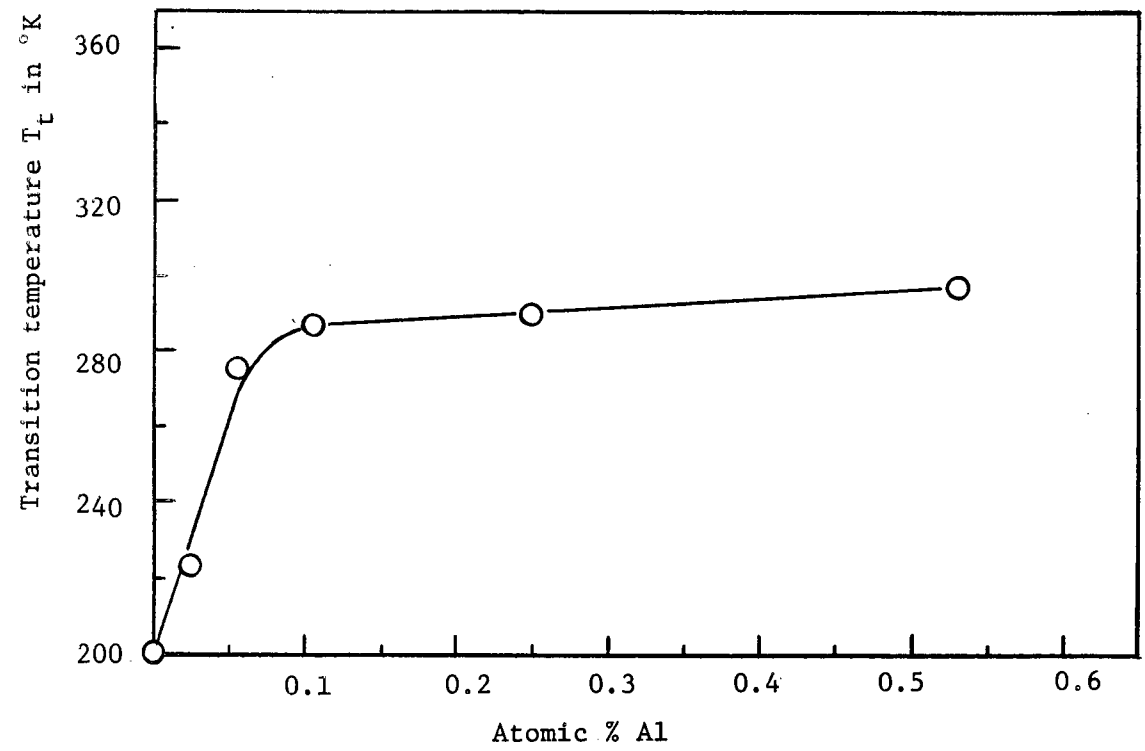

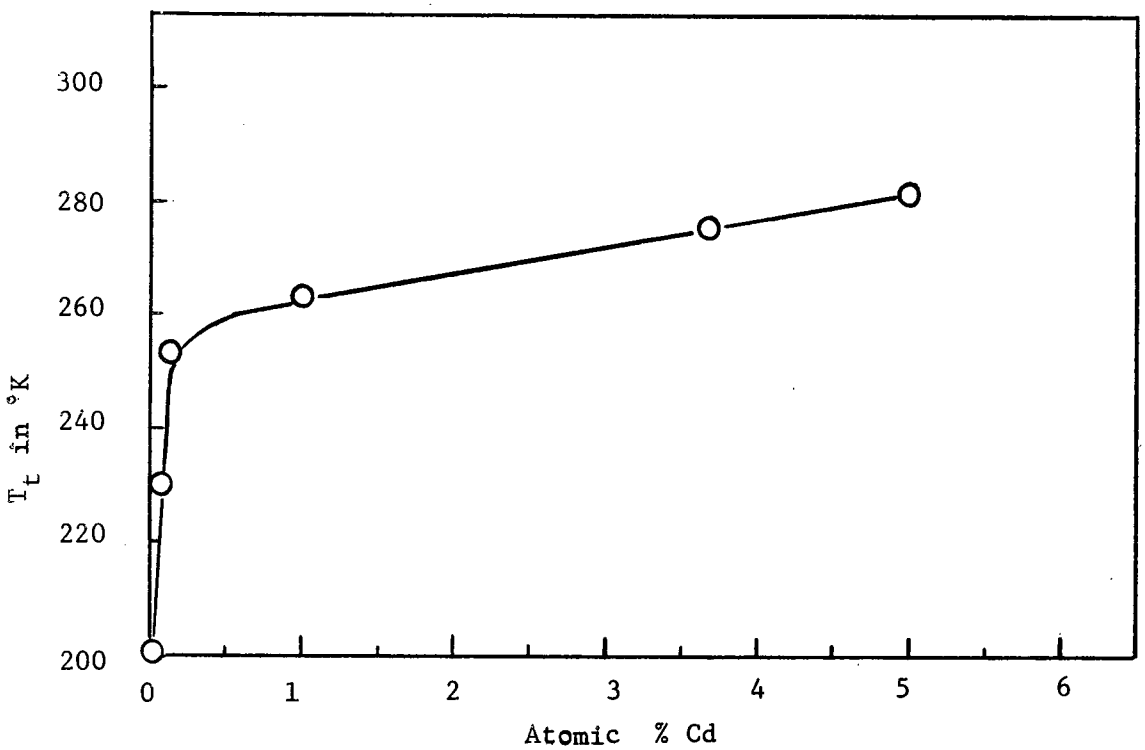

Fig. 10. The composition dependence of T_t in Mg-Al and Mg-Cd alloys.

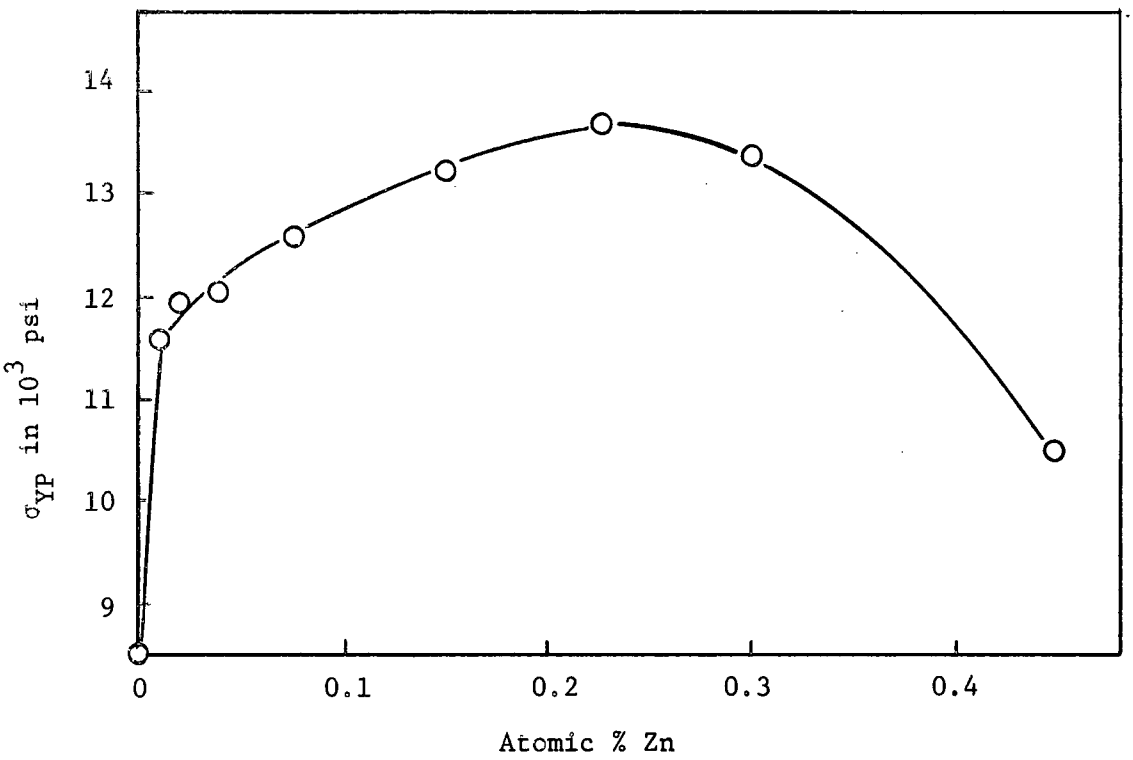

Fig.11. Yield stress-concentration plot for Mg-Zn alloys.

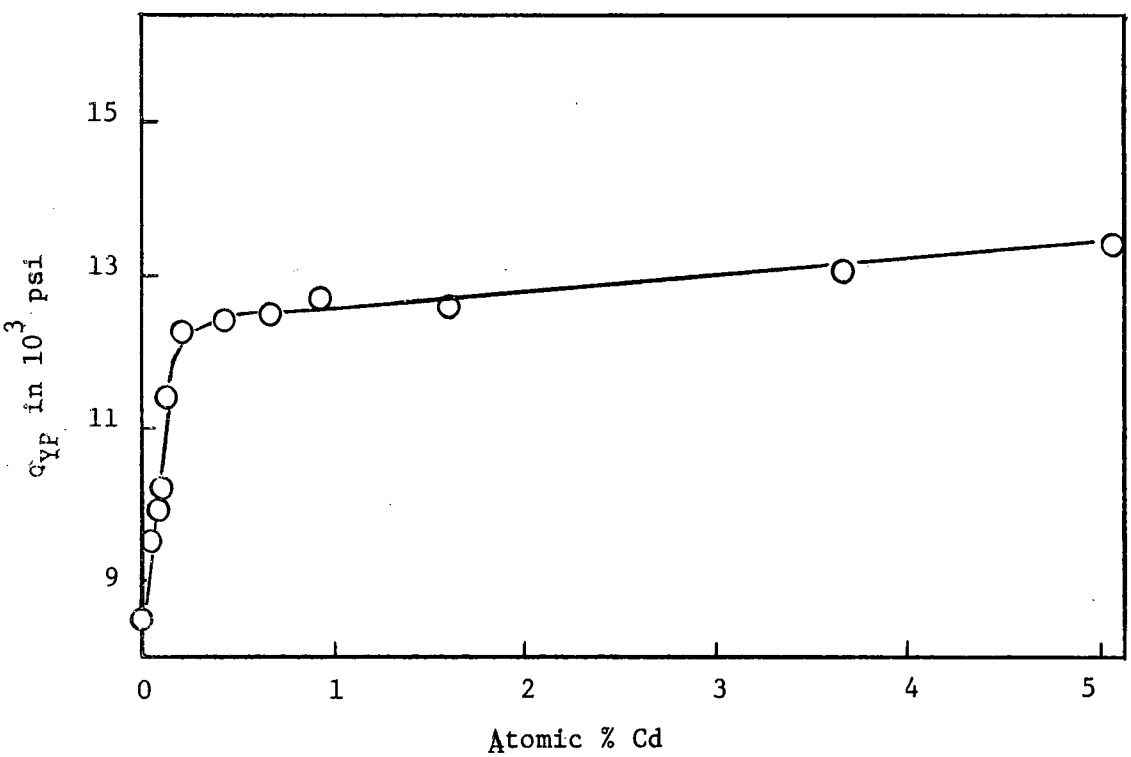

Fig. 12. Yield stress-concentration plot for Mg-Cd alloys.

stage strengthening effect in Mg-Li alloys, similar to that observed in the present work. However, neither study was sufficiently complete to provide the necessary information.

1.3.2.3. Solution Strengthening in Stage I:

The stage I regions for all the five systems examined at room temperature are shown in fig. (13), and clearly reveal the relative strengthening effect of the various solutes in the order Zn, Al, Pb, Cd, In. The solution strengthening rate $(\frac{d\sigma}{dc})'$ in stage I for various solutes are listed in Table I along with other relevant data.

The stage I slope has been plotted as a function of the size difference, Δr between magnesium and the various solutes as shown in fig. (14). It is seen that the strengthening effect of the solute increases as the difference in size between the solvent and the solute becomes larger. In attempts to correlate the hardening effect to the size difference, it is important to note that the concept of an atomic size in an alloy is problematic and hence care must be exercised while making quantitative interpretations involving the use of such a parameter. There are two methods in use for the evaluation of the size misfit parameter. The one involving the use of the change in lattice parameter due to alloying is the more commonly used method, which relates the strengthening effect of the solute as follows:

$$\frac{d\sigma}{dc} = K \left(\frac{1}{a} \frac{da}{dc} \right)^n$$

where a is the lattice parameter, $da/_{dc}$, its variation with solute concentration, K and n are adjustable parameters. The changes in the lattice parameters of magnesium due to alloying have been tabulated by Busk[17],

TABLE I

Solution hardening parameters for polycrystals tested at 295°K

SOLUTE ELEMENT	SOLUBILITY at %		CRITICAL CONCENTRATION C_T	STAGE I SLOPE $\frac{d\sigma'}{dc}$	STAGE II SLOPE $\frac{d\sigma''}{dc}$	YIELD STRESS AT C_T σ_T
	Max.	at 25° C	at %	psi/at % solute	psi/at % solute	in psi
Zn	4.0	0.5	0.01	345×10^3	9×10^3	11,950
Al	11.5	1.6	0.067	59.5×10^3	0.9×10^3	12,500
Pb	8.0	1.5	0.068	42.6×10^3	0.6×10^3	11,400
Cd	Complete	12	0.16	22.7×10^3	0.254×10^3	12,360
In	19.0	13	0.25	11.0×10^3	0.65×10^3	11,250

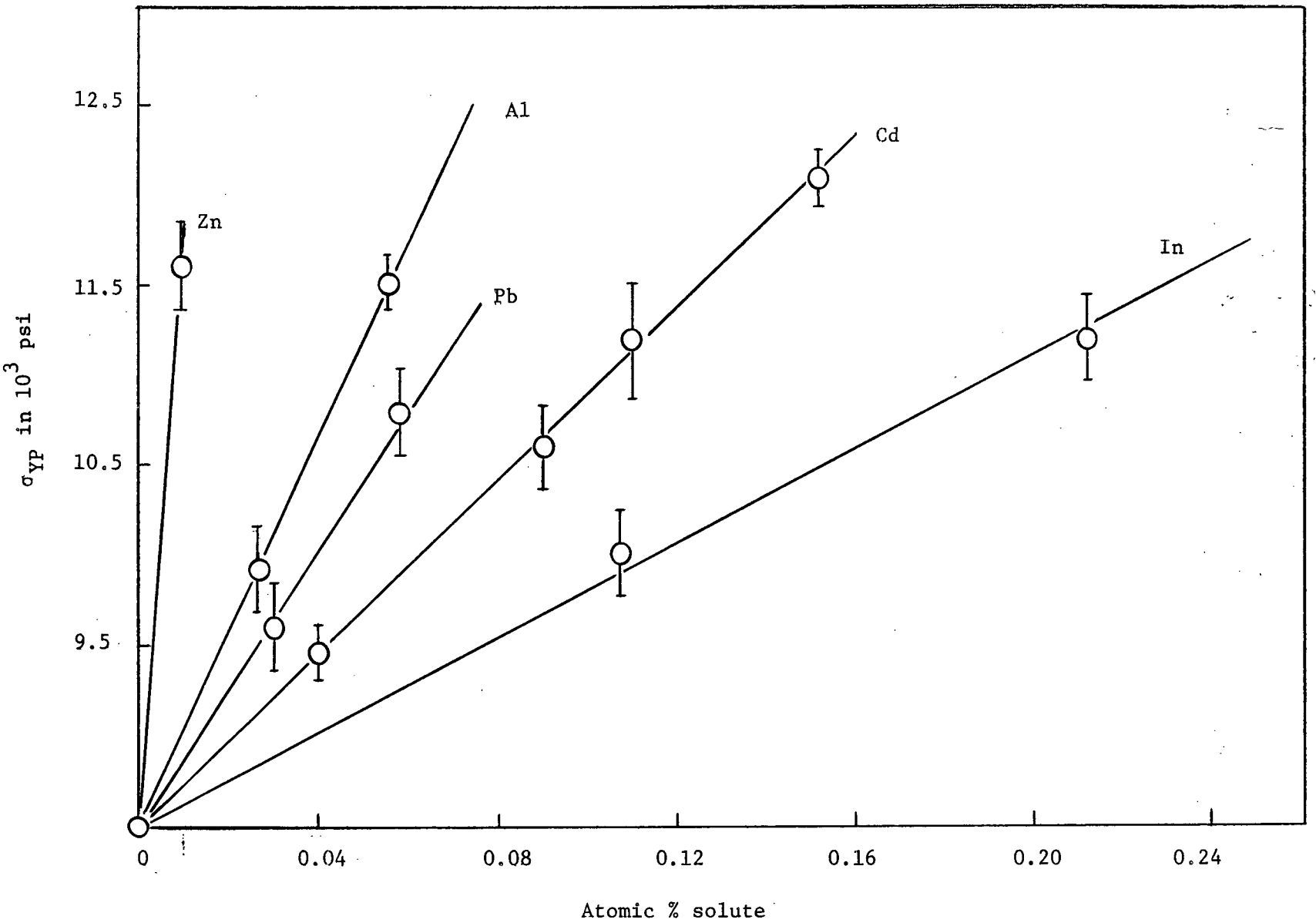

Fig. 13. Stage I solution hardening at 295°K for various alloys.

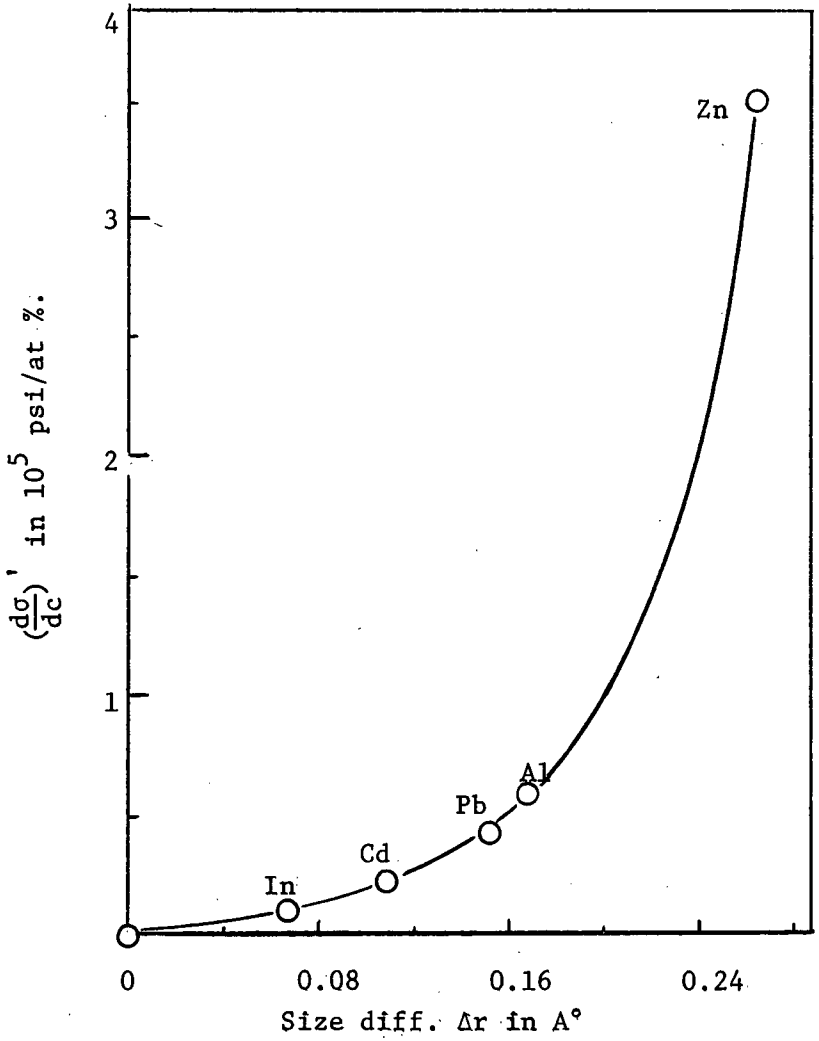

Fig. 14. Stage I slope vs size misfit parameter.

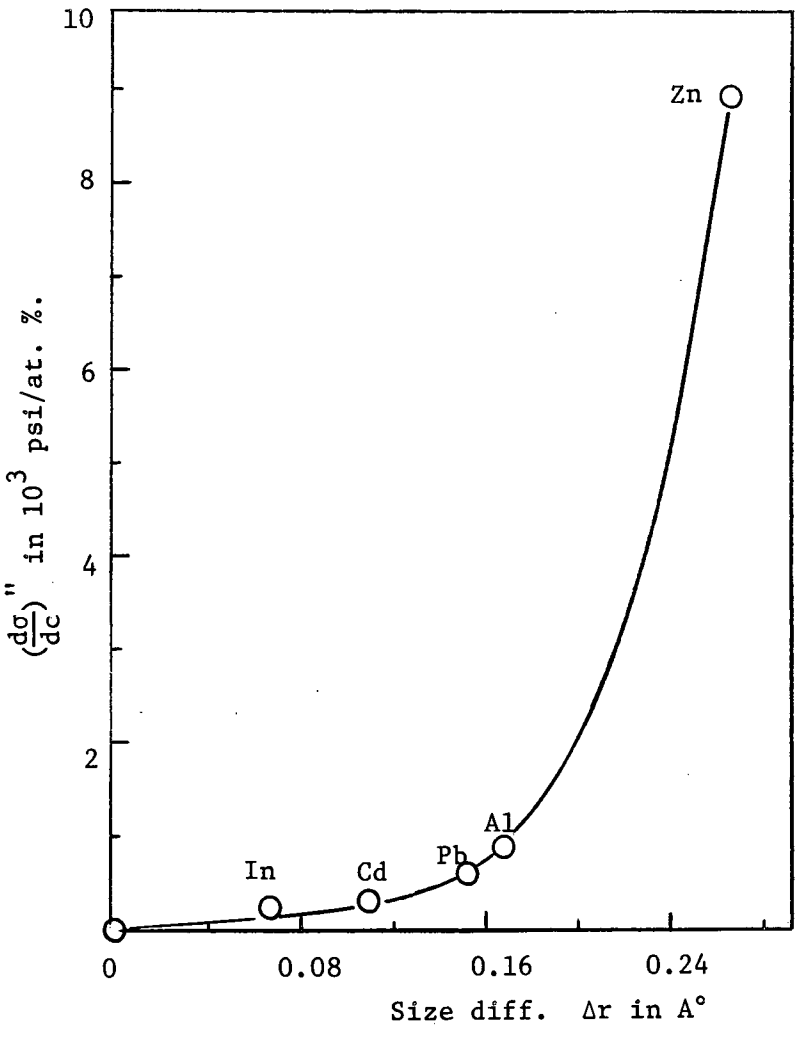

Fig. 15. Stage II slope vs size misfit parameter.

Hardie and Parkins[31], von Batchelder and Rauchle[32] and King[33]. However, no single combination of n and K could give a satisfactory fit for the present results. Alternatively, the difference in size between the pure metals can be used as a size misfit parameter. The last mentioned approach has been taken in the present work. Atomic radii tabulated by Van Vlack[34] have been used here.

It is important to note that the change in the shear modulus of the material due to alloying is also a contributing factor in solution strengthening. In the absence of experimental data relating to the variation of the shear modulus with solute content, however, this factor has not been considered here.

1.3.2.4. Strengthening Above C_T:

The solution hardening rates in stage II, at room temperature are listed in table I for all solutes examined. Fig. (15) shows the dependence of $(\frac{d\sigma}{dc})''$ on the size misfit parameter, which follows the same general trend as $(\frac{d\sigma}{dc})'$ against Δr. Although stage II extends over a much wider range of compositions the hardening rate is an order of magnitude lower compared to that in stage I. Stage II merged with stage III with a gradual decrease in σ_{YP}. Stage III was observed only in Mg-Al and Mg-Zn alloys.

1.3.2.5. The Temperature Dependence of the Solution Strengthening Parameters:

The solution hardening curves for Mg-Al and Mg-Cd alloys deformed over a range of temperatures are shown in figs. (16) and (17) respectively. The multistage nature of strengthening prevails at all temperatures. The extent of stage I increases with decreasing temperature

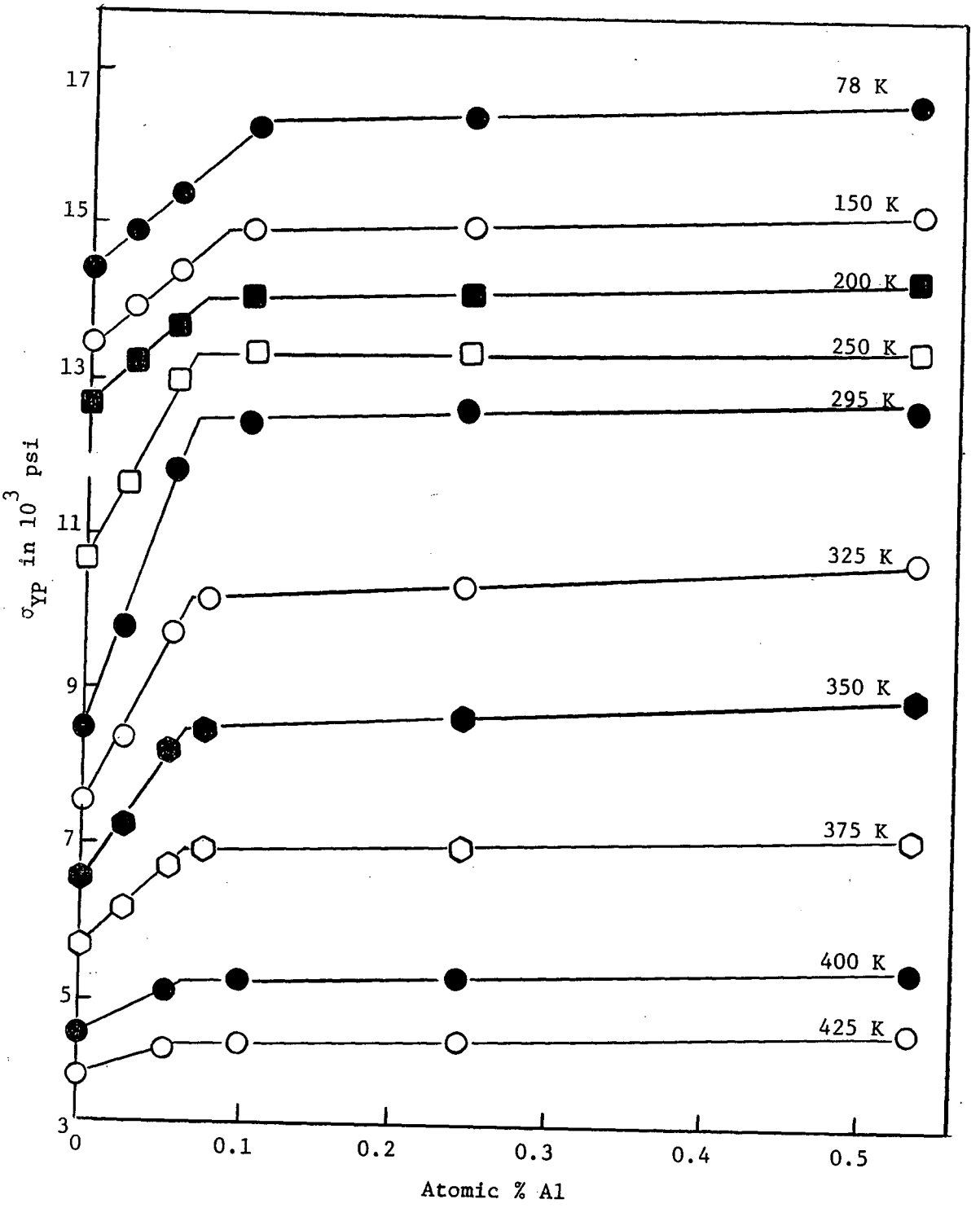

Fig. 16. The effect of temperature on the solution hardening curve for Mg-Al alloys.

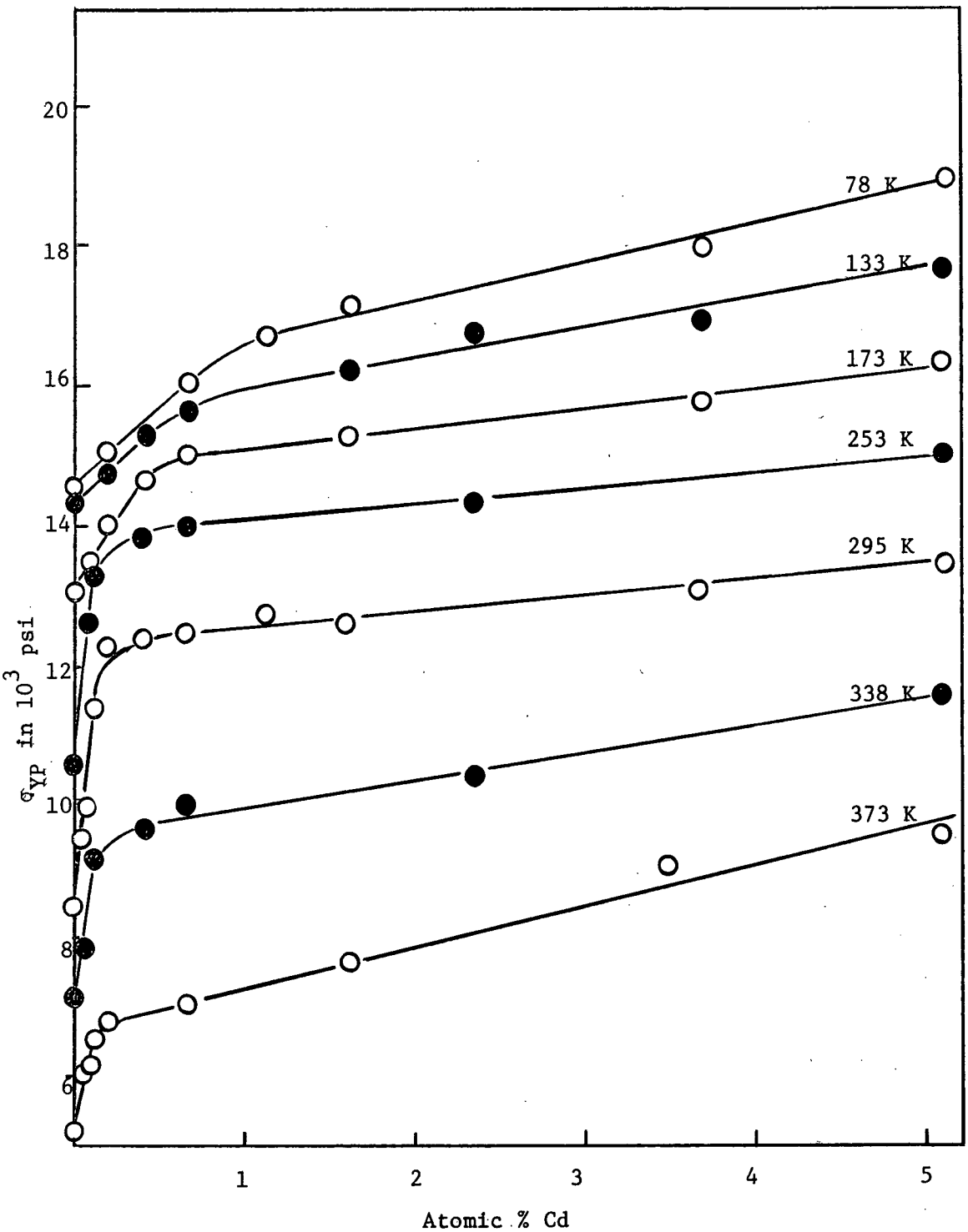

Fig. 17. The effect of temperature on the solution hardening curve for Mg-Cd alloys.

below 250°K. Above this temperature, however, C_T remains independent of temperature. The temperature dependence of C_T for the Mg-Cd and Mg-Al alloys is shown in figs. (18) and (19) respectively.

The variation of the solution hardening rate with temperature is shown in fig. (20) for the Mg-Cd alloys. It is observed that between 78°K and 140°K $(\frac{d\sigma}{dc})'$ is affected very slightly by temperature, whereas a pronounced increase is apparent between 140 and 260°K. $(\frac{d\sigma}{dc})'$ attains a maximum in the vicinity of room temperature and starts to decrease thereafter with increasing temperature. $(\frac{d\sigma}{dc})''$, on the other hand, decreases rapidly from 78°K, reaches a minimum around room temperature and increases thereafter with increasing temperature. Fig. (21) shows the variation of $(\frac{d\sigma}{dc})'$ with temperature in the Mg-Al alloys which is similar to that in the Mg-Cd alloys. However, $(\frac{d\sigma}{dc})''$ was found to be independent of temperature in the Mg-Al alloys.

1.3.3. The Critical Transition Concentration:

The temperature variation of C_T has already been described earlier. The numerical values of C_T for the five alloy systems examined at room temperature are listed in table I . The transition concentration could be related to the size misfit as can be seen from the Δr-C_T plot in fig. (22). For a large value of Δr, C_T is small. As the size misfit parameter Δr is decreased, C_T increases, indicating a very large value as Δr approaches zero. This is as expected, for the addition of a solute with $\Delta r = 0$ i.e. magnesium itself.

From the C_T - Δr relationship in fig. (22), the transition concentration for lithium as solute turns out to be $\approx$0.2 at.%. A

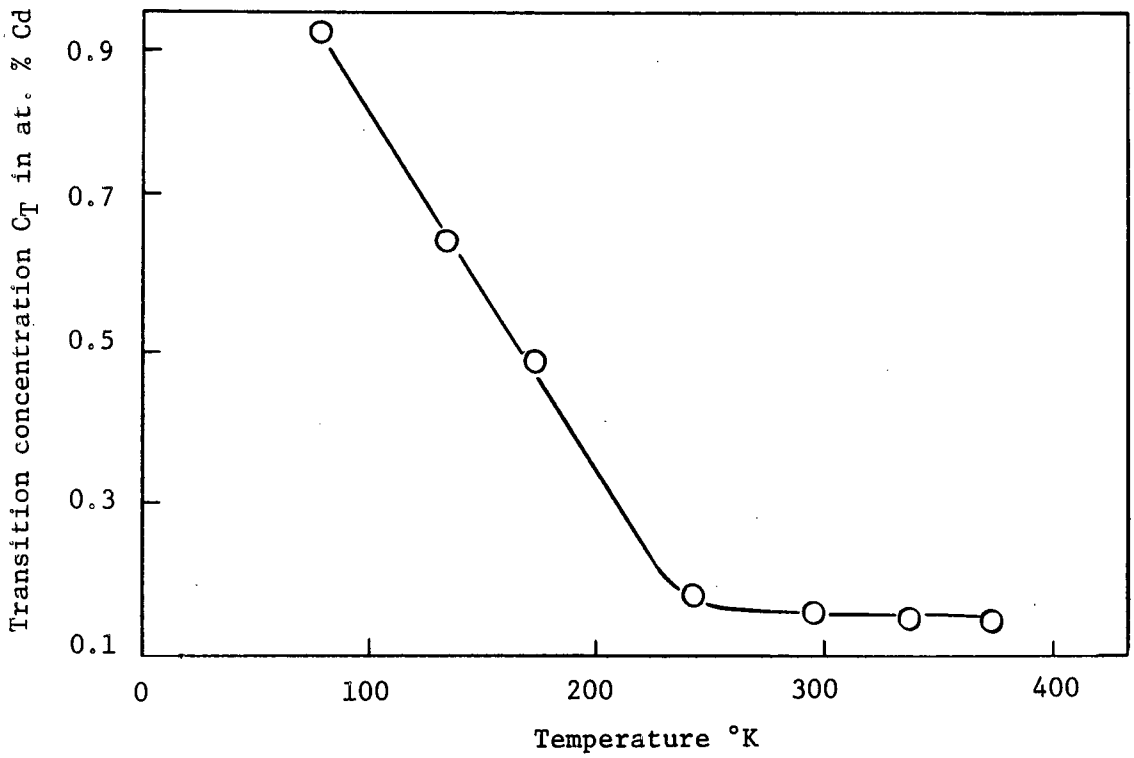

Fig. 18. Critical transition concentration, C_T from stage I to stage II vs. temperature for Cd solute.

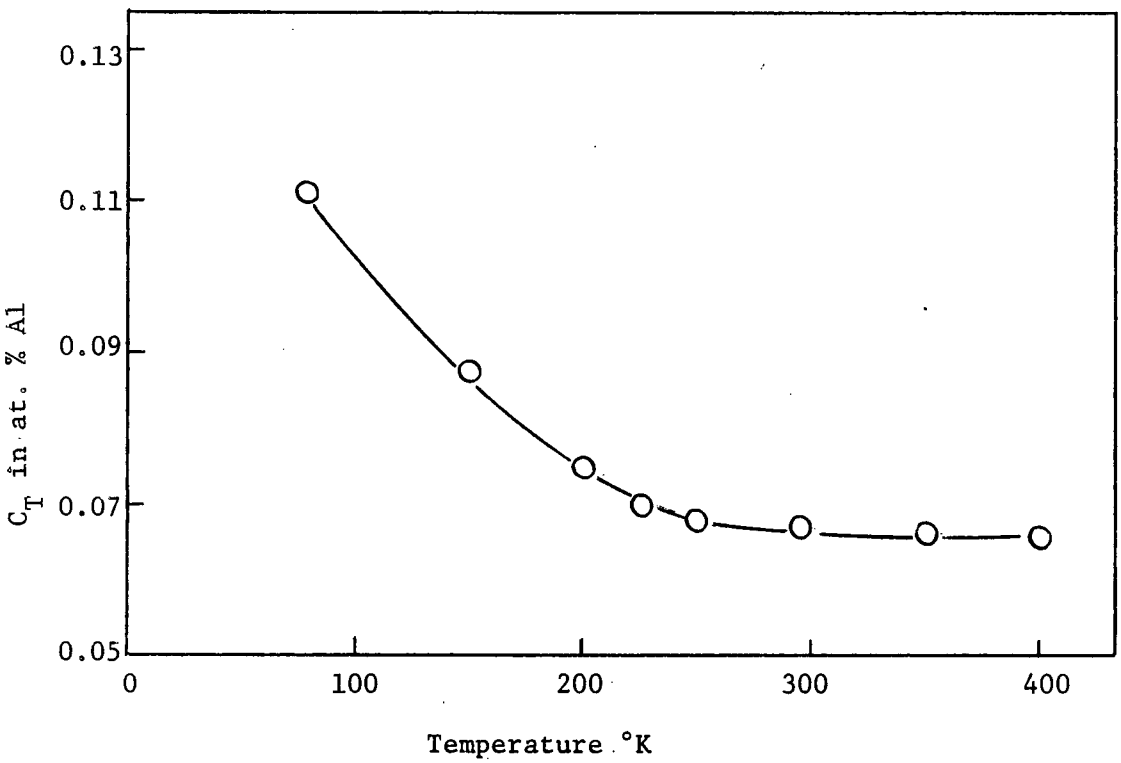

Fig. 19. C_T vs temperature for Al solute.

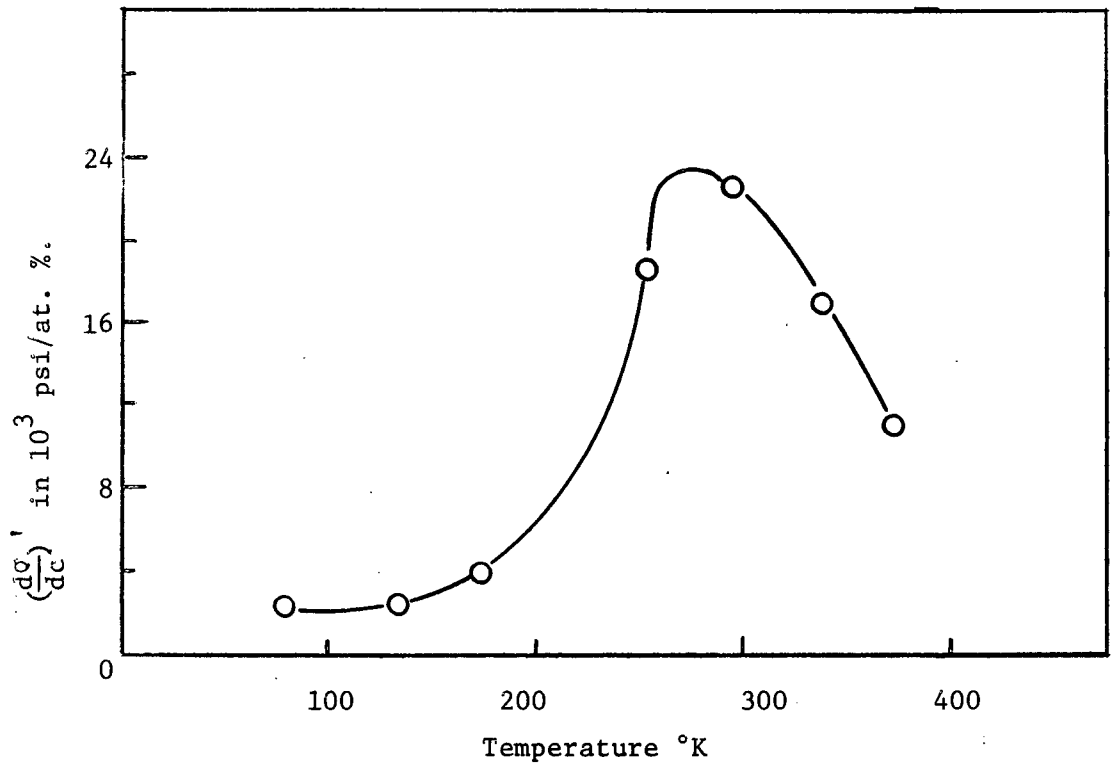

Fig. 20(a) Stage I slope vs temperature for Mg-Cd alloys.

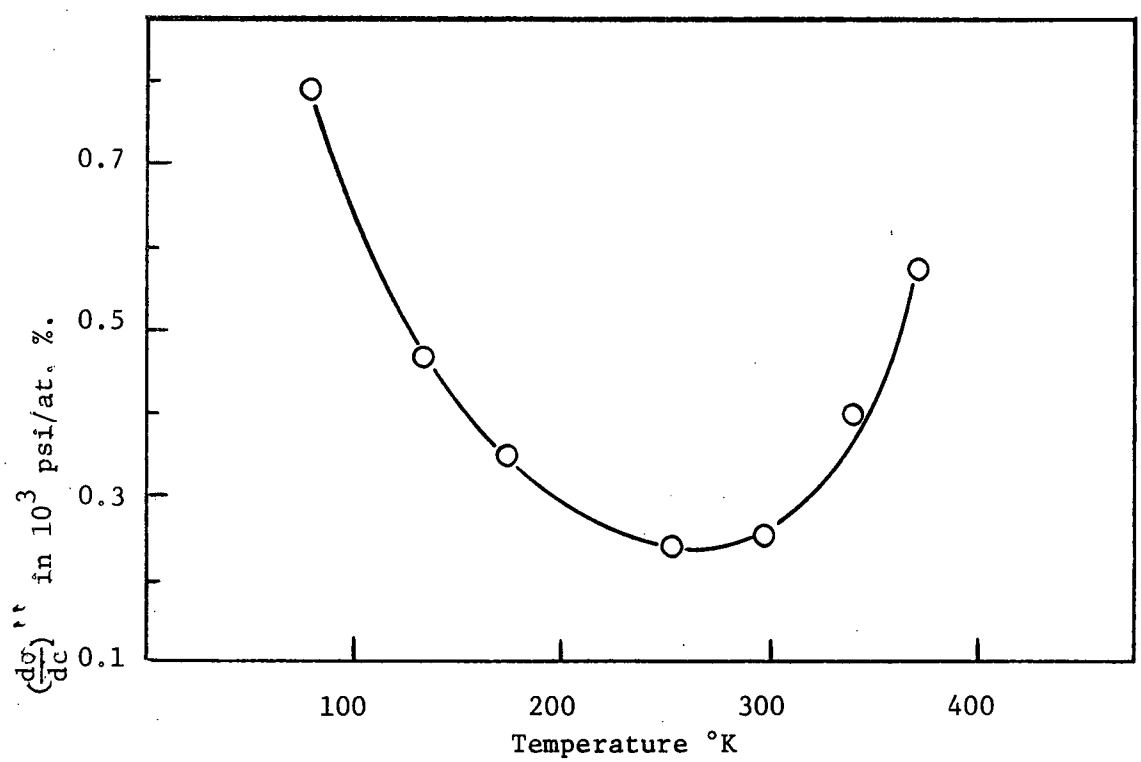

Fig. 20(b). Stage II slope vs temperature for Mg-Cd alloys.

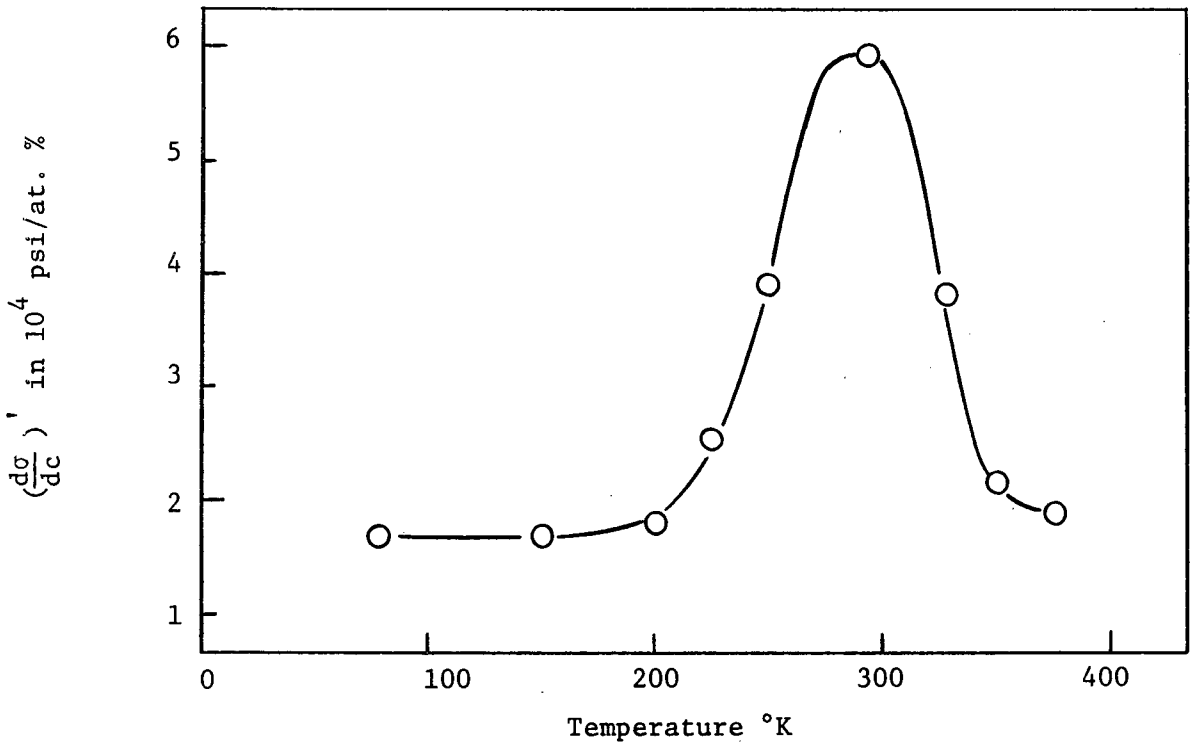

Fig. 21. Stage I slope vs temperature for Al solute.

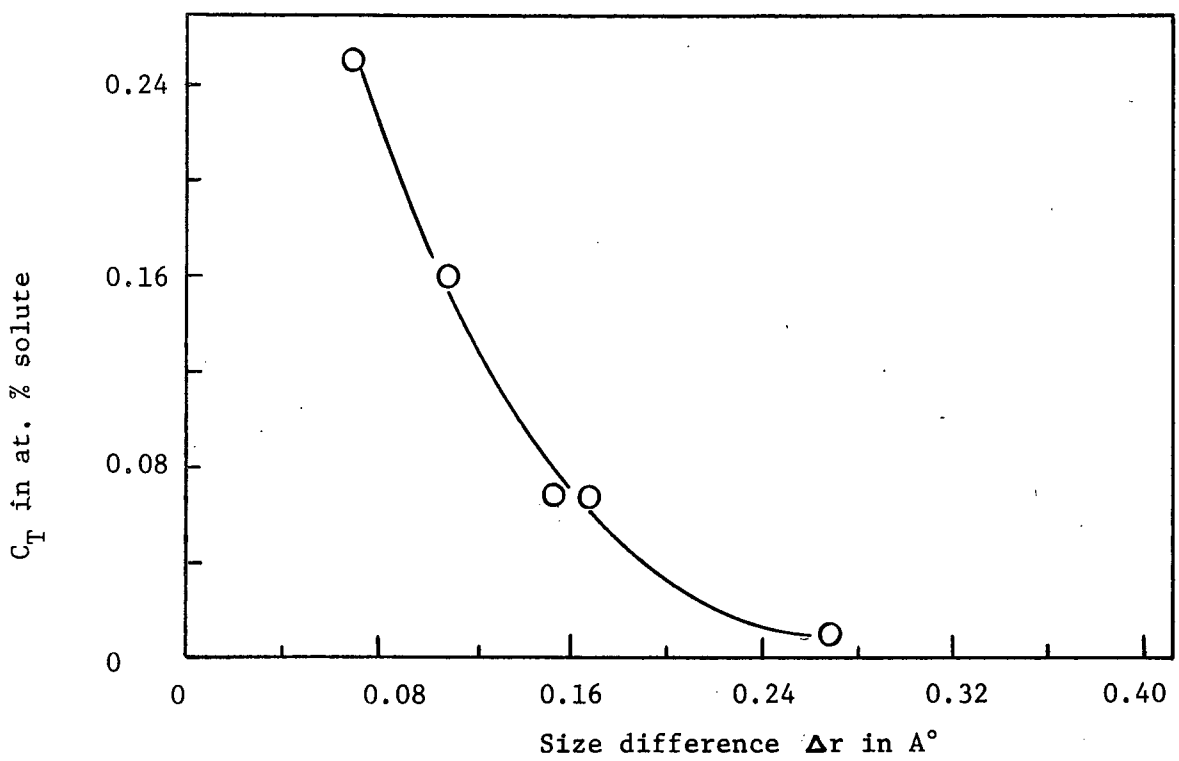

Fig. 22. Critical transition concentration, C_T from stage I to stage II vs size misfit parameter.

direct experimental verification of this estimate is not possible from the present results, since lithium has not been included in the present study. Earlier experiments on the Mg-Li alloy polycrystals have never been carried out at sufficiently low concentrations of lithium as to verify the above conclusion either. Indirect evidence in support of the correctness of the above estimate, however, comes from the single crystal data on Mg-Li alloys. This will be discussed in a later chapter.

1.3.4. The Maximum Stress Variation with Temperature and Alloying:

The temperature dependence of the fracture mode in polycrystalline magnesium is outlined in chapter (1.4.2.). In the "brittle fracture" region the maximum stress is equal to the fracture stress, however, at higher temperatures Mg does not undergo fracture at the maximum stress. Therefore, at higher temperatures the term maximum stress refers to the stress at the onset of negative work hardening.

The temperature dependence of the maximum stress for Mg as well as a series of Mg-Al alloys is shown in fig. (23). The transition temperature from brittle to ductile transition in pure Mg having an average grain size of 65 μ is 225°K in the present work. Unlike the transition in σ_{YP} - temperature relationship the transition temperature in the maximum stress temperature plot was found to be unaffected by solute. The brittle fracture stress of alloys containing solute less than C_T was found to be lower than that of magnesium. Beyond C_T, the brittle fracture stress increased with increasing solute concentration.

The variation of maximum stress with solute concentration is shown in fig. (24) for the Mg-Cd alloys deformed at room temperature.

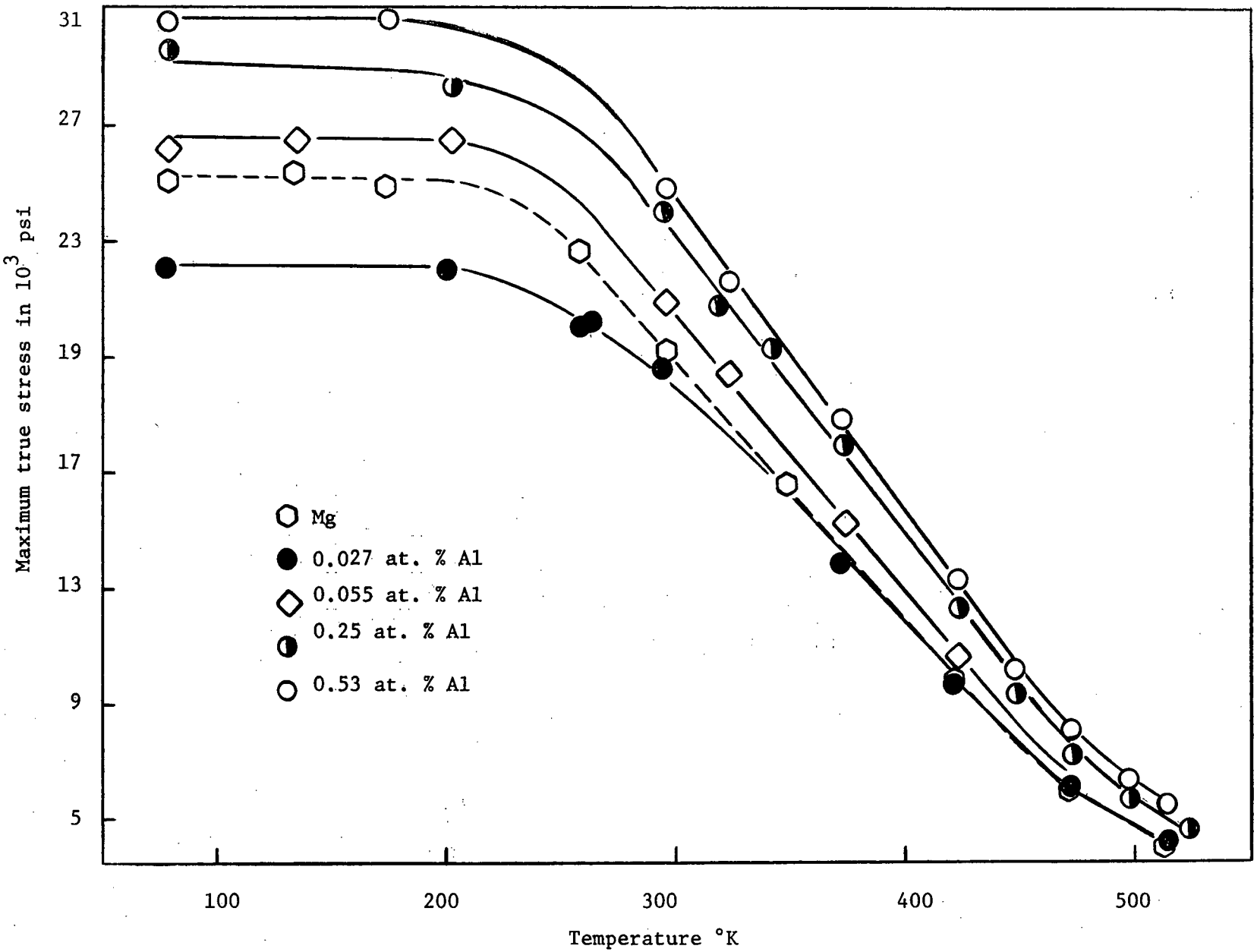

Fig. 23. Maximum stress vs. temperature for Mg-Al alloys.

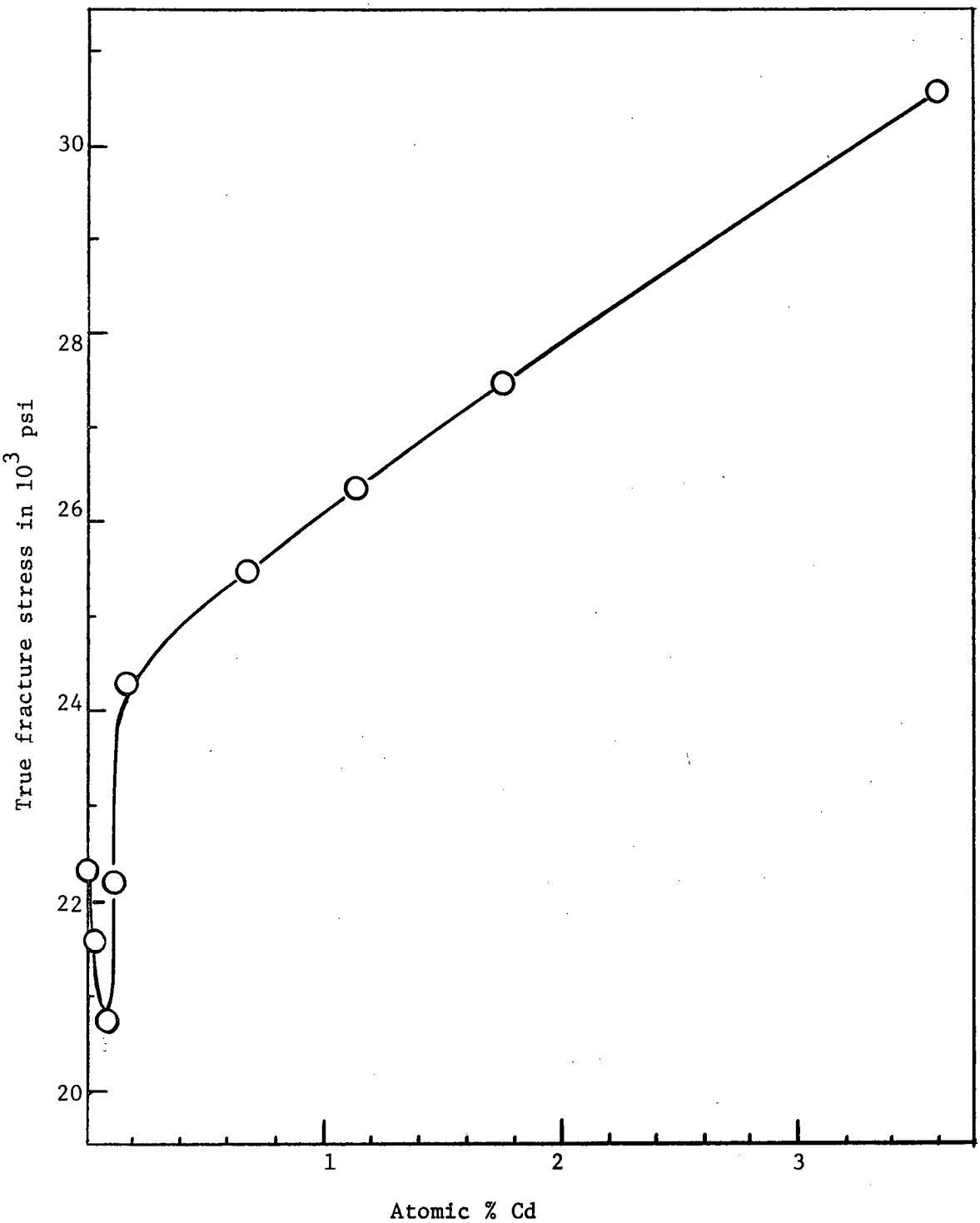

Fig. 24. Fracture stress vs. composition for Mg-Cd alloys tested at 295°K.

The minimum in fig. (24) which is at a concentration of solute slightly less than C_T disappears at higher testing temperatures (not shown here).

1.3.5. Flow Stress in Relation to Temperature and Alloying:

Flow stress temperature relationships for pure Mg and a representative set of Mg-Al alloys are shown in figs. (25, 26 and 27). It is observed that the flow stress-temperature curves for any specified strain are of the same shape as the yield stress-temperature curves, therefore, the terminology used in defining the three stages in the σ_{YP} - T curves will also be applied to the flow stress curves. A noticeable feature of figs. (25, 26 and 27) is the effect of increasing strain on the transition temperature from stage I to stage II. In the case of pure magnesium and alloys containing solutes in large excess of C_T, the transition temperature T_t was observed to be affected only slightly with increasing strain, however, an alloy containing solute close to C_T (fig. (26)) exhibited a pronounced decrease in T_t with increasing strain as shown in fig. (28).

The concentration dependence of the flow stress in Mg-Zn alloys tested at room temperature is shown in fig. (29). At any fixed strain the flow stress increases rapidly with alloying upto a concentration of solute equal to C_T. Beyond C_T a continuous decrease is observed with increasing solute content. The decrease in flow stress at 0.2% strain was observed to commence at 0.3 at % Zn, however, at higher strains all alloys containing solute in excess of C_T had flow stresses lower than that at C_T. Similar results have been obtained for the Mg-Al alloys tested between 78°K and 423°K.

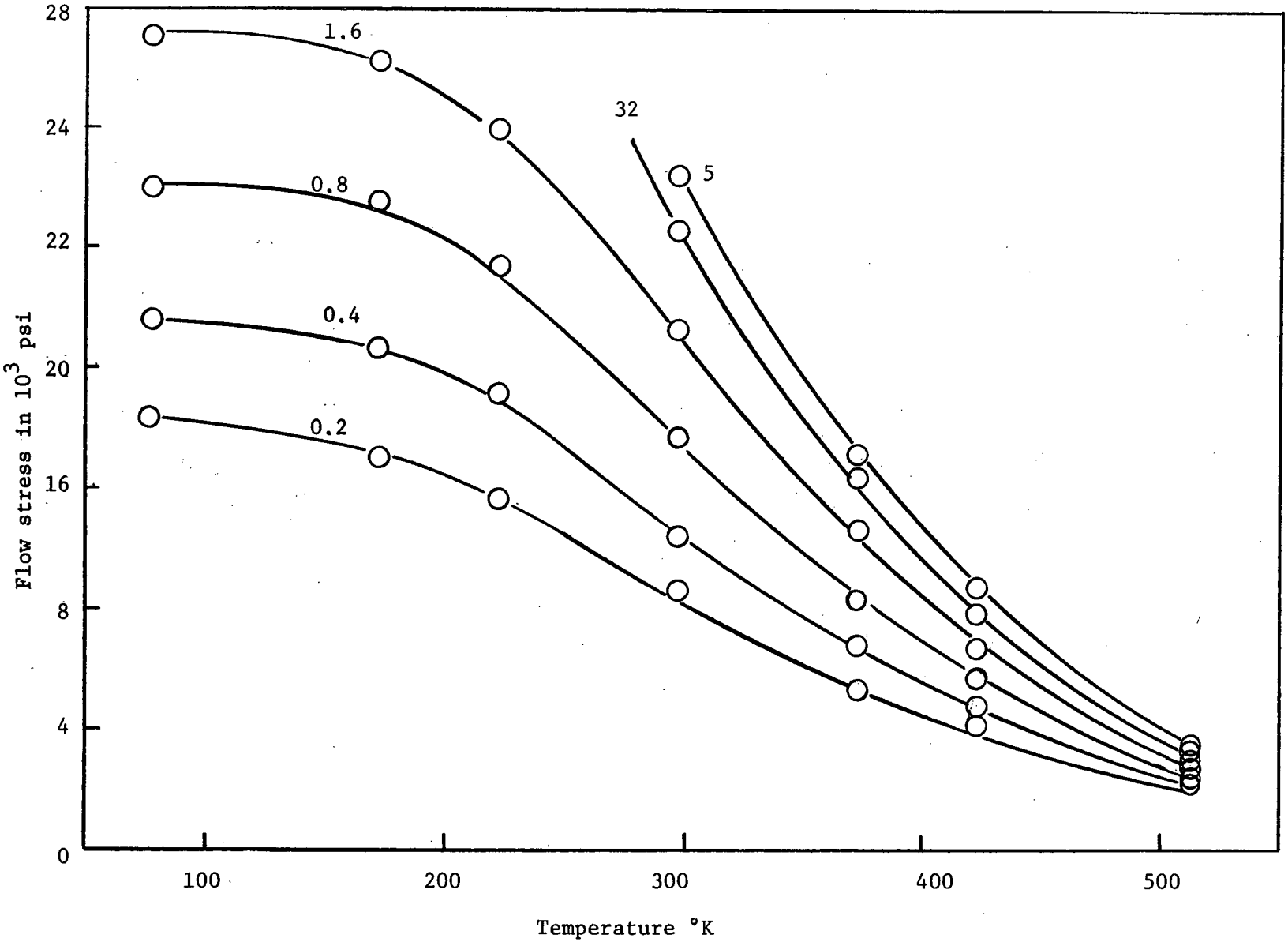

Fig. 25. Flow stress vs. temperature for 65μ Mg.

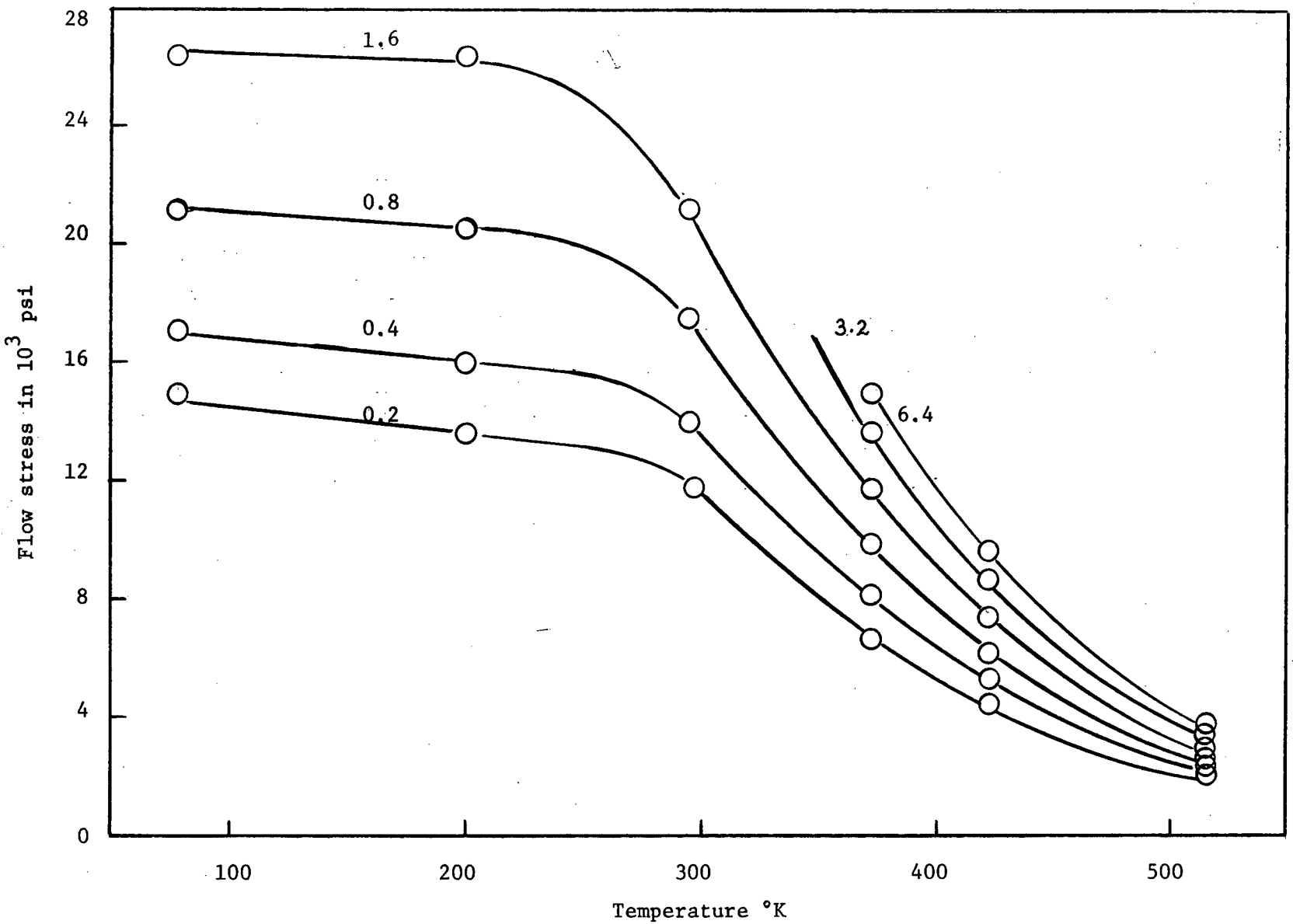

Fig. 27. Flow stress vs. temperature for Mg + 0.055% Al alloy.

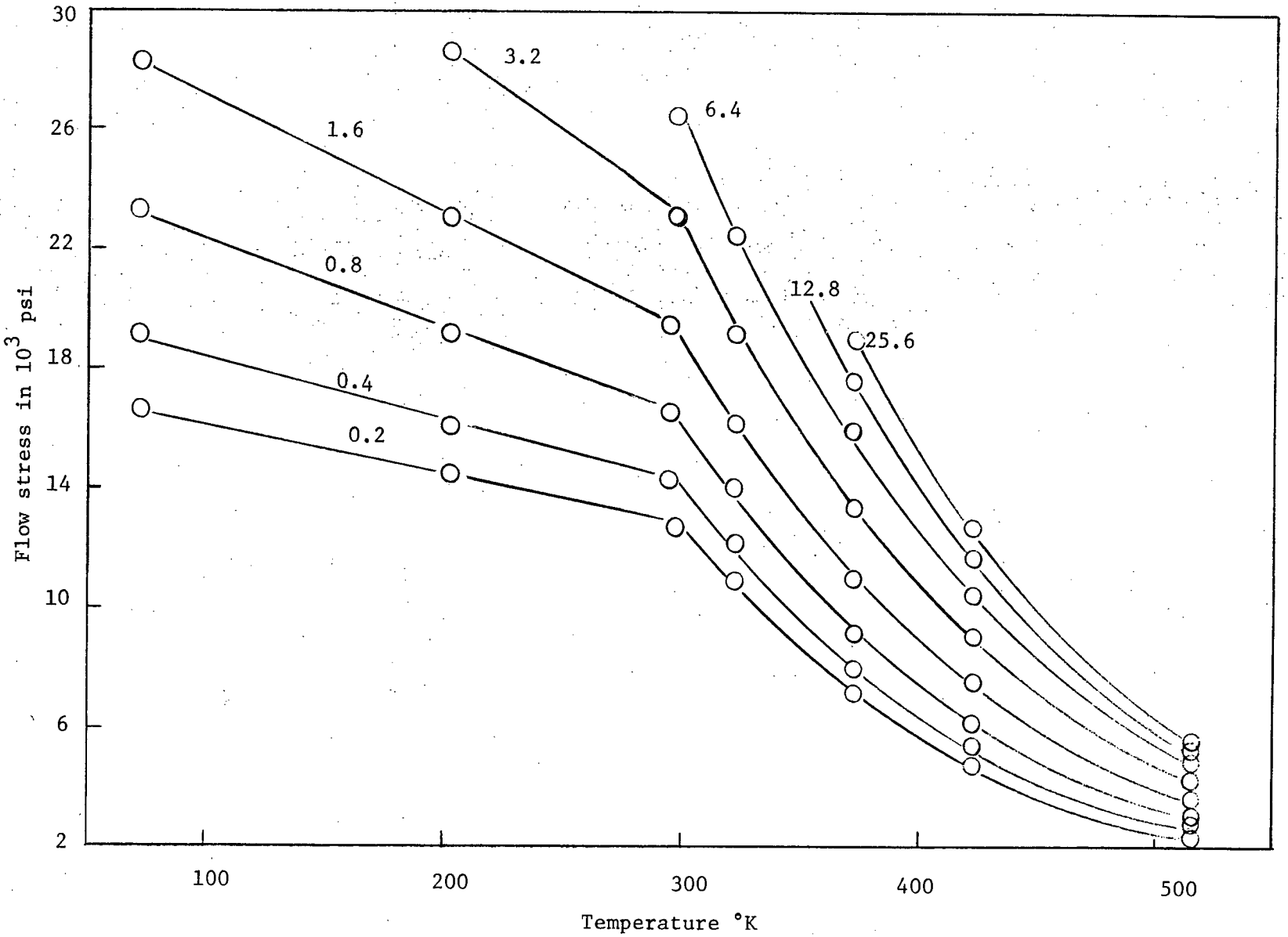

Fig. 27. Flow stress vs. temperature for Mg + 0.53 at.% Al alloy.

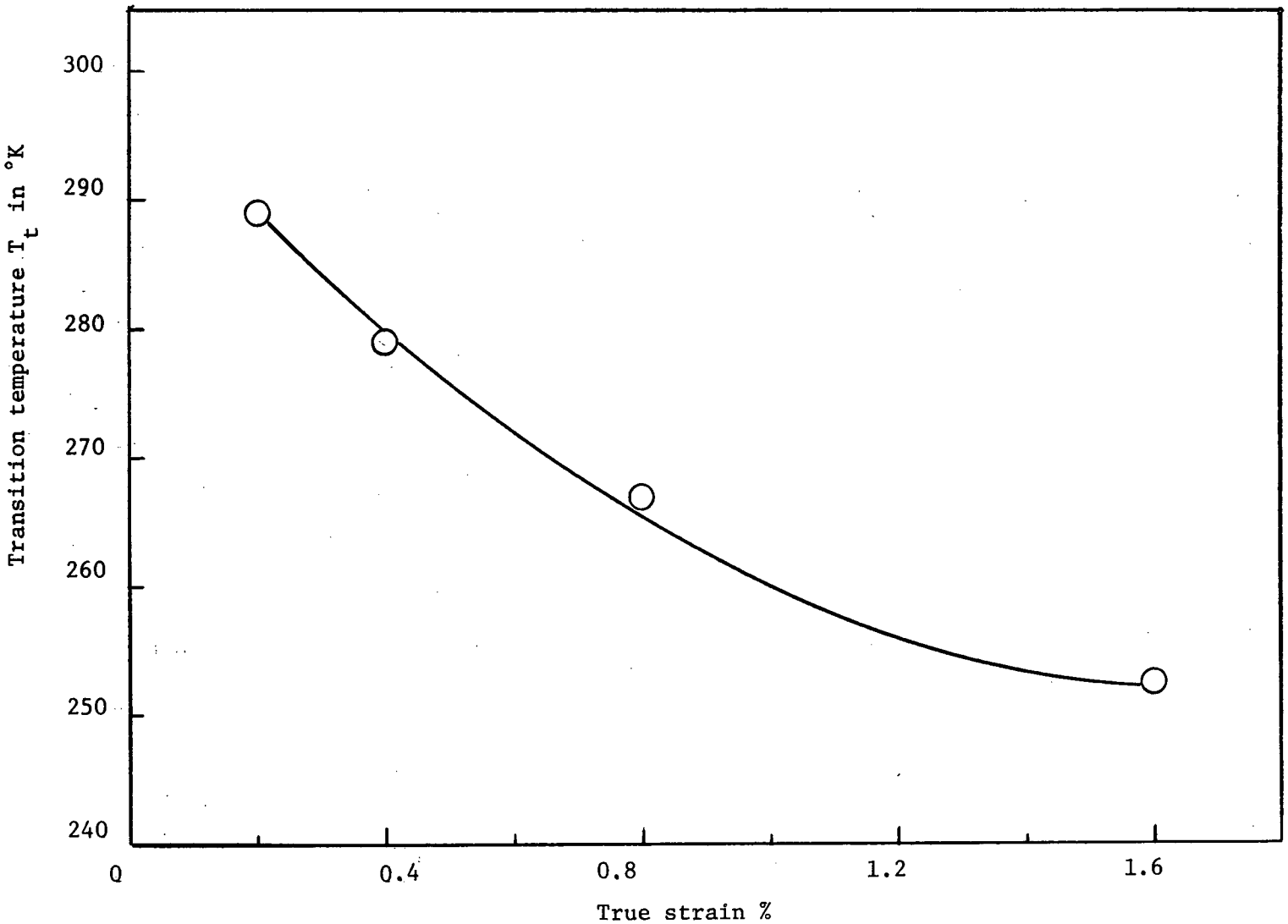

Fig. 28. Transition temperature from stage I to stage II in the flow stress-temperature curves of Mg + 0.055 at.% Al alloy vs. strain.

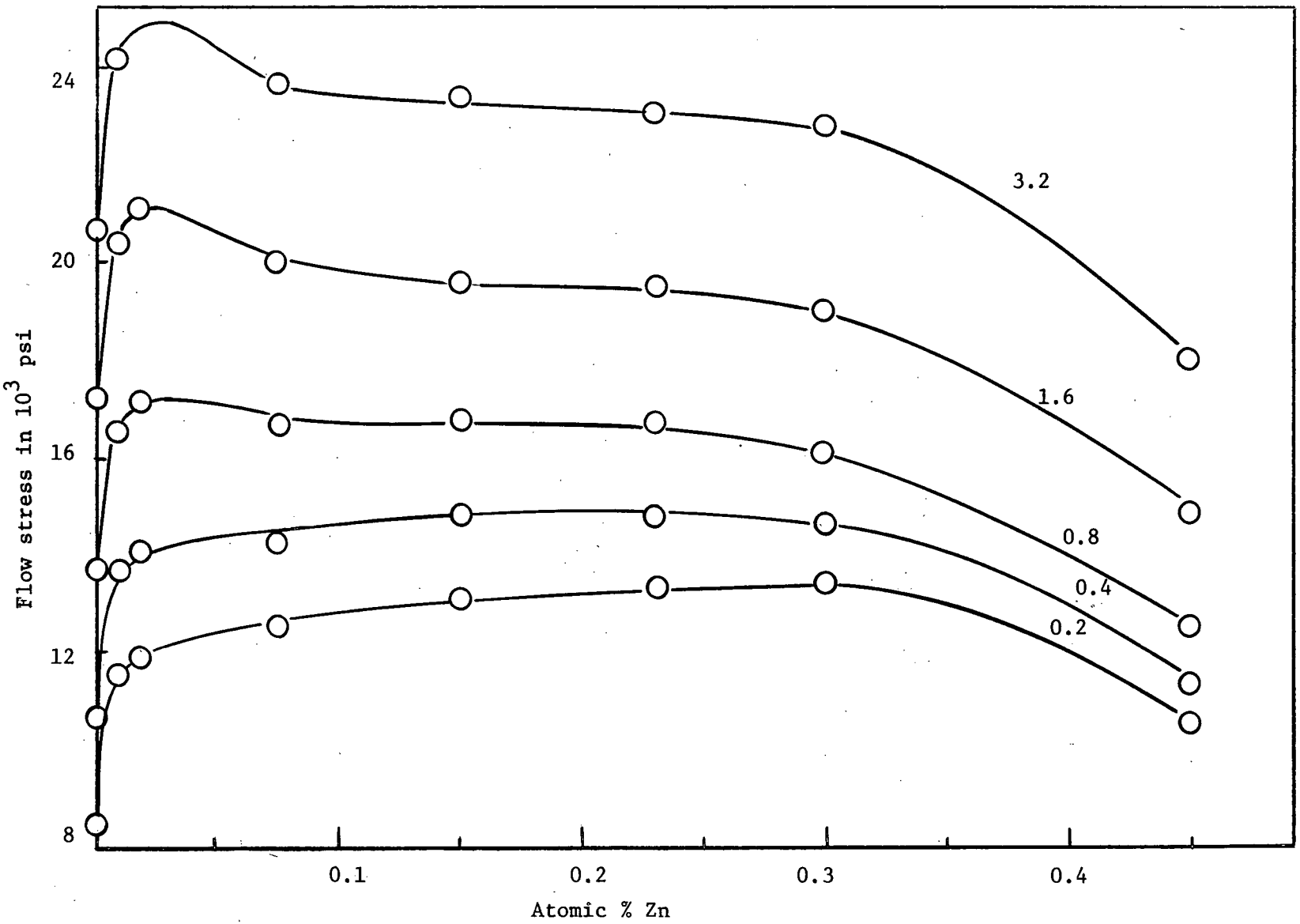

Fig. 29. Flow stress vs. composition for Mg-Zn alloy.

1.3.6. Ductility:

Percent elongation or true strain based on the uniform extension of the gauge-length was used as a measure of ductility, as it was not practical to obtain reduction in area values because of the specimen dimensions.

1.3.6.1. Alloying Effect:

A plot of ductility against concentration for each solute examined at room temperature is shown in fig. (30). It is readily observed that the strain to fracture decreases until a concentration close to C_T is reached, and then increases with further increase in the alloy content. It is interesting to note that the solutes were effective in increasing the ductility in the order Zn, Al, Cd and In paralleling their relative strengthening effects.

1.3.6.2. The Temperature Dependence of Ductility:

Because of the large amount of strain associated with the negative work hardening at temperatures above 373°K, it was necessary to indicate the strain to maximum stress, in addition to the true strain to fracture.

The effect of temperature on the strain to fracture for magnesium and a series of binary Mg-Al alloys is shown in fig. (31). Upto approximately 300°K, the ductility of magnesium is affected very slightly with changes in temperature and alloying. Also irrespective of the testing temperature, alloying upto the transition concentration has little effect on the ductility of magnesium, although σ_{yp} increases dramatically in the same range of concentrations. Between 300°K and 400°K,

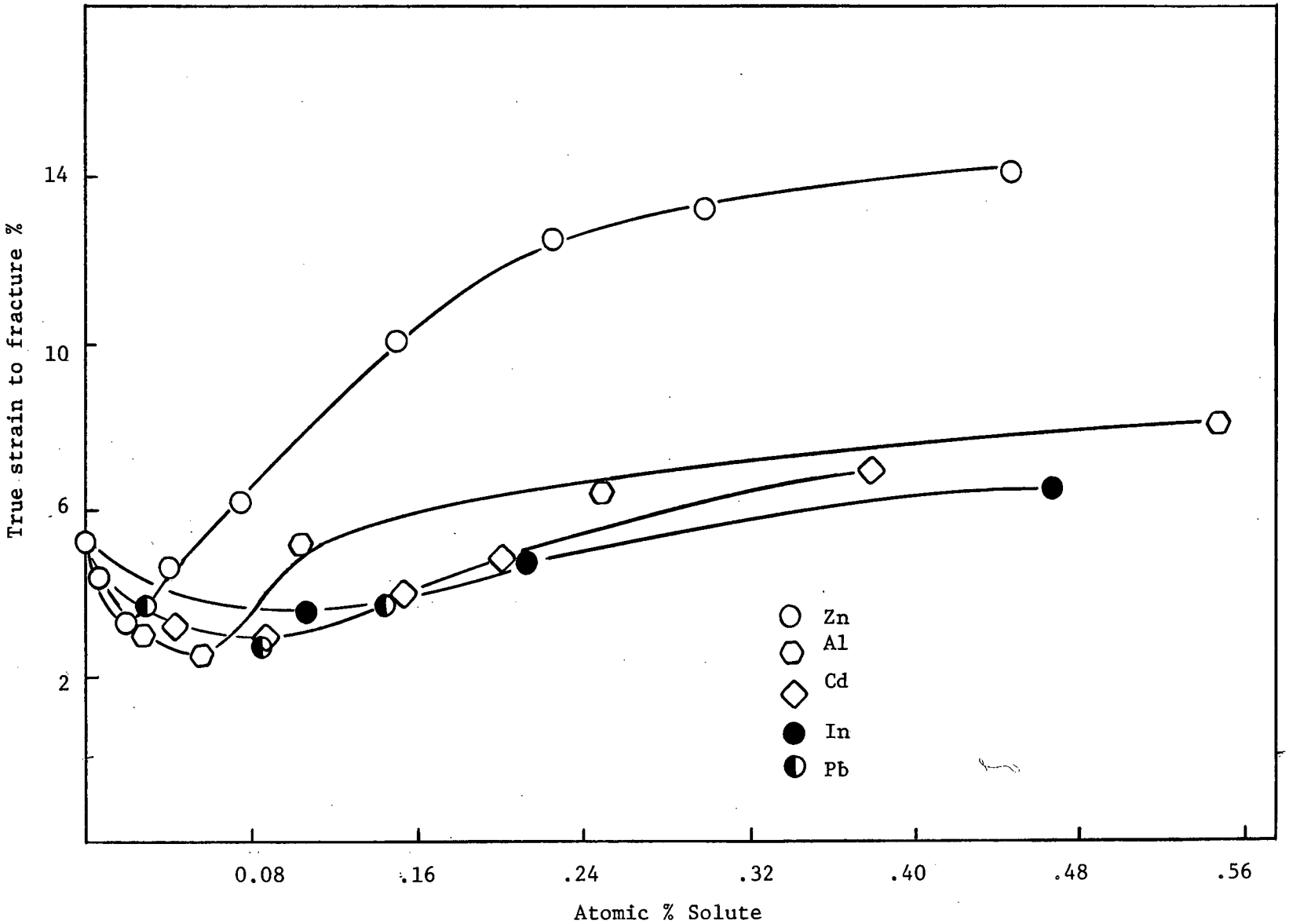

Fig. 30. Ductility vs. concentration for various solutes.

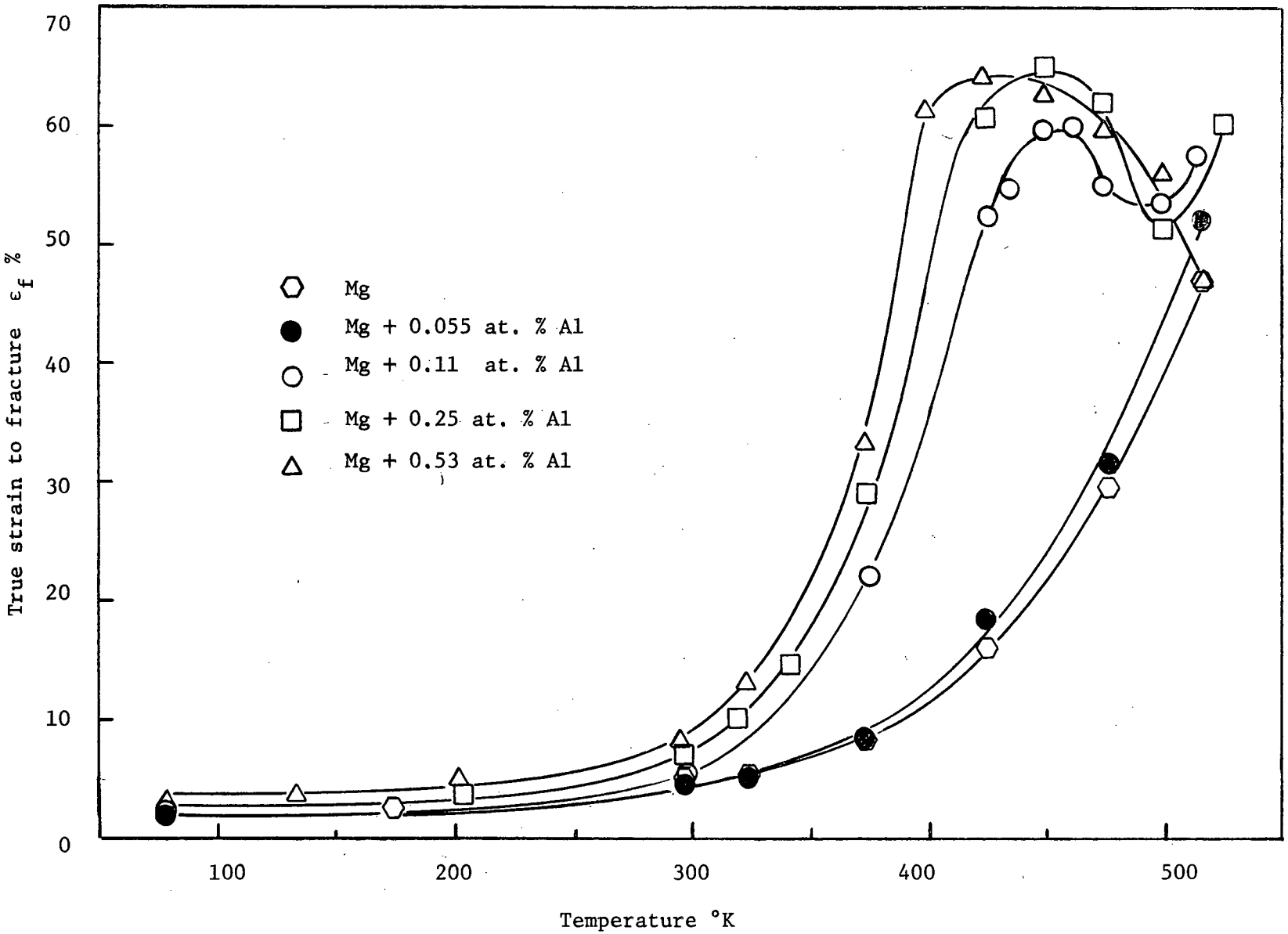

Fig. 32. True strain to fracture vs. temperature for Mg-Al alloys.

however, alloying additions in excess of C_T have a profound effect in increasing the ductility. Magnesium and alloys containing solute less than C_T show a progressive increase in ductility with temperature in this interval. The higher alloys show maxima and minima in ductility in the temperature interval between 400° and 500°K. The shape and position of the maxima show a systematic variation with solute concentration. In constant strain rate tests, the ductility peak becomes broader and shifts to lower temperatures with increasing aluminum addition.

The temperature dependence of the true strain to maximum stress and that associated with the negative work hardening are shown in figs. (32) and (33) respectively. The strain associated with the negative work-hardening is very small below room temperature. Above room temperature, however, the strain to maximum stress and that associated with the negative work hardening follow a trend similar to the temperature variation of the strain to fracture, with the exception that the peaks do not broaden. The maxima in the case of strain to maximum stress were observed at about 450°K, whereas those in the case of the strain associated with the negative work hardening are in the vicinity of 420°K.

Ductility maxima similar to those in the present work have been observed earlier by Greenwood et al[35] in Mg-0.2% Pb alloy and in Mg-0.8% Al alloy by Stacey[36].

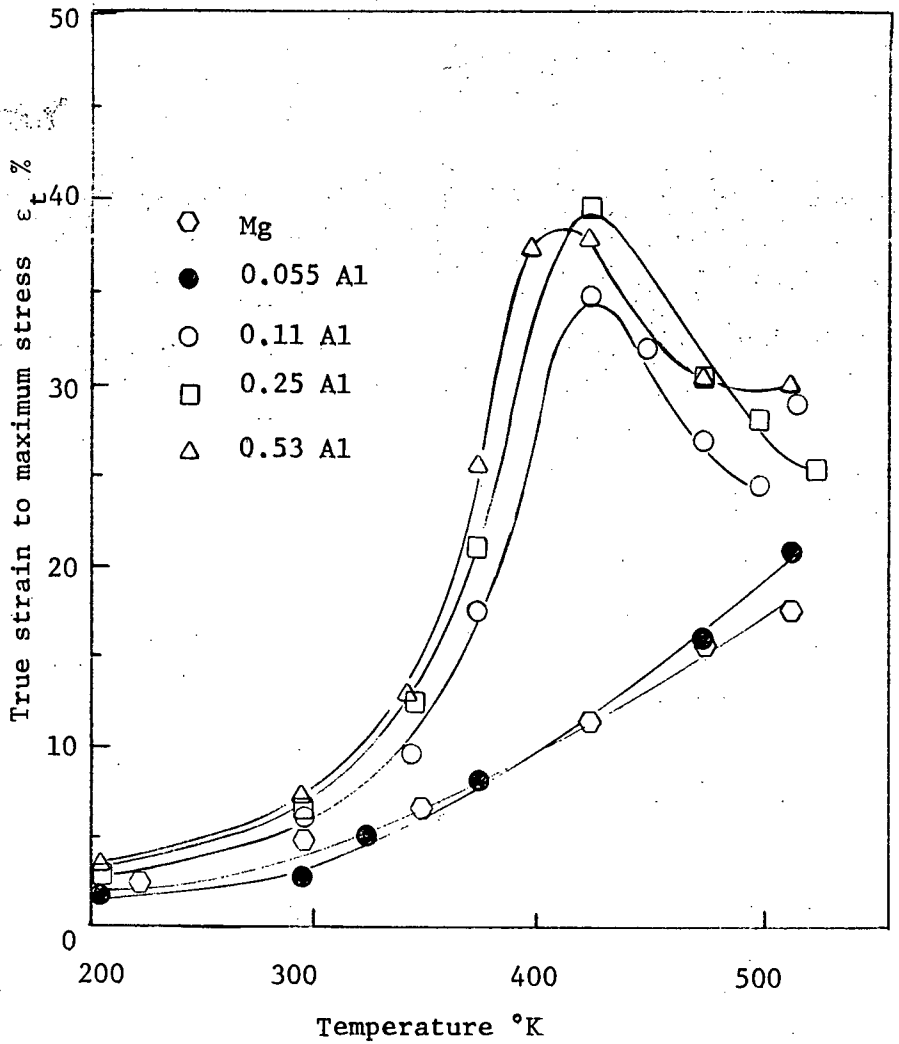

Fig. 32. True strain to maximum stress vs. temperature for Mg-Al alloys.

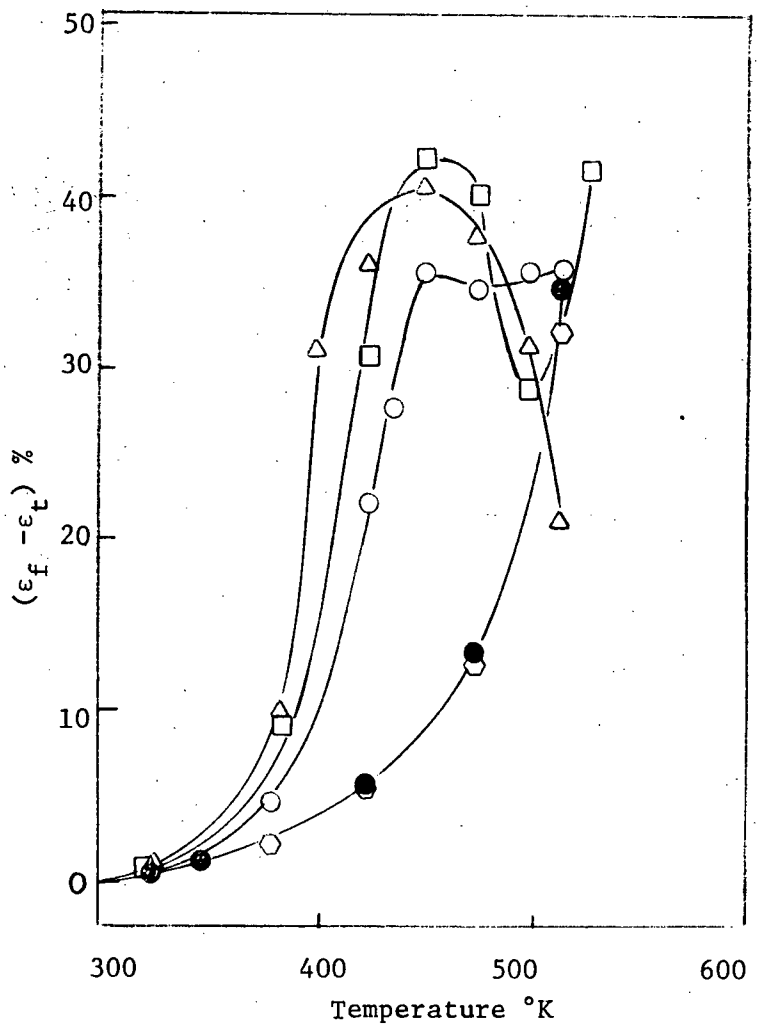

Fig. 33. True strain associated with negative work hardening vs. temperature for Mg-Al alloys.

1.4. DISCUSSIONS

In order to understand the mechanism of solution strengthening in polycrystalline aggregates, it is essential to have a knowledge of the crystallographic deformation modes available, and their effect on the macroscopic flow and fracture characteristics of the material. Keeping this in mind it appears logical to give a brief review of the earlier work on the deformation and fracture of magnesium followed by a discussion of the effects of solute on the various flow parameters.

1.4.1. Deformation Modes in Magnesium:

In 1928 von Mises[19] first pointed out that a necessary condition for a polycrystal to be ductile when it deforms by crystallographic slip in its grains is that the number of independent slip systems available be five. The total number of slip systems is given by the crystal structure. Usually there is one slip mode and a number of slip systems for this mode as determined by the point group symmetry. Groves and Kelly[20] and Kocks[21] have examined the number of independent slip systems in various crystal structures. von Mises' finding has been used in the studies of face centred cubic metals in finding the number of slip systems found to operate near the grain boundary[37] and also in theoretical attempts to deduce the polycrystalline stress strain curve from that of single crystal[22] . In many systems, however, other mechanisms such as twinning, grain boundary shear and cell structure formation may occur thereby reducing the number of independent slip systems required. It is helpful to remember that the von Mises criterion is taken to be a necessary condition for any polycrystal ductility whatsoever, not as one that determined different degrees of ductility.

1.4.1.1. Crystallographic Slip:

Magnesium undergoes slip predominantly on the basal system $\{0001\}\langle 11\bar{2}0\rangle$. The shortest slip vector which preserves the ABAB basal or close packed plane stacking is of magnitude a and direction $\langle 11\bar{2}0\rangle$. The total strain energy is lowered by the dissociation in the basal plane of the dislocation into two partials having the Burgers vector $\frac{a}{3}\langle 10\bar{1}0\rangle$ [38]. A stacking fault exists in a ribbon between the two partials. Although no direct way of measuring the fault energy is available for magnesium, Seeger estimates it to be in the range 200 - 400 ergs/cm^2 [39]. This leads to a predicted separation of the partials at room temperature of the order of an interatomic distance. Slip vectors of the form other than $\langle 11\bar{2}0\rangle$ have never been observed in magnesium. Non-basal slip vectors of the form $\langle 11\bar{2}3\rangle$ have been observed in addition to the basal $\langle 11\bar{2}0\rangle$ vector in other hexagonal close packed metals like Cd [40,41] Zn [42] and Be [43]. The temperature dependence of the CRSS for basal slip has been studied by Sheely and Nash [13], Conrad and Robertson [6] and by Basinski [3].

Small amounts of non-basal slip are seen after room temperature deformation of pure Mg [14]. It has been a popular belief that if and when non-basal slip does occur it will do so much more readily in systems which have c/a ratio equal to or less than the ideal value of 1.633. This argument follows from relative close packing considerations. Seeger [44] has suggested that in addition to the c/a ratio, the stacking fault energy will have a strong influence on the deformation modes in as much as it controls the cross slip process. Stoloff and Davies [45] using hexagonal close packed Zn-Ag alloys of slightly varying axial ratios have

shown that the c/a ratio is not the only criterion for non-basal slip. Zirconium and beryllium serve as good examples to show that the occurrence of non basal slip is not determined entirely by c/a ratio and the stacking fault energy of the material. Although both these metals have approximately the same c/a ratio (less than ideal) and have high stacking fault energies, whereas basal slip predominates in beryllium [47], Zr deforms mainly by prismatic $\{10\bar{1}0\}\langle 11\bar{2}0\rangle$ slip[46].

The earliest observations of non-basal slip in magnesium were made by Schmid[48] who concluded that the $\{10\bar{1}1\}\langle 11\bar{2}0\rangle$ pyramidal system became operative at 225°C and above. Later work on the compression of thin single crystal wafers by Bakarian and Mathewson[49] confirmed the significance of this temperature and contributed the first extensive evidence on the waviness of elevated temperature slip lines on this system. Burke and Hibbard[50] observed only basal slip in high purity single crystals of magnesium at room temperature except in the region close to the grip where $\{10\bar{1}1\}\langle 11\bar{2}0\rangle$ system was operative due to the grip constraints. Thus, up until 1955 there was an acceptance of 225°C as the temperature below which no slip system except $\{0001\}\langle 11\bar{2}0\rangle$ would operate in Mg without the imposition of unusual stress systems.

In 1955, Dorn et al[11] began to examine rather critically the deformation in tension of polycrystalline pure magnesium. Small amounts of non-basal slip were seen at room temperature and the temperature dependence of non-basal slip was found to be not as simple as thought before. Hauser et al[12] observed prism $\{10\bar{1}0\}\langle 11\bar{2}0\rangle$ basal $\{0001\}\langle 11\bar{2}0\rangle$ cross slip between 78°K and 298°K at triple points which are susceptible sites for stress concentration.

Reed-Hill and Robertson[51] studied the tensile deformation of magnesium single crystals with the stress axis close enough to the basal plane so that basal slip and mechanical twinning on $\{10\bar{1}2\}$ were suppressed. This orientation is of considerable practical significance in the tensile deformation of polycrystalline sheet and extruded metal because the texture of these materials is such that the basal plane tends to align itself with the direction of rolling or extrusion. Reed-Hill found that $\{10\bar{1}0\}\langle 11\bar{2}0\rangle$ slip occurred at 93°K and 298°K. At low temperatures the slip lines had a minimum spacing of less than 5×10^{-5} cm. Fine prism slip lines were seen to be cross slipped by basal slip at both these temperatures. The variation of the critical resolved shear stress for prismatic slip over the temperatures ranging between 78°K and 800°K has been investigated by Ward-Flynn, Mote and Dorn[9] and by Horiuchi and Yoshinaga[52]. These results are supplementary to the data obtained by Reed-Hill and are in excellent agreement with those of Hauser et al.

First order pyramidal slip $\{10\bar{1}1\}\langle 11\bar{2}0\rangle$ has been observed in magnesium single crystals[51] deformed at elevated temperatures. Reed-Hill found that with the geometry of his crystals the slip lines were so irregular and diffuse that direct trace analysis of their system was not possible. However, a careful study of the asterism in Laue X-ray photograms made from the deformed crystals showed them to be interpretable as the result of predominantly $\{10\bar{1}1\}\langle 11\bar{2}0\rangle$ pyramidal slip. Large discrete $\{10\bar{1}1\}$ pyramidal slip bands were also observed on specimens strained in tension at 298°K with the tensile axis in the basal plane and approximately 17° from a $\{10\bar{1}0\}$ direction. However, the high loads to fracture, the limited ductility at 298°K and the apparent rarity of

$\{10\bar{1}1\}$ slip bands all point to the fact that pyramidal slip is not an important mode of plastic deformation at room temperature[53]. There appears to be no conflict between these results and those of Schmid[48] and Bakarian[49] except that the significance of the 225°C is lost.

Chaudhri et al[54,55] have investigated the high temperature deformation of coarse grained polycrystalline magnesium in tensile creep at 533°K. From a careful trace analysis coupled with the waviness of the bands of slip lines they concluded that although $<11\bar{2}0>$ direction was invariant, slip occurred with microscopic alternation on prism and pyramidal planes.

Second order pyramidal $\{11\bar{2}2\}$ slip bands have also been observed by Reed-Hill[53] on single crystal specimens strained in tension at 83°K with the tensile axis in the basal plane and approximately 2° from a $<10\bar{1}0>$ direction. The asterism found in a Laue back reflection photograph and microscopic observation of slip lines indicated that the slip direction is probably $<10\bar{1}0>$. Although Cd, Zn and Be show $\{11\bar{2}2\}$ $<11\bar{2}3>$ pyramidal slip bands, non basal slip vectors have never been observed in magnesium.

In hexagonal metals the operation of the second order $\{11\bar{2}2\}$ $<11\bar{2}3>$ pyramidal slip is a necessary as well as sufficient condition for the availability of five independent slip systems. As reviewed by Dorn and Mitchell[56] this system is the only one which can promote extensive deformation parallel to the c axis. Table II shows the number of independent systems for each of the prominent slip systems.

Table II

Slip Systems in Hexagonal Metals
(After Dorn[56])

No.	Slip Systems	Burgers Vector	Number of Independent Systems
1	$\{0001\}\ \langle 11\bar{2}0\rangle$	a	2
2	$\{10\bar{1}0\}\ \langle 11\bar{2}0\rangle$	a	2
3	$\{10\bar{1}1\}\ \langle 11\bar{2}0\rangle$	a	4
4	$\{11\bar{2}2\}\ \langle 11\bar{2}3\rangle$	c + a	5
5	1 + 2 + 3	a	4

No combination of $\{0001\}\langle 11\bar{2}0\rangle$, $\{10\bar{1}0\}\langle 11\bar{2}0\rangle$ and $\{10\bar{1}1\}\langle 11\bar{2}0\rangle$ can provide the five independent systems required. Since the second order pyramidal slip of the type $\{11\bar{2}2\}\langle 11\bar{2}3\rangle$ is absent in magnesium, plastic deformation of the polycrystalline aggregate is not possible, in principle, from slip alone. However, considerable plasticity is observed. This is due to cell formation, twinning, compression banding and grain boundary deformation, which supplement slip in order to satisfy von Mises criterion.

1.4.1.2. Plastic Deformation by Twinning

Twinning systems are often not included as possible deformation modes for the purpose of satisfying compatibility conditions, because of the limited amount of deformation achieved even when the entire volume has been twinned. Also twinning can accommodate either c-extension or c- contraction but not both. However, the profusion of two or more twinning systems, some leading to an extension and the others leading

to a contraction in the c direction, can assume the role of independent deformation modes. For instance Re[57], Ti[58] and Zr[46,59] exhibit essentially unlimited ductility although (c + a) slip has never been identified in any of them. Kocks and Westlake[60] have attributed the large ductility in these materials to the profusion of $\{11\bar{2}1\}\langle\bar{1}\bar{1}26\rangle$ and $\{11\bar{2}2\}\langle11\bar{2}\bar{3}\rangle$ twinning. The former leads to an extension and the latter to a contraction in the c-direction.

The twinning system most common to magnesium is the $\{10\bar{1}2\}\langle\bar{1}011\rangle$ type. $\{10\bar{1}2\}$ twinning results in an extension in the c-direction and is favoured by compression parallel to the basal plane and tension perpendicular to it.

The complete formation of a twin under conditions where the parent crystal has no restraint to the resulting shear is a simple case, not usually met in practice. In general accommodation to the shear is accomplished by a phenomenon known as accommodation kinking. The plane of accommodation is usually called a bend or a kink plane. Accommodation may be expected on both $\{10\bar{1}0\}$ and $\langle11\bar{2}0\rangle$ planes. Non-crystallographic boundary formation has also been observed in magnesium. Dorn[11],[12] found that in many cases they crossed grain boundaries. He postulated that these boundaries formed because of the bending of the lattice associated with the non-homogenous deformation of the underlying grains.

The temperature dependence of $\{10\bar{1}2\}$ twinning has never been studied thoroughly under conditions where the variables of strain rate and orientation were fixed. Twinning in polycrystalline magnesium becomes less important at elevated temperature, but whether this is intrinsic to the twinning mechanism or not cannot be said, since the critical stress

for nonbasal slip and grain boundary deformation decrease rapidly with increasing temperature.

From the studies of deformed polycrystalline specimens Roberts[61] reported the existence of a twinned structure apparently on the habit of $\{30\bar{3}4\}$. Couling and Roberts[62] identified the habit as $\{30\bar{3}4\}$. This was confirmed on magnesium single crystals by Reed-Hill[63]. The twins are uniquely narrow and they exist in bands forming interesting arrays at low strain levels. These twins are formed when tension is applied perpendicular to the c axis. The rolling texture of magnesium effectively places the grains in an orientation unfavourable to both basal slip and $\{10\bar{1}2\}$ twinning. However $\{30\bar{3}4\}$ twins are formed when tension is applied in the direction of rolling. Also, since they are responsible for brittle fracture of Mg they have been studied in somewhat greater detail than the $\{10\bar{1}2\}$ twins. The $\{30\bar{3}4\}$ lamellae are formed as a result of a primary twinning on the $\{10\bar{1}1\}$ plane followed by a second order $\{10\bar{1}2\}$ twin formed in the primary twin. Using electron microscope replicas Hartt and Reed-Hill[64] have shown that the irrational habit of these twins is probably the direct result of a need to accommodate the second order twinning shear. A model has been presented which explains the accommodation resulting in both an external shear in the matrix and an internal shear in the lamella. Similar twins have been observed by Wonsiewicz and Backofen[65] in the complex straining of magnesium single crystals at higher temperatures and in some alloys of Mg by Hosford, Jr. et al[66] at room temperature. The detailed understanding of these twins explains the compression banding and the rolling texture in magnesium[67]. However, the established twin systems in magnesium cannot assume the role of an

independent deformation mode mainly because they are formed at places of special stress concentrations and are incapable of accommodating both expansion and contraction in the c-direction.

Twinning on $\{10\bar{1}3\}$,$\{10\bar{1}4\}$, $\{11\bar{2}4\}$, $\{10\bar{1}5\}$ [63] as well as on $\{11\bar{2}1\}$ [62] have been reported. However, their existence is not well established.

1.4.1.3. Grain Boundary Deformation:

The operation of grain boundary shearing under tension at room temperature was proved in the polycrystalline aggregate by Hauser et al[11]. The importance of the process in the creep of polycrystalline magnesium at elevated temperatures has been demonstrated by Couling and Roberts[68]. They found that the high temperature grain boundary deformation in polycrystalline magnesium is a two stage process involving alternate boundary shearing and migration. Increasing test temperatures and decreasing strain rates favour larger contributions to the over all strain from boundary deformation. In the limiting case it appears that all the deformation would be localized at the boundaries. A mechanism which explains the observations is the alternation of anelastic boundary shears with the capture of these shears when the boundaries migrate to new positions. The number of cycles necessary to produce the measured shear has been calculated and found to agree qualitatively with metallographic observations.

1.4.1.4. Cell Formation:

Cell formation results from a stress-accelerated polygonization process caused by non-homogenous distortion[54,55]. Chaudhri et al[54] have noticed in the case of Mg (especially coarse grained aggregates) that the breakdown of the metal into cells is marked in the grain boundary region. Polygonization can be so pronounced in the grain boundaries that it actually leads to recrystallization. Due to the lack of availability of five independent modes, cell formation plays an important role in the deformation of magnesium. For example, the transition in fracture stress and ductility of magnesium in the vicinity of room temperature is thought to be associated with the onset of cell formation and recrystallization[69]. Recently, however, Reed-Hill[64] has associated this transition with the operation of $\{10\bar{1}1\}$- $\{10\bar{1}2\}$ double twinning.

Suiter and Wood[70] have suggested a mechanism for the formation of cell structures. This depends on the relative movements of the grain boundaries causing rumpling and twisting of the structure. Dislocation movements relieve the strain associated with the deformation and lead to the formation of sub-boundaries which develop into the observed cell structures.

Cell formation has also been observed in Mg-Pb alloys[35] and Mg-Al alloys[36] details of which will be discussed later.

1.4.2. Fracture of Magnesium Polycrystals:

Studies on the flow and fracture stress characteristics of high purity magnesium carried out by Hauser et al[30] and by Toaz and Ripling[69] have revealed that fine grained Mg fractures at low but rather constant stress below about 250°K. Above this range, the fracture stress decreases rapidly with increasing temperature and the ductility increases markedly. The temperature at which this change occurs is regarded by Hauser et al as the transition point from brittle to ductile fracture. A true transition temperature refers to the situation where a change from brittle to ductile behaviour occurs with no thermal instability of the microstructure and where negligible deformation occurs prior to fracture in the brittle range. The use of the term brittle fracture range is not strictly justified in the case of magnesium, since a fair amount of plastic deformation precedes fracture. However, the characteristics of the low temperature fracture of magnesium are in many ways similar to those of brittle fracture. For example, the fracture stress increases linearly with the reciprocal of the square root of grain diameter in accordance with the Hall-Petch relation[71], the transition temperature increases with increasing grain size and the low temperature fracture stress as well as fracture strain are found to be relatively independent of the strain rate.

On the basis of some metallographic studies Toaz and Ripling conclude that the discontinuity (in the fracture stress-temperature relationship) in the case of pure magnesium results from the entrance of recrystallization during deformation[69]. It has been observed by Risebrough[72] that the negative work hardening in the stress strain curves

of polycrystalline Zn and Cd is associated with recrystallization. Metallographic examination of the test samples before and after the onset of the negative work hardening in the present work suggests recrystallization to be responsible for the work-softening of magnesium. The strain associated with the negative work hardening, which was taken as the strain to fracture less the limiting strain to maximum stress, was found to decrease with decreasing temperature, becoming vanishingly low at about 250°K. This observation tends to support the conclusion of Toaz and Ripling on the nature of the transition temperature.

The fracture of Mg and its alloys near and below room temperature results primarily from the joining of the intragranular cracks by a moderate amount of intergranular cracking. The twinned structures which have been identified as $\{30\bar{3}4\}$ twins and the higher order planes such as $\{10\bar{1}4\}$, $\{10\bar{1}5\}$ and $\{11\bar{2}4\}$ are the crack nucleation sites in intragranular fracture. At elevated temperatures, however, the grain boundaries play an important role in the fracture of magnesium and its alloys. This will be considered at a later stage.

1.4.3. Solution Hardening:

Earlier assessments of solution strengthening in magnesium alloys have considered the possible effects of various solute species on such quantities as the cohesive strength, surface tension and flow stress[14]. However, such considerations are rarely helpful in defining the detailed processes involved. Accordingly, it is more profitable to attempt a direct assessment of the deformation modes and the way in which solute additions affect them.

As outlined in the last section the deformation of polycrystalline Mg occurs predominantly by slip on the basal $\{0001\}\langle 11\bar{2}0\rangle$ system with additional slip on the prismatic $\{10\bar{1}0\}\langle 11\bar{2}0\rangle$ system accompanied by a double twinning in the sequence $\{10\bar{1}1\}$ - $\{10\bar{1}2\}$ and some grain boundary sliding. Prism slip occurs predominantly at grain corners which are sites of high stress concentration, and thus acts as a stress relief mechanism contributing to increased ductility. Furthermore, the yield strength of polycrystalline magnesium will be governed by the CRSS for both basal and prismatic slip. The most comprehensive data available are based on studies on the Mg-Li system by Dorn and his colleagues[14,15,73]. These experiments have shown that addition of lithium to magnesium causes an increase in the CRSS for slip on the basal system, but a decrease in the CRSS for slip on the prism system. They have also shown that, for polycrystals, the yield stress of these alloys, varies with concentration of lithium roughly in a manner similar to that found in the present work, and that a similar variation of ductility with concentration was also found. Yoshinaga and Horiuchi[16] have also investigated the deformation behaviour of Mg-Li polycrystals as a function of lithium concentration. Although both groups of workers found similar variation in yield stress with solute concentration, the ductility minimum was observed at 0.4 at.% Li by Horiuchi and Yoshinaga while Dorn et al found the minimum at 4 at.% Li.

The interpretation offered by Dorn et al is that the yield stress of the polycrystalline aggregate is the combined result of the CRSS for both basal and prismatic slip. The initial rapid increase was attributed to the dominant solution hardening for basal slip, while the

subsequent reduced rate of hardening and increased ductility was attributed to the increasing importance of prismatic slip as an available deformation mode. Twinning and boundary shear were considered to be of minor importance.

Paralleling these conclusions is the observation that increasing lithium content results in a reduction of the c/a ratio, and hence the decrease of CRSS for prismatic slip is the expected result of the decreasing Peierls stress. The work of Ahmadieh and Dorn[73] has shown Peierls stress to be the rate controlling mechanism for prismatic slip at low temperatures.

These ideas cannot account adequately for the present results. Consider, first, the dependence of CRSS for basal slip on concentration. Levine, Sheely and Nash[74] have measured the CRSS for basal slip in single crystals of dilute alloys of magnesium with Zn, Al, Tl, Cd and In and their results are reproduced in fig. (34). These authors conclude that the solute strengthening effect is linear with concentration for Zn, Al and Tl and that for Cd and In there is no hardening at low concentrations followed by a linear hardening at higher concentrations. A closer examination of these data indicates that if lines of truly best fit are drawn through the points, then in no case do they extrapolate back to the CRSS for pure magnesium. Such lines are drawn in fig. (35), and show that for all solute species, the CRSS for basal slip is unaffected by solute addition up to a concentration, approximately the same as C_T in the present work. This conclusion has been confirmed in Mg-Zn alloys, details of which are discussed in a later chapter.

Clearly, then the present observation of the very rapid increase in σ_{YP} with solute addition from pure Mg to C_T cannot be

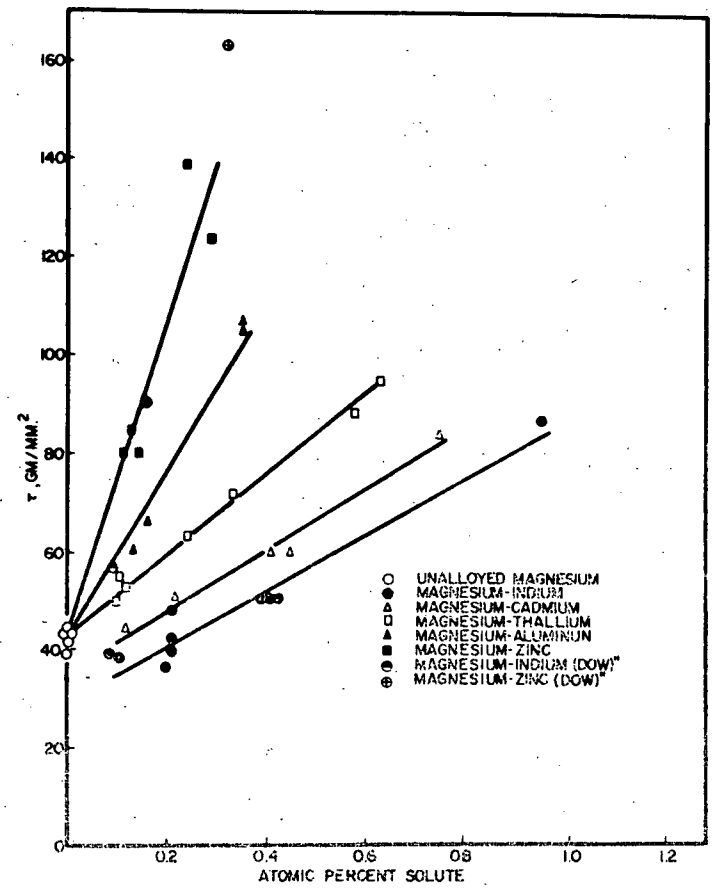

Fig. 34. CRSS for basal slip vs. concentration. (After Levine et al[74]).

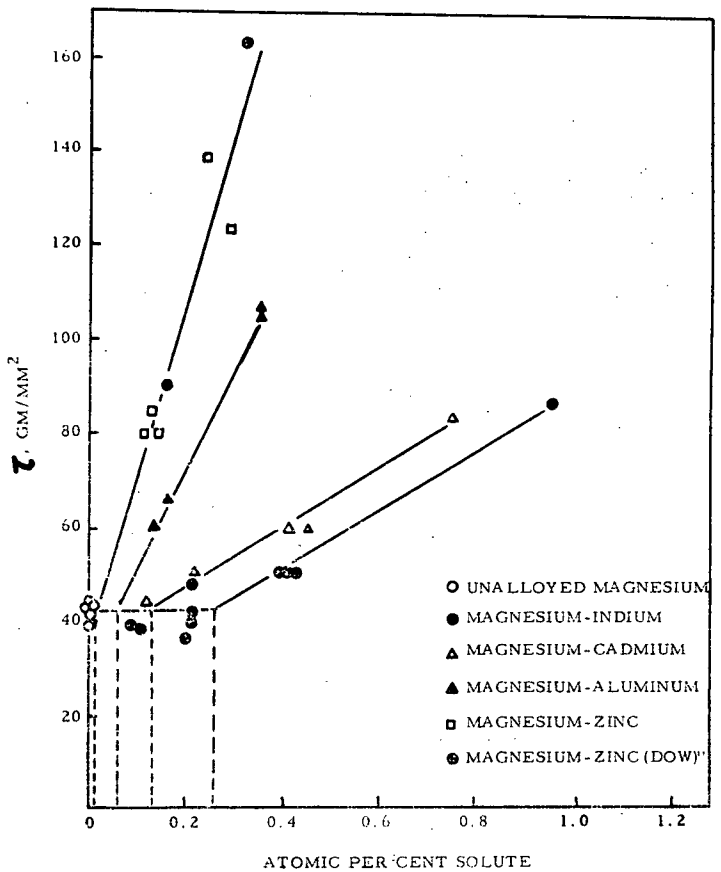

Fig. 35. Revised curves drawn for data from ref. 74.

attributed to a change in CRSS for basal slip. It would appear logical therefore, to conclude that this increase in σ_{YP} must be due to an increase in the CRSS for prismatic slip.

So far, there are no reports in the literature on the variation of CRSS for prismatic slip at very low solute concentrations. Accordingly, such measurements have been carried out in the present work and the results for Mg-Zn alloys are shown in fig. (93). These confirm the conclusion that the CRSS for prismatic slip does, in fact, increase with increasing solute concentration up to C_T. Details of this work are discussed in a later chapter.

1.4.3.1. The Variation of σ_{YP} and Ductility with Solute Concentration:

The variation of both σ_{YP} and ductility with solute concentration are now more readily understandable. The yield stress in polycrystalline material is determined by the stress necessary to activate both basal and prismatic slip. The initial high rate of solution hardening is due to the rapid increase in the CRSS for prismatic slip, while the CRSS for basal slip remains unchanged upto C_T (at and above room temperature). Due to slip on the basal system, stress concentrations will arise which may be relieved either by crack formation or by plastic flow on the prismatic slip system. As the CRSS for prismatic slip increases from pure magnesium to C_T, less plastic deformation is possible prior to fracture and the ductility is reduced.

1.4.3.2. The Solution Hardening Rate $(\frac{d\sigma}{dc})'$:

The critical resolved shear stress for basal slip in magnesium is approximately two orders of magnitude lower than that for

prismatic slip. For example at room temperature the numerical values for the two systems are 51 gm/mm^2 and 4600 gm/mm^2 respectively. Thus it may seem rather unlikely that prismatic slip should operate at the yield stress of the polycrystalline aggregate. However, in view of the strong rolling and recrystallization texture of magnesium and its alloys the operation of prismatic slip is not at all surprising. These materials have a texture such that the basal plane remains inclined to the rolling or extrusion direction within 10°. The Schmid factor for basal slip in this orientation is about 4-5 times lower than that for prism slip plane. Thus the deformation behaviour of the polycrystalline aggregate should show a closer similarity to that of single crystals oriented for prismatic slip rather than for basal slip. Qualitatively, the stress-strain curves of the polycrystals do show a closer resemblance to the stress-strain curves of the single crystals oriented for prismatic slip.

It would be interesting at this juncture to compare the observed initial solution hardening rate of the polycrystals with that of single crystals in prism slip orientation. Single crystals and polycrystals of both Mg-Al and Mg-Zn systems have been deformed at room temperature in the present work. This is shown in Table III. For converting the shear stress to tensile stress the following relationship $\sigma = 2\tau$ has been used.

Table III

Comparison of Solution Hardening Rates in Single Crystals With Polycrystals

System	$(\frac{d\sigma}{dc})'$ in psi For polycrystals at 295°K	$(\frac{d\sigma}{dc})'$ in psi For prismatic slip at 295°K
Mg-Zn	3.45×10^5	4.74×10^5
Mg-Al	5.95×10^4	6.24×10^4

It is apparent from the table that the solution strengthening rate of the polycrystalline aggregatesis close to that of single crystals oriented for prism slip.

No attempt will be made here to compare the effect of temperature on $(\frac{d\sigma}{dc})'$ in the polycrystals with that in single crystals. The effect of grain boundary sliding and cell formation in polycrystalline material above room temperature (0.31 T_m) makes such a comparison difficult. Below room temperature on the other hand it is not the prismatic slip system alone which is affected by the addition of solute up to C_T. This amount of solute is effective also in increasing the CRSS for basal slip below room temperature. These considerations do not permit a quantitative comparison at temperatures below room temperature.

1.4.3.3. Hardening Beyond C_T:

For all the alloy systems considered here the c/a ratio increases with increasing solute concentration; that is, the effect is opposite to that for Mg-Li system. Yet reference to fig. (93) shows that for increasing concentrations beyond C_T, the CRSS for prismatic slip decreases. This decrease cannot be accounted for, then, in terms of a decreasing Peierls stress resulting from a reduction in the axial ratio, as in the Mg-Li case.

The decreasing CRSS for prismatic slip can account for both the decreased rate of solution hardening and the increasing ductility beyond C_T. The reduced rate of hardening and increased ductility in stage II can be attributed to the increasing importance of prismatic slip as an operative deformation mode. The operation of prismatic slip in the polycrystals is made slightly easier due to the increase in CRSS for basal slip in the alloys containing concentrations of solute

in excess of C_T. Thus yield in these alloys will be achieved by a balance between basal and prismatic slip. The initial work hardening rate will become lower with increasing solute concentration (beyong C_T), because of the increasing ease of stress relief by prismatic slip.

This line of argument can be extended further to explain the observed lowering of σ_{YP} in stage III. The yield stress was evaluated at 0.2% plastic strain. An alloy containing solute concentration close to C_T will have a high initial work hardening rate due to the difficult operation of prismatic slip. This will lead to a large flow stress at 0.2% strain. On the other hand an alloy containing solute in large excess of C_T will have a lower initial work hardening rate and as a result, the flow stress at 0.2% strain will become smaller than at a lower solute concentration.

1.4.3.4. The Transition Concentration C_T:

Above 300°K the CRSS for basal slip remains unchanged in stage I of solution strengthening, whereas that for prismatic slip increases. Hence in polycrystals the existence of a critical transition concentration is a manifestation of a transition in the CRSS - concentration relationship for prismatic slip. This conclusion is supported by the equality of the transition concentration observed in polycrystalline aggregate at room temperature (0.01 at.% Zn) to that obtained in crystals oriented for prismatic slip (0.006 at.%). It should be noted that at all temperatures the transition concentration in crystals oriented for prismatic slip remains constant.

The situation is, however, rather complicated at low temperatures, as discussed earlier. Therefore, the critical transition

concentration, as obtained from the σ_{YP} of the polycrystalline aggregates tested below room temperature, is rather a complex quantity which cannot be discussed at the present.

1.4.3.5. The Flow Stress:

Toaz and Ripling[69] have found that the transition in the maximum stress-temperature curve results from the entrance of recrystallization. Staceys work on magnesium and its alloys containing small amounts of Al has indicated that cell formation precedes recrystallization[36]. Metallographic studies on pure Mg and Mg-Al alloys deformed between 200 and 300°K up to a strain of 2%, in the present work, have failed to reveal recrystallized grains, although the transition in the flow stress from stage I to stage II occurs in the same temperature interval.

It is proposed, therefore, that the onset of cell formation (sub grains) is responsible for the transition in the flow stress-temperature curves. This can be better understood as follows.

When deformation proceeds at a fixed strain rate there is stress concentration at the grain corners. This stress concentration will not be relieved by slip in the adjacent grains, due to von Mises' criterion not being satisfied. The operation of prismatic slip, at the grain corners, will only partly relieve the stresses because basal and prismatic slip combined cannot provide five independent modes of deformation. At lower temperatures this stress concentration is finally relieved by crack nucleation and subsequent fracture, whereas at higher temperatures stress accelerated polygonization will relieve the stress concentration and deformation will proceed at a lower flow stress than at lower temperatures.

This explanation involving polygonization and cell structure formation is consistent with the observed strain sensitivity of the transition temperature in the flow stress-temperature curves for 0.055% Al alloy (fig. (28)). The corresponding transition temperature in pure Mg and Mg - 0.53% Al alloy are observed to be less sensitive to the strain at which the flow stress is measured. (0.055 at % Al is close to C_T and therefore the CRSS for prismatic slip in this alloy will be higher than in pure Mg or the higher alloys). Therefore, at a fixed strain rate the extent to which stress relief will be achieved by the operation of prismatic slip will be small, thus making cell formation an important mechanism. Since cell formation is a stress accelerated polygonization process, it will operate at a lower temperature, the higher the applied strain, as is the case with 0.05 at. % Al alloy. The strain sensitivity will be lowered with the increasing ease of prismatic slip, because more stress relief will be achieved through the operation of prismatic slip; thereby making cell formation a less important process than in the 0.05 at. % Al alloy.

1.4.4. The Effect of Temperature on Ductility:

The effect of solute on ductility at constant temperature has been rationalized in terms of the relative ease of prismatic slip. However, there are two observations which are still unexplained. They are

1) The increase in ductility of Mg as well as its alloys with temperature, above room temperature.

2) The observed maxima and minima in the ductility - temperature curves of the Mg-Al alloys.

The ductility transition in mangesium has been attributed to the onset of recrystallization[69]. As the temperature increases the CRSS for prismatic slip decreases and also the ease of polygonization is enhanced. Both these processes lead to an increased stress relief and make longer time available for recrystallization to proceed. Therefore, the ductility of magnesium increases continuously with temperature beyond 295°K. The addition of solute up to C_T increases the flow stress for prismatic slip and therefore, the ductility of these alloys is observed to be slightly lower than that of magnesium. At higher solute concentrations, however, the effectivensss of the stress relief increases due to the lower flow stress for prismatic slip and higher flow stress for basal slip leading to an increased ductility in these alloys. It is important to note that up to 420°K pyramidal slip $\{10\bar{1}1\}\langle 11\bar{2}0\rangle$ does not operate in magnesium[51].

1.4.4.1. The Ductility Maxima:

Ductility maxima have been observed in Mg-alloys containing 0.2% Pb and 0.8% Al. Green Wood et al[35] have found extensive grain boundary cavitation in the Mg-0.2 % Pb alloy in the temperature interval in which the loss in ductility is encountered. It was suggested that grain boundary cavitation is responsible for the early fracture. A shift in the ductility maximum to lower temperatures was also observed with decreased strain rate, which could be accounted for in terms of the longer time available for vacancies to diffuse, coalesce and form intergranular voids at a slower strain rate.

Stacey[36] reported the occurrence of ductility peaks in Mg-0.8% Al alloy and explained his results in terms of a combined effect of cavitation and the formation of cell structure adjacent to the grain boundaries. Since the grain boundary movements increase with increasing temperature, the strain to be accommodated by lattice bending should accordingly decrease. Thus the formation of cell structure, which according to Stacey is at least in part responsible for the ductility peak, may be expected to be well developed at slower strain rates and at an intermediate temperature range, which in turn will be determined by the strain rate.

The present results on the high temperature ductility of Mg-Al alloys can now be better understood. The effect of alloying up to C_T is to increase the CRSS for prismatic slip. Therefore, in these alloys the attainment of stress relief through prismatic slip is even less than in pure magnesium. The strain rate used in the present experiments (75%/hr) is rather high so that there is neither much time available for recrystallization to proceed, nor can the vacancies coalesce to form intergranular voids. This explains the lower ductility and the absence of maxima in these alloys.

Increasing the alloying content in excess of C_T is in effect equivalent to reducing the strain rate. This equivalence can be understood as follows. The flow stress for prismatic slip decreases with increasing solute addition beyond C_T. Since prismatic slip acts as one of the mechanisms causing stress relief at the grain corners, the effective-length of time available for the recrystallization to proceed, therefore, increases at higher solute concentrations. As a

result, the fine grained structure adjacent to the boundaries is better developed when the solute concentration is high. This explains the increased ductility with solute concentration.

However, the coalescence of vacancies to form intergranular voids, being a time dependent phenomenon, is also enhanced with increasing solute content thereby leading to a shift in the ductility peak to lower temperatures.

1.4.5. Strengthening Effects in Multicomponent Solid Solutions:

It has been frequently noted that the strength of a multicomponent solid solution can be obtained by adding up the strengthening effects of the corresponding binary solid solutions. The above conclusion has been empirically established for face centred cubic alloys. However, even in the absence of comprehensive data on binary and ternary systems such behaviour should not be expected in polycrystalline solid solutions having hcp structure. Unlike the polycrystalline aggregates of fcc structure, which deform by the operation of one slip mode (having more than five slip systems and hence satisfying von Mises criterion), the hcp materials undergo plastic flow by the simultaneous operation of two or more deformation modes. Since the various deformation modes are affected differently by the addition of solute, the yield stress of the polycrystalline aggregate represents a balance between these deformation modes and the additive nature of solutes is unlikely to be observed in hcp materials.

In the present work this conclusion was verified on a Mg-In-Zn alloy tested at room temperature. The strength calculated from the Mg-In

and Mg-Zn binaries was found to be much higher than the observed strength of this alloy. The Mg-In-Zn ternary was chosen because it involved the component responsible for the maximum strengthening effect (Zn) and also the one giving the minimum strengthening effect (In), of all the solutes examined. The ternary alloy examined had concentration of each solute in excess of the transition concentration for the corresponding binary system. A critical examination of the observed strength of this alloy suggested that the stage I strengthening is achieved by one component only and the solute in excess of C_T for this component as well as the total amount of solute of the other component, have additive effect in stage II. The calculated value using Mg-In and Mg-Zn binaries was found to agree closely with the experimental value of σ_{YP} of the ternary, if Zn is assumed to be the preferred solute responsible for stage I strengthening. Details of this are given in appendix (B).

In order to gain some insight, the investigation of the ternary systems was carried further. Two series of Mg-Zn-In alloys were prepared containing 0.004 at.% and 0.007 at.% Zn respectively (both less than C_T for Zn) and In additions up to 1.1 at.% were made. The results are shown in figs. (36,37). Since Zn concentration is lower than C_T, In should contribute partly to the stage I strengthening. Experimentally then, a three stage solution strengthening curve is obtained, as expected. The results show that the stage I slope (Ib in ternary) is reduced, the stage II slope is increased and the transition concentration is reduced from the corresponding values for the Mg-In binary. The implication may be that solution strengthening results from a type of solute atom dislocation interaction with preference for prism plane dislocations and large size difference solutes to be involved.

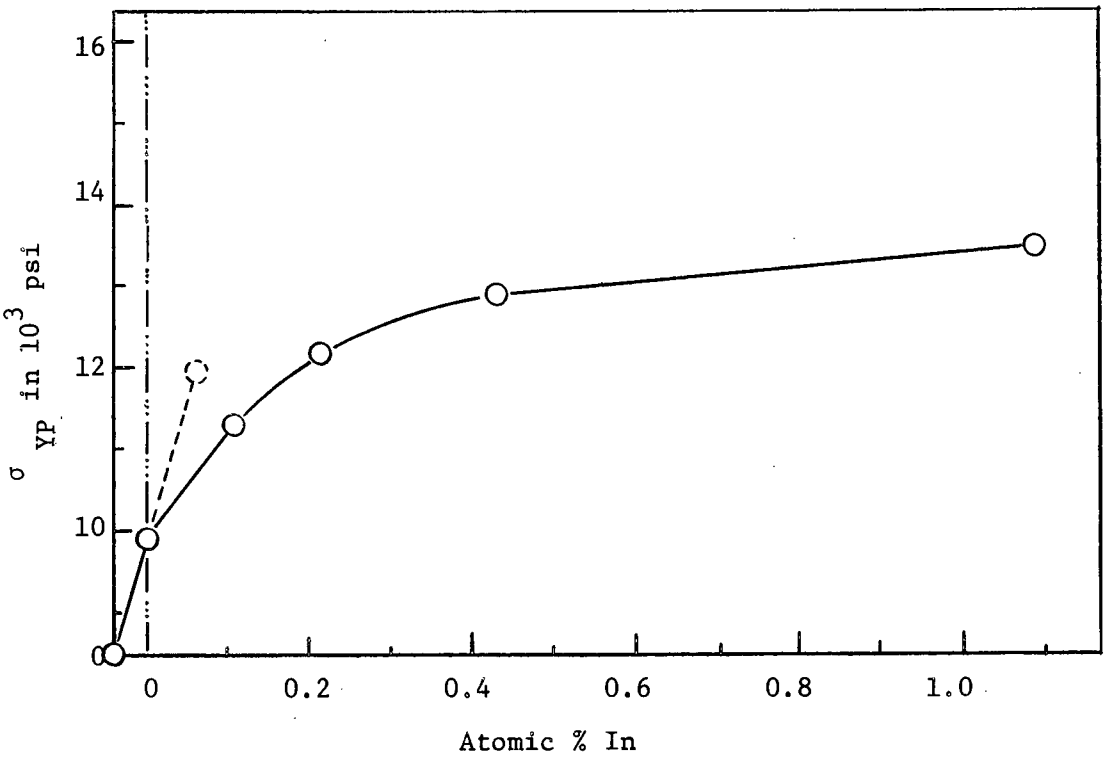

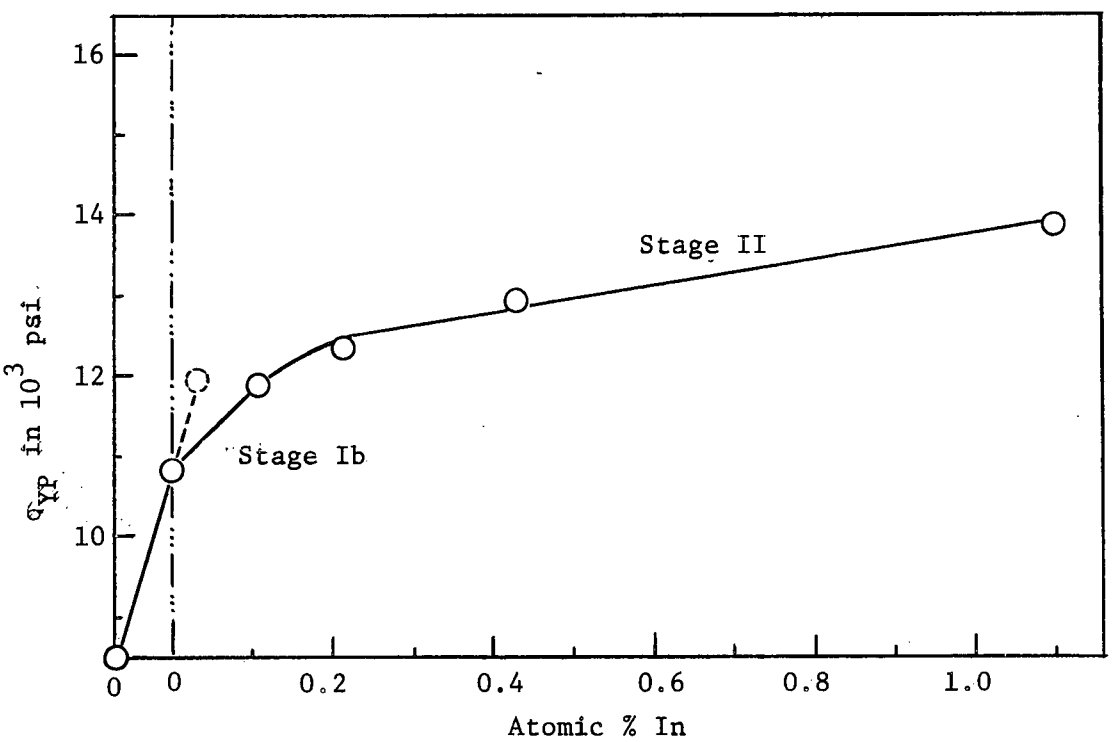

Fig. 37. Solution hardening curve for Mg-Zn-In ternary alloys tested at 295°K with Zn concentration fixed at 0.007 at.%.

PART II

2. Solution Hardening in Alloy Single Crystals

2.1. INTRODUCTION AND OBJECTIVES:

The study of single crystals has the advantage of avoiding the difficult problem of dealing with the constraining conditions imposed by the grain boundaries during the deformation of the polycrystalline aggregates. This simplicity, which enables one to obtain a better knowledge of shear stress conditions on particular slip planes, has disadvantages due to the poor reproducibility of the flow stress values of different single crystals, because of the effects of slight changes in such factors as substructure, impurity concentration, orientation and initial dislocation density. Additional complications arise in alloy single crystals grown from the melt, due to the solute segregation.

Single crystals of dilute solid solutions of magnesium containing Zn in amounts up to 0.45 at % have been studied in the present investigation.

The study of the dilute alloys was undertaken because of three main reasons. The solution hardening rate in the polycrystals in Mg dilute solutions is extremely high. The first logical step in pursuit of an explanation of the hardening in polycrystals is to study the solution hardening in single crystals of low alloys.

Another objective of the dilute solution study was to determine the indirect strengthening effect of solute arising due to a change in the dislocation density. Strengthening is possible in close packed structures through an increase in the dislocation density, caused by the presence of the solute. This indirect effect of the solute is believed to be significant

at low concentrations of solute.[75]

Lastly, much of the current theory of solution strengthening assumes either an ideal or a regular solution model. Since these models are better descriptions at low solute concentrations, they can be tested more exactly in dilute solutions only.

The choice of Zn as solute was made because of its strong hardening effect as observed in the Mg-Zn polycrystals. This strong hardening effect was hoped to make the study of dilute solutions easier. Zn is a hexagonal close packed metal which constitutes a substitutional solute in magnesium at the Mg rich end of the phase diagram. Additional reasons for the choice of Zn are outlined in the section on prismatic slip. The experimental procedure for specimen preparation is given earlier.

2.2. STRESS-STRAIN RELATIONSHIPS IN BASAL SLIP:

2.2.1. The Stress-Strain Curves:

It is now well recognized that the stress-strain curves of a variety of crystal structures show certain similarities. Thus the three stages in the basic work hardening curve are common to the face centred cubic metals and alloys[76,77], the alkali halides[78], some intermetallics[79], body centred Niobium[80] and Germanium[81]. However, the work hardening curve of hexagonal metals consists of two or three stages[3,29,82,83].

The shear stress-vs-shear strain curves of pure Mg crystals deformed at temperatures between 78°K and 423°K at a constant strain rate are shown in fig. (38). It is observed that the stress increases in a parabolic manner at low strains; a minimum rate of work hardening is

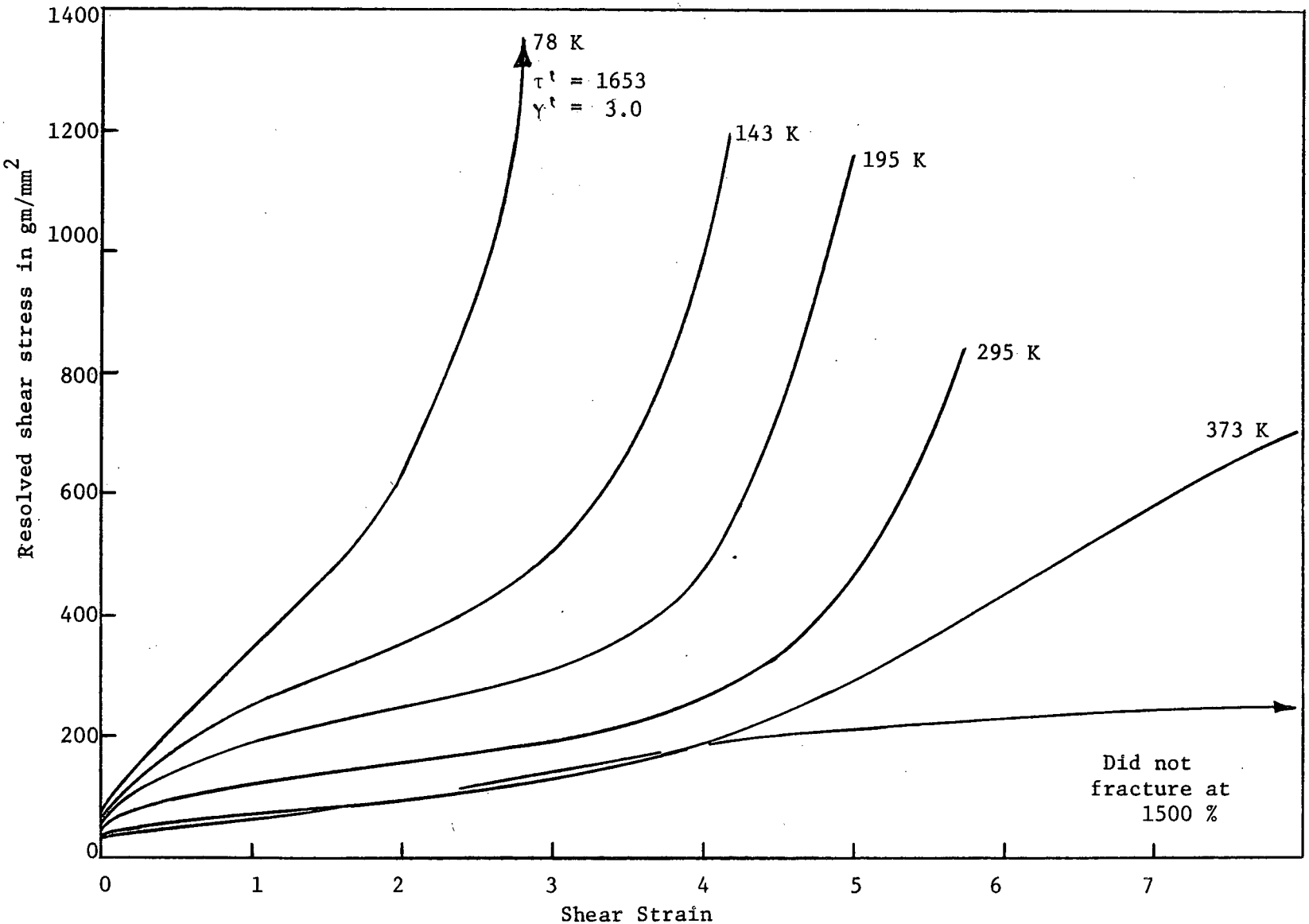

Fig. 38. Resolved shear stress-shear strain curves for Mg single crystals oriented for basal slip.

attained at intermediate strains, followed by a region of rapid hardening. A third stage with a decreasing work hardening rate is also observed in crystals deformed at and above room temperature.

Following the common tendency to break stress-strain curves into sections of similar work hardening rates, the three stages of deformation will be defined as shown schematically in fig. (39).

It is interesting to note that whereas the low initial work hardening rate (10^{-4} -10^{-5}G) and an extensive range of easy glide are common to many hexagonal metal crystals, the "Sigmoidal Shape" is a characteristic feature of magnesium only. The initial stage of work hardening becomes sub-divided into two linear regions in Zn[84]- and Cd[72] crystals deformed at room-temperature, however, this was not observed in Mg crystals in the present work. These differences in the work hardening behaviour place Mg in a category quite different from most of the other common hexagonal metals.

2.2.2. The Effect of Substructure on Work Hardening:

In order to make a quantitative comparison of the work hardening parameters in dilute alloys possible, it is important to keep the effect of other variables on these quantities to a minimum. One such variable is a low angle boundary running parallel to the tensile axis of the crystal. Ordinary etchants and X-ray back reflection technique will not detect a single sub-boundary in a large crystal. However, optical micrographs of specimens, exhibiting a high rate of work hardening extended only small amounts, show boundaries of twinning and enhanced deformation not observed in the other specimens. An example of such a boundary in Mg-0.054 at.% Zn alloy deformed at room temperature is shown in fig. (40).

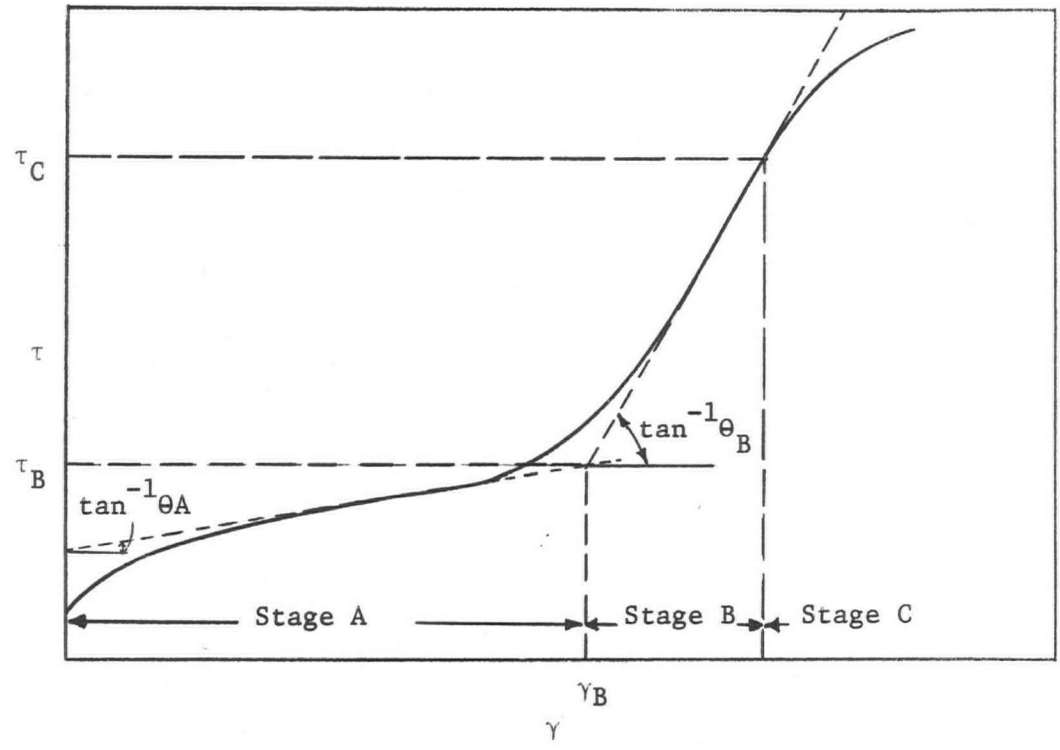

Fig. 39. Schematic resolved shear stress-shear strain curve.

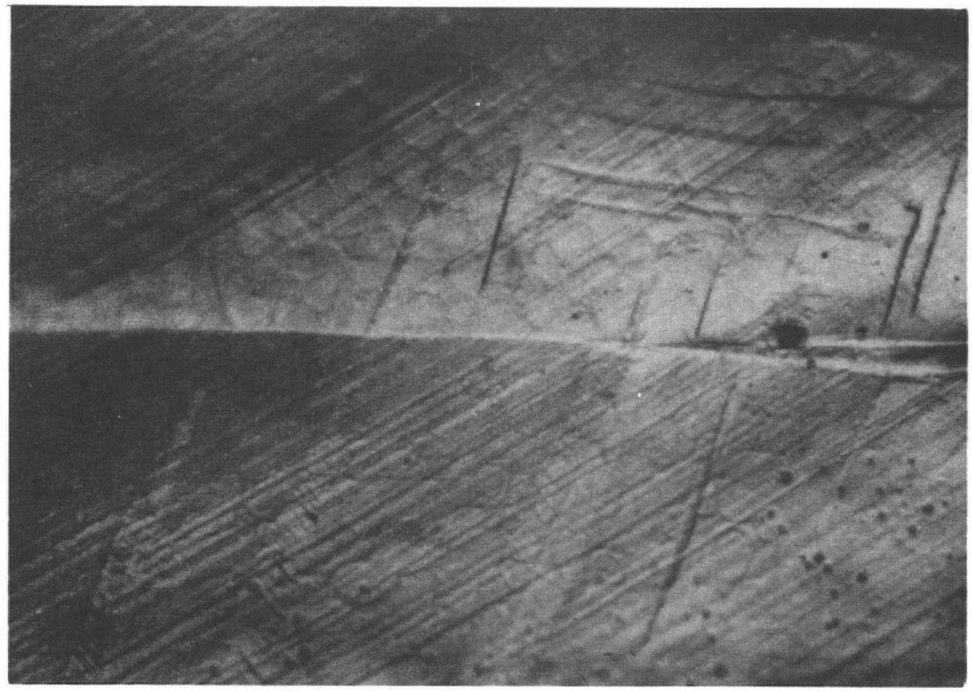

Fig. 40. Sub-boundary running parallel to the tensile-axis in a Mg + 0.054 at.% Zn alloy crystal deformed in easy glide at room temperature. 140X

It has been suggested earlier by Hirsch and Lally[29] that this high rate of work hardening is associated with the said sub-boundaries. These investigators have observed that the presence of a single sub-boundary of the order of a degree leads to a reduction in the extent of easy glide by a factor of five, an increase in the initial work hardening rate by an order of magnitude and a loss in the sigmoidal shape of the stress-strain curve. However, the work hardening rate in stage B remains unaffected by the presence of sub-boundaries.

The stress-strain curves of Mg crystals deformed by various workers at room temperature are summarized in fig. (41). The inconsistency apparent in fig. (41) is not surprising in view of the dramatic effect of sub-boundaries on work hardening. In most of the earlier investigations the growth rate has been > 1"/hr. In the present work, however, it was observed that 1"/hr is about the limiting growth rate beyond which the crystals contain many sub-boundaries, as observed by the splitting of the back reflection spots. Therefore, in order to obtain good crystals a growth rate of 0.4"/hr was used. All tensile test specimens for one composition were taken from one single crystal and tests were conducted in duplicate. Repeat tests were considered necessary when the extent of easy glide in the first two crystals differed by more than 50%.

2.2.3. The Stress-Strain Curves of the Mg-Zn Alloys:

Stress-strain curves of a representative set of Mg-Zn alloys are shown as a function of the test temperature in figs. (42,43). In order to facilitate comparison of the work hardening behaviour as a function of solute, at a constant temperature, the stress-strain curves

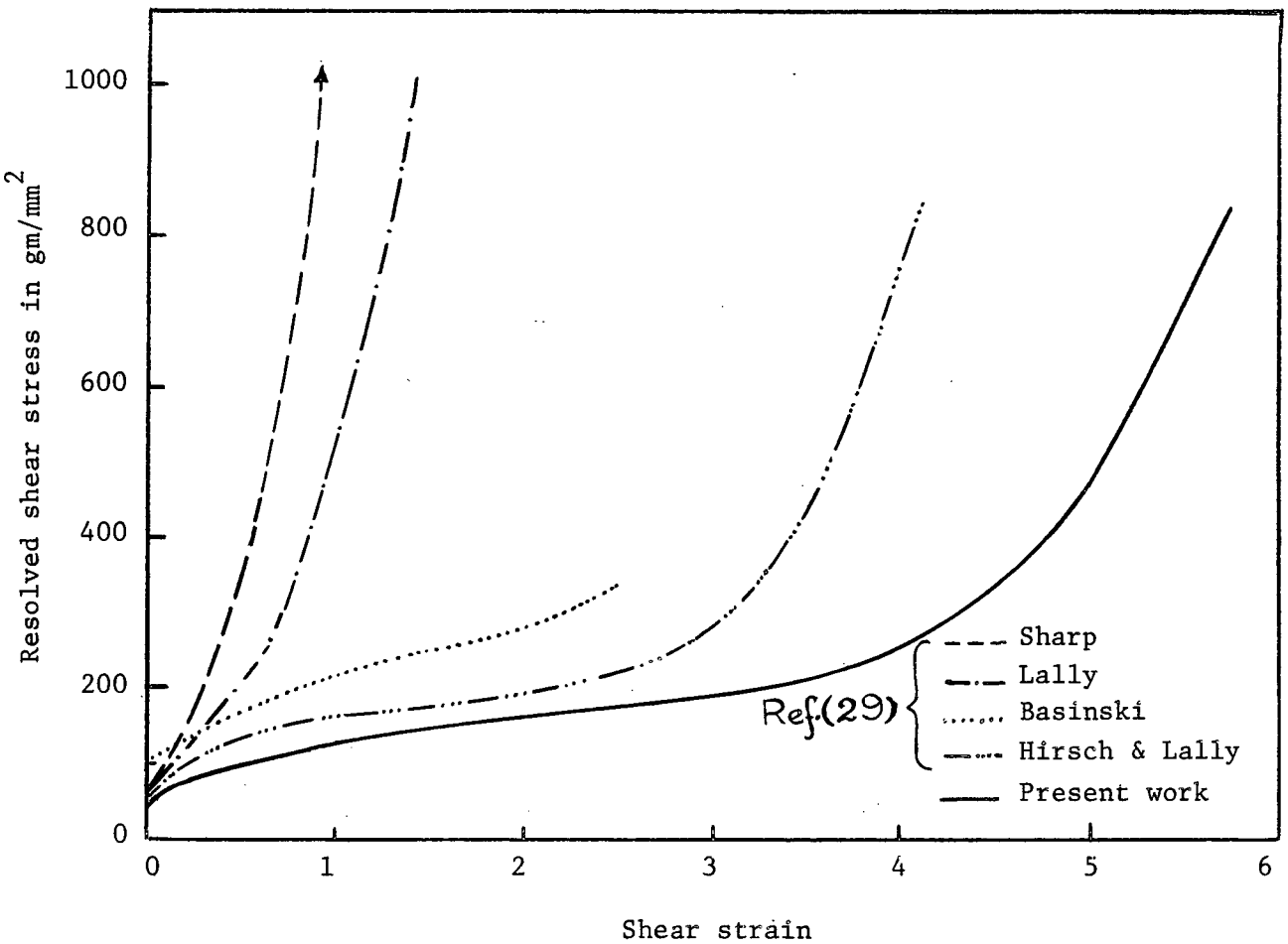

Fig. 41. Resolved shear stress-shear strain curves for Mg single crystals deformed by various workers at room temperature.

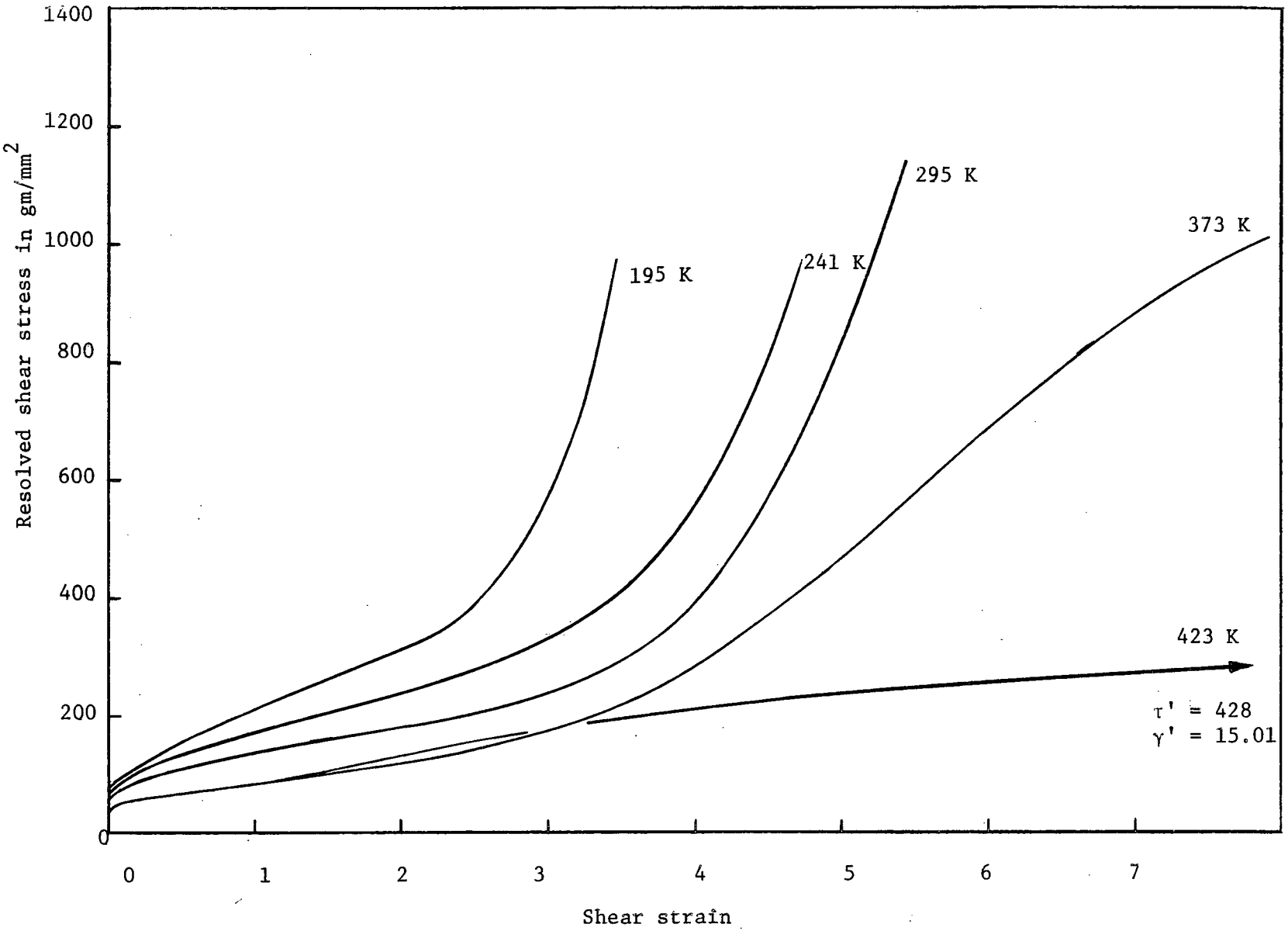

Fig. 42. Resolved shear stress vs. shear strain curves for Mg + 0.019 at.% Zn alloy single crystals.

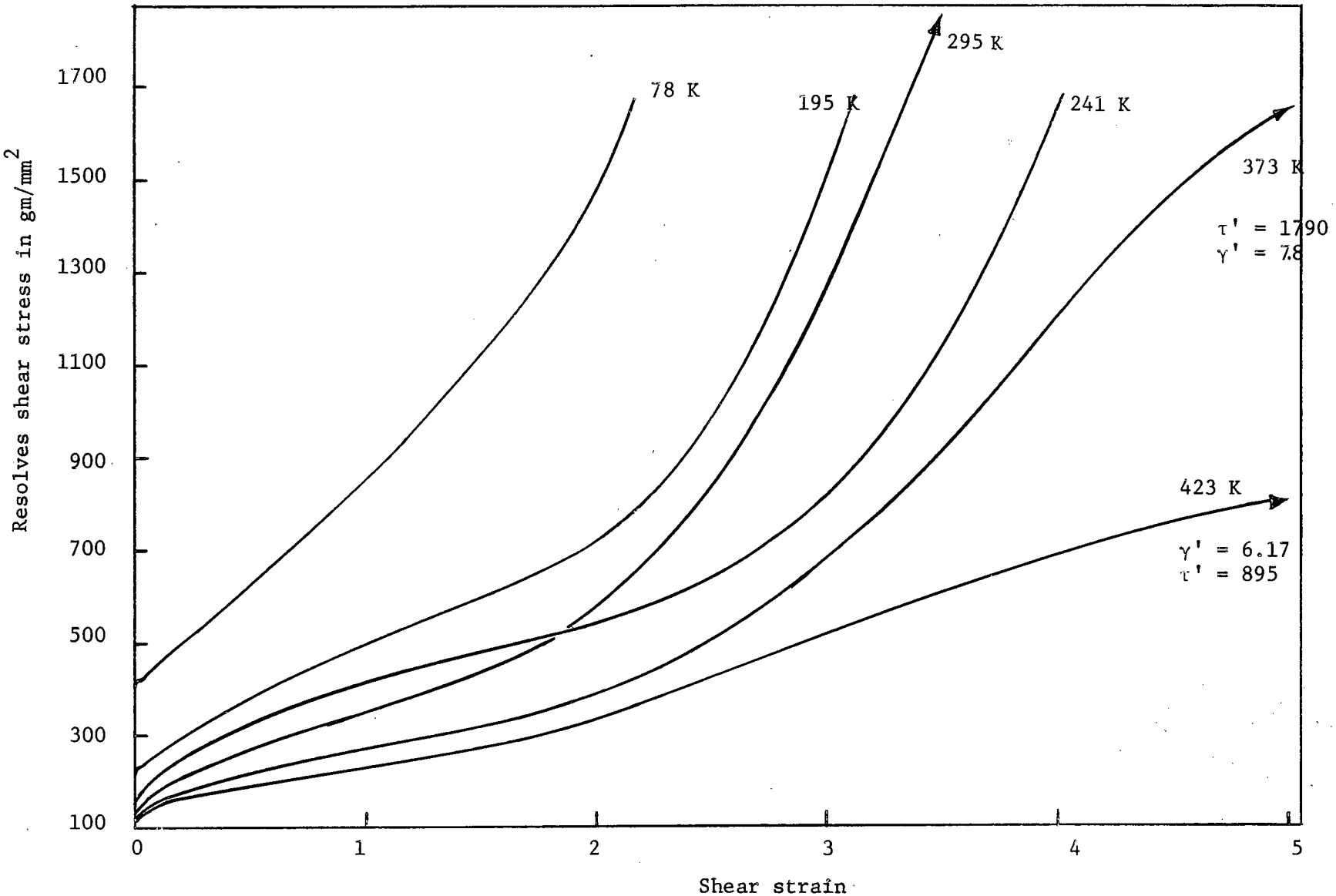

Fig. 43. Resolved shear stress vs. shear strain curves for Mg + 0.258 at.% Zn alloy single crystals.

of alloys containing different amounts of solute are grouped together as shown in figs. (44,45, and 46).

It is observed that the "S" shape of the curves is retained up to a concentration of solute equal to 0.258 at.% Zn. The sigmoidal shape is most pronounced in an intermediate temperature range between 143°K and 295°K. Both above and below this temperature interval the region of easy glide tends to become linear. The alloy containing 0.45 at.% Zn is an exception in that yield points were observed in this alloy at and below room temperature, leading to the absence of the sigmoidal shape of its stress-strain curves.

2.2.4. Yield Points:

Yield points have been observed in Mg-Zn alloys in the present work at low temperatures. When tested at 78°K, only a slight yield point was observed in 0.054 at.% Zn alloy, however, a well defined yield drop became apparent on increasing the solute concentration to 0.45 at.%. The yield points continued to appear at increasingly higher temperatures, as the solute content was increased. For example, the appearance of yield points was limited to 78°K only in the case of 0.054 at.% Zn alloy, to temperatures below 200°K in the case of 0.258 at.% Zn and in the case of Mg-0.45 at.% Zn alloy yield points could be seen in specimens tested at room temperature.

In addition to the initial yield points, multiple yield points have been observed in alloys containing 0.019 at.% Zn when tested at 423°K. The serrated yielding starts immediately after the material undergoes plastic flow and continues up to a certain strain, which increases with increasing solute addition. Beyond this strain the stress-strain

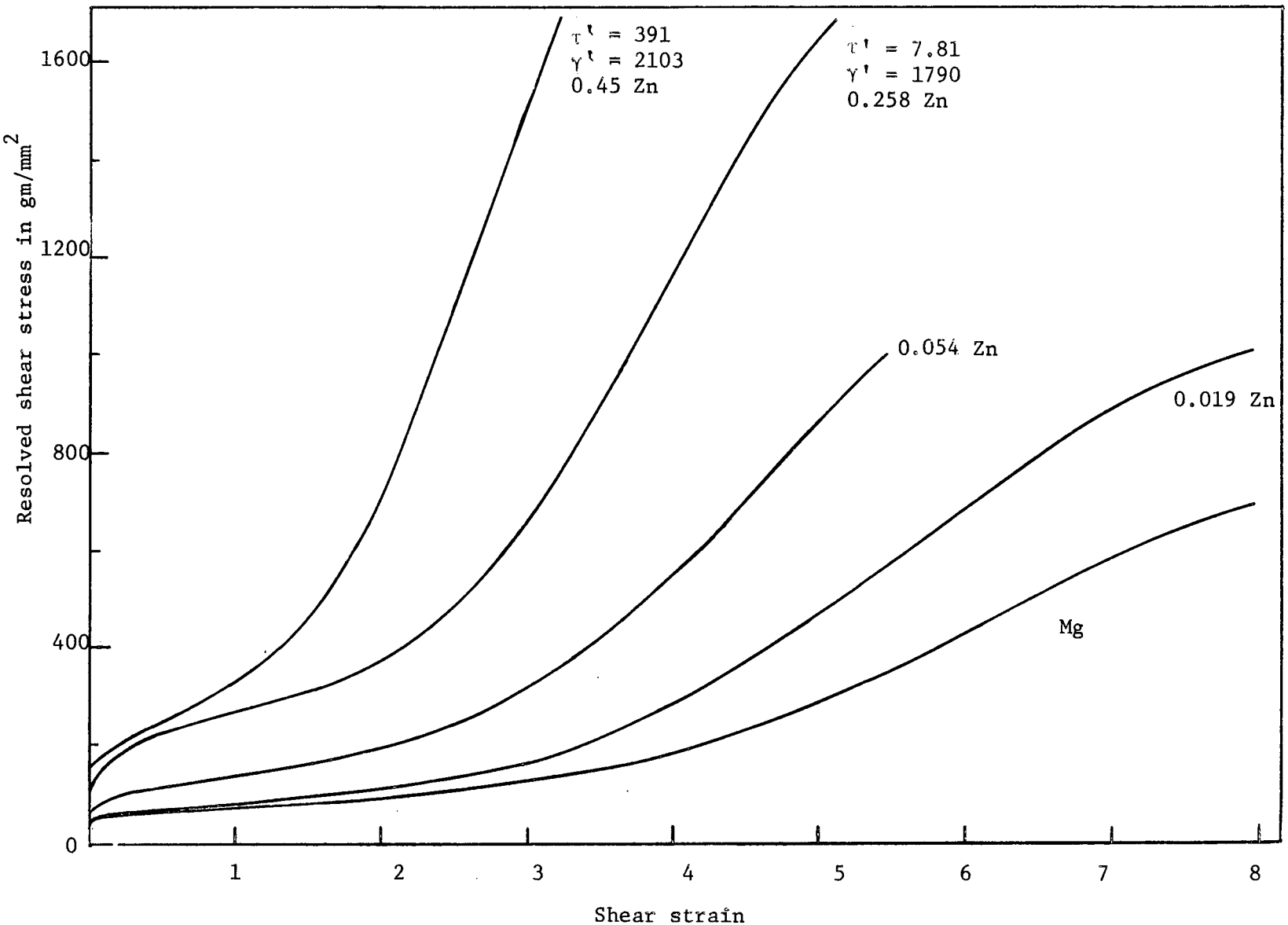

Fig. 44. Resolved shear stress vs. shear strain curves for Mg-Zn single crystals deformed at 373°K.

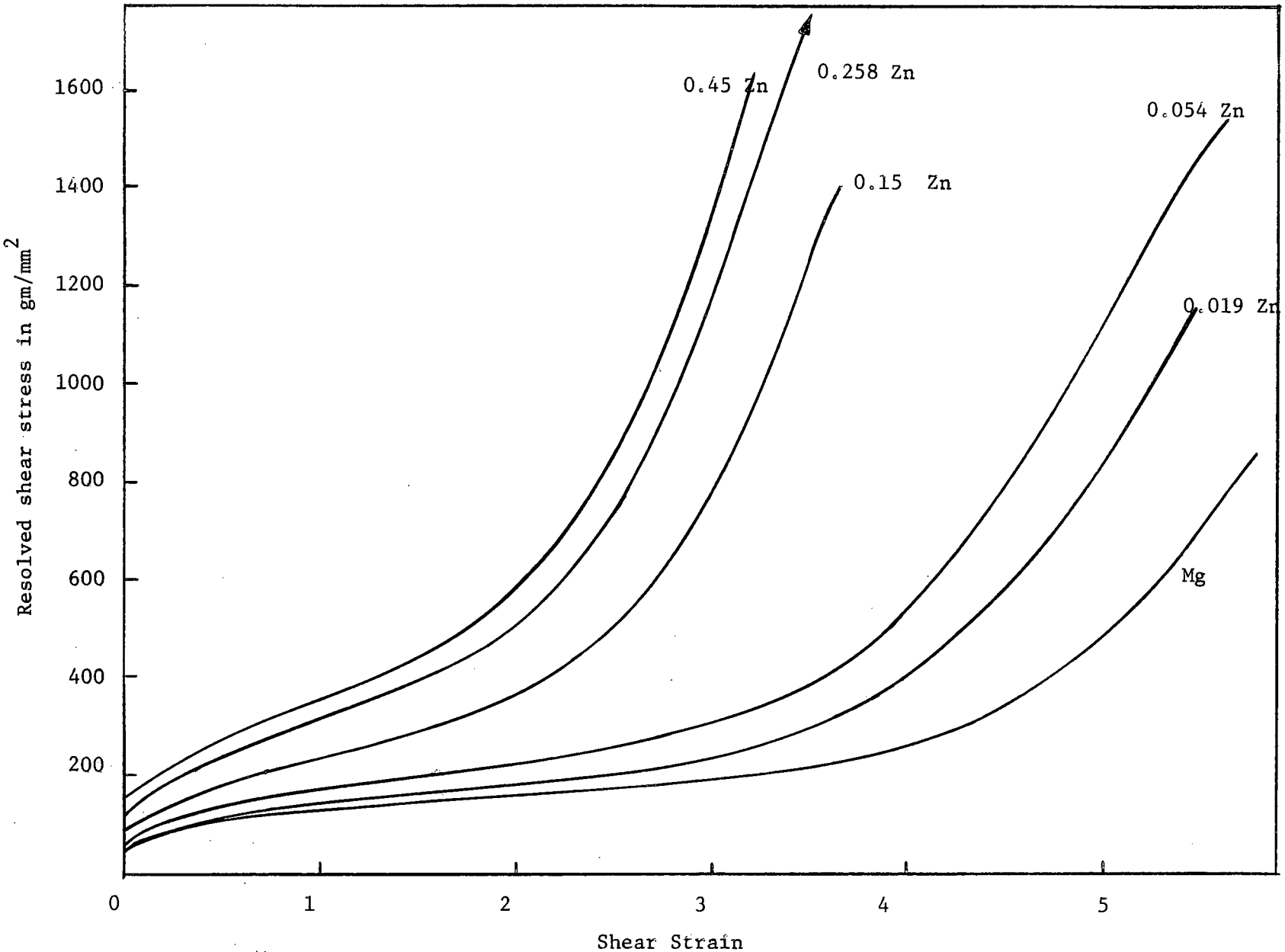

Fig. 45. Resolved shear stress vs. shear strain curves for Mg-Zn alloy single crystals deformed at 295°K.

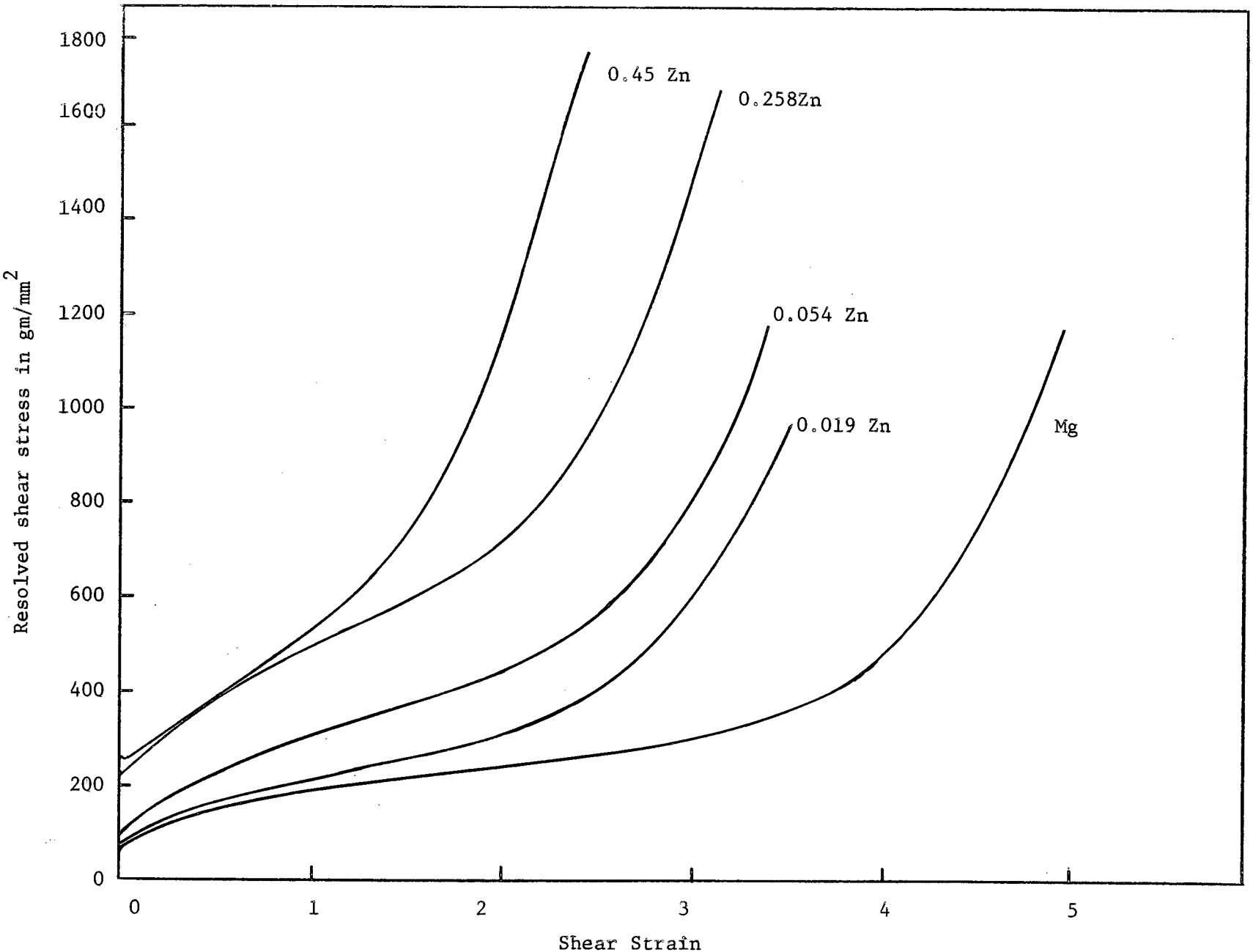

Fig. 46. Resolved shear stress vs. shear strain curves for Mg-Zn alloy single crystals deformed at 195°K.

curve remains smooth till fracture occurs.

2.2.5. The Critical Resolved Shear Stress:

The CRSS of Mg crystals are shown as functions of composition and testing temperature in fig. (47). Gross plastic flow was considered to begin at the first departure from linearity. Sometimes CRSS is obtained by the extrapolation of stage I to zero strain, however, such a procedure was not practical because of the "S" shape of the stress-strain curves.

It is clear from fig. (47) that the CRSS of Mg decreases linearly from 74 gm/mm^2 at 78°K to 41 gm/mm^2 at 330°K. Beyond 330°K the CRSS remains essentially independent of temperature, varying slightly due to a change in shear modulus with temperature. The present trend of the temperature dependence of CRSS in Mg is in agreement with the earlier findings[6,13,89].

The strengthening effect of Zn on Mg is seen to be strongly dependent on temperature. For example, the difference in CRSS between pure Mg and 0.258 at.% Zn crystal tested at 78°K is approximately 4-5 times higher than that at room temperature and above.

It is interesting to note that beyond 330°K, the alloys containing Zn in amounts up to 0.02 at.% have the same CRSS as that of Mg. However, the same alloys when tested at 78°K show a substantial increase in CRSS over that of Mg.

The strengthening effect of Zn as a function of the solute concentration is shown in fig. (48) for various testing temperatures. The data at 0°K have been obtained by the extrapolation of the curves in fig. (47) to absolute zero. It is apparent from fig. (48) that the strengthening effect of the solute on Mg is not a simple linear function of the solute

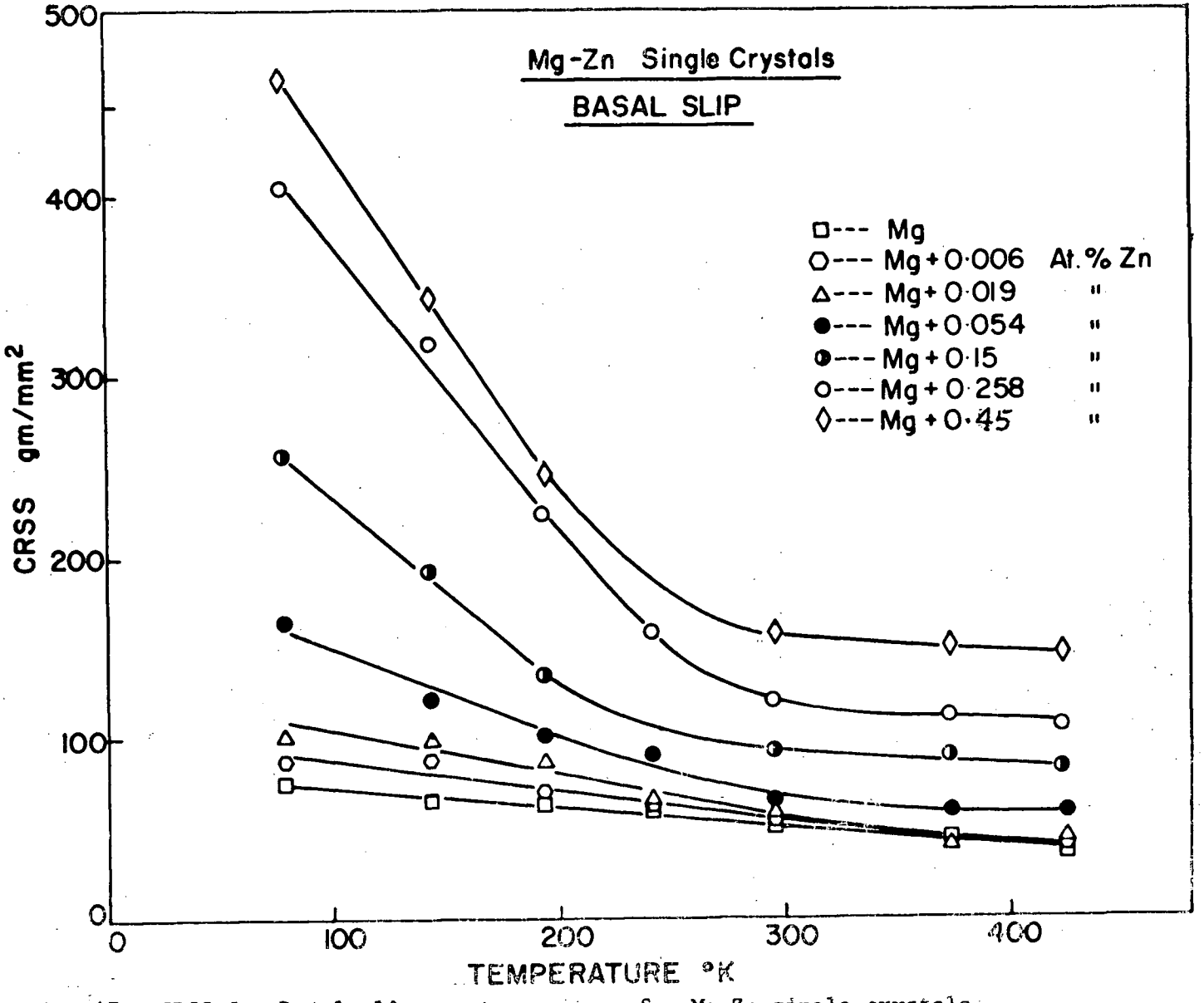

Fig. 47. CRSS for basal slip vs. temperature for Mg-Zn single crystals.

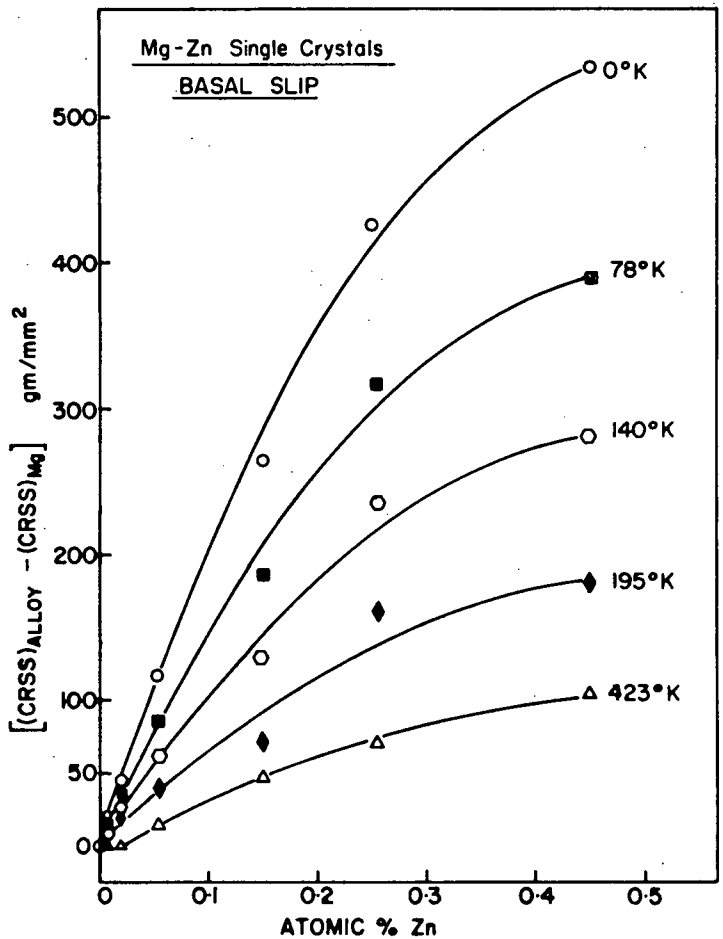

Fig. 48. Solution strengthening in basal slip vs. concentration for Mg-Zn alloys.

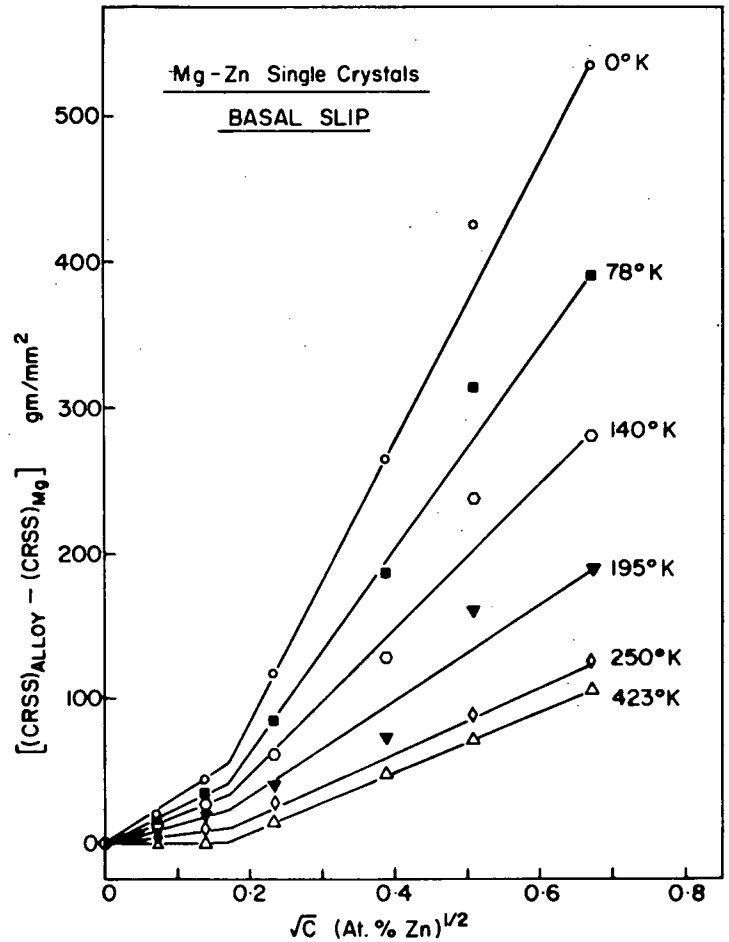

Fig. 49. Solution strengthening in basal slip vs. square root of the solute concentration.

concentration as reported earlier by Levine, Sheely and Nash[74].

Fig. (49) shows a plot of the increase in CRSS of the alloy over that of magnesium against $C^{\frac{1}{2}}$, where C is the concentration of the solute in at.%. It is clear that the solution hardening occurs in two linear stages, I and II. Stage I continues up to a concentration of solute equal to 0.025 at.% Zn, followed by stage II which has a slope approximately 3 times higher than in stage I. The transition concentration from stage I to stage II is observed to be independent of temperature. The occurrence of a two stage solution hardening behaviour in the CRSS-$C^{\frac{1}{2}}$ plot similar to that in the present work has been recently reported in the dilute Ag-base (face centred cubic) solid solutions containing In solute[85].

2.2.6. The Rate of Solution Strengthening:

The non-linearity of solution hardening with respect to zinc concentrations makes it difficult to define a single parameter representing the strengthening rate over a range of compositions. However, solution hardening rate can be conveniently described by the slopes S_I and S_{II} of the two linear parts of the curves in fig. (49). It is important to note that the solution hardening rate at any solute concentration is related to the solute concentration and the corresponding slope of the CRSS-$C^{\frac{1}{2}}$ curve as follows:

$$\left(\frac{\partial \tau}{\partial C}\right)_C = \frac{1}{2C^{\frac{1}{2}}} \cdot \frac{\partial \tau}{\partial C^{\frac{1}{2}}} = \frac{S}{2C^{\frac{1}{2}}} \qquad (1)$$

2.2.6.1. The Temperature Dependence of S_I:

The temperature dependence of S_I is shown in fig. (50). It is apparent that S_I decreases linearly from 316 gm/mm^2/(at.%)$^{\frac{1}{2}}$ at 0°K to zero at 330°K. In alloys containing solute up to 0.025 at.% Zn (i.e. stage I) no solution hardening is observed above 330°K. The critical resolved shear stresses of Mg and the alloys containing solute in amounts up to 0.025 at.% Zn become athermal at 330°K.

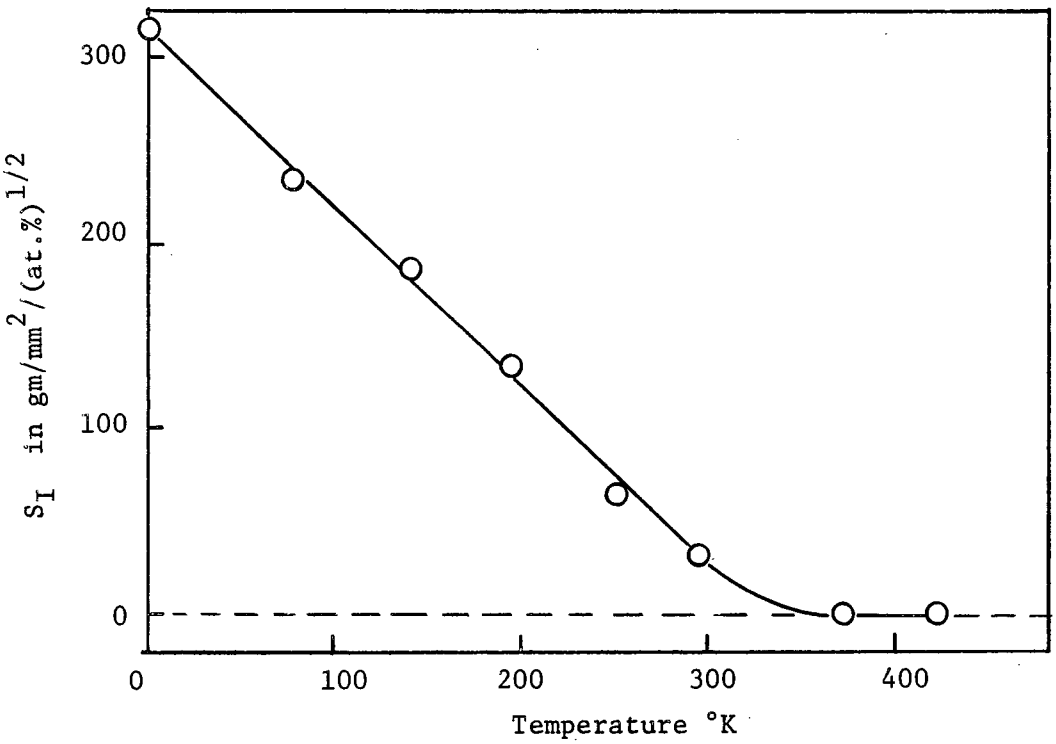

Fig. 50. The variation of the solution strengthening parameter S_I with temperature.

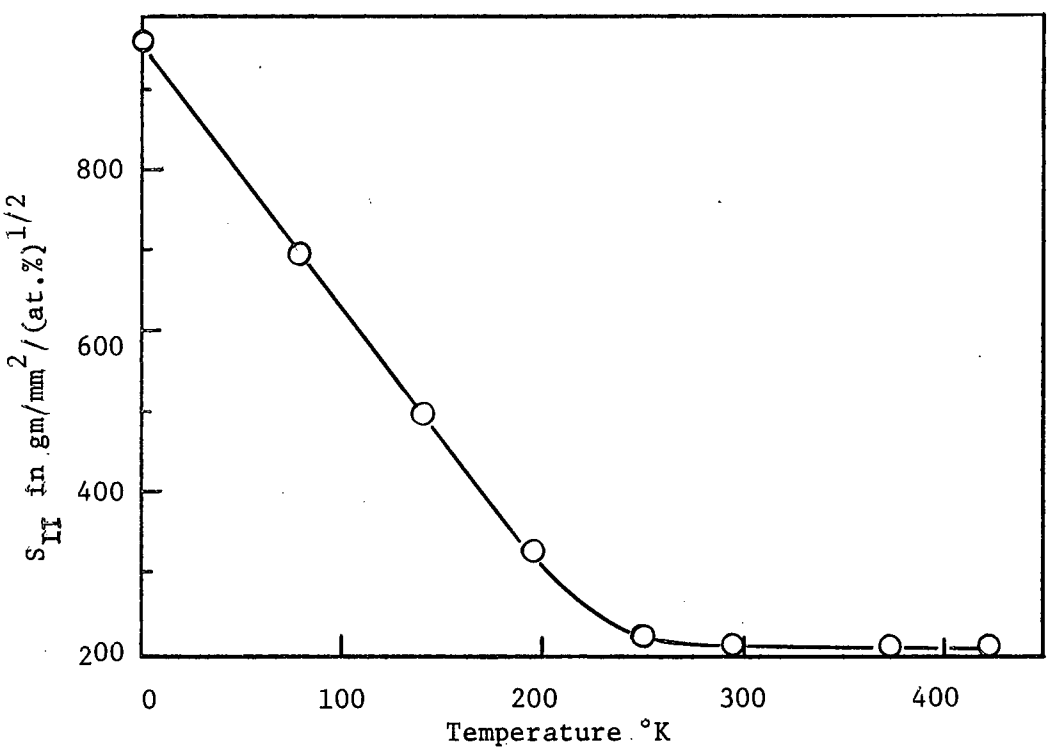

Fig. 51. The variation of the solution strengthening parameter S_{II} with temperature.

2.2.6.2. The Variation of S_{II} With Temperature:

The effect of temperature on S_{II} is shown in fig. (51). The solution hardening parameter decreases from 960 gm/mm^2 (at.%)$^{1/2}$ at 0°K to 225 gm/mm^2/(at.%Zn)$^{1/2}$ at 250°K. Beyond 250°K, S_{II} decreases very slightly with increasing temperature.

2.2.7. Work Hardening:

The work hardening parameters have been defined in an earlier section. The effect of solute on these quantities will be considered here. Because of the inconsistency in the work hardening parameters of Mg reported earlier in the literature, it was considered necessary to investigate the strain hardening behaviour of Mg over a range of temperatures.

2.2.7.1. The Work Hardening Rate in Stage A, θ_A:

The work hardening rate during stage A deformation, θ_A, is shown in fig. (52) as a function of composition and temperature. It is conventional to express the work hardening rate as θ/G where G is the shear modulus; however, in the absence of data relating to the concentration dependence of G, θ is reported here without taking G into account. In order to make comparison with other metals possible, θ/G values at a few selected temperatures and compositions are indicated in fig. (52). The values of shear modulus for this purpose have been taken from the work of Slutsky and Garland[86] and Koster[87].

The temperature dependence of θ_A for Mg is shown in fig. (53). The values of θ_A reported in the literature earlier are also included for comparison. The present results indicate that θ_A decreases rapidly

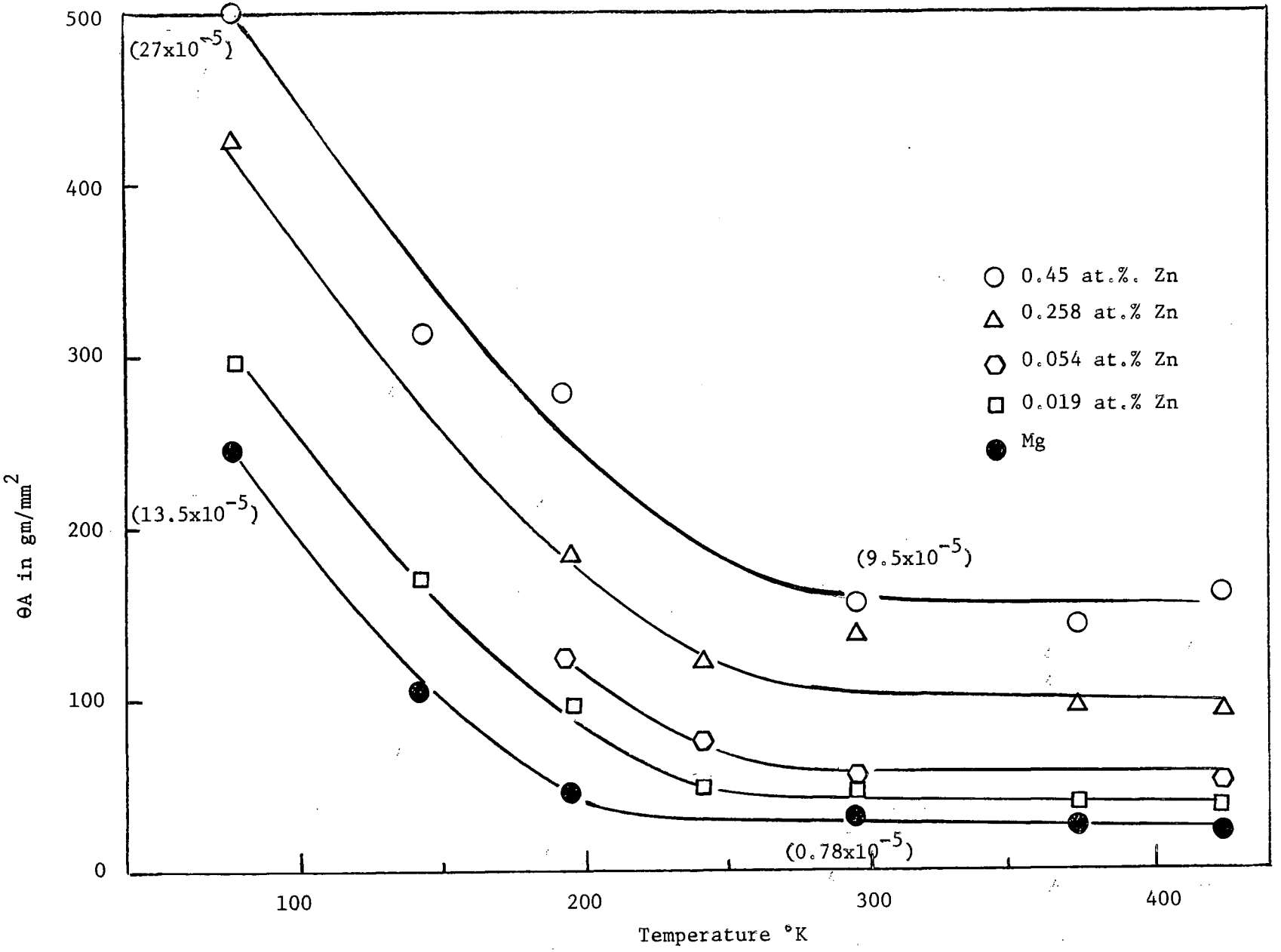

Fig. 52. The work hardening rate in stage A vs. temperature for Mg-Zn single crystals.

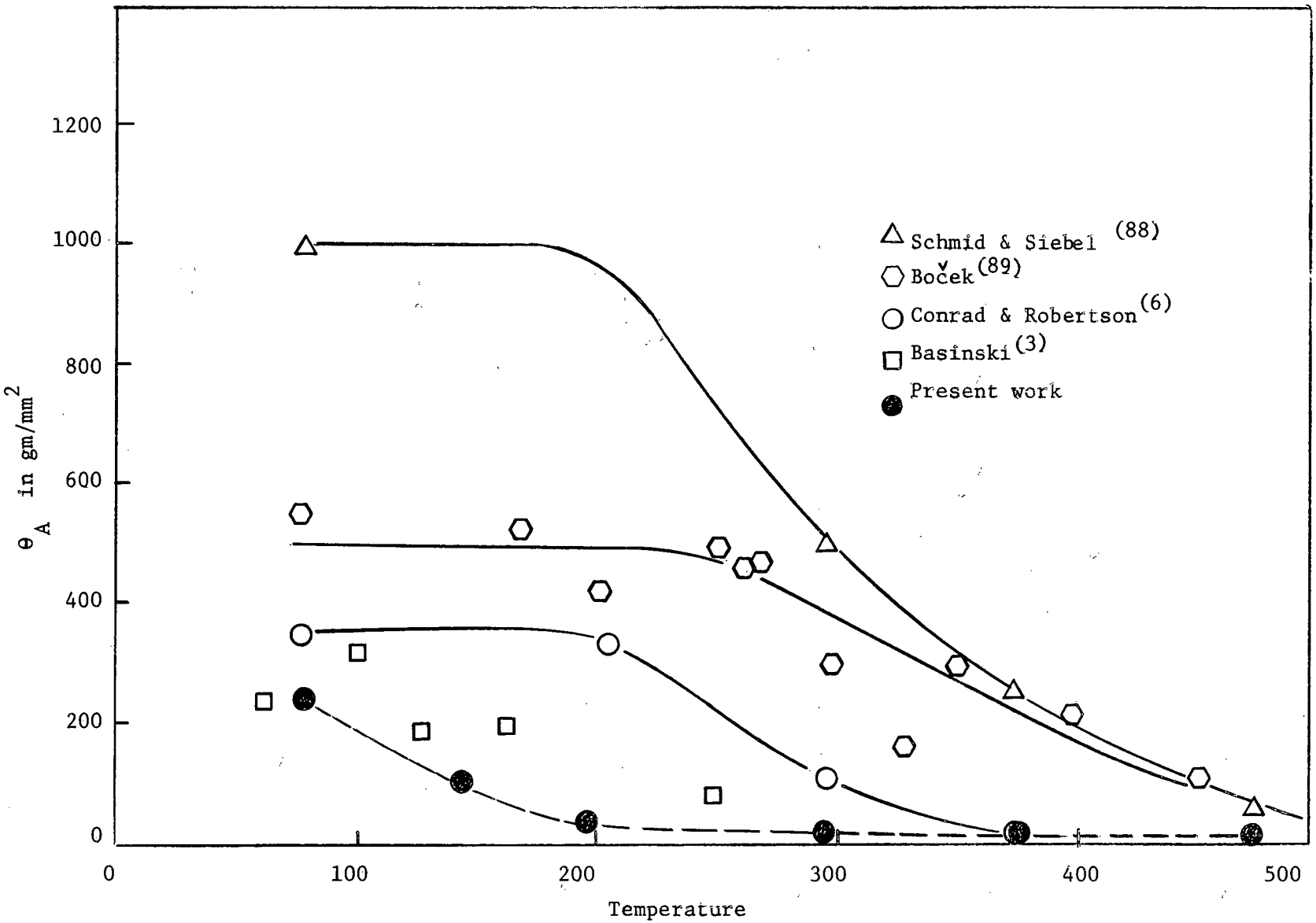

Fig. 53. The temperature dependence of the work hardening rate in the easy glide of Magnesium as reported by various workers.

with increasing temperature from a value of θ_A/G equal to 1.38×10^{-4} at 78°K to 1.07×10^{-5} at about 250°K. Beyond 250°K, however, θ_A/G remains independent of temperature. The large scatter in data[89] and the high values of θ_A reported earlier[88] may have been a result of the sub-boundaries, which are likely to be present in these crystals (because of the fast rate of growth used by these workers). The existence of a temperature insensitive θ_A below 200°K as reported by Schmid[88], Boček[89] and Conrad[6] is, however, surprising.

The concentration dependence of θ_A for the Mg-Zn alloys is shown in fig. (54) for a representative set of temperatures. These curves have been constructed by taking isothermal sections from fig. (52). It is clear that the work hardening rate increases in a parabolic fashion with increasing Zn content. The linear dependence of θ_A on $C^{1/2}$ is apparent from fig. (55).

2.2.7.2. The Extent of Easy Glide:

The strain at the end of easy glide, γ_B, is shown in fig. (56) as a function of temperature for a representative set of Mg-Zn alloys. In pure Mg, γ_B increases from approximately 230% shear strain at 78°K to 470% at room temperature. Beyond room temperature γ_B decreases with increasing temperature. Although the effect of Zn is to decrease γ_B, the trend in the temperature dependence of γ_B remains the same in the alloys as in Mg. A plot of the $\left[(\gamma_B)_{Mg} - (\gamma_B)_{alloy}\right]$ against solute concentration for different temperatures (fig. 57) indicates that the decrease in the extent of easy glide caused by alloying is independent of temperature between 195° - 373°K.

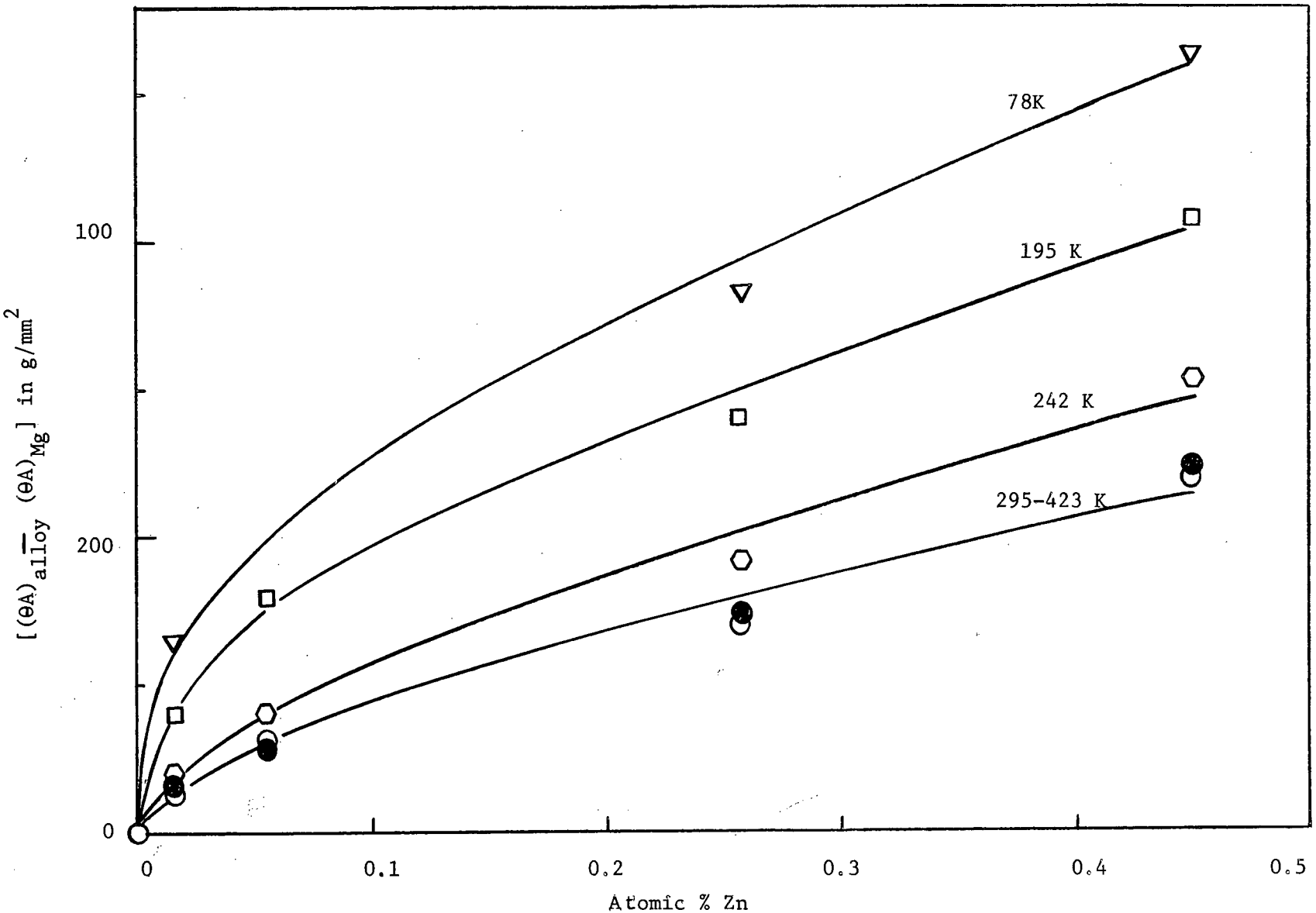

Fig. 54. The increase in work hardening rate in easy glide vs. Zn concentration.

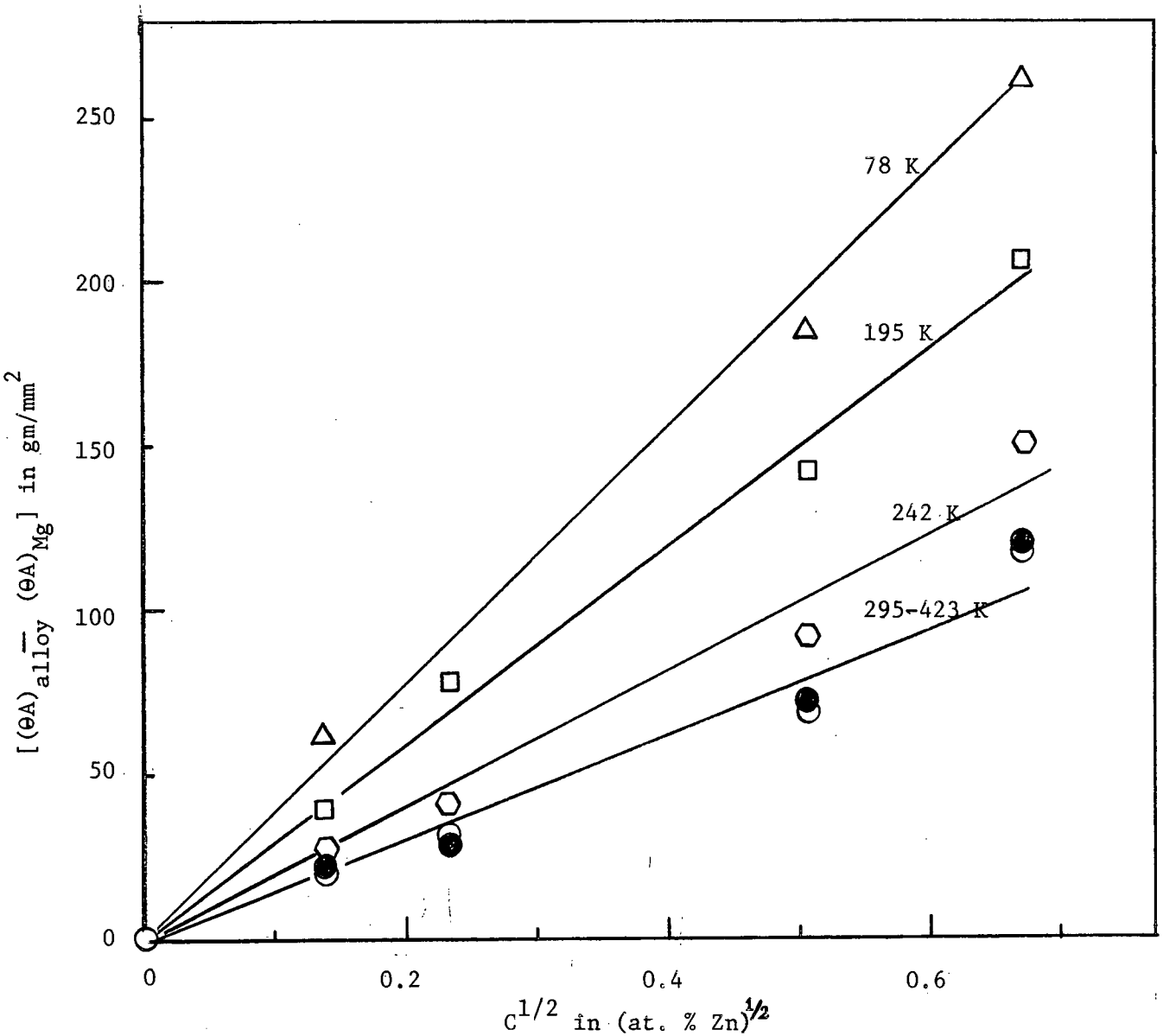

Fig.55. The increase in work hardening rate in easy glide vs. square root of the Zn concentration.

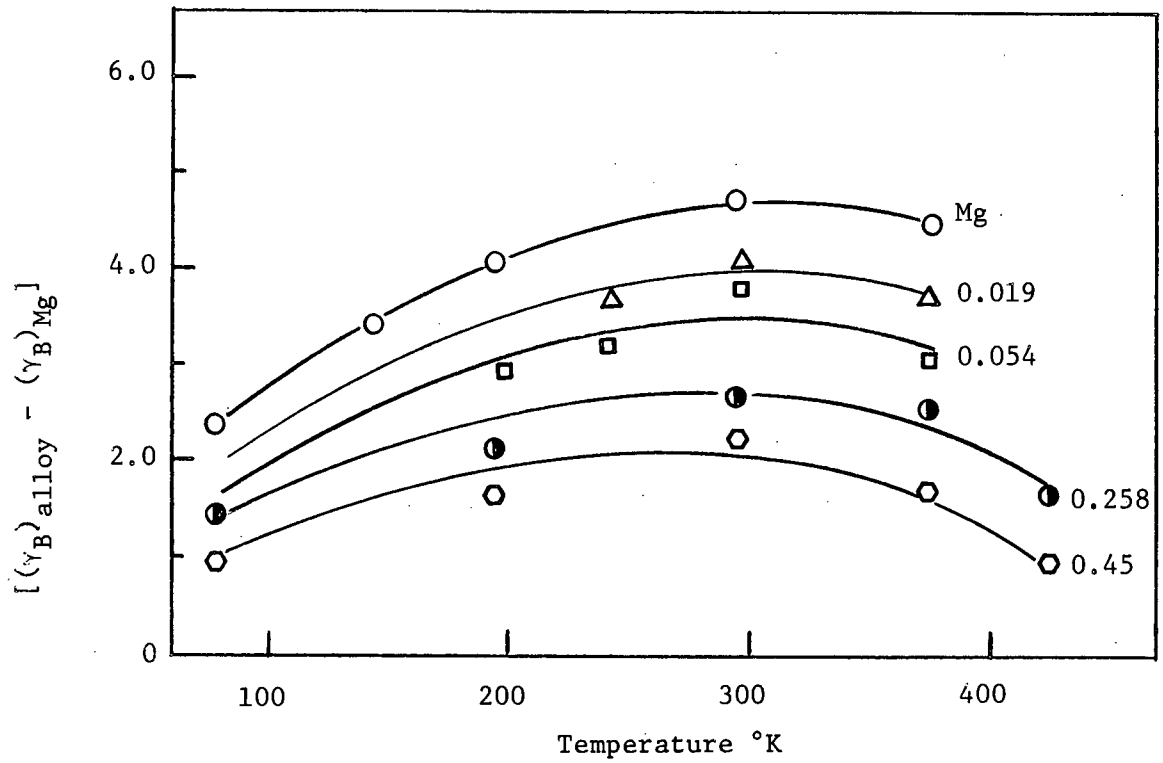

Fig. 56. The extent of easy glide as a function of temperature for Mg-Zn single crystals.

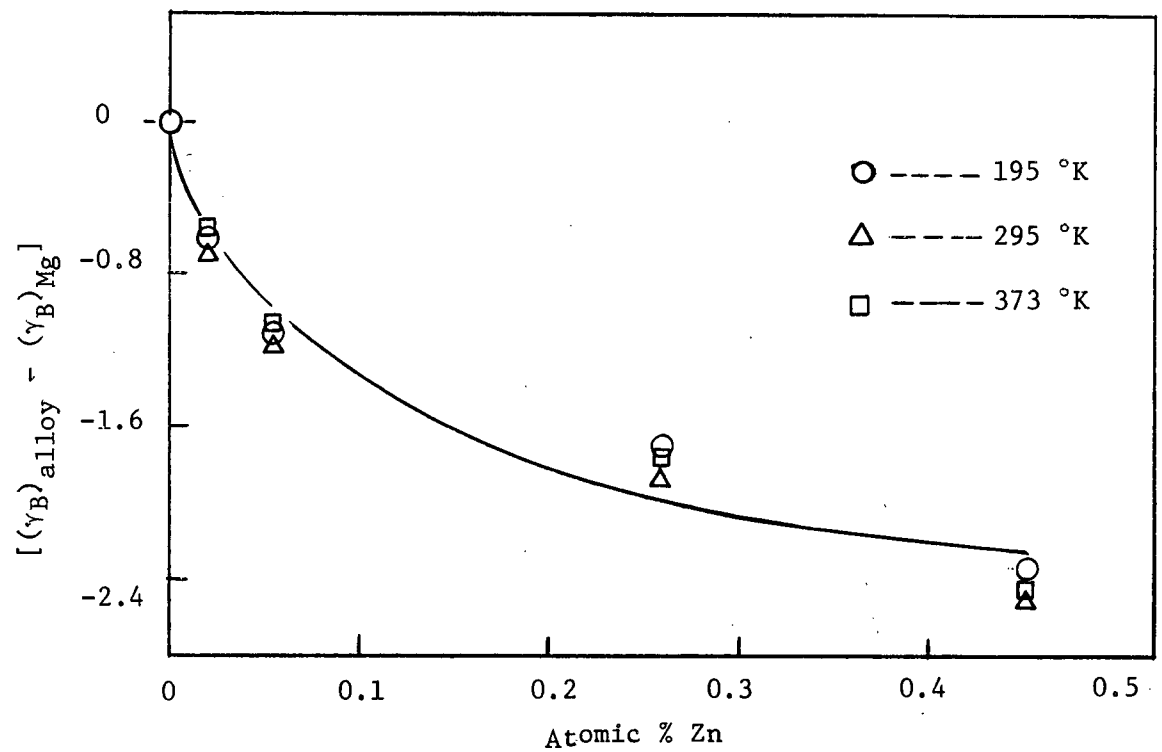

Fig. 57. The decrease in the extent of easy glide as a function of the solute concentration.

2.2.7.3. Stress at the Onset of Stage B, τ_B:

Stage B was considered to begin at a stress determined by the intersection of the extrapolated linear stages A and B. However, since stage B was not clearly defined below room temperature, the values of τ_B below room temperature are not reliable and hence will not be reported here.

The variation of τ_B with Zn concentration is shown in fig. (58). It is apparent that τ_B increases with increasing solute concentration. Also it is interesting to note that $[(\tau_B)_{alloy} - (\tau_B)_{Mg}]$ remains independent of temperature above 295°K for any fixed solute concentration.

2.2.7.4. The Work Hardening Rate in Stage B, θ_B:

For most of the crystals tested below room temperature, the work hardening rate in stage B was found to increase with strain till fracture occurred. Under such circumstances θ_B cannot be evaluated accurately. Therefore, the results of the tests conducted above room temperature will be presented here.

The temperature dependence of θ_B for Mg and four Mg-Zn alloys is shown in fig. (59). The work hardening rate θ_B decreases with increasing temperature.

The effect of alloying on θ_B is shown in fig. (60). It is apparent that the work hardening rate increases in a near parabolic manner with increasing Zn content and that the effect is more pronounced the lower the temperature.

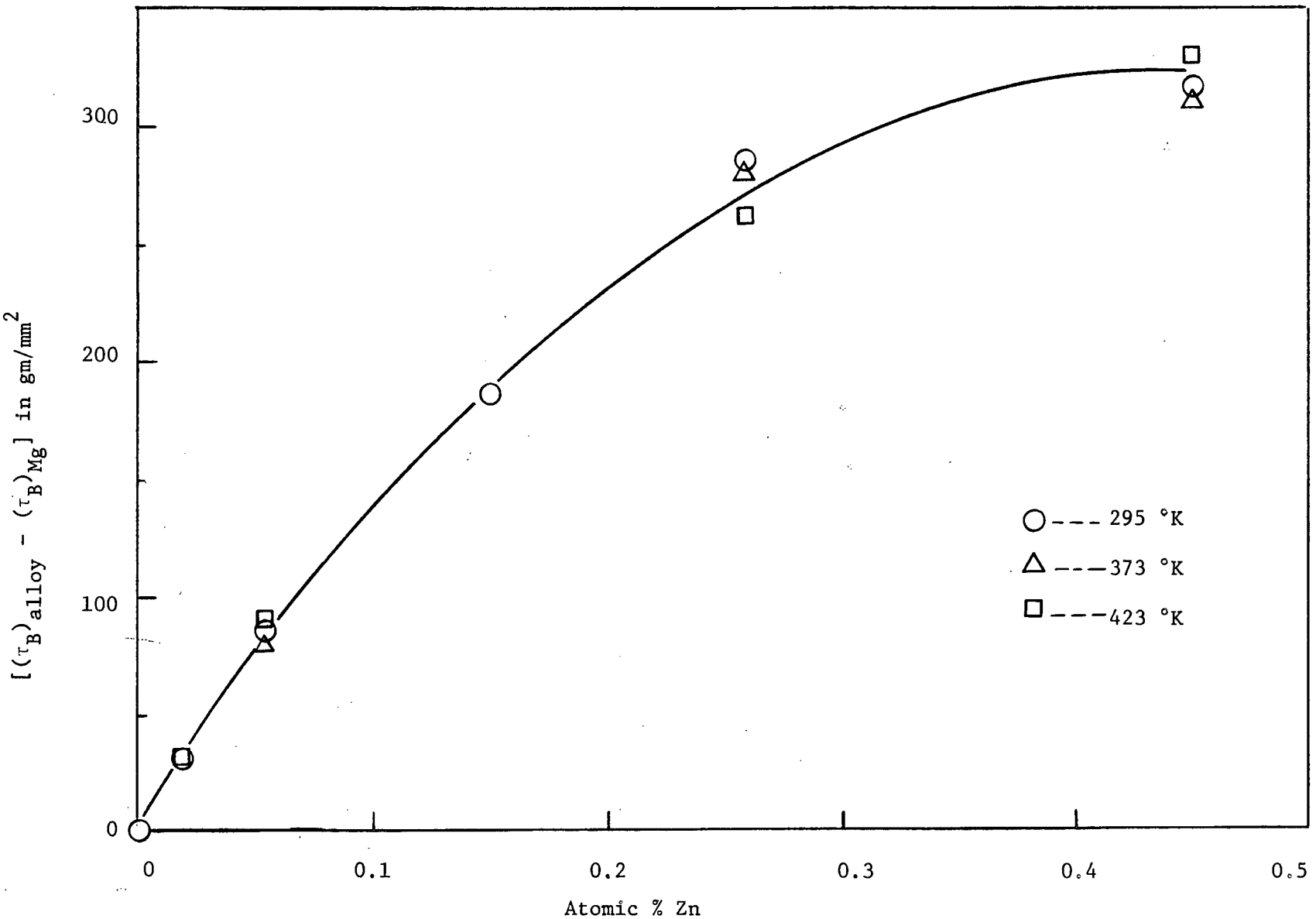

Fig. 58. The effect of temperature and solute concentration on the stress at the onset of Stage B.

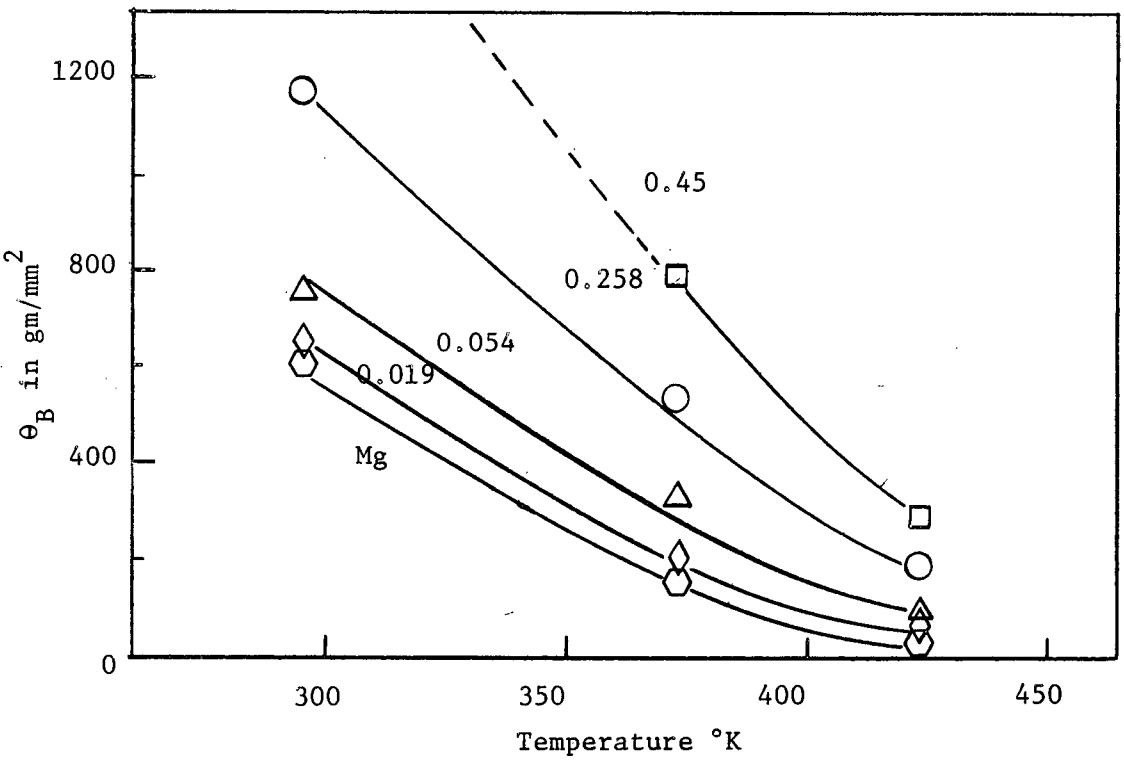

Fig. 59. The effect of temperature on the work hardening rate of Mg-Zn crystals in Stage B.

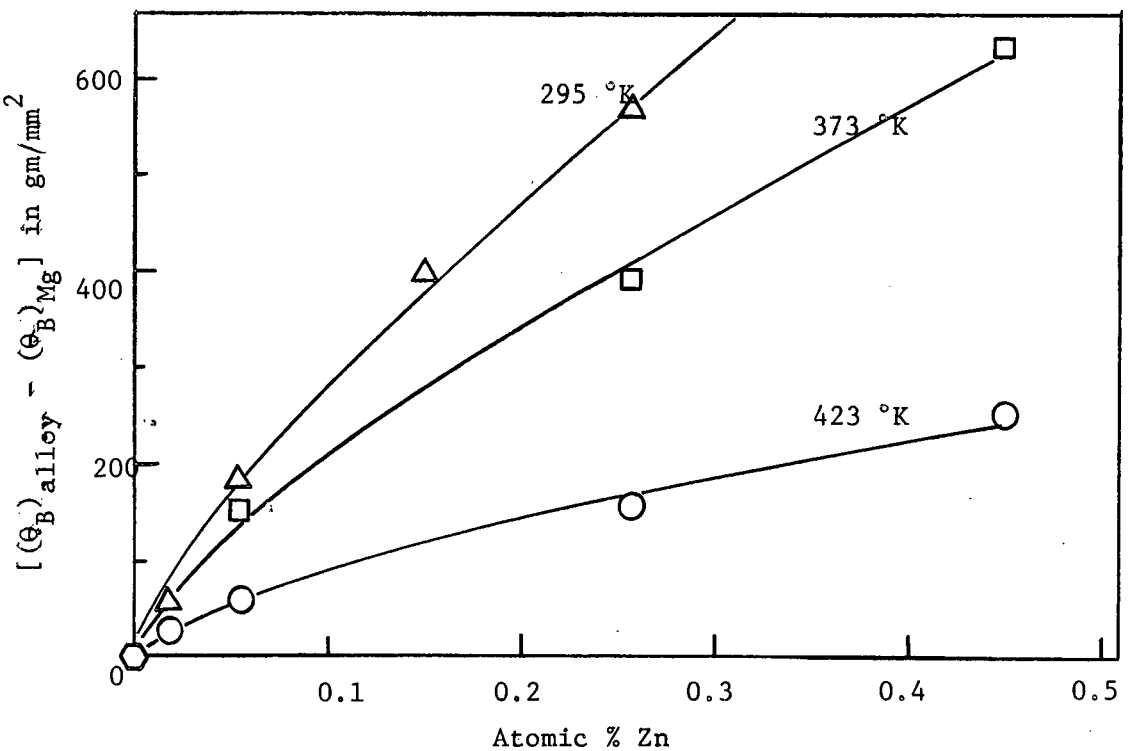

Fig. 60. The increase in the work hardening rate in Stage B vs. Zn concentration.

2.2.7.5. Deformation in Stage "C":

Stage C immediately follows the stage B, and is characterised by a decreasing work hardening rate with increasing strain. Stage C was clearly observed above room temperature only.

The stress corresponding to the first deviation from linearity at the end of stage B will be termed τ_C. The variation of τ_C with Zn concentration is shown in fig. (61) for 373°K and 423°K. It is observed that τ_C increases with alloying in a near parabolic manner.

2.3. THE EFFECT OF SOLUTE ON THE DISLOCATION DENSITIES:

It has been pointed out by Seeger[75] that solution hardening is possible in close packed structures, as a result of a change in the dislocation density through the presence of a solute. This indirect hardening effect is thought to be most pronounced at low solute concentrations, especially when the difference in size between the solvent and the solute is large[90,91]. Bearing in mind that the difference in size between Mg and Zn is large and that the alloys investigated in this work contain low concentrations of the solute, an examination of the dislocation densities in these alloys deserves attention.

There are two ways possible through which strengthening may be achieved due to an increase in dislocation density. The glide dislocation density may increase leading to an increase in the long range stress field i.e. the athermal component being affected. Alternatively, or simultaneously, the forest dislocation density may vary thereby changing the short range dislocation-dislocation interaction leading to a change in the thermally activated component of the flow stress.

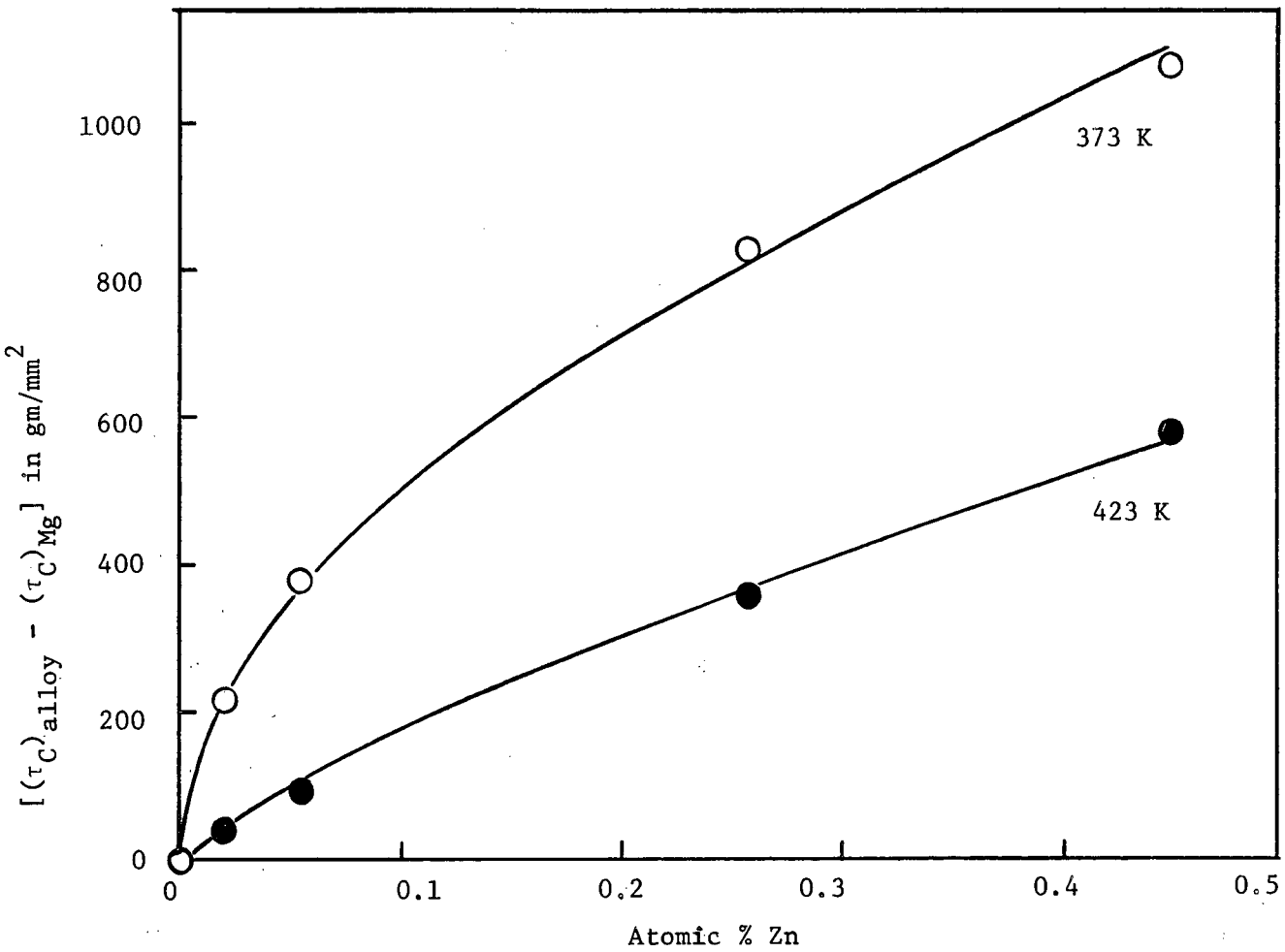

Fig. 61. The stress at the onset of Stage C vs. Zn concentration.

In the face centred cubic structures a knowledge of the dislocation density on the glide plane provides information on the forest dislocation spacing as well, since the glide dislocation and the forest dislocations lie on crystallographically similar planes. However, differences are to be expected in hexagonal metals, because the two sets of dislocations are not contained on crystallographically similar planes. Thus it has been decided to examine the two sets of dislocations independently of one another.

2.3.1. The Basal Dislocation Density:

Transmission electron microscopy of thin foils has been used in the present investigation to measure the basal dislocation density.

There exists considerable controversy in the literature concerning the degree to which dislocation arrangements observed in thin foils are representative of the bulk material[92-94]. It is believed that the degree of rearrangement due to stress relaxation increases, the higher the stacking fault energy. In fact, experiments on Al-Ag solid solutions[95] have revealed that more than 60% of the dislocations are lost during the process of thinning.

In the present study the easy glide plane {0001} was kept parallel to the foil surface, thus lowering the probability of losing dislocations through cross-slip. This foil orientation has been used earlier by Hirsch and Lally[29] in examining the variation of dislocation density as a function of deformation in magnesium. Through the examination of a carefully chosen set of nonbasal sections, these authors have come to the conclusion that the arrangement and densities of dislocations in the basal sections are typical of the bulk material.

2.3.1.1. Foil Preparation:

Considerable difficulty was encountered in obtaining foils, free from oxide film, of the Mg-Zn alloys. Therefore, it was decided to study Mg-Al crystals instead, at a comparable concentration level. The choice of Al as solute was mainly due to the large size difference between Mg and Al atoms, which is comparable to that between Mg and Zn. The distribution coefficients of the two alloy systems at low concentration levels are also comparable.

The foils were prepared by the chemical polishing of 0.1" crystal sections parallel to the {0001} plane. The polishing solution consisted of 10% nitric acid in water. Shallow cavities were created on each face of the slice by impinging a jet of acid-water mixture. The final thinning was done by immersing the specimen in the centre of a beaker containing the thinning solution. Perforations were seen first at the cavities. The narrow region between two perforations was found most suitable for the electron microscopy work.

2.3.1.2. Observations:

A representative portion of the dislocation structure in Mg is shown in fig. (62). The main features are the long dislocation dipoles at A, B and C. The presence of unidentified dark particles in the electron micrographs of Mg have been reported earlier[29]. In the present work such particles have been observed in varying amounts in all specimens (fig. (62)) and are often surrounded by dislocation loops. On tilting the specimen the dislocations go out of contrast but the dark spots remain in contrast suggesting them to be particles. However, their size was too small for identification using selected area diffraction. A

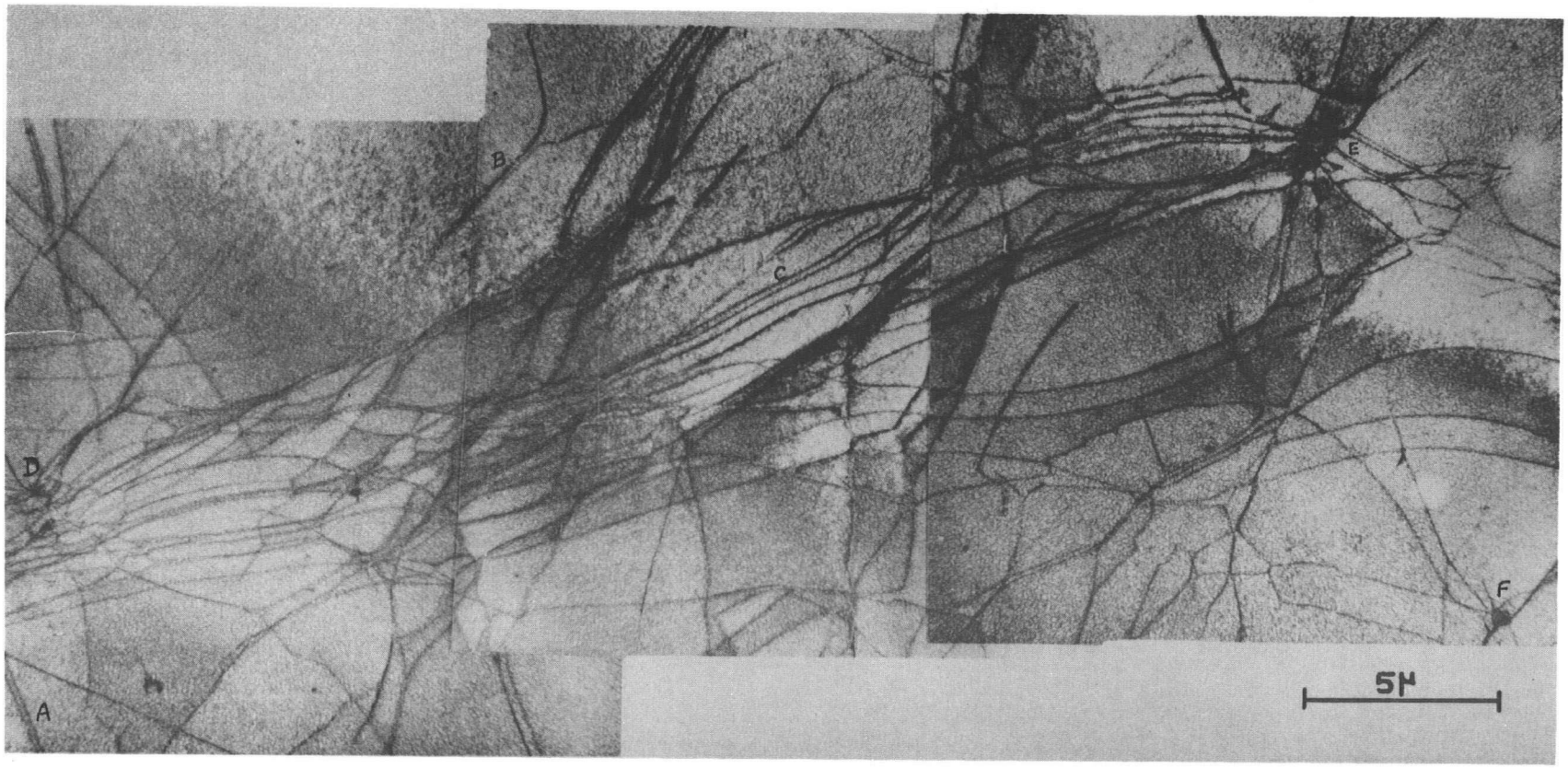

Fig. 62. Typical dislocation structure in as grown Mg crystals. Foil parallel to {0001} plane. Note particles at D, E, and F, and the high density of dipoles.

higher magnification micrograph of such a particle and the sourrounding dislocations is shown in fig. (63). Sometimes these particles have been observed to emit dislocation spirals under the heat of the electron beam.

Typical dislocation structures in alloys containing 0.18 at.% and 0.36 at.% Al are shown in figs. (64) and (65) respectively. It is observed that the closely spaced dipoles become fewer, and the dislocations become more evenly distributed as the alloying content is increased.

2.3.1.3. The Technique of Dislocation Density Measurement and its Limitations:

A modification of the random line intersection method[97,98] of Ham was used in the present work. The random lines consisted of six circles with random centres drawn on a transparent template.

The observed length of the dislocation line becomes the actual length (not a projection) if it is assumed that the dislocations run very nearly parallel to the basal plane. Under these conditions the dislocation density ρ_G will be given by

$$\rho_G = \pi N/(2Lt) \qquad (2)$$

where

N is the number of intersections of the random circles with the dislocation lines.

L is the total length of the circumference of the circles.

t is the thickness of the foil in the region under examination.

Much difficulty was encountered in determining the foil thickness. Because slip traces cannot be obtained in basal sections, the foil thickness had to be estimated by counting the number of the extinction

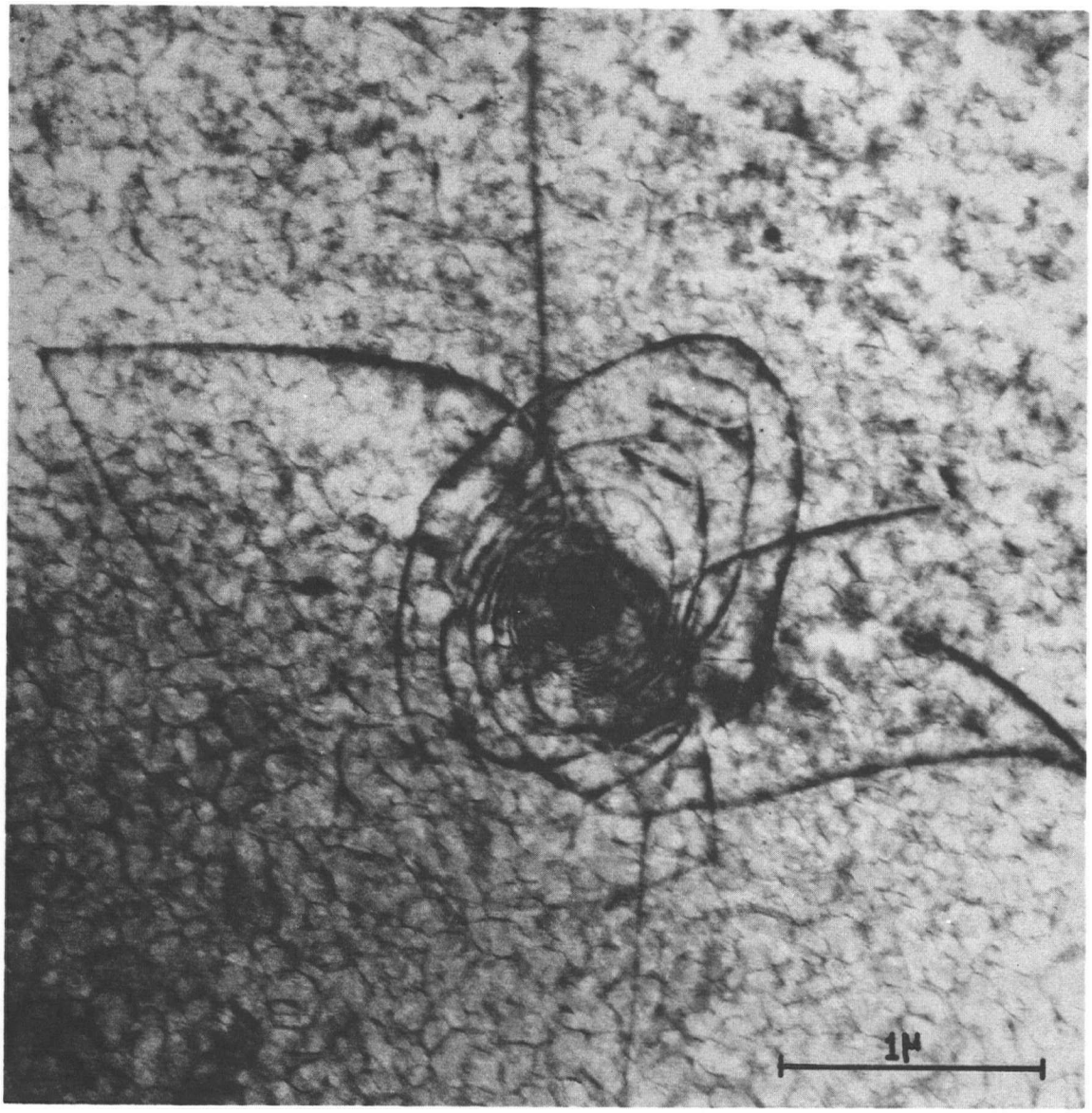

Fig. 63. Electron micrograph showing dislocations surrounding a particle.

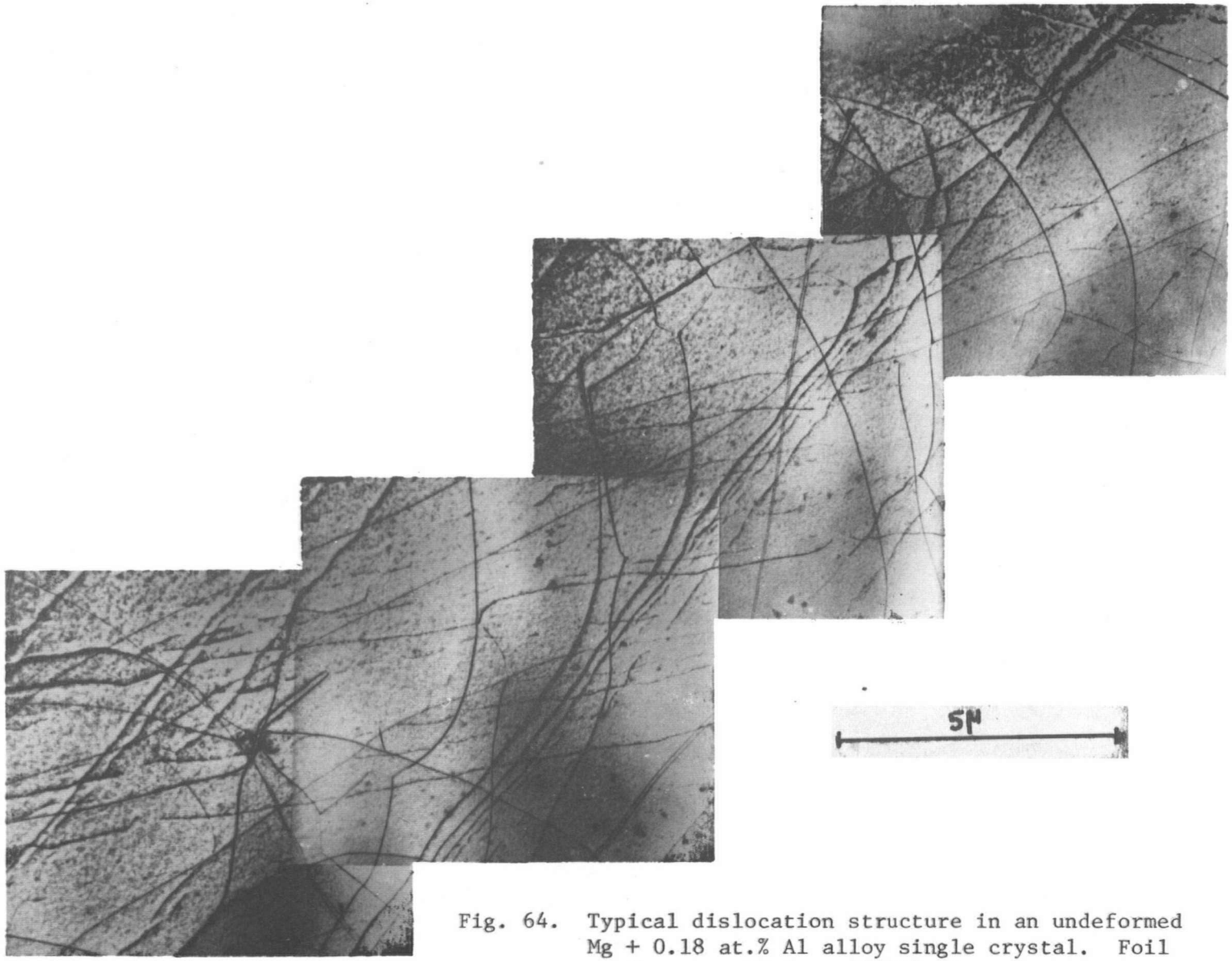

Fig. 64. Typical dislocation structure in an undeformed Mg + 0.18 at.% Al alloy single crystal. Foil surface parallel to {0001} plane.

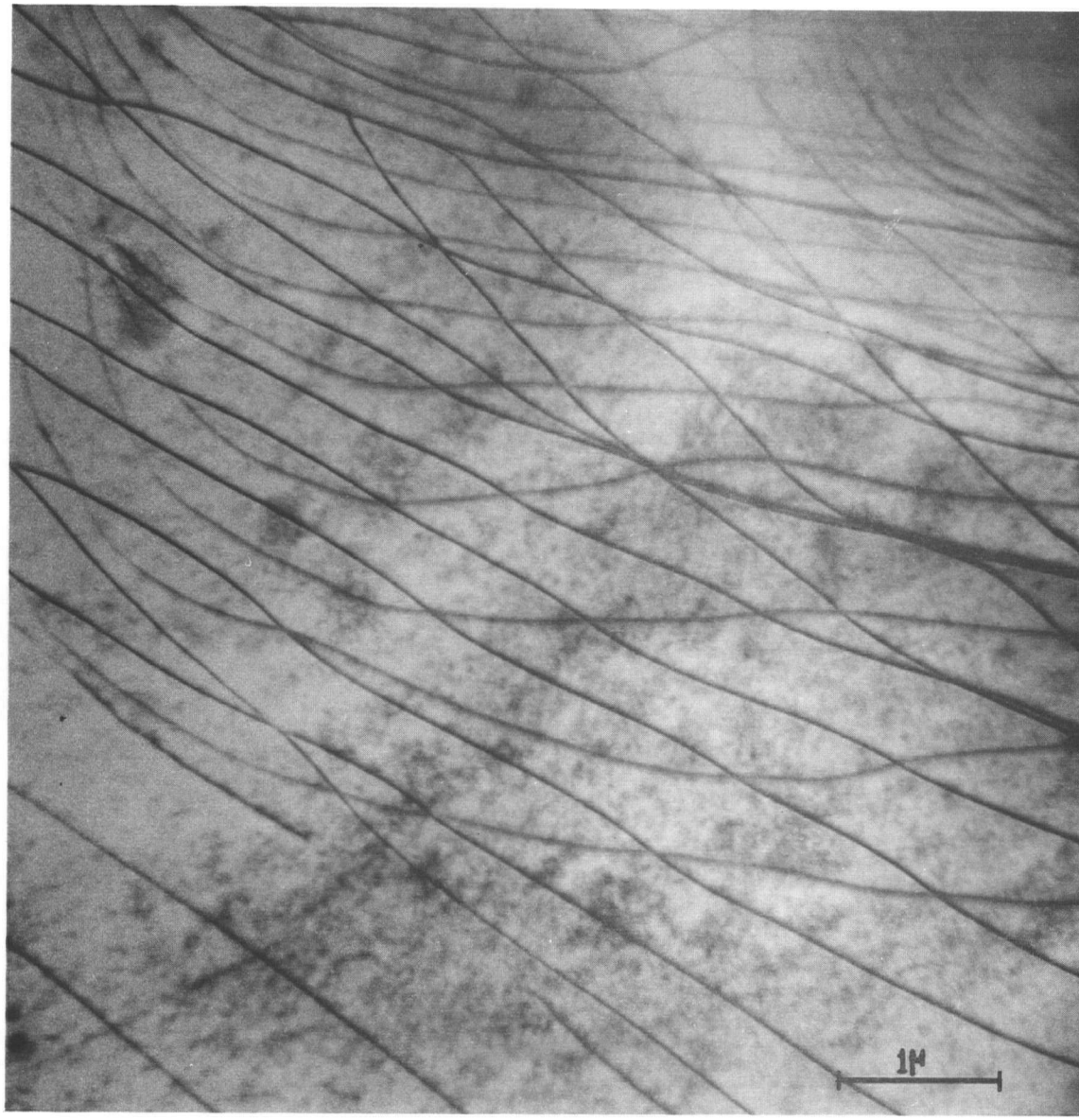

Fig. 65. Typical dislocation structure in an undeformed Mg + 0.38 at. % Al alloy single crystal. Foil parallel to {0001} plane.

fringes from the foil edge.

In order to obtain an average dislocation density, counts were made on at least three different areas on each specimen. The total random line length used on each specimen was at least 200 μ.

Burgers vectors of kind other than $\langle 11\bar{2}0 \rangle$ have never been observed in magnesium, neither have dislocations sharply inclined to the basal plane been seen[29]. Thus with the foil orientation chosen in the present work, all the dislocations were in contrast. This eliminated the need for correcting the measured density for dislocations out of contrast.

The number of short lengths of dislocations meeting the surface at closely separated points (indicating that they are inclined to the basal plane) was much smaller than the long segments lying in the basal plane, hence the measured density may be taken as the basal dislocation density.

2.3.1.4. The Effect of Solute on the Basal Dislocation Density:

In pure magnesium a density of 2.4×10^8 lines/cm^2 was observed, which is close to 2.2×10^8 reported earlier by Hirsch and Lally[29]. Tsui[96], however, has obtained a density of the order of $10^3 - 10^6$/cm^2 in Mg single crystals.

It is seen from a plot of ρ_G against $C^{\frac{1}{2}}$ in fig. (66) that the dislocation density increases in a parabolic manner with Al concentrations. Numerically ρ_G increases by a factor of three due to an addition of solute equal to 0.38 at.%.

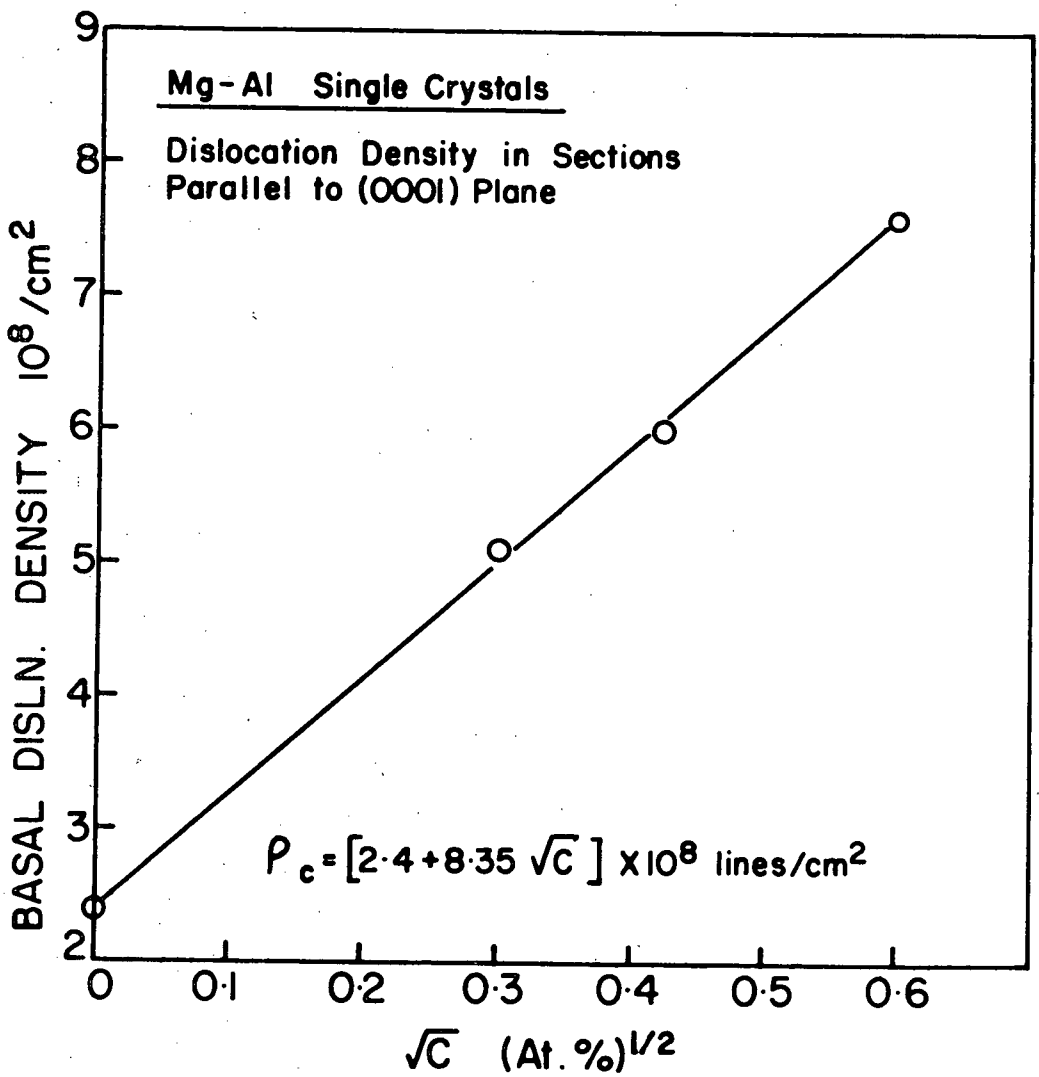

Fig. 66. Basal dislocation density vs. square root of solute concentration for Mg-Al alloys.

From the straight line plot of $C^{\frac{1}{2}}$ against ρ_G in fig. (66) the following relationship is obtained.

$$(\rho_G)_C = [2.4 + 8.35C^{\frac{1}{2}}] \times 10^8 \text{ lines /cm}^2 \qquad (3)$$

Assuming this relationship holds good up to the limit of solid solubility (1.6 at.%), the dislocation density in the highest alloy will be only 5 times higher than in Mg. This is in agreement with the earlier findings in fcc solid solutions that the dislocation density in the alloys is less than an order of magnitude higher than in the solvent pure metal[2].

2.3.2. The Forest Dislocation Density:

The forest dislocations were revealed by an etch pitting technique, which was developed in the course of the present investigation.

2.3.2.1. Crystal Orientation and the Pit Characteristics:

The {0001} plane of magnesium is the most suitable surface for etching, since it will not reveal the basal dislocations, whereas the nonbasal dislocations of edge character, which constitute the forest dislocations can be preferentially revealed. All screw dislocations will be parallel to the {0001} plane and hence will not be revealed by etching. Crystals of Mg and Mg-Zn alloys were spark eroded to obtain 0.1" thick slices parallel to the {0001} plane within 2 degrees. The spark damaged layer was removed by chemical polishing in 10% HNO_3 and the specimen was washed in ethanol and dried.

The etchant consisted of a 20% solution of HNO_3 in water and the etching was carried out by dipping the polished specimen for about 10 secs. in warm nitric acid solution kept at 30-35°C.

The etch pits obtained in this manner were circular in shape. Hexagon shaped etch pits were, however, produced by etching in a 30% HNO_3 solution maintained at room temperature. Such geometric shapes are characteristic of the dislocation etch pits. Some of the hexagon shaped pits are shown in fig. (67). For counting the number of dislocations, however, it was found convenient to use the circular pits.

The etched surfaces of a representative set of Mg-Zn alloys are shown in figs. (67(a),(b) and (c)).

2.3.2.2. The Study of Spark Erosion Damage in Mg Using the Dislocation Etch Pit Method:

In order to examine the damaging effect of spark erosion a sample was etched without removing the entire damaged layer. A micrograph of such a specimen is shown in fig. (68). It is apparent that small twins are formed at the edge of the specimen and the nonbasal edge dislocations can be seen at the twin boundaries. On further chemical polishing and subsequent etching the twins disappear, suggesting that they are confined to a narrow surface layer.

The etch pit density decreased till a surface layer approximately 150μ in thickness was removed from the surface. Below this depth the density remained constant.

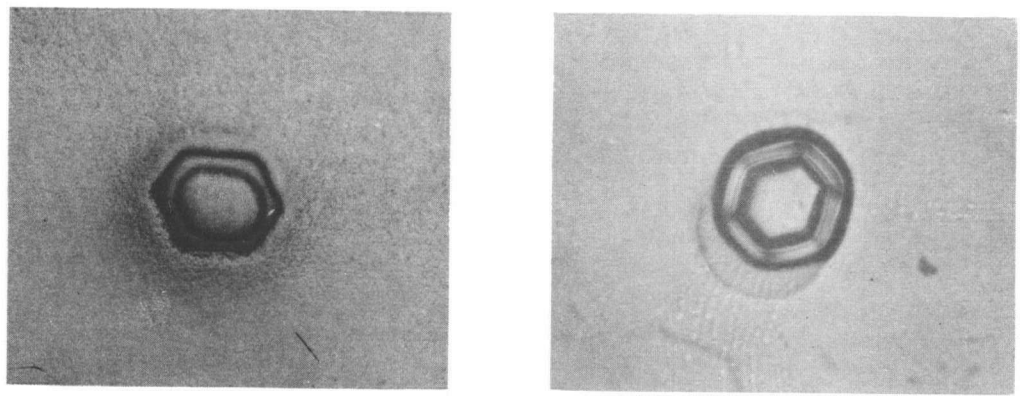

Fig. 67(a). Hexagonal shape of the etch pits.

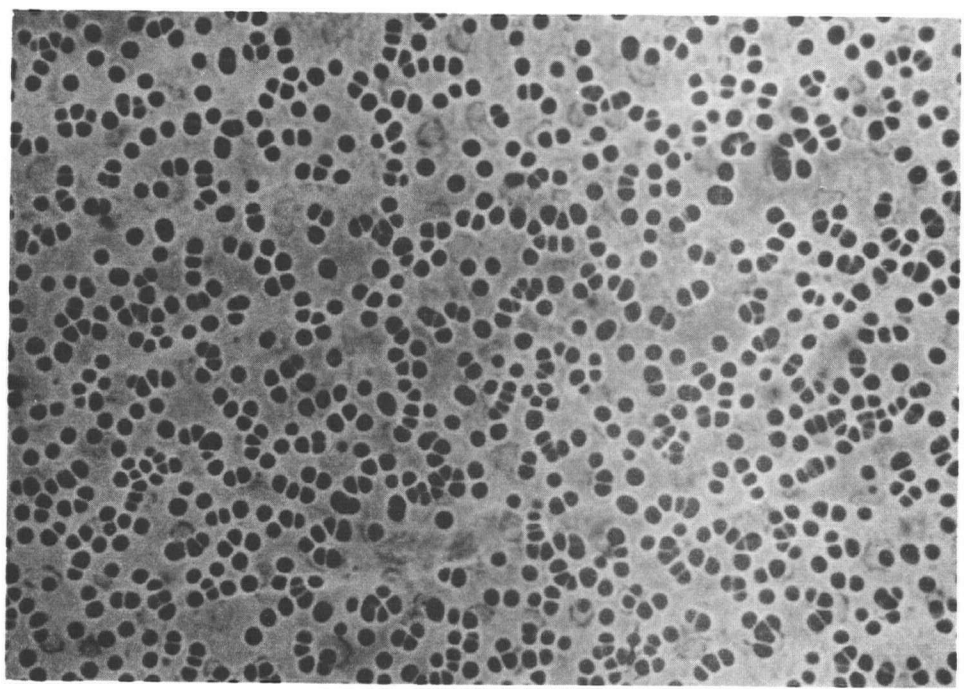

Fig. 67(b). Distribution of etch pits in a Mg + 0.019 at.% Zn alloy crystal. 84X.

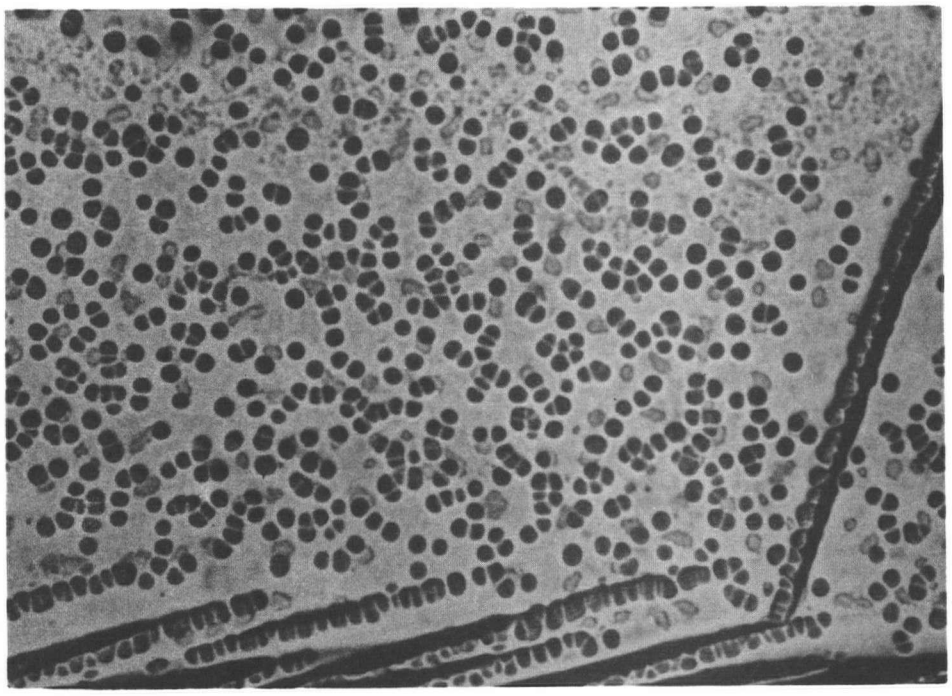

Fig. 68. Dislocation etch pits on the {0001} plane of Mg single crystal. Note non-basal edge dislocations at the twin boundaries. 75X

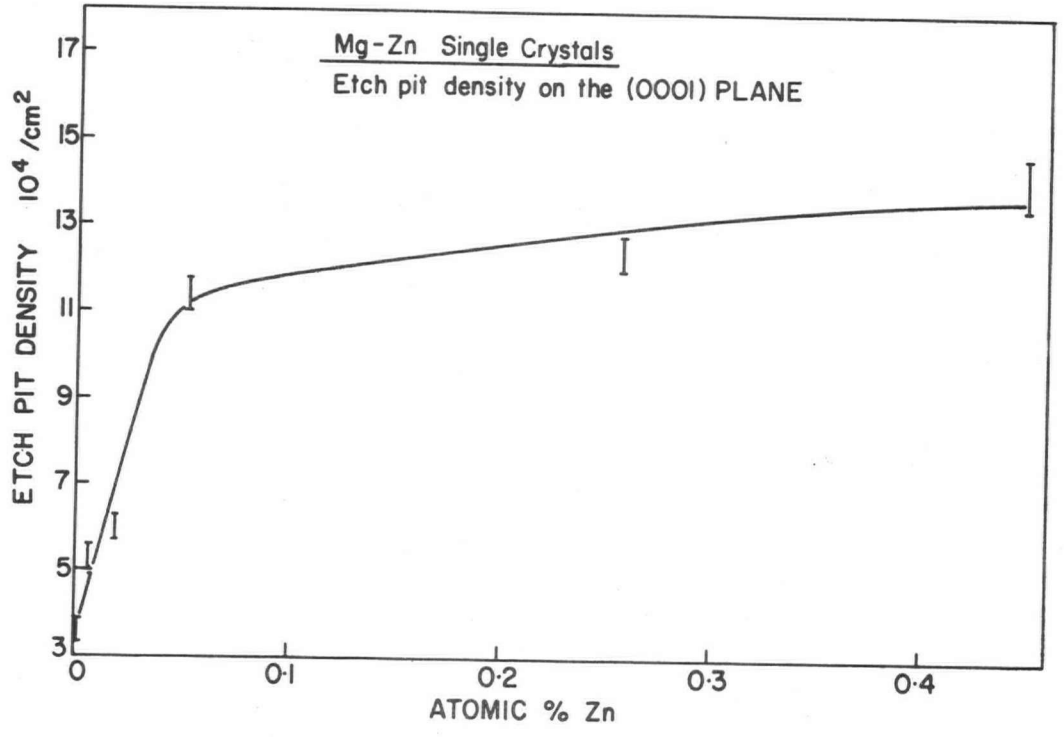

Fig. 69. Etch pit density vs. Zn concentration.

2.3.2.3. Variation of the Etch Pit Density with Alloying:

The concentration dependence of the number of etch pits per unit area is shown in fig. (69). In order to avoid local differences, counts were made at a magnification such that at least 800 pits were in the field of view at one time. Three different regions were examined on each specimen. The variation from specimen to specimen is shown in fig. (69) by the scatter bars.

It is apparent that the etch pit density increases rapidly with alloying up to approximately 0.05 at.% Zn, followed by a very slight increase up to 0.45 at.% Zn.

It is interesting to note that the etch pit density in magnesium is $3.5 \times 10^4/cm^2$. From activation volume measurements on the other hand Conrad[4] has arrived at a forest density of the order of $10^7 - 10^8/cm^2$. Transmission electron microscope studies on non-basal sections (basal plane almost parallel to foil normal) made by Hirsch and Lally[29], however, indicate that the forest dislocation density is unlikely to be as high as $10^8/cm^2$.

2.4. DISCUSSIONS:

Much progress has been made in the understanding of the solid solution strengthening mechanisms in metals after the development of the dislocation theory. Most of the important mechanisms of interaction were proposed within a few years after the study of the behaviour of dislocations in solid solutions had been undertaken.

In the past decade, however, the major problem has been the one of deciding which mechanisms are important in a given experimental situation and unravelling the contributions of the various mechanisms.

The results of the present study on Mg-Zn alloys are examined in the light of the various strengthening mechanisms, followed by a discussion of the effect of solute on the work hardening parameters of magnesium.

2.4.1. The Critical Resolved Shear Stress:

The CRSS of single crystals is perhaps the only satisfactory parameter which can be used for a quantitative comparison with the theoretical predictions without any adjustable parameters. In the case of polycrystalline aggregates such adjustable parameters become important, because of the constraining conditions imposed by the grain boundaries.

The experimental results can be best viewed against the background of the theory of temperature dependence of the flow stress as developed by Seeger[38] and Friedel[99]. According to this theory the applied stress can be considered as the sum of two components such that

$$\tau_{(T)} = \tau_G + \tau^* \qquad (4)$$

τ^* is referred to as the thermal component of the applied stress and is associated with short range obstacles which can be overcome with the aid of thermal energy.

τ_G is the athermal component that arises due to the long range elastic interactions such as those between parallel glide dislocations at distances large compared with b, the Burgers vector. Such obstacles cannot be overcome with the aid of thermal energy.

The consequence of Seeger's postulate is schematically shown in fig. (70), for the situation where the mechanism of yield does not change with temperature. τ_G varies with temperature only through a change in the shear modulus G such that τ_G/G becomes independent of temperature. Seeger has modified his definition of τ_G later to include a short range elastic interaction term[92].

The effect of solute on the two components of the CRSS will now be considered separately.

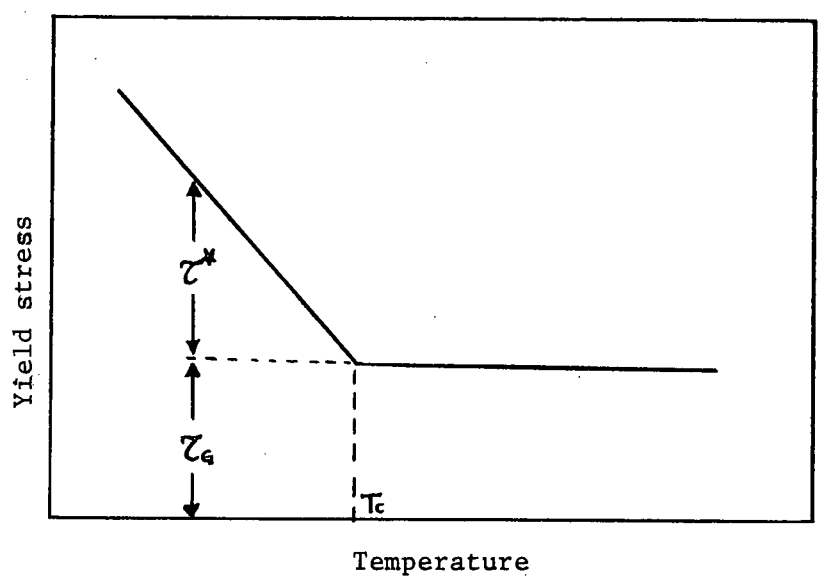

Fig. 70. The temperature dependence of yield in terms of the stress components (after Seeger[35]).

2.4.2. Solution Strengthening in the Athermal Region:

The critical resolved shear stresses of magnesium and its alloys containing Zn in amounts up to 0.45 at.% Zn become athermal above 330°K (fig. 47). It is apparent from fig.(49) that the addition of Zn in amounts up to 0.025 at.% has no effect on the CRSS of Mg above 330°K (i.e. $S_I = 0$), however, τ_G increases linearly with the square root of Zn concentration above 0.025 at.%. Another characterisitc feature of the solution hardening in the athermal region is the constancy of the strengthening parameter S_{II}.

As mentioned earlier τ_G is the stress required to overcome the long range obstalces in the crystal. The long range stress field can be affected by one or more of the following interactions involving the solute and the dislocations:

1) A change in the basal dislocation density.
2) Elastic interaction.
3) Chemical interaction.
4) Short range order.
5) Long range order.
6) Friction stress due to random distribution of solute.

Of these, the change in dislocation density is an indirect effect of solute leading to strengthening. The remaining five arise due to a direct interaction between the solute and the dislocation.

2.4.2.1. The Basal Dislocation Density:

Seeger[75] has shown that the long range stress field τ_G is related to the glide dislocation density ρ as follows:

$$\tau_G = \alpha\, b\, G \sqrt{\rho} \qquad (5)$$

where α is a constant,

b is the Burgers vector,

and G is the shear modulus in the slip direction.

The dislocation density of magnesium has been evaluated as a function of shear stress by Hirsch and Lally[29]. These authors came to the conclusion that the flow stress of Mg at room temperature (the thermally activated component of the flow stress is very small at room temperature and hence the CRSS may be taken to be equal to τ_G) can be related to the dislocation density by the following expression

$$\tau = \tau_o + 2.7 \times 10^{-3} \sqrt{\rho} \qquad (6)$$

where τ is the flow stress

and τ_o is a constant equal to 40 gm/mm^2.

It has been shown earlier in this thesis that the basal dislocation density can be expressed as a function of Al concentration by the relation

$$\rho_C = [2.4 + 8.35 \sqrt{C}] \times 10^8 \text{ cm}^{-2} \qquad (3)$$

where C is the concentration of solute. The subscript G has been dropped for convenience.

Combining equations (6) and (3)

$$\Delta\tau = 40.5 \left[1 - \sqrt{1+3.48\ C^{\frac{1}{2}}} \right] \qquad (7)$$

where $\Delta\tau$ is the strengthening at a concentration C.

The values of $\Delta\tau$ obtained using equation (7) are plotted in fig. (71) along with the experimental results of Sheely, Levine and Nash[74] on the CRSS of Mg-Al alloys tested at room temperature. It is seen that equation (7) gives a constantly increasing value of τ_G with solute concentration. However, the present results have established that τ_G remains unaffected in Mg-Zn alloys upto a certain minimum concentration of solute. Also earlier in this thesis it has been shown that this concentration independence of τ_G is common to a host of Mg-solid solutions including the Mg-Al alloys. Thus at low solute concentrations equation (7) is a poor description of the effect of solute, and it is apparent that at higher solute concentrations the predicted values of τ_G are far smaller than those observed experimentally.

It should be noted here that ρ in equation (6) comprises the grown in dislocations plus those generated due to work hardening, whereas equation (3) describes only the grown in dislocation density variation due to solution effect. Thus, whereas in the former case dislocation-dislocation interaction is a contributing factor, it is absent in the latter case. In view of this fact the combination of equations (6) and (3) to yield equation (7) is not fully justified. However, equation (7) will be considered as a close approximation for the sake of comparison with the experimental results.

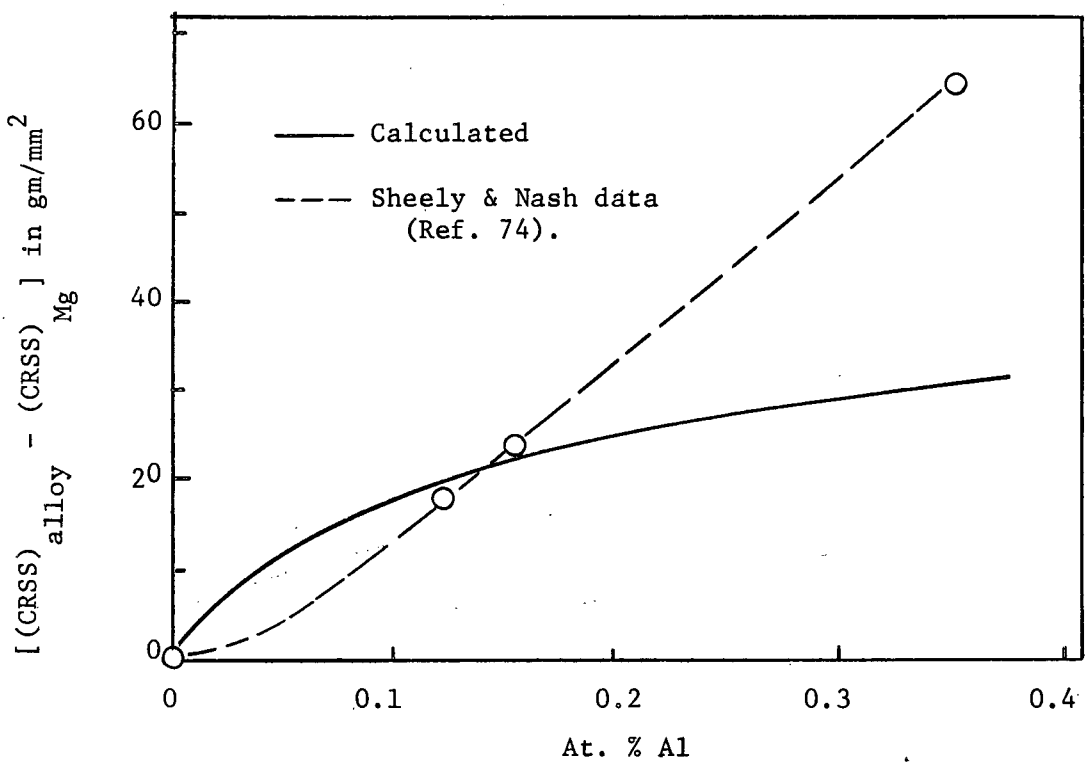

Fig. 71. Comparison of the observed solution strengthening with that expected from the increase in the basal dislocation density.

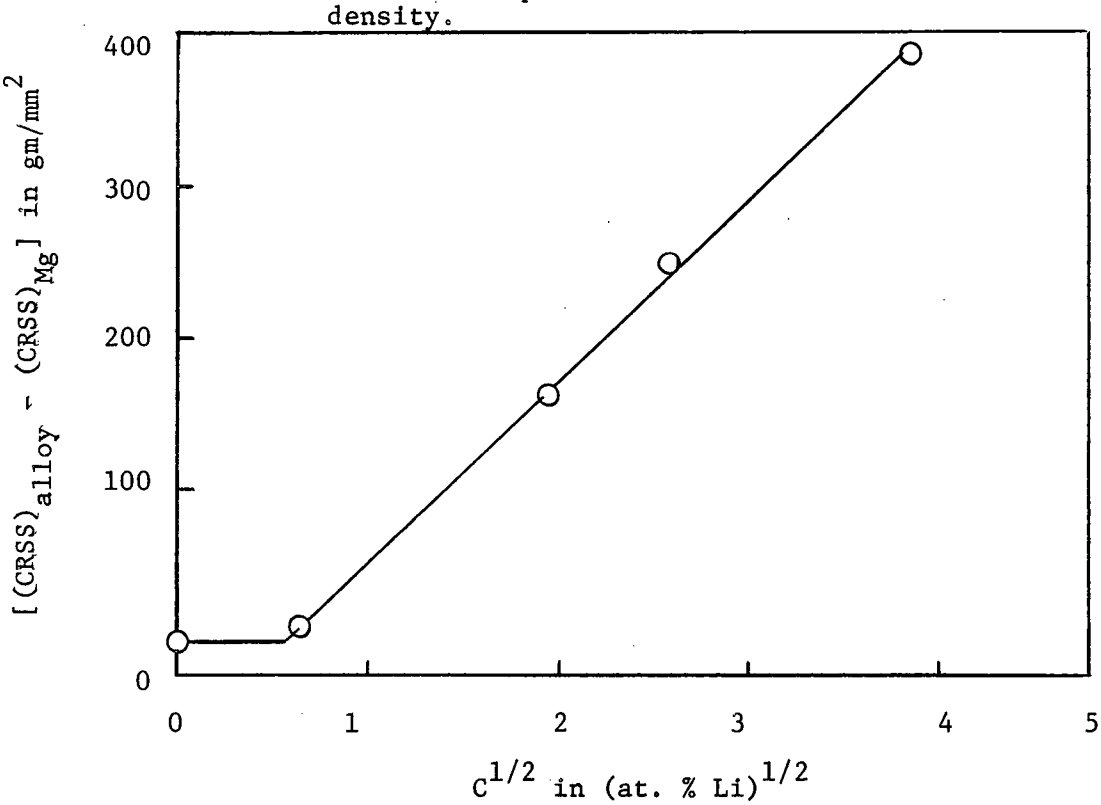

Fig. 72. The increase in CRSS of Mg vs (Li concentration)$^{1/2}$ in Mg-Li alloy single crystals (Data from Horiuchi and Yoshinaga[16]).

Therefore, it is reasonable to conclude that the change in the basal dislocation density is not an important factor in solution strengthening of magnesium. Similar conclusion has been arrived at by Adams, Vreeland and Wood in the case of Zn base solid solutions containing Al[118].

2.4.2.2. Elastic Interaction:

The mechanism of elastic interaction was originally proposed by Cottrell[100] to explain the yielding of Fe-C alloys. Strengthening arises from the elastic interaction between the stress field of a dislocation and the stress field due to the lattice distortion resulting from the misfit of the solute atom. The problem has been treated by the methods of classical elasticity by several authors[102-104] and has been successfully applied to many cases of interstitial solutes.

An analysis for the substitutional solutions has been given by Suzuki[101] using the concept of continuously varying composition and lattice parameter in the neighbourhood of the dislocation. As pointed out by Suzuki, the solution hardening in substitutional alloys due to this mechanism decreases markedly with temperature by thermal activation and becomes practically negligible at higher temperatures.

The present results on Mg-Zn alloys at higher temperatures, however, do not conform to the requirements of this mechanism. The CRSS of Mg-Zn alloys is almost independent of temperature above about 330°K, yet solution strengthening effect is quite pronounced above 330°K (fig. 47). Therefore, the elastic interaction theory cannot be applied to the case of solution hardening in Mg-Zn alloys tested above room temperature.

2.4.2.3. Chemical Interaction:

It is now well established that the stacking fault energy can be a function of composition for alloys in which the dislocations are extended. Evidence for this has been obtained from X-ray measurements of stacking fault occurrences in deformed alloys[105], from direct electron microscopic observations of extended dislocations[146] and from the temperature and strain rate sensitivity of τ_{III}[141,142] in the stress strain curves of single crystals having fcc structure. As suggested by Suzuki[106], this variation in stacking fault energy with composition should result in a difference in composition between the faulted area of extended dislocations and the bulk material. A surface thermodynamic treatment of the problem has also been given by Guard and Fine[107]. Experimentally, Spreadborough[105] has shown that a difference in the chemical reactivity between the faulted area and the bulk material exists which is evidence that segregation does occur. This segregation has a pinning effect on the dislocations. Suzuki's theory has later been extended to regular solutions and in its final form stands as follows:

$$\tau = \frac{m_A m_B}{RT} \quad \frac{V}{bt} \left(\frac{\partial \gamma}{\partial m_A^f}\right) \quad \left[1 - \frac{m_A m_B}{RT} \left(\frac{\partial^2 \Delta H}{\partial m_A^2}\right)\right]^{-1} \qquad (8)$$

where τ is the increase in the critical shear stress of the alloy over that of the pure metal, m_A, m_B are the mole fractions of the solute and the solvent respectively,

V is the molar volume of the alloy,

b is the Burgers vector,

t is the thickness of the faulted region,

γ is the stacking fault energy,

m_A^f is the mole fraction of the solute in the faulted region,

ΔH is the integral heat of mixing,

R is the gas constant,

and T the absolute temperature at which equilibrium is attained.

It is seen from equation (8) that a knowledge of the variation of stacking fault energy with solute concentration (in the stacking fault) is essential in determining the applicability of the equation to a particular situation. In the case of pure magnesium the stacking fault energy has been estimated, from theoretical considerations, to be equal to 200 ergs/cm^2 [39]. Quantitatively, however, this value of γ has never been verified using electron microscopy. Because of the rather long extinction distance in magnesium and its low shear modulus, it is difficult to observe the alternate extension and contraction of the nodes in the hexagonal network formed by the interaction of two sets of screws with different basal Burgers vectors [29]. Stacking fault energy can also be estimated by having a knowledge of the stress required to induce cross slip. The method has been applied successfully to the case of crystals with face centred cubic structure. However, this method has never been applied to the hcp materials mainly because the stress to induce cross slip is not apparent from the stress strain curves of this group of crystals. Bearing in mind that $(\frac{\partial \gamma}{\partial m_A^f})$ for Mg-Zn alloys is not at hand and that the thermodynamic functions of the system are also unknown, an attempt will be made to calculate the extent of Suzuki hardening under certain assumptions. First, we will assume an ideal mixing and therefore $\frac{\partial^2 \Delta H}{\partial m_A^2} = 0$. Secondly, $\left(\frac{\partial \gamma}{\partial m_A^f}\right)$ will be calculated using the

stacking fault energies of pure Zn and pure magnesium. Also assuming the stacking fault to be two atomic layers thick equation (8) reduces to the following:

$$\tau = \frac{1}{2} \frac{c}{a} \frac{m_A m_B}{RT\ V} \cdot Q^2 \qquad (9)$$

where c/a is the axial ratio of the crystal,

and $$Q = \frac{V\ (\gamma_{Zn} - \gamma_{Mg})}{2c} \qquad (10)$$

the other symbols having their usual meaning.

Substituting $\gamma_{Mg} = 200$ ergs/cm^2

$\gamma_{Zn} = 70$ ergs/cm^2

and $V = 14$ cm^3/mole

$T = 458°K$ i.e. $0.5\ T_m$. This value is reasonable in that the diffusion of solute atoms to the stacking faults will be negligible below $0.5\ T_m$. τ for 0.45 at.% Zn alloy comes out to be 21 gm/mm^2. On the other hand the experimental value of $(\tau)_{0.45Zn} - (\tau)_{Mg} =$ 105 gm/mm^2. Thus it is seen that the chemical hardening mechanism cannot adequately account for the observed strengthening. Additional discrepancy is encountered in the composition dependence of solution strengthening. At low solute concentrations (upto 0.45 at.% Zn) equation (9) predicts an almost linear relationship between τ and C whereas the experimental data follow a $C^{\frac{1}{2}}$ trend.

2.4.2.4. Short Range Order:

The energy of a solid solution varies linearly with the degree of local order while the entropy varies roughly logarithmically; therefore, unless the interaction between like and unlike neighbours is identical, the equilibrium state will be one with a non zero local order[108].

As pointed out by Fisher[109] this order need not be very great to make a significant contribution to the strengthening. According to Flinn[110] the short range order interaction would lead to a temperature independent friction stress i.e. τ_G should increase with alloying if SRO interaction is present.

Applying the theoretical result of Flinn to the case of basal slip in hcp metals,

$$\tau = \frac{8}{\sqrt{3}} \frac{(m_A m_B)^2}{a^3 kT} \cdot \nu^2 \qquad (11)$$

where ν is the interaction energy for like bonds.

When the value of ν/kT is small, ν can be calculated using the following approximate formula

$$\nu = \frac{\alpha_1 kT}{2m_A m_B} \qquad (12)$$

Here α_1 is the local order parameter which can be determined by X-ray or neutron diffraction experiments. However, such experiments have not been carried out with Mg-Zn alloys. In the absence of experimentally determined values of the short range order parameter equation (11) cannot be used to calculate the strengthening due to short range order in the Mg-Zn system. Nevertheless, the fact that equation (11) predicts a C^2 dependence of the friction stress speaks against SRO hardening. In the present work the observed hardening follows a $C^{\frac{1}{2}}$ relation.

Lately it has been shown by Koppenal[111] that neutron irradiation does not influence the strength of Cu-14% Al crystals upto a dose where radiation induced short range ordering is already complete. This also is against the idea that SRO can strongly contribute to the long range stress field.

2.4.2.5. Strengthening Due to a Random Distribution of the Solute:

The earliest theory of solution strengthening based on a random distribution of the solute was propounded by Mott and Nabarro[102,112]. This theory computes the average magnitude of the stress in the matrix of a dilute solid-solution due to replacing atoms of the matrix by ones that are larger or smaller, (i.e. size effect) thus straining the lattice. Although considering sign, the average stress on a dislocation is zero, relatively short lengths experience stresses of the order of the average stress magnitude and hardening results. The theory cannot adequately account for the athermal solution strengthening in general due to two reasons. As pointed out by Fleischer[113] the theory of Mott and Nabarro applies only to dislocations whose stress fields have dilation associated with them, and hence pure screw dislocations are able to move freely. However, the main objection to the theory was the experimental failure[114,115] of the parameter δ (defined as $\delta = \frac{1}{b} \cdot \frac{db}{dc}$, where b is the lattice parameter) to be a proper index of the relative hardening when different solute atoms are added to a metal. It has been observed that the valency of the added element is a strong factor.

Fleischer has extended the analysis further to include two interactions responsible for solution strengthening[113,116]. One is caused by the hydrostatic component of the stress field of a dislocation interacting with the volume change produced by inserting a foreign atom (size or δ interaction) and the other occurs because the inserted atom represents a small region of different elastic properties from the matrix, so that a dislocation interacts because it must do more (or less) work

than usual in elastically shearing the impurity atom (modulus or η interaction). This second interaction is first order for either edge or screw dislocations since both have shear strains. The size interaction with a screw dislocation, however, is zero to a first order, since a screw dislocation has no hydrostatic stress according to linear elasticity. On the other hand there is a second order elastic interaction caused by an expansion, which in essence arises from the atomic roughness of the planes in a crystal. These planes are forced apart as they are sheared across one another; thus there exists a hydrostatic component of stress around a screw dislocation. Taking the δ and the η interactions into account, the dependence of the room temperature plateau stress on concentration of solute comes out as follows

$$\tau_G = Z.G.C^{\frac{1}{2}} . \varepsilon^{3/2} \qquad (13)$$

where Z is a constant calculated by Fleischer to be equal to 1/760 for screws.

$$\varepsilon = \eta' - \alpha\delta \qquad (14)$$

δ is already defined.

$$\eta' = \frac{\eta}{1+\frac{1}{2}|\eta|} \qquad (15)$$

where

$\eta = \frac{1}{G} . \frac{dG}{dC}$, G being the shear modulus.

The value of α lies between 3 and 16 for interaction with screw dislocations whereas it is greater than or equal to 16 for interaction with edge dislocations. For polycrystalline Cu-solid solutions α is estimated to be about three implying a screw dislocation solute atom interaction[116]. Recently Saxl[117] has extended Fleischer's calculation of the dislocation solute interaction starting from first principles and gets rather similar results.

The present results conform to the predicted square-root C dependence of the friction stress (fig. 49). However, in order to make a quantitative verification possible, a knowledge of the concentration dependence of the lattice parameters and the shear modulus is necessary. The concentration dependence of the lattice parameters in the case of Mg-Zn alloys has been determined by a number of workers[31,119]. The linear size factor of 0.2 as computed by King[33] will be used in the present calculations. The parameter η has never been evaluated for Mg-Zn alloys. However, elastic constants of some of the Mg-base alloys have been evaluated as a function of solute concentration in the case of Ag, In and Sn solutes[120]. From these results it appears that those elements belonging to group I of the periodic table tend to increase the shear modulus of magnesium whereas those belonging to group III and IV decrease it. Therefore, since Zn belongs to the same group in the periodic table as magnesium, it would be logical to conclude that η will be small in the case of Mg-Zn alloys. Now if we neglect η in comparison with δ and substitute the values of $\frac{d\tau}{dC^{\frac{1}{2}}}$, G and ε_{screw} after differentiating equation (13) with respect to $C^{\frac{1}{2}}$, Z comes out to be $\frac{1}{377}$, whereas if ε_{edge} is used then Z becomes $\frac{1}{4,800}$. It is apparent that edge dislocation solute atom interaction does not give a satisfactory fit. The value of Z can be improved if we assume a linear dependence of τ_G on ε_S. By substituting ε_S instead of $\varepsilon_S^{3/2}$ the best fit is obtained with $Z = \frac{1}{500}$. This value of Z would become closer to $\frac{1}{760}$ (as estimated by Fleischer) if η is positive; however, this speculation cannot be justified until η is evaluated experimentally. The linear dependence of τ_G on ε_S instead of $\varepsilon_S^{3/2}$ has, however, been observed in the case of Ag base solid solutions[121].

The only other hexagonal alloy system in which the room temperature plateau has been measured is the Mg-Li system. Yoshinaga and Horiuchi[16] have attributed the hardening to the Suzuki chemical strengthening mechanism, although the experimental data conform to the theoretical prediction only upto 6 at.% Li. Above this concentration of Li the observed hardening is much smaller than is required by the Suzuki hardening mechanism. Yoshinaga and Horiuchi's data has been plotted by the present author against $C^{\frac{1}{2}}$ as shown in fig. (72). It is apparent that $C^{\frac{1}{2}}$ dependence holds good in the case of Mg-Li alloys too. Thus it is seen that the friction stress mechanism does explain adequately the observed variation of the room temperature plateau - stress with solute concentration in the Mg-Zn and Mg-Li solid solutions.

2.4.2.6. Strengthening at Low Solute Concentrations:

An interesting feature of figs. (49) and (72) is that the straight line through the experimental points in the τ_G against $C^{\frac{1}{2}}$ plot does not pass through the origin. The intersection on the $C^{\frac{1}{2}}$ axis corresponds to a composition equal to 0.025 at.% in the Mg-Zn system and 0.29 at.% in the case of Mg-Li alloys. A critical examination of Rogausch's[121] data reveals that this feature is common to the Ag-base solid solutions too. Rogausch's data are reproduced in fig (73). This effect has, however, not been explained earlier.

The concentration independence of τ_G will be better understood in the light of a knowledge of the low temperature rate controlling mechanisms in the Mg-Zn alloys. This will be discussed in a later chapter.

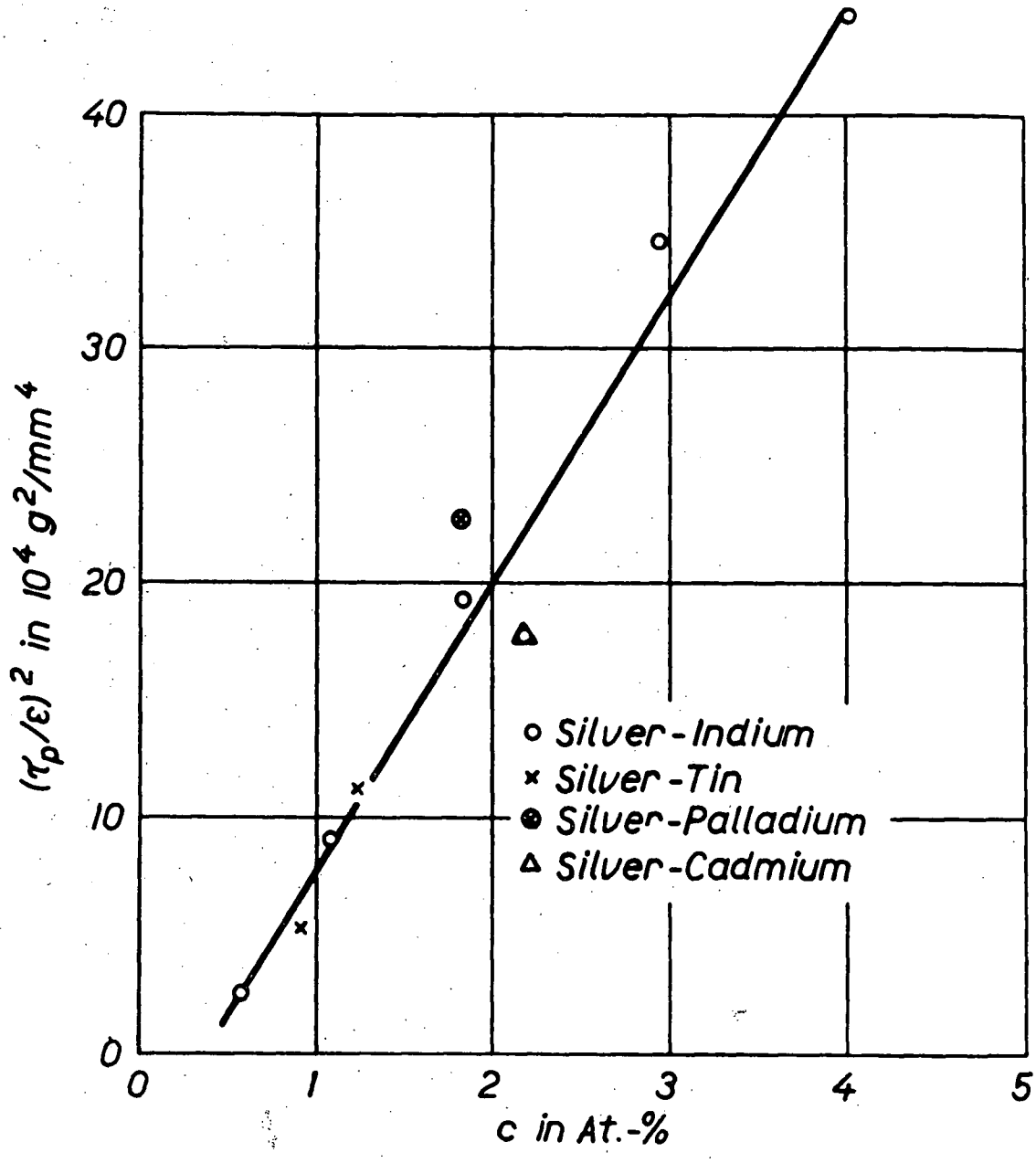

Fig. 73. τ_G vs concentration for Ag solid solutions (after Rogausch[2]).

2.4.2.7. Valency Effect:

It has been observed by several investigators that the relative valency of the solvent and the solute is an important factor contributing to solution strengthening[114,115,122]. However, since the present results are best explained in terms of the size and modulus interactions, the valency effect is of no consequence. Valency effect is in fact incorporated in the modulus interaction term.

2.4.2.8. Other Hardening Mechanisms:

The only other hardening mechanism not covered so far is the long range order hardening. This mechanism is of importance when dealing with the deformation of the super lattices only and is of no consequence in the present study, which deals with dilute solutions.

2.4.3. Solution Strengthening at Low Temperature:

Before entering into the detailed discussions of the low temperature strengthening mechanismsit is profitable to examine the various possible ways in which the τ-T curve can be altered by the addition of solute. Principally this can happen in three ways as shown schematically in fig. (74).

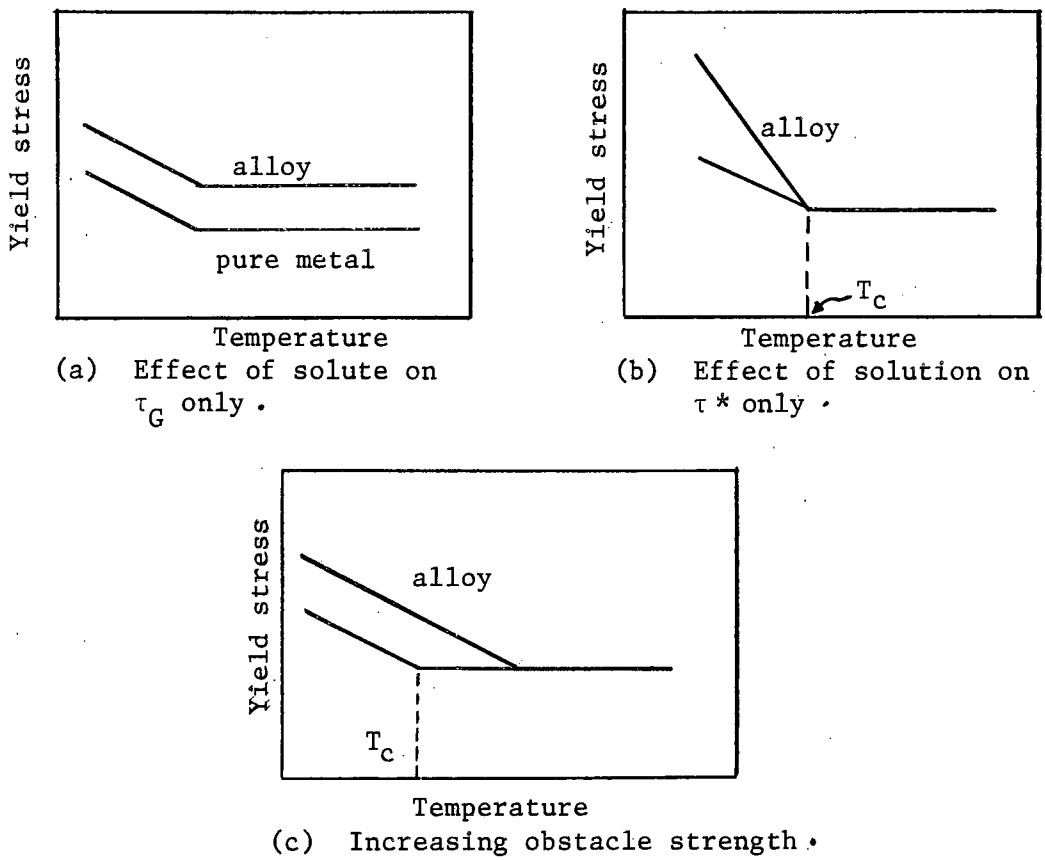

(a) Effect of solute on τ_G only.

(b) Effect of solution on τ^* only.

(c) Increasing obstacle strength.

Fig. 74. The effect of solute on the τ-T curve (Schematic).

a) By increasing τ_G which uniformly elevates the τ-T curve.

b) By increasing the density of the short range obstacles. If this is done strengthening will be limited to temperatures below T_c.

c) By introducing stronger obstacles. This will shift T_c to higher temperatures.

Experimentally the alloys containing 0.006 and 0.019 at.% Zn conform to the situation in (b). At higher Zn concentrations both τ_G and τ^* increase, however, the τ-T curve is not uniformly elevated. This is apparent from fig. (75), where only τ^* is plotted against temperature for various solute concentrations. Here τ^* has been obtained by subtracting τ_G from the measured CRSS (after applying the shear modulus correction to τ_G). It is observed that the temperature sensitivity of τ^* increases with increasing solute content. This again suggests that the short range order is not an important hardening mechanism in these alloys. Short range hardening is inherently athermal, since the energy for nucleating forward slip never reaches a maximum value. As a segment of dislocation bows out the energy continuously increases due principally to the disordering that is induced across the slip plane. For this mechanism, therefore, deformation must be induced exclusively mechanically by the application of a sufficiently high stress to cause disordering. Therefore, in order that short range ordering is the principal strengthening mechanism, $(\frac{\partial \tau^*}{\partial T})$ at low temperatures should be unaffected by the amount of solute present, which is different from what is observed experimentally.

It is recognized that some mechanisms are thermally activatable under some conditions and athermal under others. For example, weak Cottrell atmosphere locking of dislocations is thermally activatable, but more concentrated and stronger Cottrell-atmosphere locking can be athermal. Suzuki locking constitutes a second example: weak Suzuki locking of partials having a narrow stacking fault ribbon is thermally activatable, but under otherwise similar conditions, in alloys that have

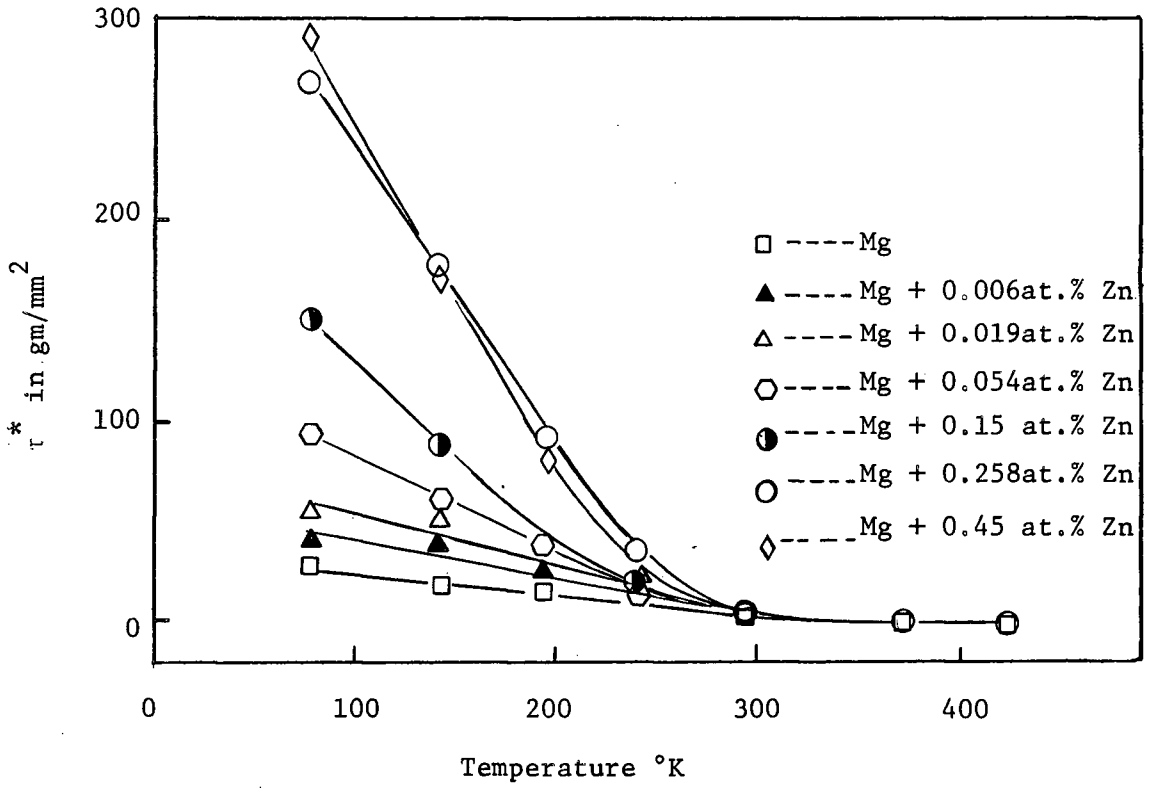

Fig. 75. τ^* vs. temperature for Mg-Zn single crystals.

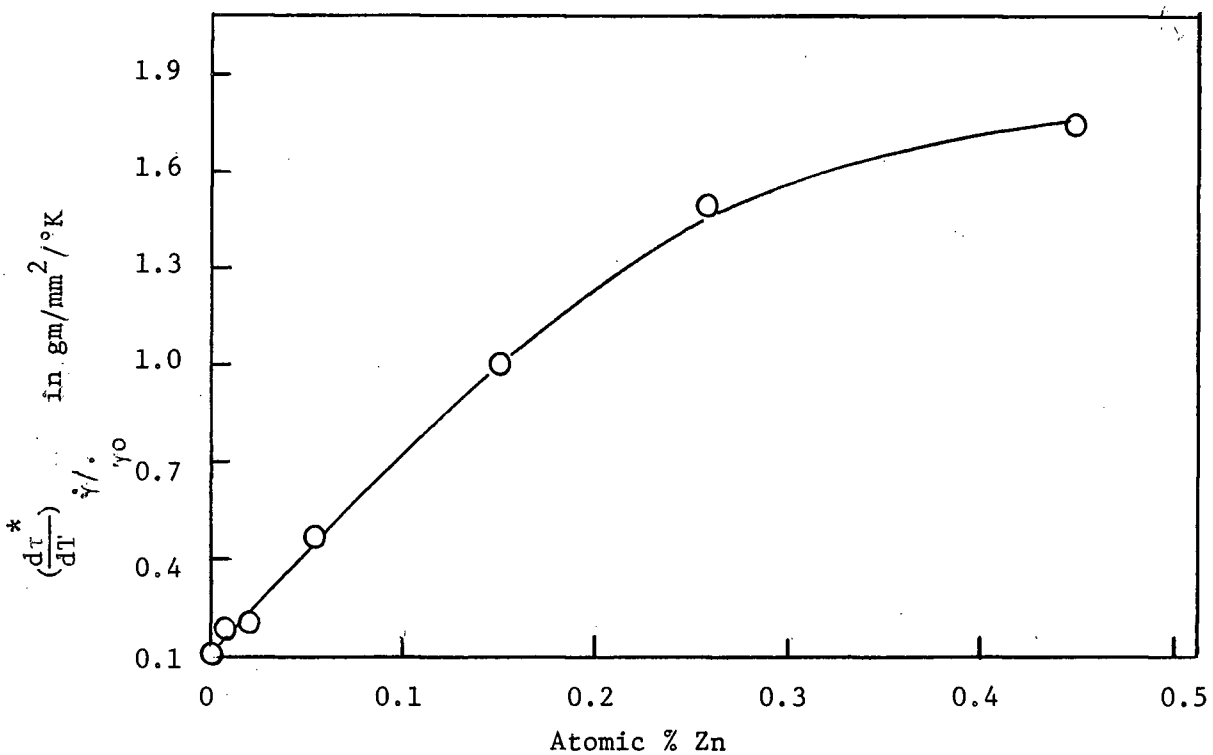

Fig. 76. $(\frac{d\tau^*}{dT})_{\dot{\gamma}/\dot{\gamma}_o}$ vs. solute concentration for Mg-Zn single crystals.

low stacking fault energies, the unlocking mechanism is athermal. The transition of Cottrell locking from a thermally activatable to an athermal mechanism is principally due to the height of the activation energy barrier, whereas this transition for Suzuki locking arises from the fact that high thermal fluctuations in energy can only occur over small volumes of the crystal. The fact that the width of the stacking fault in magnesium is rather narrow (due to high stacking fault energy) makes Suzuki locking a possibility and secondly the low solute concentrations involved may be taken to include Cottrell locking as a possible athermal mechanism in the Mg-Zn alloys. However, with the help of arguments, similar to those described in connection with the variation of τ_G, it can be shown that neither in trend nor quantitatively does Suzuki hardening explain the observed low temperature strengthening. Moreover, no single mechanism can explain the observed break in the τ-$C^{\frac{1}{2}}$ plot at 0.025 at.% Zn. Therefore, at this juncture the identification of the short range obstacles in Mg and the Mg-Zn alloys may be helpful in determining the mechanism of solution strengthening at low temperatures. The justification for such a procedure comes from the following analysis.

It is now widely accepted that the obstacles giving rise to the short range stress τ^* in close packed metals are the forest dislocations. Therefore, the low temperature strengthening in Mg can arise from an indirect effect of solute, namely the change in the forest dislocation density. From the present etch pit counts it is apparent that the forest dislocation density increases with increasing amounts of solute. However, experimentally there is little change in the forest

spacing beyond 0.04 at.% Zn, although the observed $(\frac{\partial \tau^*}{\partial T})$ (fig. 76) continues to increase rapidly even at concentrations beyond 0.04 at.% Zn. This implies that the change in the forest spacing may be the important factor in solution strengthening at low solute concentrations, but at higher solute concentrations the short range obstacles must be different from the forest dislocations.

The rate theory will be used in an effort to identify the short range obstacles which determine the thermal component of the flow stress at higher solute concentrations. The possible role of the change in the forest dislocation spacing as a solution strengthening mechanism can also be ascertained by comparing the observed activation length with the measured etch pit spacing.

2.4.3.1. Thermally Activated Deformation:

It has been pointed out earlier that obstacles are essentially of two types, short range obstacles are effective over distances less than ten atomic diameters and long range obstacles possess stress fields of the order of ten atomic diameters or greater. Thermal energy is able to assist the applied stress in pushing the dislocation past the short range obstacles, but cannot aid in getting dislocations past the stronger long range obstacles. Above T_c all thermal barriers become transparent and dislocations move through the lattice unimpeded once the applied stress has overcome the athermal barriers. Below T_c, however, thermal barriers must be overcome by the assistance of stress and thermal energy if an applied strain-rate is to be maintained. Of the several thermal barriers encounted, the strongest determines the rate at which dislocations can move under given conditions of stress, strain rate and temperature.

Provided the thermally activated processes occur in sequence and that the same event is rate controlling throughout the lattice, the macroscopic strain rate $\dot{\gamma}$ may be expressed as[123]

$$\dot{\gamma} = \dot{\gamma}_o \, e^{-\Delta F/kT} \tag{16}$$

where $\dot{\gamma}_o$ depends on the number and arrangement of the dislocations and their vibrational frequency. ΔF is the change in Gibbs' free energy of the system in surmounting the strongest obstacle. On the other hand, if the thermally activated processes occur independently and the rate controlling step is not the same throughout the lattice, then the strain rate will follow the relationship[124];

$$\dot{\gamma} = \sum \dot{\gamma}_{oi} \, e^{-\Delta F/kT} \tag{17}$$

where the subscript "i" refers to the i^{th} kind of mechanism. Under such circumstances the application of the rate theory for the identification of the rate controlling mechanism is not possible, since the extrapolation of the macroscopic thermodynamic measurements to a single activated event occurring in a specific region of the lattice is no longer possible.

The change in free energy for the thermally activated event can be expressed as[72];

$$\Delta F = \frac{\Delta H + T \frac{\partial G}{\partial T} \cdot \frac{\tau^* V^*}{G}}{1 - \frac{T}{G} \cdot \frac{\partial G}{\partial T}} \tag{18}$$

where G is the shear modulus and ΔH is the activation enthalpy, given by

$$\Delta H = -kT^2 \left(\frac{\partial \ln \dot{\gamma}/\dot{\gamma}_o}{\partial \tau^*} \right)_T \cdot \left(\frac{\partial \tau^*}{\partial T} \right)_{\dot{\gamma}/\dot{\gamma}_o} \tag{19}$$

V* is identified as the activation volume and is equal to

$$V^* = -\left[\frac{\partial(\Delta F)}{\partial \tau^*}\right]_T = kT\left[\frac{\partial \ln \dot{\gamma}/\dot{\gamma}_o}{\partial \tau^*}\right]_T \qquad (20)$$

The concept of activation volume arises when one considers the work W done on the system during an activation event by the effective stress τ^* pushing a dislocation segment of length l a distance d (the activation distance) where b is the Burgers vector of the dislocations. The term (bdl) is called the activation volume.

The evaluation of the activation parameter ΔF, ΔH and V* involves an evaluation of the partial differentials $(\frac{\partial \tau^*}{\partial T})_{\dot{\gamma}/\dot{\gamma}_o}$ and $\frac{\partial \ln \dot{\gamma}/\dot{\gamma}_o}{\partial \tau^*}_T$ at constant density, arrangement and number of mobile dislocations. For different alloys these factors will be different, however, here the constancy refers to the situation when one alloy is examined over a range of temperatures. Assuming the yield stress to be governed by the same thermally activated mechanism over the range of temperatures of interest, one can consider that the structure is relatively constant at yield[125]. Hence, on subtracting τ_G from τ (i.e. CRSS) a plot of τ^* against temperature is obtained (fig. (75)) and the slope $(\frac{\Delta \tau}{\Delta T})$ may be taken as $(\frac{\partial \tau^*}{\partial T})$. The second partial $\frac{\partial \ln \dot{\gamma}/\dot{\gamma}_o}{\partial \tau^*}$ is usually evaluated from differential strain rate change tests on a single specimen during flow at a fixed temperature. The flow stress difference accompanying instantaneous changes of strain rate may be taken as variation in effective stress $\Delta \tau^*$ with $\dot{\gamma}$ if it is assumed that the structure remains constant during the instant of change.

Differential tests corresponding to a strain rate change by a factor of 10^2 were carried out by varying the cross head speed on the instron from 0.002 to 0.2 ipm and vice versa using a push button speed selector. Experiments were performed at temperatures ranging from

78°K to 295°K covering the entire range of temperature senitive yielding. The details of the strain rate change tests are described in appendix (C).

2.4.3.2. The Effect of Solute on the Apparent Activation Parameters:

From the relationship

$$V^* = kT \left[\frac{\ln \dot{\gamma}_2/\dot{\gamma}_1}{\Delta\tau} \right]_T \qquad (20)$$

activation volumes were calculated for a series of Mg-Zn alloys. The effect of the applied stress and the solute concentration on the activation volume is shown in fig. (77). These tests were conducted at 78°K and the activation volumes are expressed in terms of b^3 where b is the Burgers vector of the glide dislocations. The measured activation volumes have been plotted against the resolved shear strain as shown in fig. (77) from which the activation volume at yield can be obtained by an extrapolation to zero strain. It is observed that in the case of magnesium the activation volume decreases rapidly at low strains, but at higher strains the rate of decrease is much smaller. The alloy containing 0.019 at.% Zn exhibits essentially similar behaviour as Mg except that the magnitude of V* is smaller than that of the pure metal at low strain levels. The difference in V* between magnesium and the low alloy, however, decreases rapidly so that at strains beyond 1.5 the two have the same activation volume at a constant strain level. The higher alloys containing from 0.15 to 0.45 at.% Zn, on the other hand, are associated with activation volumes which are less sensitive to both stress and strain. This is apparent from the fact that whereas in Mg the activation volume decreases from 4500 b^3 at yield to 400 b^3 at fracture, the corresponding change in the case of an alloy containing 0.45 at.% Zn is from 320 b^3 to 230 b^3.

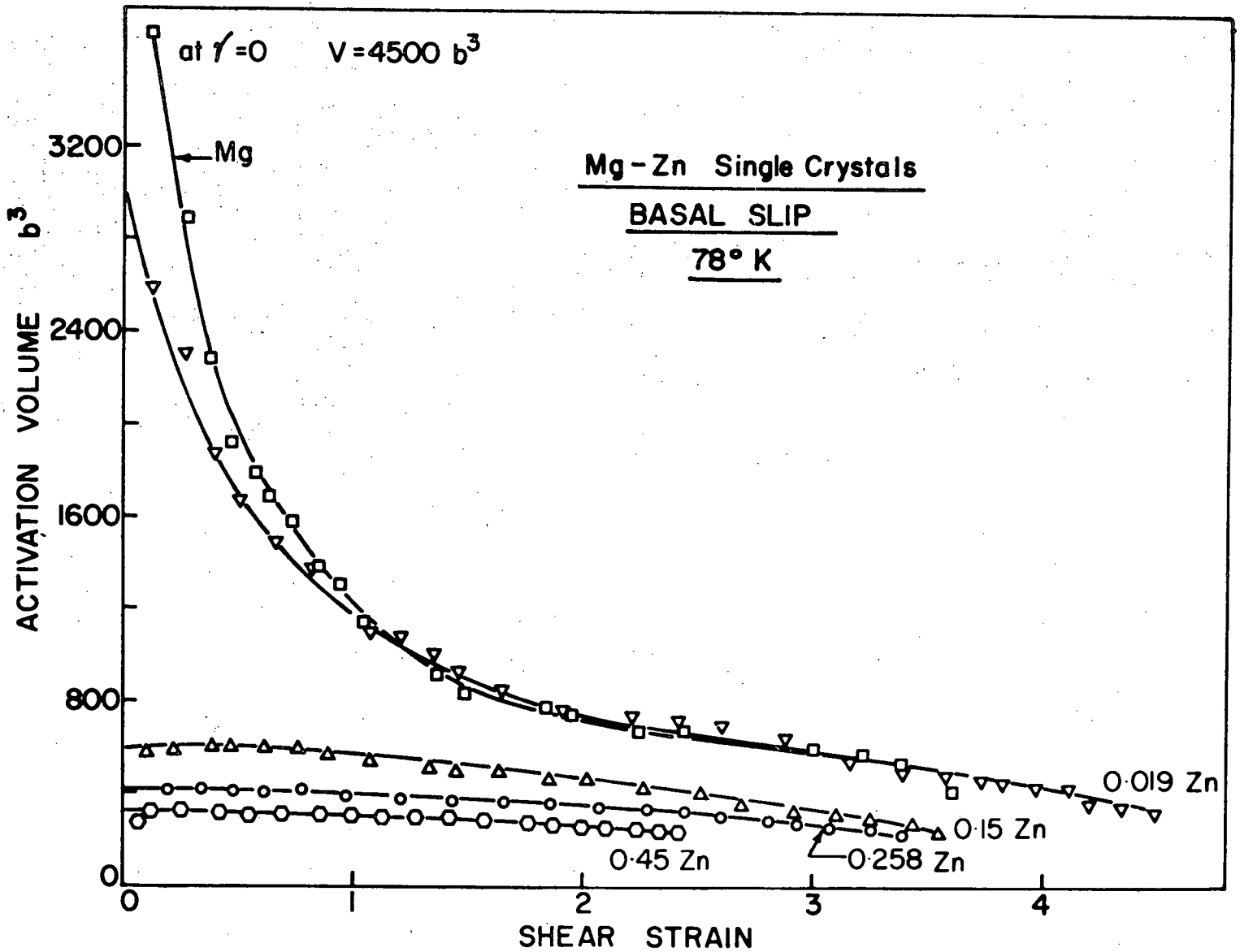

Fig. 77. Activation volume vs. shear strain for Mg-Zn single crystals.

2.4.3.3. The Activation Volume at Yield:

A direct measurement of the activation volume at yield is rather difficult because of the uncertainty in measuring $\Delta\tau$ at low strains. In order to minimize error, the extrapolated value of V^* to zero strain has been used. The concentration dependence of the activation volume at 78°K is shown in fig. (78). It is clear that V^* decreases dramatically from 4500 b^3 in pure magnesium to less than 1500 b^3 by the addition of as little as 0.05 at.% Zn. Between 0.05 and 0.45 at.% Zn, on the contrary, the activation volume decreases very slightly. From figs. (77) and (78) it appears that the alloys containing solute in amounts less than 0.05 at.% belong to a category different from the one which the higher alloys belong to.

The temperature dependence of the activation volume at yield is shown in fig. (79). Two compositions were chosen for this purpose, Mg being the representative of the group containing upto 0.05 at.% solute while 0.45 at.% Zn alloy belonging to the latter category. The activation volume at yield was once again obtained by the method of extrapolation to zero strain.

The activation volume is observed to increase rapidly with temperature in the case of magnesium, whereas the temperature sensitivity of V^* in the case of 0.45 at.% Zn alloy is considerably lower; especially at temperatures below 200°K. Profitable information may be obtained if V^* is plotted against τ^*. This has been done for Mg and 0.45 at.% Zn alloy as shown in fig. (80). The activation volume decreases drastically with increasing values of τ^* in the case of magnesium whereas there is only a moderate decrease in the case of 0.45 at.% Zn alloy. The values

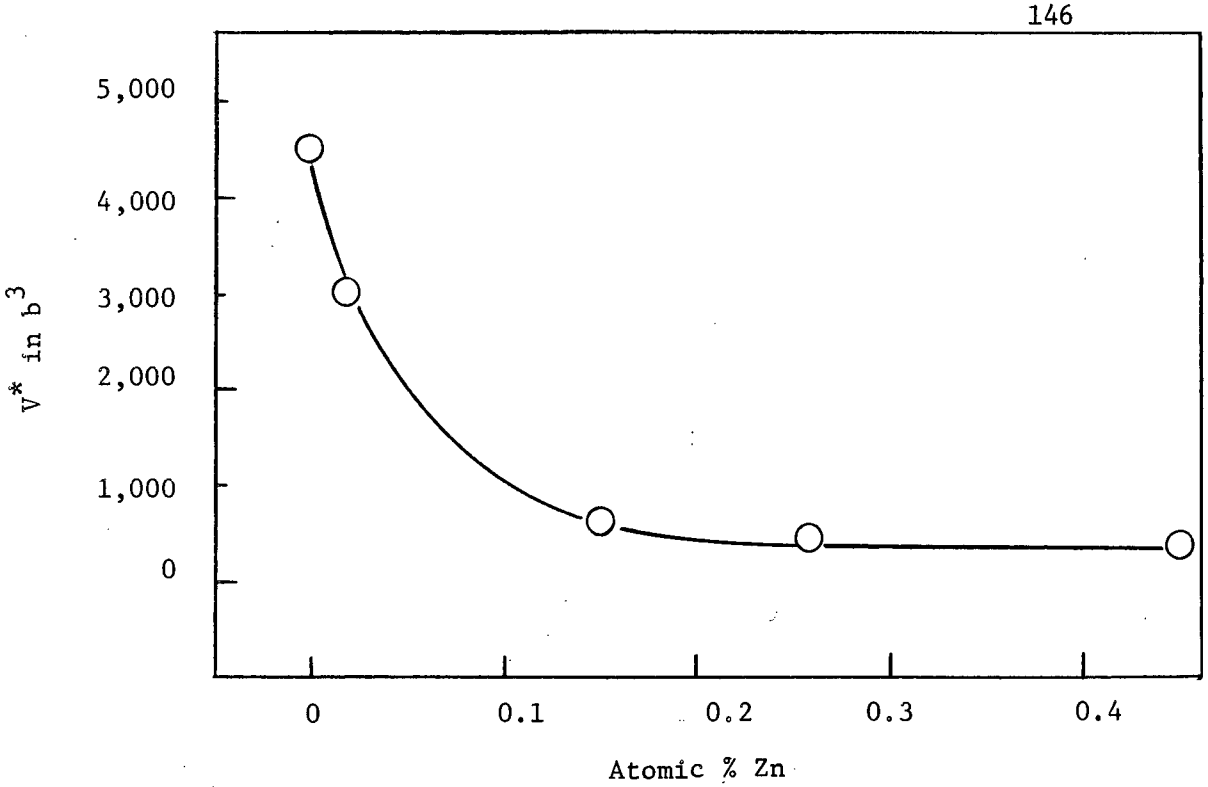

Fig. 78. Activation volume at yield vs. Zn concentration.

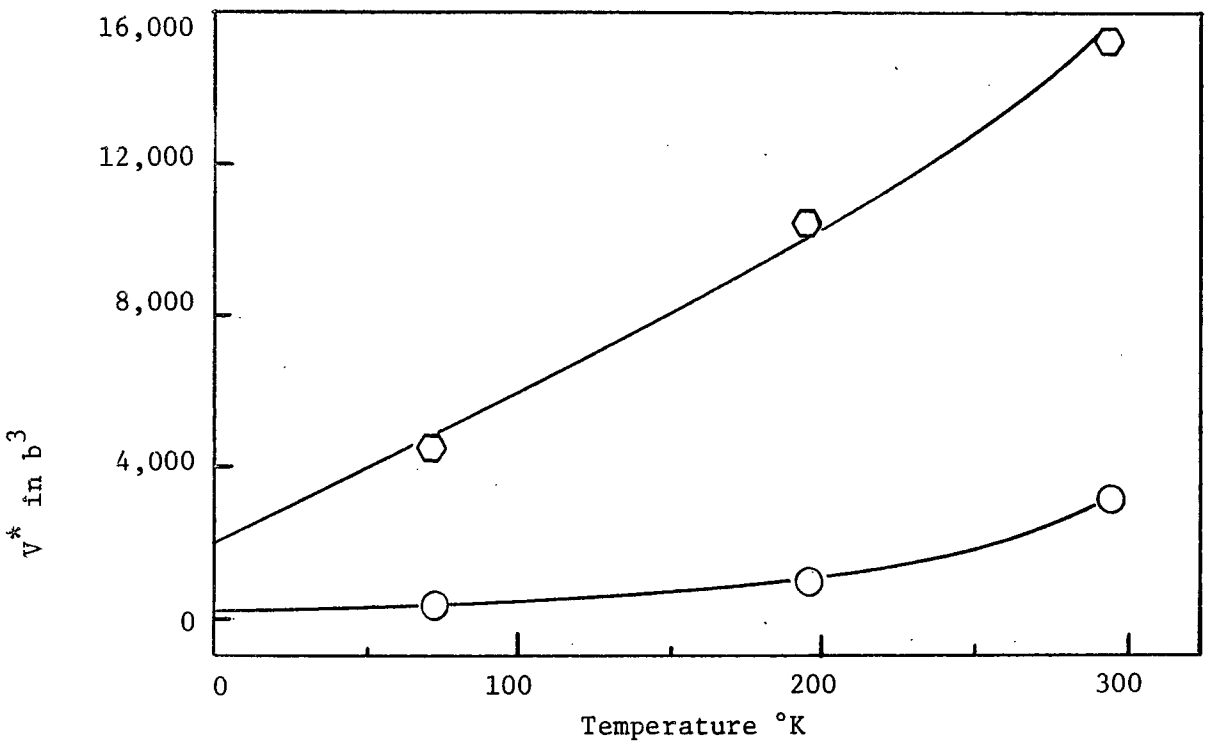

Fig. 79. Activation volume at yield vs. temperature for Mg and Mg + 0.45 at. % Zn alloy single crystals.

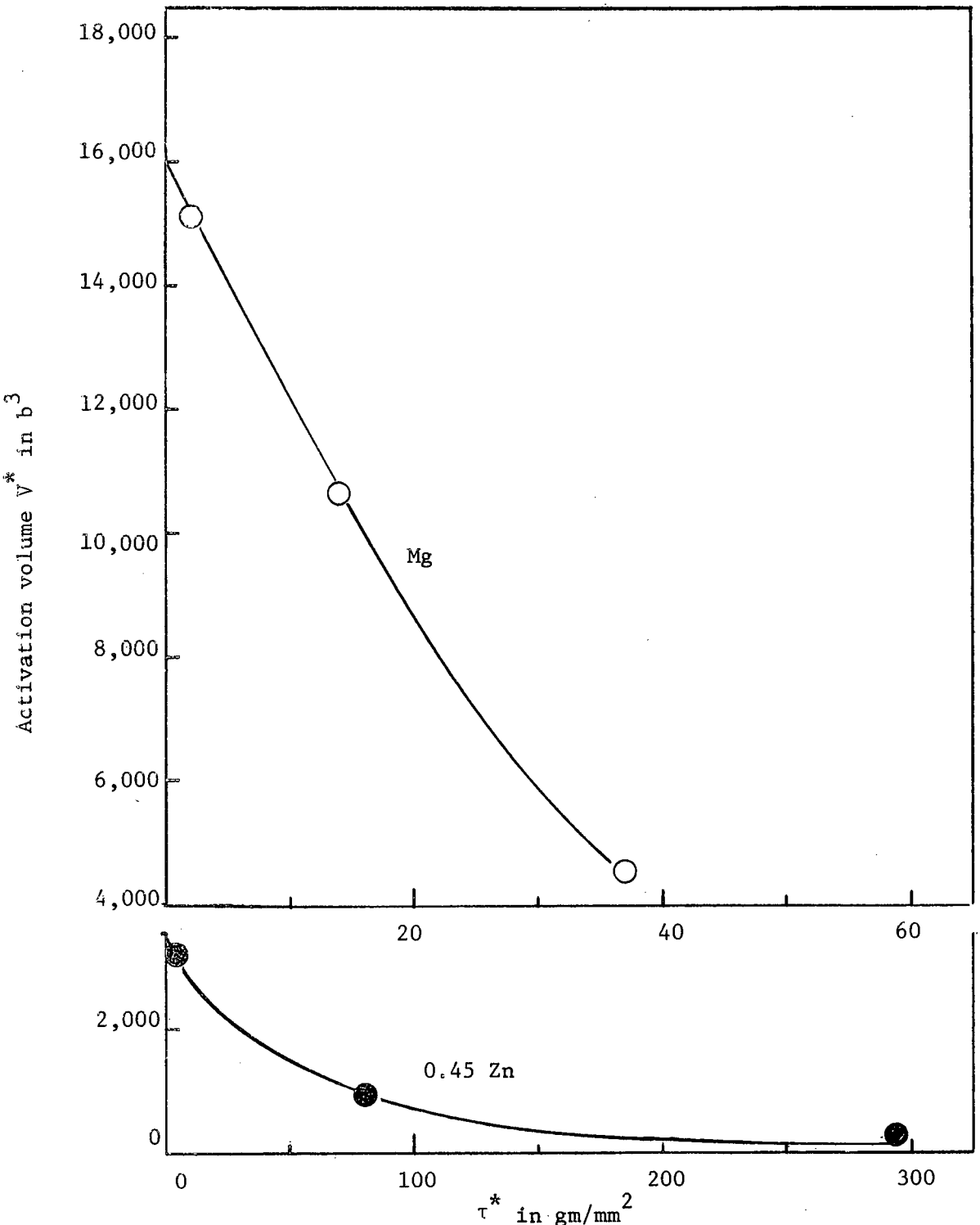

Fig. 80. Activation volume at yield vs. τ^* for Mg and Mg + 0.45 at. % Zn alloy single crystals.

of V^* at $\tau^* = 0$ for Mg comes out to be approximately 16,000 b^3 and that for 0.45 % Zn alloy is 3,300 b^3. Conrad,[5] using an intersection model for Mg single crystals, has shown that the nature of the force-distance curve may vary slightly with temperature (i.e. with τ^*) due to the influence of stress on the amount the gliding dislocations bow out on the slip plane thereby changing the effective forest spacing "l". This decrease in activation volume with strain has been interpreted by Basinski as arising due to an increase in the forest dislocation density[3]. Therefore, if the activation volume is to be used in determining the forest spacing at yield, then it is essential that the value at $\tau^* = 0$ be chosen. In this connection it is worth noting that the temperature variation of the activation volume can be caused by the temperature dependence of the stacking fault energy, which in turn determines the activation distance "d". However, in materials having high stacking fault energy (e.g. Mg) the distance between the partials is unlikely to be altered much through changes in temperature and hence the activation distance "d" is not likely to be the factor responsible for the temperature dependence of V^*.

2.4.3.4. Solution Effect on the Apparent Activation Energy:

Substituting for ΔH and V^* in equation (18) the activation Gibbs free energy becomes

$$\Delta F = -kT^2 \left[\frac{\partial \ln \dot{\gamma}/\dot{\gamma}_o}{\partial \tau^*}\right]_T \left[\left(\frac{\partial \tau^*}{\partial T}\right)_{\dot{\gamma}/\dot{\gamma}_o} - \frac{\partial G}{\partial T} \cdot \frac{\tau^*}{G}\right] \qquad (21)$$

The term $\left(\frac{\partial G}{\partial T} \cdot \frac{\tau^*}{G}\right)$ is small and hence will be neglected compared to $\left(\frac{\partial \tau^*}{\partial T}\right)$. ΔF can then be approximated to ΔH i.e.

$$\Delta F \simeq \Delta H \simeq - V^* T \left(\frac{\partial \tau^*}{\partial T}\right)_{\dot{\gamma}} / \dot{\gamma}_o \qquad (22)$$

It is important to note that when ΔH is substituted for ΔF, it is assumed that the entropy term $e^{\Delta S/k}$ is incorporated in the pre-exponential term $\dot{\gamma}_o$. This approximation is valid only when the entropy change does not have significant contribution to the over all free energy change.

The term ΔH calculated using equation (19) does not include the work done by the effective stress during thermal activation. Correcting for this work done the total activation energy (enthalpy) ΔH_o is then expressed as

$$\Delta H_o = \Delta H + V^* \tau^* \qquad (23)$$

where $V^* \tau^*$ is the work done during thermal activation.

The variation of ΔHo with Zn content has been calculated using equations (19,20) and (23) and is shown in fig. (81).

The term ΔHo should be labelled "apparent" activation enthalpy, since the effective stress before the activation event is unknown. ΔH_o would be the true activation enthalpy only when $\tau^* = 0$. However, this has not been done in the present work.

2.4.3.5. Zinc Alloying and the Thermally Activated Flow:

In solid solutions the mechanism of thermally activated deformation can be any one of the following:

1) Intersection of forest dislocations,
2) Dislocation pinning by single solute atoms,
3) Tetragonal strain centres,
4) Peierls, Pseudo Peierls, and Recombination mechanism,
5) Cross slip,
6) Cottrell-Lomer Dissociation,

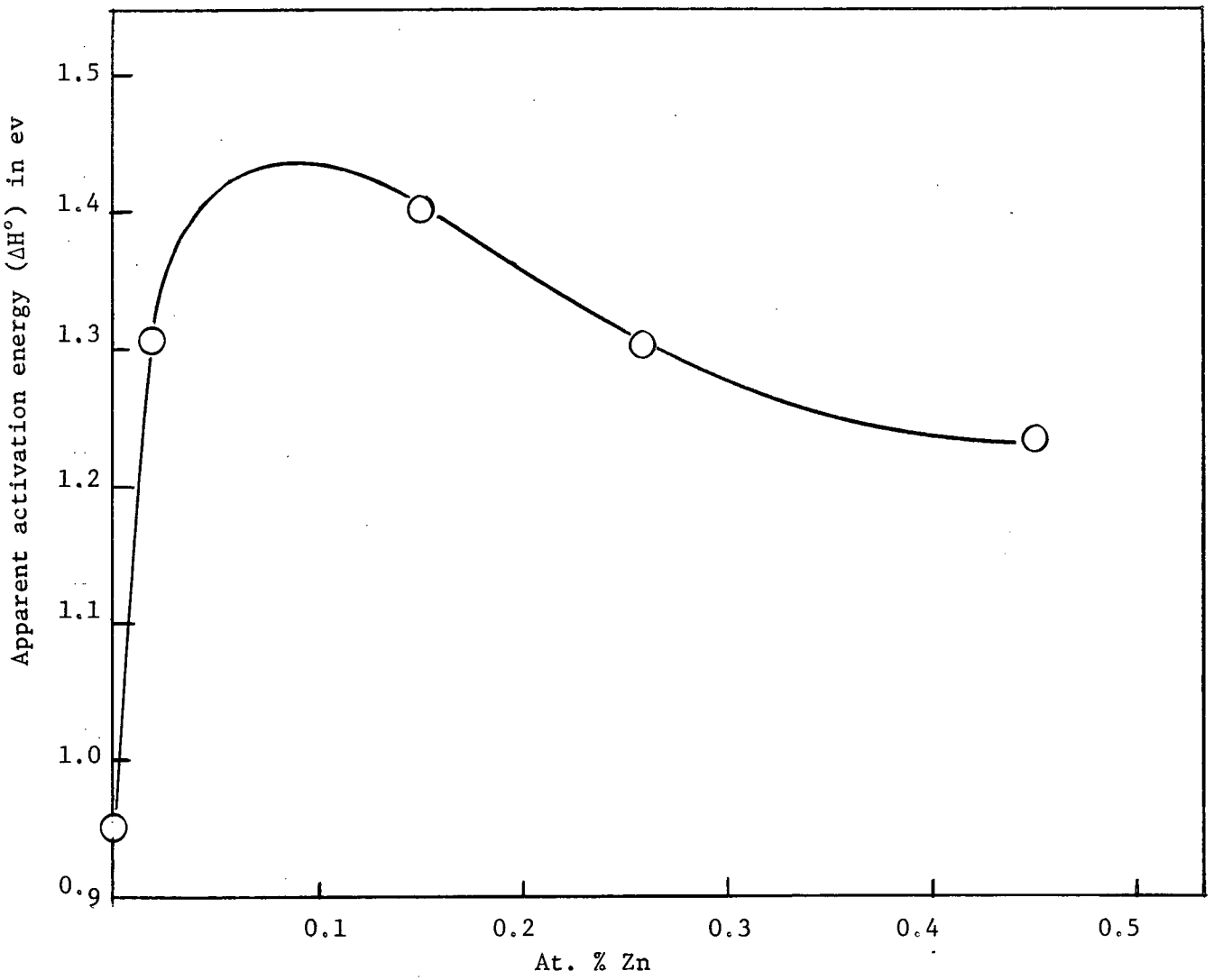

Fig. 81. Apparent activation energy vs. Zn concentration.

7) Fisher locking,

and 8) Suzuki locking.

Some of these mechanisms have been discussed earlier. For example Fisher and Suzuki locking mechanisms do not apply to the present case as shown in the earlier part of this section. The mechanism of Cottrell-Lomer dissociation does not apply to the case of hexagonal structures. Also the case of Tetragonal strain centres is inapplicable since it applies to interstitial impurities only, while Zn is a substitutional solute in Mg.

The remaining four will be discussed in the following pages.

2.4.3.5.1. Cross Slip:

The activation volumes associated with the cross slip process[73] are of the same order as those for intersection, both being greater than 100 b^3. The experimentally determined V^* in the Mg-Zn alloys are also greater than 100 b^3. However, activation volume alone cannot be taken to decide between the cross slip and the intersection mechanisms. Additional information may be obtained from the following considerations.

In the range of temperature investigated, the only established cross slip planes in magnesium are the basal {0001} and the prism $\{10\bar{1}0\}$ planes. The CRSS for prismatic slip in each of these alloys is about two orders of magnitude higher than that for basal slip. Therefore, it is unlikely that cross slip would be possible at the onset of plastic flow. This conclusion is supported by the absence of cross slip markings on the surface of the deformed crystals, although the slip line observations should not be taken as conclusive when optical microscopy is used for their

examination. Cross slip does play a significant role in the work hardening of magnesium in the stage A of deformation[29], however, this is of little consequence when CRSS is the parameter under consideration. Thus it may be concluded that cross slip cannot be the rate controlling mechanism in basal slip.

2.4.3.5.2. Peierls, Pseudo-Peierls and Recombination Mechanisms:

Peierls mechanism concerns the thermal activation of dislocation motion past linear obstacles. A rather complete review of this mechanism has been given recently by Guyot and Dorn[126]. The pseudo-Peierls mechanism was originally proposed by Dorn to explain the thermally activated flow of Mg-Li alloys. It is a slight modification of the Peierls mechanism for the case where the two partials are very close together (0.5 to 2b). The stacking fault energy plays a significant role in the Pseudo Peierls mechanism whereas the Peierls-Nabarro theory does not take this into consideration[127]. These mechanisms will be discussed in greater detail in connection with prismatic slip.

Recombination is thought to be a successful mechanism in explaining effectively the orientation dependence and the initial rates of strain hardening in bcc metals[127].

Without going into any further details of the above three mechanisms, it should be pointed out that the activation volume associated with each of these mechanisms is less than 80 b^3, whereas the experimentally determined values of V^* are greater than 300 b^3. Therefore, these mechanisms are not applicable to the present case.

2.4.3.5.3. The Intersection Model:

It is now well recognized that the obstacles determining τ^* in the basal glide of magnesium are the forest dislocations. In view of the fact that the grown in dislocation density does change in many instances of close packed structures by the addition of solute, there is reason to believe that the indirect solution strengthening due to such a change can be of importance if the strengthening due to direct interaction is relatively small. In the past attempt has been made by Hendrickson and Fine[128] to explain the observed strength of the Ag-Al alloys in terms of increased grown in dislocation densities. However, such an explanation requires the presence of dislocations upto 10^{10} cm^{-2} in the as grown crystal, which is too high to be met in practice. The case of Mg-Zn will now be examined in the light of the grown in forest dislocation density (the increase in basal dislocation density can contribute to τ_G only and therefore will not be considered here since τ^* is being dealt with at the present).

The activation volume at 78°K for each of the Mg-Zn alloys tested is greater than 100 b^3 (fig. 78) thus forest intersection can be the rate controlling mechanism in these alloys.

From fig. (80) the values of V^* at $\tau^* = 0$ can be used to calculate the forest dislocation density at yield in Mg and 0.45 at.% Zn alloy using the following expression.

$$V^* = b.d.l. \qquad (24)$$

If a simple assumption is now made that the activation distance "d" can be approximated by the Burgers vector "b" then

$$V^* = b^2.l \qquad (25)$$

Again, assuming a square array, the forest dislocation density $\rho = \frac{1}{l^2}$ (26)

Such calculations in the two cases yield $\rho_{Mg} = 3.8 \times 10^6$ cm^{-2} and $\rho_{0.45\ Zn} = 9 \times 10^7$ cm^{-2}. A similar calculation in Mg by Conrad yielded $l_o = 1.5 \times 10^{-4}$ cm in one set of experiments[6,8] and $l_o = 3.0 \times 10^{-4}$ cm in another[5]. Conrad has attributed this inconsistency in his results to the difference in growth conditions, impurity content and the effect of recovery treatment on l_o.

The calculated $\rho_{Mg} = 3.8 \times 10^6$ is two orders of magnitude higher than the etch pit density. This discrepancy has been discussed already. Here we will compare the ratio ρ_{alloy} / ρ_{Mg} with the corresponding etch pit figure. From the activation volume measurements $\rho_{0.45\ Zn} / \rho_{Mg} = 24$ whereas the corresponding ratio of etch pits = 4. This implies that either the assumption that "d" remains constant is not true or the basic assumption that the rate controlling mechanism in Mg 0.45 at.% Zn alloy is one of intersection is wrong. Now let us consider the variation of "d" with solute concentration. If it is the width of the stacking fault that is determining "d", then "d" cannot decrease to a value less than 0.5 - 2 b, which is the distance between the partials in Mg. Therefore, the only other possibility is that "d" increases. If it does then the ratio $\frac{\rho_{alloy}}{\rho_{Mg}}$ becomes even larger than 24, making the discrepancy worse.

Therefore, the first assumption that the rate controlling mechanism in 0.45 at.% Zn alloy is one of intersection of forest trees must be wrong.

a) Intersection Model at Low Solute Concentrations:

The etch pit density increases rather rapidly by the addition of Zn upto 0.04 at.% and the break in the $C^{1/2} - \tau$ plot is at 0.025 at.% Zn. Therefore, it is likely that the addition of solute in such small quantitites will not alter the rate controlling mechanism of magnesium and hence strengthening could be due to increased forest density. In order to put this suggestion to test let us compare $\frac{\rho_{0.025\ Zn}}{\rho_{Mg}}$ derived from activation volume measurements with the ratio of etch pits at a comparable situation. In the absence of the value of V^* for 0.025 Zn alloy at $\tau^* = 0$, the activation volumes at 78°K will be used. This will not be too erroneous because the temperature effect on V^* will be approximately of the same order in the two cases. $\frac{\rho_{0.025\ Zn}}{\rho_{Mg}}$ evaluated in this manner is equal to 3.2, the corresponding etch pit ratio being 2.5. In view of the experimental error involved in the measurement of the activation volume this may be regarded as a good agreement.

Hence the thermally activated mechanism in Mg and the alloys containing upto 0.025 at.% Zn is one of intersection. What remains to be seen is which of the rate controlling mechanisms can account for the flow in the higher alloys. The only mechanism not discussed so far is the single solute atom dislocation pinning mechanism. This will be applied to both low and high Zn alloys in order to see if it can provide an alternative to the intersection model and to test its applicability at higher concentrations of solute.

2.4.3.5.4. Dislocation Pinning by the Solute Atoms:

A model for the low temperature short range solute dislocation interaction has been formulated by Friedel[104]. According to this model the dislocation moves in a zigzagging fashion from one position of maximum core interaction energy to the next. The situation is schematically represented in fig. (82).

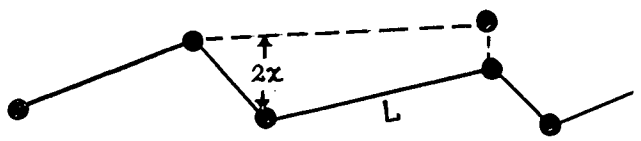

Fig. 82. Dislocation pinning by solute atoms giving rise to low temperature friction stress (Schematic).

The stress τ_o^o to do this at T = 0 is determined by the interaction energy U_m and the concentration C of the solute according to the equation:

For T= 0; $$\tau_o^o \, bLx = U_m \qquad (27)$$

In the case of hexagonal close packed metals,

$$V_o = bLx = \text{Activation Volume} = \frac{2}{\sqrt{3}} \cdot \frac{b^3}{C} \text{ , and} \qquad (28)$$

in fcc metals $bLx = b^3/C$ (note C is atom fraction, not at.%)

$$\tau_o^o = \frac{U_m}{V_o} \qquad (29)$$

for T>0 $$\tau_o(T) = \frac{\sqrt{3}}{2} \cdot C \, \frac{U_m - kT\ln(\dot{\gamma}_o/\dot{\gamma})}{b^3} \qquad (30)$$

At finite temperatures the friction stress is decreased by thermal activation expressed in its simplest form in equation (30).

In order to make a comparison between the theory and the experiment we will first calculate the activation volume as a function of the solute concentration according to equation (28). Since the measured activation volume varies with temperature it is essential to extrapolate these values to 0°K and then compare with the V_o obtained from equation (28). This has been done in fig. (83). The solid line represents the calculated value whereas the dashed line follows the extrapolated values of the activation volume to 0°K. It is apparent that the theroetical prediction agrees with the experimental results only at concentrations of solute greater than 0.3 at.%. There is marked deviation at low concentrations specially at concentrations below 0.05 at.% Zn, implying that the pinning of dislocation by single solute atoms is an unlikely mechanism at low concentrations, although at higher concentrations such a mechanism is possible. Additional support for the dislocation pinning by single solute atoms comes from the fact that the higher temperature flow stress is adequately explained by the friction stress mechanism in these alloys, which again involves the concept of single solute atoms interacting with dislocation lines.

Using τ_o^o for 0.45 at.% Zn alloy and the activation volume at 0°K the value of U_m is found to be 0.48 e.V., which is much too low compared to that obtained by the strain ratio change tests at 78°K. (H_o° = 1.237 e.V.). A similar discrepancy was encountered by Rogausch[121] in the case of Ag-In alloys.

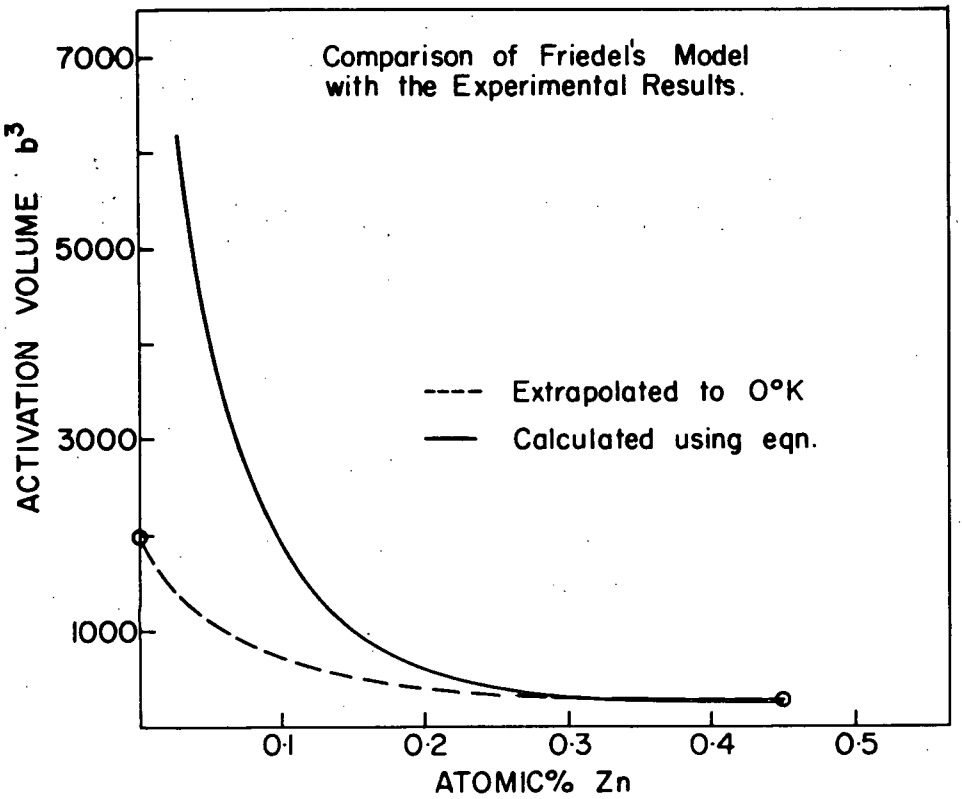

Fig. 83. Comparison of the experimental results with the composition dependence of activation volume as predicted by Friedel's model.

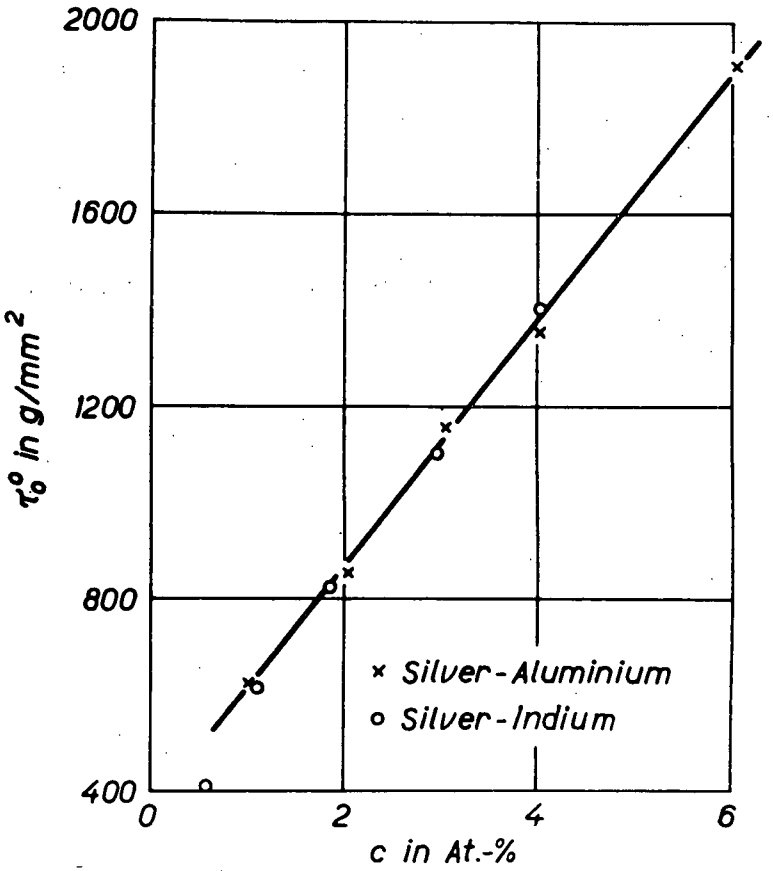

Fig. 84. Concentration dependence of CRSS extrapolated to 0°K for Ag-In and Ag-Al single crystals (after Haasen[2]).

Finally a remark may be made on the predicted linearity of τ_o^o on C as represented by equation (30). The present values of τ_o^o do not show a linear relationship with C. Earlier experiments of Rogausch on Ag-In[121] and those of Hendrickson and Fine on Ag-Al alloys[128] reveal that τ_o^o is a linear function of the solute concentration. The two sets of data plotted together are reproduced in fig. (84). A closer examination of these data shows that the straight line when extrapolated to zero concentration of solute gives τ_o^o for Ag = 380 gm/mm^2 whereas the actual τ_o^o from Rogauschs' data comes out to be less than 150 gm/mm^2. What this implies is that τ_o^o is not a linear function of C at low solute concentrations. The present experiments were performed on dilute Mg-Zn alloys and this is why τ_o^o is non-linear with respect to C. The reason for such a non linearity being that in this concentration range there exists a transition from the intersection mechanism to the solute atom dislocation pinning mechanism.

Recent experiments of Hendrickson[85] on Ag solid solutions suggest that the dislocation density is not affected much by solute addition. However, the scatter in the dislocation density measurements was too high in Hendricksons' experiments to distinguish the change of density by a factor of two or three.

2.4.3.6. Strengthening Mechanism in Dilute Alloys:

The solution strengthening parameter S_I when plotted against temperature, shows a linear decrease upto 330°K, above this temperature, however, no solution strengthening is observed. The most obvious conclusion would be that the addition of solute upto 0.025 at.% Zn does not contribute to the long range stress field.

Moreover, since solution strengthening is observed at low temperatures, it must be due to some sort of a short range interaction process. It was shown in a previous section that the rate controlling mechanism in Mg and the low alloys under consideration is one of intersection of forest dislocations. Also, since the experimental results have shown that the forest dislocation density does increase rapidly with alloying in the low alloys, it is most likely that solution strengthening is caused by the presence of a larger number of forest dislocations. The constancy of T_c in the CRSS-temperature plot further substantiates the above conclusion.

In the presence of available data on the extent of increase in the forest density with solute concentration, it is possible to make a quantitative comparison between the observed strength of the alloy with that predicted by the higher forest density.

Assuming the forest dislocations to form a regular "square" array, Seeger[148] has developed an equation which relates the stress required for the intersection process to the forest spacing l_s as follows:

$$\tau = \tau_G + \left[\frac{\alpha \Gamma d}{b l_s d} - \frac{kT}{b l_s d} \ln \frac{\rho b^2 \nu_o}{f \dot{\gamma}} \right] \qquad (31)$$

where ρ is the density of the glide dislocations,

f is the fraction of the slip plane over which the maximum average amplitude is τ_G

ν_o is the Debye frequency,

Γ is the average line energy,

$\dot{\gamma}$ is the strain rate,

d is the effective diameter of the forest dislocations,

α is a strength factor such that,

$\alpha\Gamma$ is the strength of the obstacle, the rest of the symbols have their usual meanings.

Moreover,

$$\tau = \tau_G \quad \text{at } T_C \leqslant T \tag{32}$$

therefore,

$$\alpha\Gamma d = kT_c \ln \frac{\rho b^2 \dot{\gamma}_o}{f\dot{\gamma}} \tag{33}$$

where T_c is the critical temperature above which thermal fluctuations in energy greater than $\alpha\Gamma d$ occur as frequently as is needed to maintain the imposed strain rate even when $\tau^* = 0$.

To this approximation the mechanical behaviour for cutting a simple type of localized obstacle, the stress to induce flow at the absolute zero is given by

$$\tau_o = \tau_{G_o} + \frac{\alpha\Gamma_o}{bl_s} \tag{34}$$

On the basis of this model the behaviour of the dilute Mg-Zn alloys will now be examined. It is clear from the CRSS-temperature relationships in fig. (47) that the flow stress of magnesium becomes athermal at 330°K. Also this value of T_c is unaffected by solute in the 0.006 and 0.019 at.% Zn alloys. This constancy of T_c implies that the strength of the obstacles remains unchanged by the addition of solute i.e. τ_G is independent of zinc concentration. Under such circumstances the thermally activated component of flow stress can be affected only through a change in l_s (bearing in mind here that τ_G is constant). In other words a change in the forest dislocation density is responsible for solution strengthening at low concentrations. Now equation (34) can be rewritten as follows:

$$\tau_o = A + \frac{B}{l_s} \tag{35}$$

where $A = \tau G_o = 40$ gm/mm^2, independent of Zn concentration and $B = \frac{\alpha\Gamma_o}{b}$.

B will also be taken as independent of Zn concentration since the variation in b and the shear modulus with concentration are much smaller than that in l_s (Γ_o is a function of the shear modulus).

Now expressing τ_o in terms of forest dislocation density

$$\tau_o = A + B\sqrt{\frac{1}{l_s^2}} \qquad (36)$$

or, $$\tau_o = A + B\sqrt{\rho_F} \qquad (37)$$

where ρ_F is the forest dislocation density.

However, at low solute concentrations

$$\rho_F = 3.4 \times 10^4 \left[1 + 5.35 \times 10^4 C\right] \text{ cm}^{-2} \qquad (3a)$$

Substituting in equation (37) the value of ρ_F

$$\tau_o = A + 184.4 \times B \left(1 + 5.35 \times 10^4 C\right)^{1/2} \qquad (38)$$

Using the data for pure magnesium, the constants A and B can be determined. A and B come out to be

$A = 48.8 \text{ gm/mm}^2$ (taking G into account)

$B = 0.196 \text{ gm/mm}$

Therefore, $$\tau_o = 48.8 + 36.2 \left(1 + 5.35 \times 10^4 C\right)^{1/2} \text{ gm/mm}^2 \qquad (39)$$

The CRSS of 0.006 and 0.019 at.% Zn alloy calculated using equation (39) are shown in the table below.

TABLE IV

Strengthening due to increased forest density.

At. % Zn	τ_o^o Extrapolated in gm/mm^2	τ_o^o Calculated in gm/mm^2
0.006	106	122
0.019	130	168

It is seen from the Table IV that the calculated values come out to be higher than the CRSS extrapolated to 0°K. However, the extrapolation is done over too large a temperature range to be considered accurate. A quantitative comparison will be meaningful only when experimental data are available close to absolute zero. Nevertheless, qualitatively the $C^{\frac{1}{2}}$ dependence of the CRSS is in agreement with the dictates of the forest intersection mechanism. Further evidence in support of this conclusion comes from the activation volume measurements. This has been discussed earlier.

It is worth while examining at this juncture the assumptions involved in the idealized prototype model of Seeger which has been used for calculating τ_o. Deviations from the predicted value can occur due to the following reasons. 1) the force displacement diagram can differ from the simple case assumed in calculating equation (35). However, in the case of magnesium this approximation is justified, because it is a case of intersection of undissociated basal glide dislocations with unreactive forest dislocations.

2.4.3.6.1. Deviations from Square Array:

Obstacles never form a regular array as assumed in formulating equation (35). Enough progress has been made on the statistical treatment of the problem to suggest that randomly dispersed obstacles give much lower stresses over the lower temperature range than is obtained from the square arrays[129,130]. Over the higher temperature range, however, the stress τ^* for the random distribution of obstacles lies above that predicted for a square array model and decreases very slowly with increasing temperature.

Whereas it was assumed that a single cutting would permit the dislocations to move only over the average area l_s^2 in the square array, it has been demonstrated by Kocks[130] and by the computerized experiments of Foreman and Makin[129], that a larger area is swept out. This arises because once a cutting has been achieved there is a certain probability the dislocation can unzip past the next neighbour etc.

In view of these limitations inherent in the theoretical formulation of equation (35) the observed values of τ_o^o may be considered to be in good agreement with the theoretical predictions.

2.4.4. Work Hardening of Mg Solid Solutions:

In the past much of the work in solution strengthening has been concerned with the understanding of the fundamental strengthening mechanisms governing the onset of plastic flow. However, attempts to correlate the stress strain curves of single crystals to those of the corresponding polycrystalline aggregates have revealed that relationships do exist between the two sets of work hardening parameters[131-135]. Keeping in mind that the ultimate objective of the single crystal study is to lead to an understanding of the macroscopic flow characteristics of the polycrystals, a study of solution strengthening would be incomplete without a discussion of the work hardening behaviour in alloy single crystals.

The work hardening characteristics of the Mg-Zn alloy single crystal oriented for basal slip are discussed below.

2.4.4.1. The Easy Glide in Magnesium:

It was first pointed out by Mott[136] that the deformation mechanisms in face centred cubic crystals in stage I and in Hexagonal close packed crystals in stage A are similar. The work hardening rate in easy glide is typically 10^{-4} - 10^{-5} G and in both cases it appears that the crystals deform almost entirely on one slip plane.

Two principal theories have been proposed to explain the work hardening in easy glide: that of Seeger et al[137] and of Hirsch and Lally[29]. Hirsch's theory has been extended further by Hazzledine[138]. Essentially both the theories assume that Frank-Read sources are present in the crystal and that they emit dislocations under applied stress. In Seeger's model it is assumed that a certain number of sources remain active throughout stage I and emit dislocations gradually during deformation. Seeger's model is a close approximation to the case of Cu, Zn, Ni-Co alloys etc. On the other hand, slip line studies[29] in Mg indicate that only a fraction of the sources are active in any small strain interval, the density of active sources is independent of strain and dislocations are emitted in bursts from the sources[138]. Hirsch's theory was originally designed for the case of Mg and hence will be discussed in brief.

In Hirsch's model the dislocations from sources operating simultaneously trap one another and form dipole bands for edges and screws; the screws annihilate by cross slip leaving edges and an excess of screws of one sign. The flow stress is controlled by the internal stress from the excess edge and screw dislocations and from those with non primary basal Burgers vectors. Since the dislocations are paired off or annihilate, their contribution to work hardening is expected to be low.

In this model the dislocation arrangement is stabilized by a frictional force of some kind and the prism segments or the jogs are believed to constitute the Frank-Read sources.

The increase in the hardening rate in Mg with decreasing temperature could be explained as follows. Since the jogs are more difficult to move at lower temperatures, the effective source length will become smaller as the temperature decreases. The number of potential sources is also likely to increase, because the minimum height of a jog which can serve as anchoring point for a source would be smaller (the stable jog height being temperature dependent). Moreover, since the CRSS for prismatic slip increases rapidly with decreasing temperature, the screws are less likely to annihilate and will probably form dipole bands. The increase in friction stress due to the presence of jogs, which are difficult to move, will lead to a situation where the dipole bands can support a larger number of excess dislocations of one sign.

Basinski[3] has observed that Cottrell-Stokes' law is obeyed in magnesium below 60°K. However, at higher temperatures deviations occur; suggesting the presence of two short-range processes. This observation has been rationalized in the light of Hirsch's theory as follows. The density of the prism segments produced by cross slip increases with increasing strain. Intersection of these segments leads to the formation of kinks, which is a thermally activated process and, therefore, contributes to the decreasing activation volume. The origin of the observed Cottrell-Stokes law can be attributed to the proportionality between the prism segments produced by cross slip, and the density of the screw dislocations (before annihilation), when annihilation occurs.

The present results are in fairly good agreement with the above theory.

2.4.4.1.2. Easy Glide in Alloy Crystals:

It is now well established that in the case of solid solutions having fcc structure, the extent of easy glide increases with solute addition, the work hardening rate in Stage I remains unaffected in systems showing limited solid solubility, and decreases where the solubility is extensive[2,139]. In body centred cubic metals the effects are irregular, possibly because of uncontrolled interstitial impurities[1].

The work hardening behaviour of hexagonal alloy single crystals, however, has not been investigated thoroughly. The early work of Schmid and co-workers had indicated that the work hardening rate in Mg increases with solute concentration in the case of Zn and Al solutes[88]. On the other hand Zn exhibits a lowering in θ_A with increasing impurity content[88,147].

An attempt will be made here to explain qualitatively the observed dependence of θ_A on Zn concentration in the light of Hirsch's theory of work hardening in Mg[29].

The dislocation sources in Mg are the prism segments or jogs. The effect of solute upto 0.025 at.% Zn is to increase the forest dislocation density. This leads to an increase in the number of Frank-Read sources resulting in a larger number of dipole bands being formed, which in turn increase the long range stress field and a more rapid hardening results. Moreover, since the CRSS for prismatic slip

becomes higher, the screws are less likely to annihilate and will probably form dipole bands, although the contribution from the latter source would be small as pointed out by Hirsch[29].

An increase in the solute content above 0.025 at.% Zn results in a rather rapidly increasing friction stress arising from the size and modulus interactions. In the presence of a higher friction stress the dipole clusters become difficult to move. In fact, the magnitude of the friction stress determines the way in which the excess dislocations distribute themselves. Thus the presence of solute will lead to a higher work hardening rate through a change in the friction stress.

2.4.4.2. The Temperature Dependence of θ_A in Alloy Crystals:

The low temperature work hardening in the easy glide of alloy crystals containing upto 0.025 at.% Zn, can be explained in much the same manner as in pure Mg. As shown earlier, the rate controlling mechanism at the onset of flow in Mg and the low alloys is one of intersection. The increase in θ_A in these alloys, however, arises due to the following reason. The presence of a larger number of jogs in these alloys increases the low temperature friction stress, enabling the dipole bands to support a larger number of excess dislocations of one sign. The increased stability of the dipole bands, leads to a more rapidly increasing flow stress with strain.

When a dislocation moves at a low temperature on the basal plane of an alloy crystal, containing solute in excess of 0.025 at.% Zn, the long range friction stress is overcome (as at higher temperatures) and also the forest dislocations are intersected. In addition a short range obstacle must also be surmounted. The friction stress arising due to this short

range solute dislocation interaction increases with decreasing temperature. Therefore, the work hardening rate θ_A should increase with decreasing temperature as the solute content is increased. Qualitatively this is in agreement with experiment as can be seen from fig. (54).

The parabolic nature of the concentration dependence of θ_A arises probably due to a $C^{\frac{1}{2}}$ relationship between the increase in forest density with solute content at low concentration and that between the friction stress as the Zn content is increased.

2.4.4.3. The Extent of Easy Glide:

The face centred cubic metals Cu, Ni and Al show a continuous decrease in γ_{II} with increasing temperature[140].

On the other hand the hexagonal metals Cd[72] and Zn[140] exhibit an increase in the extent of easy glide with increasing temperature.

The present results on magnesium indicate an increase in γ_B with temperature upto 295°K. Above this temperature, however, easy glide is followed by a parabolic hardening, which masks stage B. Hence the decrease in γ_B beyond 295°K as shown in fig. (56) should be accepted with reservation.

The reason for the termination of easy glide and the onset of the rapid hardening is not the same in all materials. For example slip on the secondary systems is known to be responsible for the onset of stage II in the fcc metals and alloys. In hcp Zn and Cd, the condensation of vacancies into sessile loops is considered responsible for the rapid hardening[137].

No well established theory, however, exists for the case of magnesium. It has been suggested by Hirsch[29] that the density of dipole bands becomes so large at the end of stage A that they trap the new dislocations formed. The stress concentration, therefore, increases leading to twins being nucleated, which subsequently act as barriers to the new slip lines. The pairing of the newly formed dislocations is largely hindered because of the twins. These dislocations pile up, leading to a stress concentration. The stress concentration is relieved by slip on the basal plane with non-primary Burgers vectors, prismatic slip and further twinning.

The observed decrease in γ_B with alloying can be rationalized in terms of an increase in θ_A with alloying. Since the work hardening rate increases with alloying, the stress to nucleate twins is reached earlier in the alloy than in Mg, provided the shear stress for twin formation remains unaffected by solute. However, even if the stress required for twinning increases with solute content, γ_B can still decrease with alloying provided the increase in θ_A is sufficiently large so as to attain the stress level necessary to nucleate twins at a strain less than γ_B in Mg.

The increase in γ_B with temperature in these alloys can perhaps be rationalized in a similar manner considering the high temperature dependence of θ_A and a low temperature sensitivity of the twinning stress.

2.4.4.4. Work Hardening in Stage B:

The work hardening rate in stage II of fcc metals is typically $\theta_{II} = 3 \times 10^{-3}$ G at room temperature.

The work hardening rate θ_B for Mg at room temperature is 3.7×10^{-4} G, which is approximately an order of magnitude lower than in fcc metals. The low work hardening rate is thought to be due to the high stress necessary to nucleate twins, which can subsequently act as barriers to the formation of slip lines[29].

The variation of θ_B with temperature has never been explained in the past. However, on the basis of a twin model such a decrease is to be expected. Stress relief at the dipole bands is attained not only through twinning, but also through slip on the basal plane with non-primary Burgers vectors and by prismatic slip. Between room temperature and 423°K the CRSS for basal slip remains unchanged, therefore, excess stress relief at higher temperature is not expected to be due to slip on basal plane with non-primary Burgers vectors. However, in this temperature range the CRSS for prismatic slip decreases rather rapidly. Thus the extent of stress concentration becomes smaller due to the operation of prism slip. This leads to a slower process of twin nucleation and hence the work hardening rate decreases.

The Effect of Solute on θ_B:

The CRSS for basal slip increases with solute content in alloys containing solute in excess of 0.025 at.% Zn, whereas the operation of prismatic slip becomes more difficult in the lower alloys. Both these processes would lead to a higher stress concentration at the dipole bands

than in Mg. The stress concentration will result in a larger number of twins being nucleated and thus the work hardening rate will be higher.

2.4.4.5. The Stage 'C' of Deformation:

The stage III of work hardening in face centred cubic solid solutions is associated with cross slip and therefore τ_{III} can be used to calculate the stacking fault energy of the material[141-142].

The origin of stage C in magnesium, however, is not well understood. Crystals deformed into stage C do not show cross slip markings when examined under optical microscope. The slip lines appear in coarse clusters. The exsistence of fine cross slip markings, however, cannot be ruled out. Replica studies of the slip lines may resolve this problem. A discussion of the effect of solute on τ_C in Mg will be premature, until the reason for the dynamic recovery is established.

2.4.5. The Effect of Solute on the Ease of Prismatic Slip:

2.4.5.1. Introduction and Objectives:

The role of prismatic slip in the deformation of the polycrystalline aggregates of Mg and its alloys has been pointed out earlier in this thesis. However, the study of single crystals oriented for prismatic slip, which should constitute the ground work for the understanding of the macroscopic deformation characteristics of Mg polycrystals has not attracted as much attention as it deserved. A rather comprehensive literature is available on the prismatic slip of Mg-Li alloys, which exhibit the so called "solid solution softening effect"[14-16,73]. It has been the conclusion of Dorn and his coworkers that only those elements which decrease the c/a ratio of magnesium would be effective in decreasing the CRSS for prismatic slip when dissolved in magnesium. Incidentally, the elements which decrease the axial ratio of Mg belong to group I of the periodic table. In contrast to this conclusion the present results on the deformation of the polycrystalline solid solutions of Mg containing solutes which belong to group II, III and IV of the periodic table (and hence increase the c/a ratio of Mg), suggest that irrespective of the type of solute added the CRSS for prismatic slip decreases with increasing amounts of solute beyond a critical concentration C_T.

Thus one of the objectives of the investigation of prismatic slip in single crystals was to evaluate the significance of c/a ratio (and hence valency) on the ease of prismatic slip. The second objective was to examine the effects of alloying at very low concentrations, where a rapid rate of solution hardening is observed in the polycrystalline alloys.

For this purpose the solute chosen was Zn. The choice of Zn was mainly due to the reason that the polycrystalline alloys of the Mg-Zn system exhibit all the three stages of solution hardening distinctly. Also the c/a ratio of Mg does not decrease by the addition of Zn. Some alloys containing Al as solute were also investigated. Aluminum belongs to a higher valency group (III) and increases the c/a ratio of Mg.

2.4.5.2. Experimental Results:

2.4.5.2.1. The Stress-Strain Curves:

The resolved shear stress vs shear strain curves of a representative set of Mg-Zn alloys are shown as a function of temperature for various compositions in figs. (85-88). It is apparent that the ductility is considerably lower in prismatic slip than in basal slip. For example pure magnesium undergoes fracture at a shear strain of 580% in basal slip whereas failure occurs at a strain less than 2% in prism slip. In prismatic slip, the shear stress increases in a parabolic manner with strain at low strain levels followed by a linear hardening at higher strains. In some cases a well defined third stage with a decreasing work hardening rate followed the linear hardening.

In order to make the effect of the solute apparent, the stress-strain curves of the alloys deformed at fixed temperatures are placed together and are shown in figs. (89-90). It is observed that at lower temperatures (78-200°K) the stress-strain curves of all the alloy single crystals fall below that of magnesium. But at temperatures above 200°K small additions of solute (up to 0.019 at.% Zn) lift the curves above that of pure magnesium. On increasing the alloying content beyond 0.02 at.%, however, the stress - strain curves fall below those for the lower alloys.

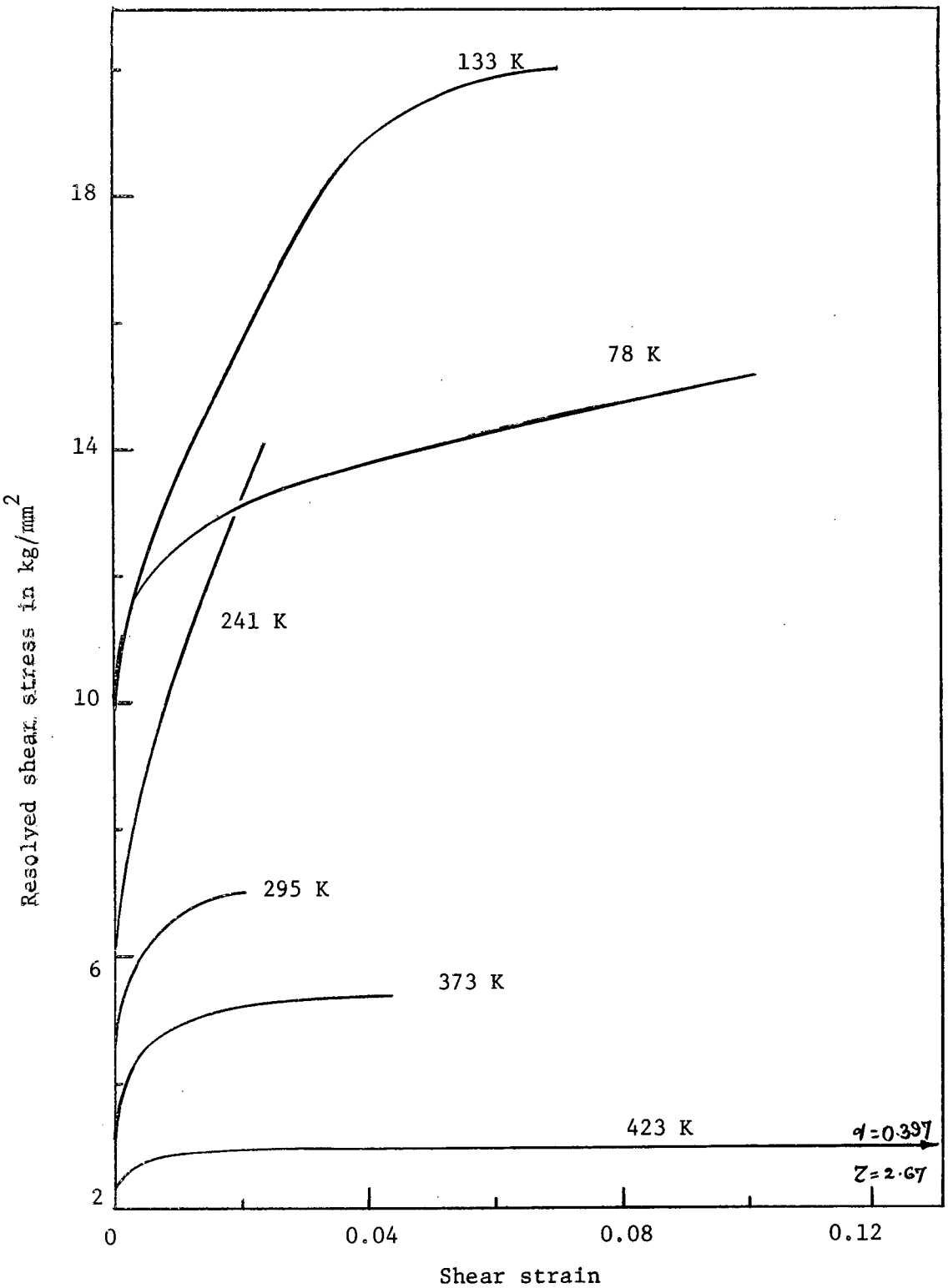

Fig. 85. Resolved shear stress vs. shear strain curves for Mg single crystals oriented for prismatic slip.

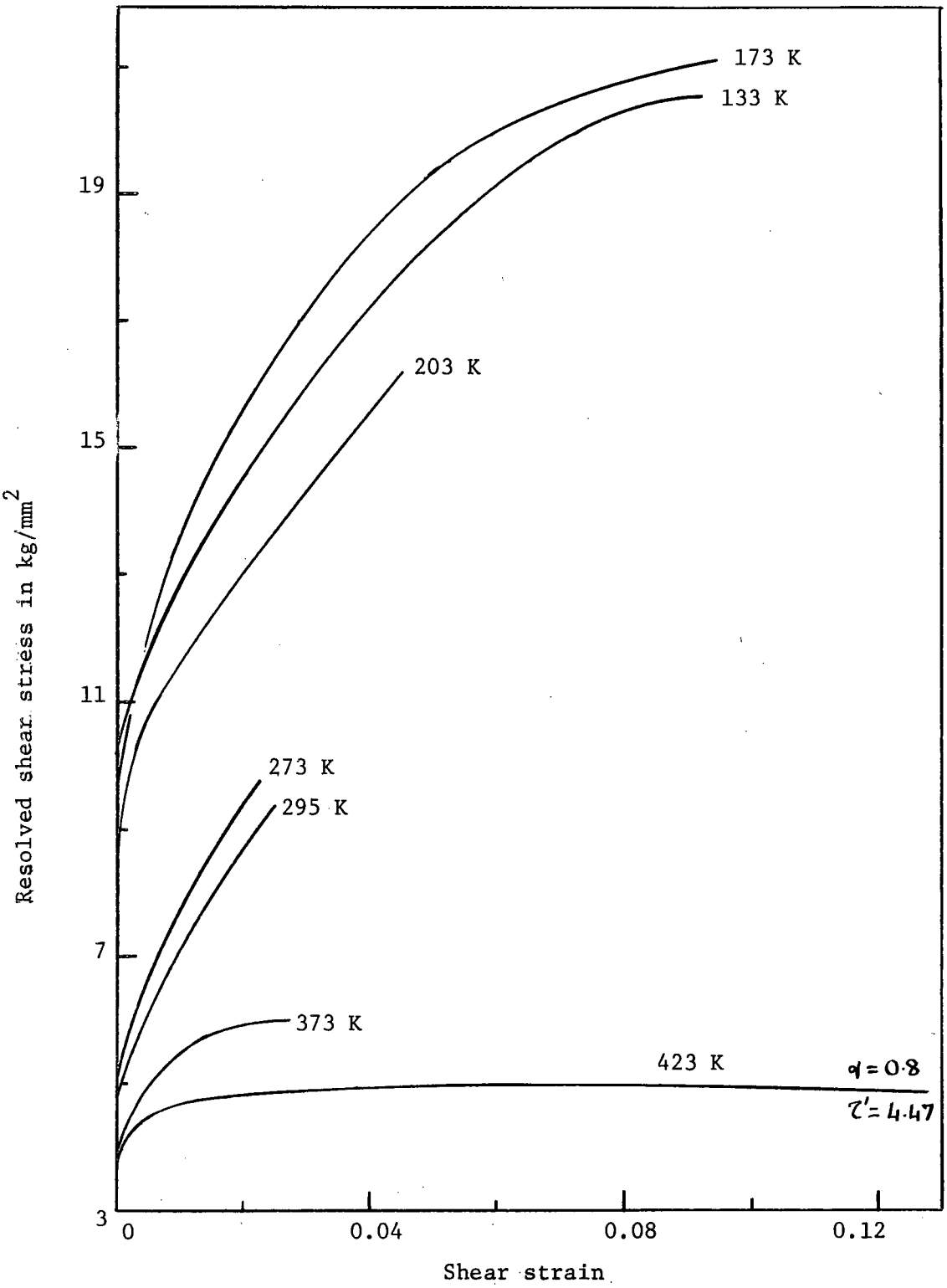

Fig. 86. Resolved shear stress vs. shear strain for Mg + 0.019 at. % Zn alloy single crystals oriented for prismatic slip.

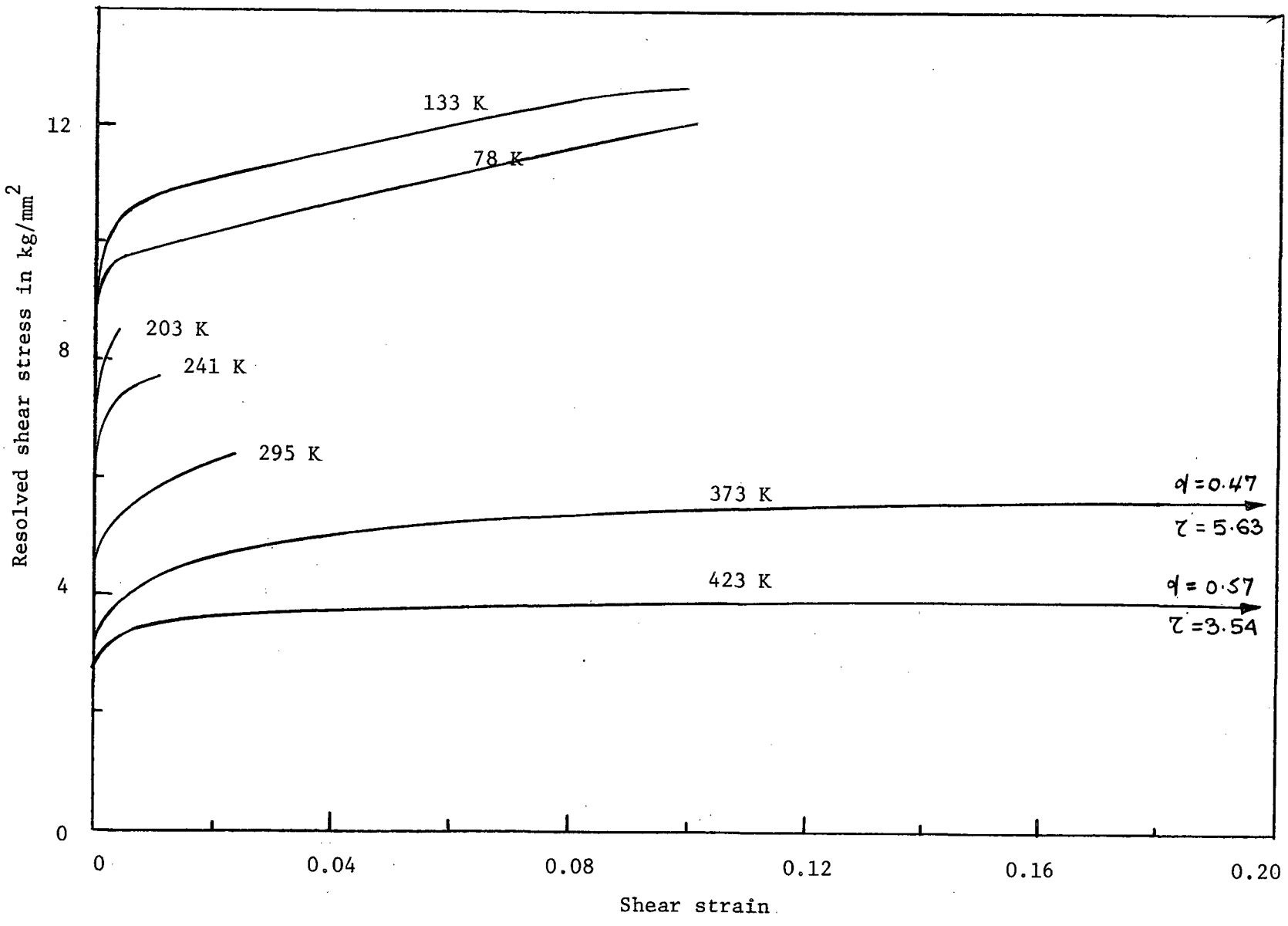

Fig. 87. Resolved shear stress vs. shear strain curves for Mg + 0.258 at. % Zn alloy single crystals oriented for prismatic slip.

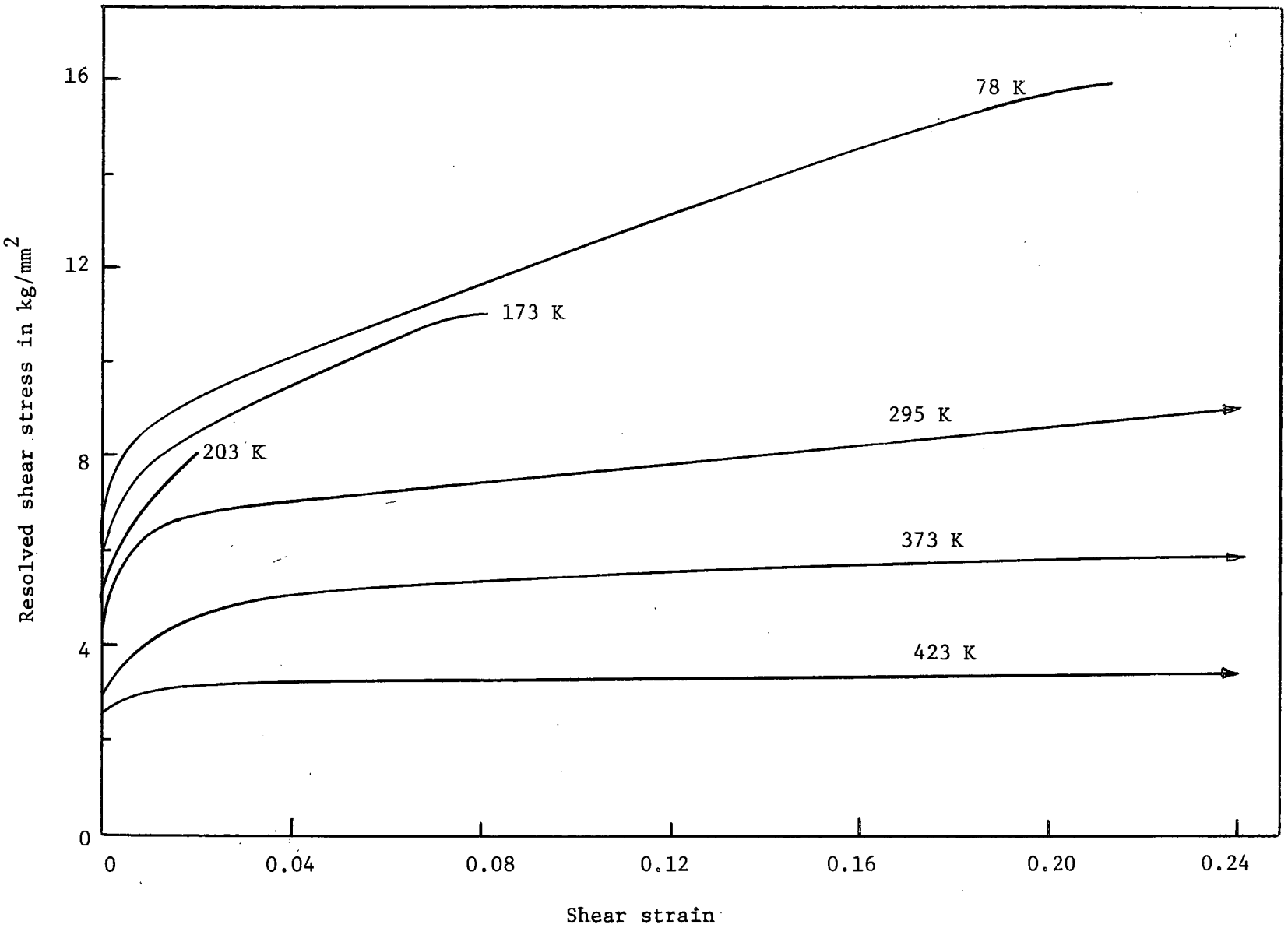

Fig. 88. Resolved shear stress vs. shear strain curves for Mg + 0.45 at. % Zn alloy single crystals oriented for prismatic slip.

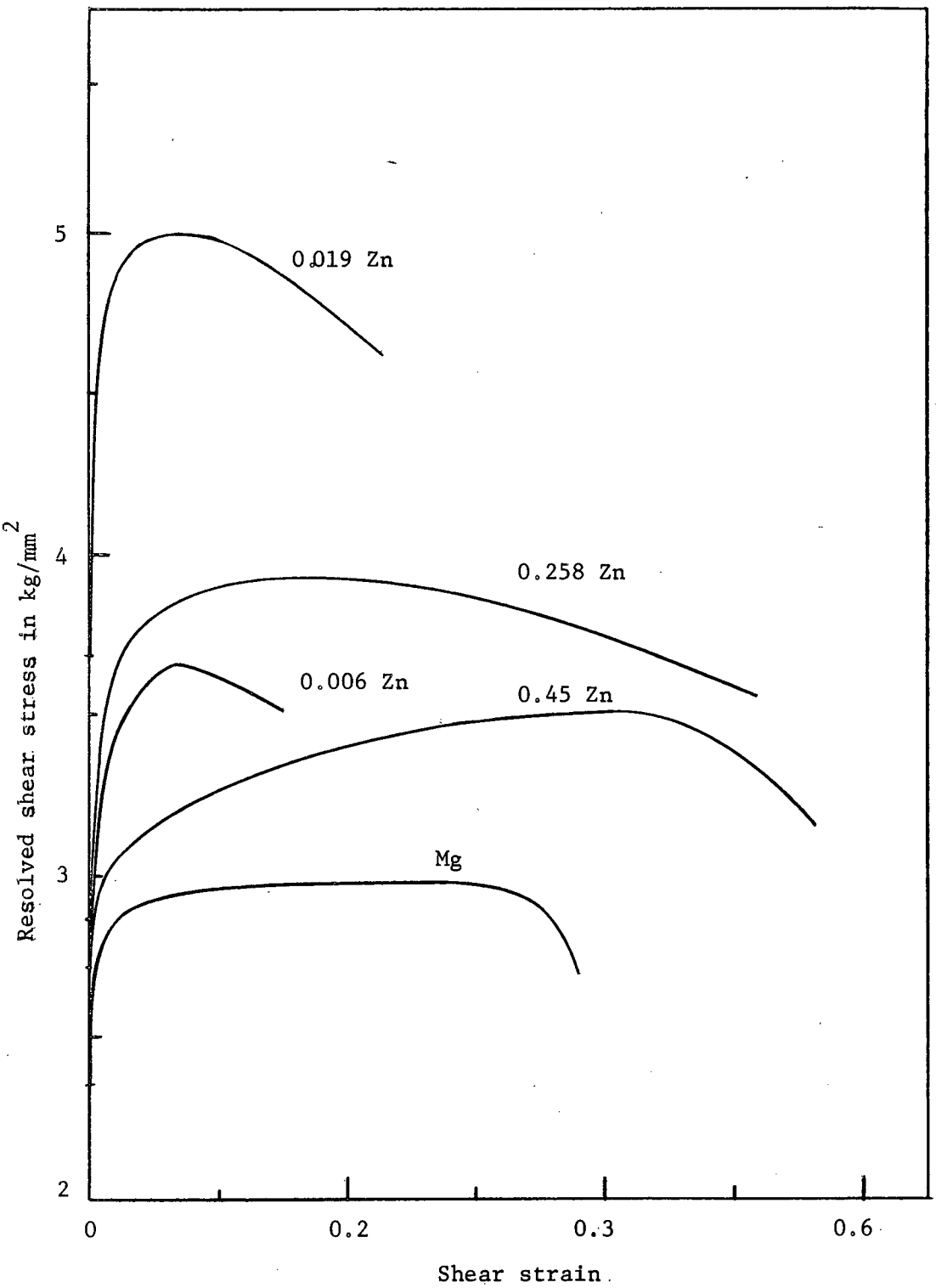

Fig. 89. Resolved shear stress vs. shear strain curves for Mg-Zn single crystals deformed at 423 °K in prism slip orientation.

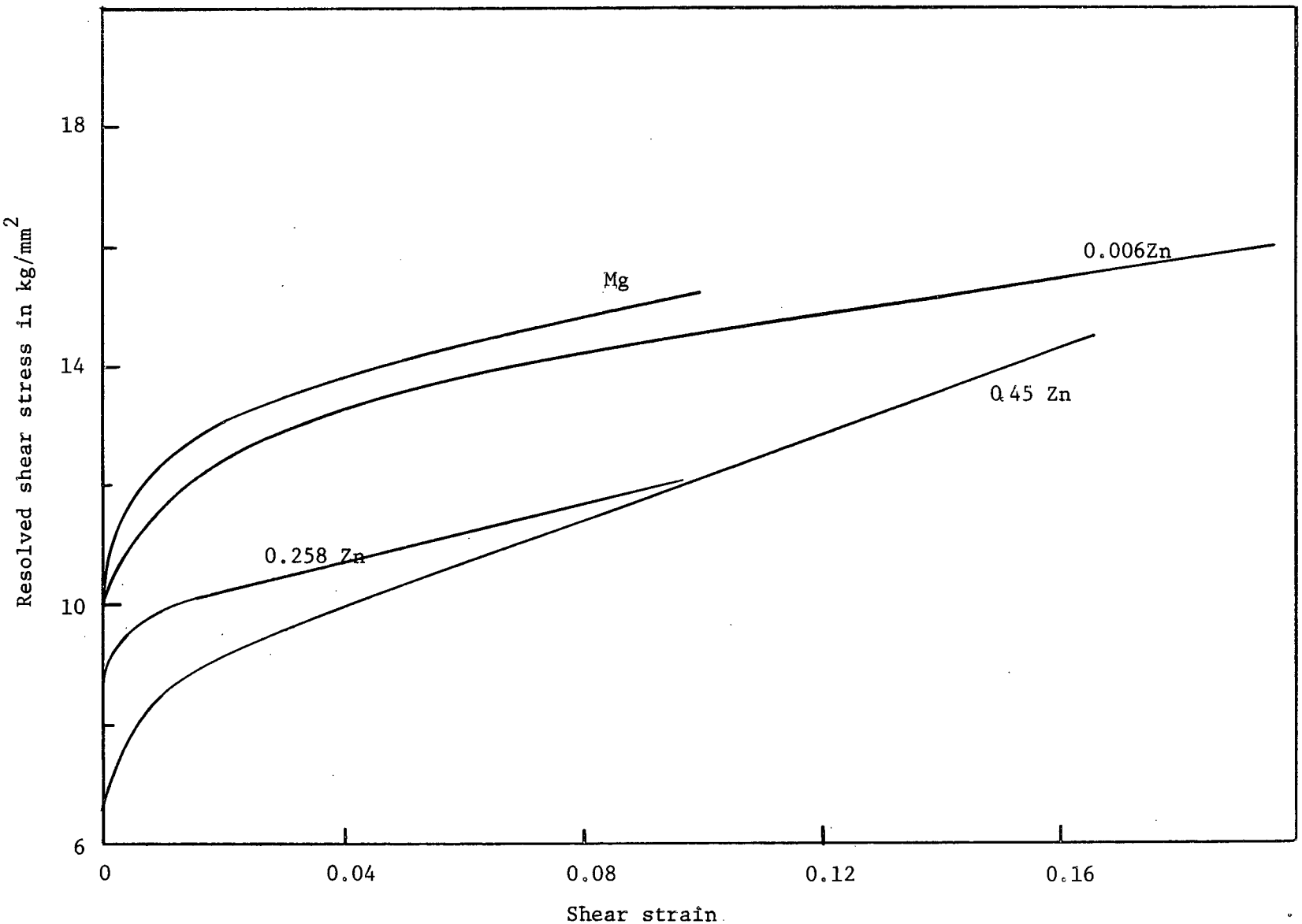

Fig. 90. Resolved shear stress vs. shear strain curves for Mg-Zn single crystals deformed at 78°K in prism slip orientation.

An interesting feature of the crystals tested at 423°K is the large amount of strain associated with work-softening. Similar work softening has been observed above room temperature in the compression of single crystals of Mg oriented such as to suppress basal slip[65]. Backofen et al[65] have attributed the softening to the onset of $\{10\bar{1}1\}$ - $\{10\bar{1}2\}$ double twinning. However, in the present tensile tests at 423°K the crystals showed necking, therefore, it cannot be concluded whether or not twinning is responsible for the loss in work hardening rate.

2.4.5.2.2. Ductility:

The shear strain to fracture is plotted against the testing temperature in fig. (91) for all the Mg-Zn alloys tested in orientations favourable to prismatic slip. It is observed that ductility decreases with increasing temperature in the range 78°-250°K and increases again at higher temperatures. A similar trend has been observed by Reed-Hill and Robertson[51] in pure Mg. In spite of the large scatter in data it can be seen that ductility decreases by small additions of solute at temperatures above 250°K, followed by a rapid increase at higher solute concentrations.

2.4.5.2.3. The CRSS for Prismatic Slip:

The first deviation from linearity was once again used as the yield criterion. The temperature and alloy dependence of the CRSS for prismatic slip in Mg-Zn alloys is shown in fig. (92).

The temperature dependence of the CRSS may be divided roughly into three regions. A relatively thermal insensitive region exists at temperatures between 78°K and 170°K, followed by a strongly temperature dependent stage. The temperature dependent stage merges gradually into a

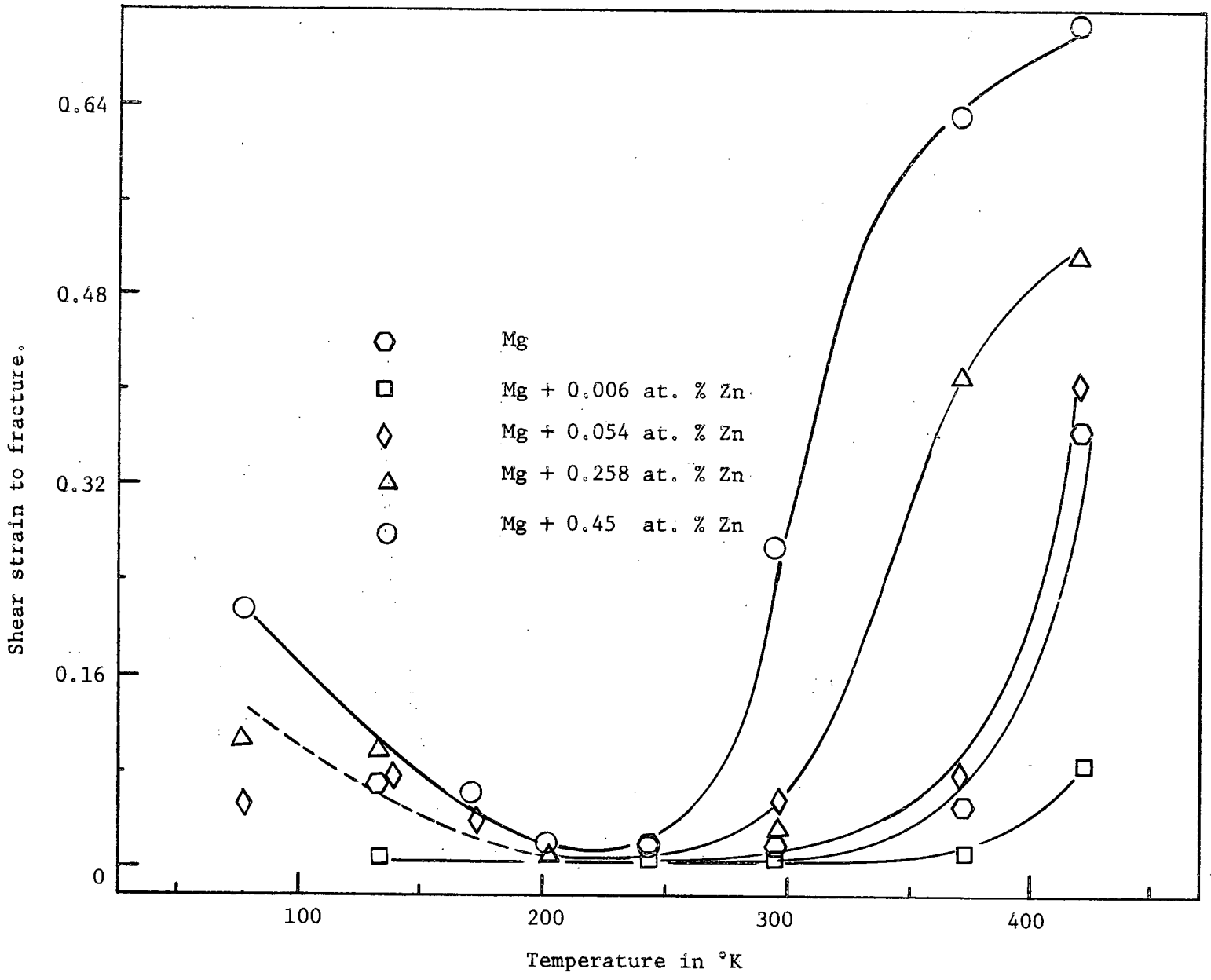

Fig. 91. Shear strain to fracture vs. temperature for Mg-Zn single crystals oriented for prismatic slip.

region of lesser temperature sensitivity at temperatures in the vicinity of 400°K. The numerical values of CRSS for Mg obtained in the present work are in agreement with the values reported in the literature[143].

2.4.5.2.4. The CRSS of Mg-Zn Alloys:

The composition dependence of CRSS for various temperatures is shown in fig. (93). From figs. (92 and 93) it is clear that at low temperatures the CRSS of magnesium remains unaffected by small additions of solute followed by a rapid decrease at higher concentrations. For example at 78°K the CRSS of Mg as well as an alloy containing 0.019 at.% Zn alloy is 9.95 kg/mm^2, whereas that for 0.45 at.% Zn alloy is 6.7 kg/mm^2.

At higher temperatures, on the other hand, the CRSS increases by small additions of Zn, followed by a decrease at higher concentrations. Above approximately 350°K the CRSS of all the alloys are higher than that of Mg.

The results of the Mg-Al alloys are shown in fig. (94). Higher alloys could not be investigated because of the difficulty encountered in growing single crystals containing more than 0.2% Al. The trend in the composition dependence of CRSS nevertheless is the same in both Mg-Al and Mg-Zn alloys. It is important to note at this juncture that the initial increase in CRSS for prismatic slip followed by a decrease at higher concentrations accounts adequately for the multistage solution hardening observed in the polycrystalline material.

Solid solution softening has previously been observed in Mg-Li alloys[73]. However, the study of single crystals oriented for prismatic slip was confined to concentrations in excess of 6 at.% Li. The existence

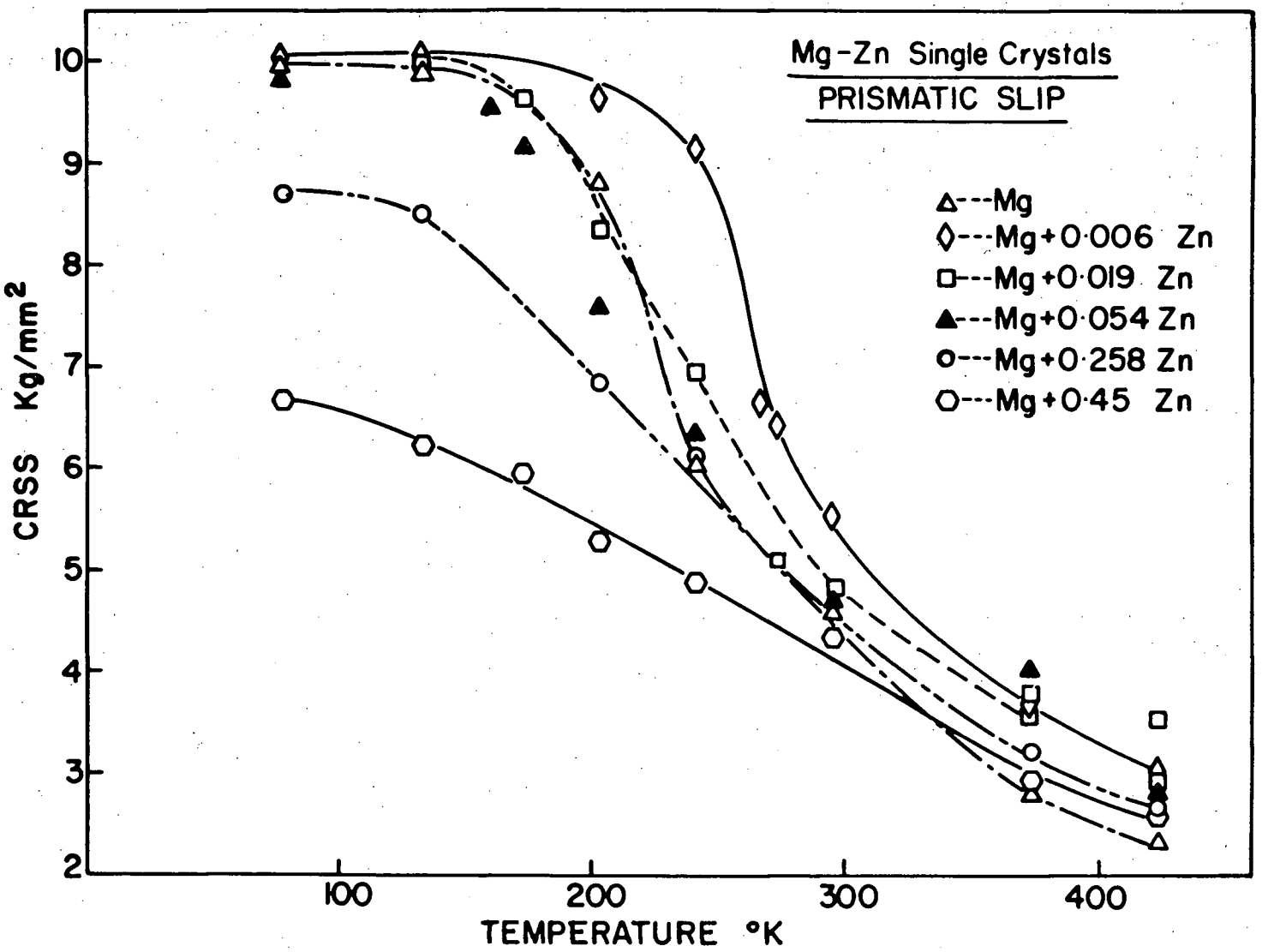

Fig. 92. CRSS for prismatic slip vs. temperature for Mg-Zn single crystals.

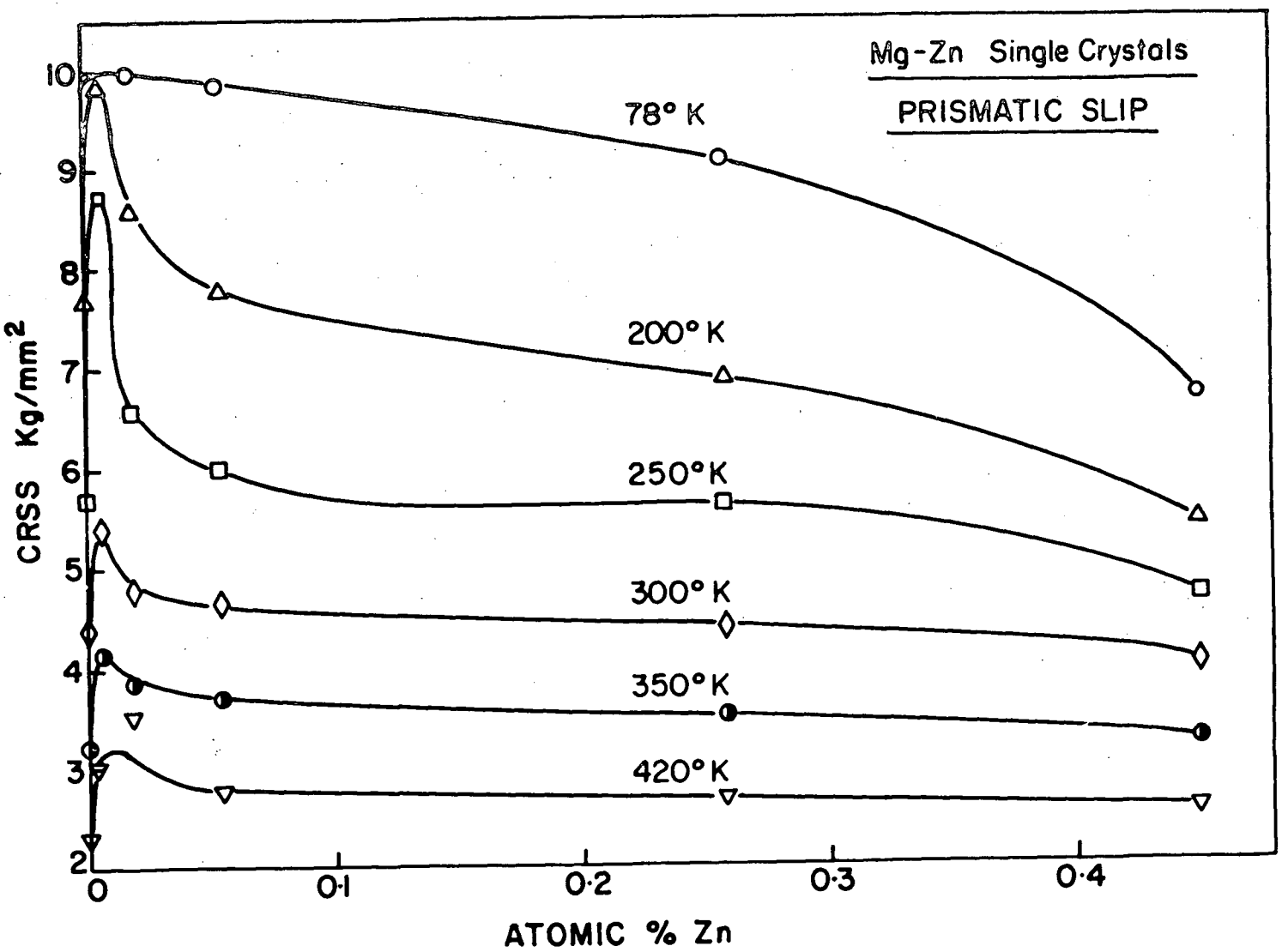

Fig. 93. CRSS for prismatic slip vs. Zn concentration.

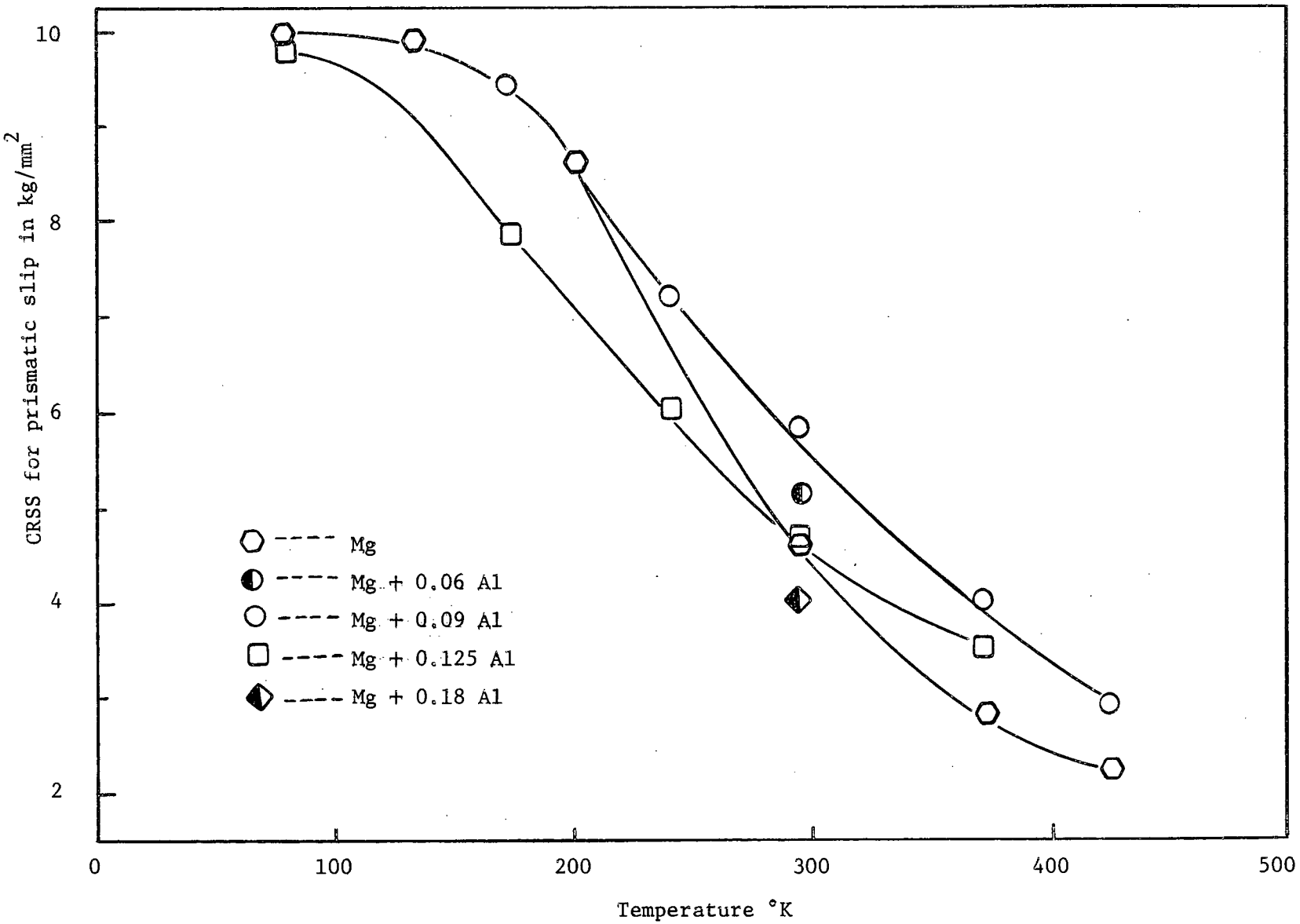

Fig. 94. CRSS for prismatic slip vs. temperature for Mg-Al single crystals.

of an initial rapid solution strengthening rate in the polycrystals of this system, however, suggests an increasing value of CRSS for prismatic slip in these alloys at low Li concentrations at room temperature.

2.4.5.2.5. The Effect of Solute on the Flow Stress:

The process of yielding in single crystals of Mg oriented for prismatic slip is rather gradual. Therefore, the interpretations based on the measurements of CRSS, which is taken as the first deviation from linearity can be erroneous, especially when the differences in the values of CRSS being examined are small (as is the case with the dilute alloys). In order to avoid this difficulty the flow stress values at various strain levels have been plotted against solute concentrations for a representative set of temperatures as shown in figs. (95 and 96).

Fig. (95) has been constructed for crystals deformed at 78°K. It is observed that the CRSS at low solute concentrations is much the same as that of Mg, but the flow stresses at higher strains decrease rapidly with Zn concentration. At the higher concentrations of solute on the other hand, the flow stress decreases less rapidly than does the CRSS.

The flow stress concentration relationship at 423°K (fig. 96) shows that the shape of the flow curves remains similar to that in the CRSS-concentration plot. The CRSS increases with solute content in the low alloys followed by a decrease at higher concentrations.

These results tend to confirm the validity of the interpretations based on the measurements of CRSS.

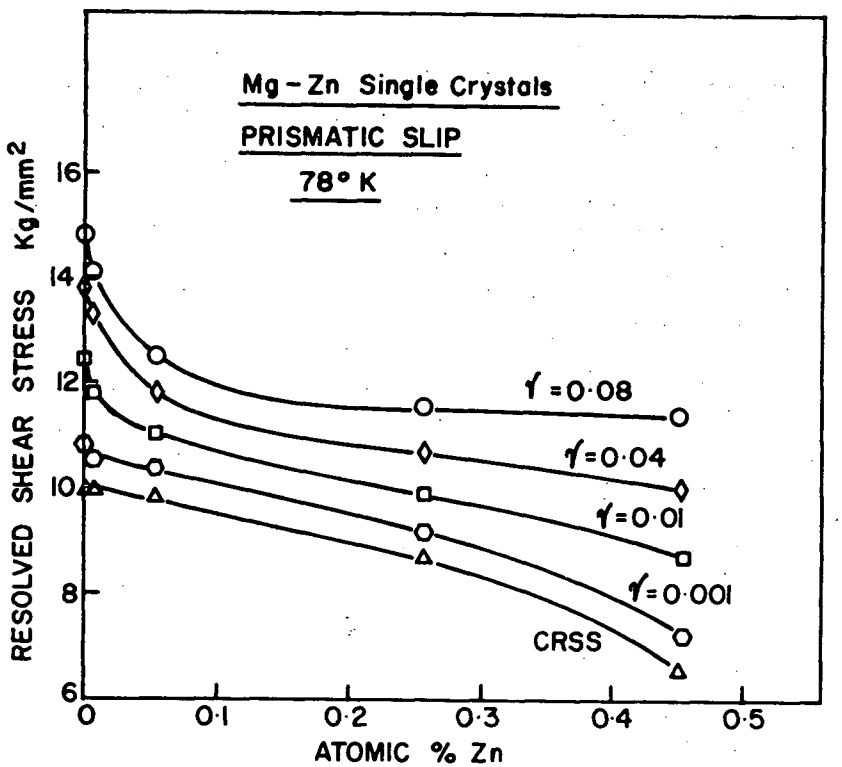

Fig. 95. Flow stress for prismatic slip vs. concentration for Mg-Zn single crystals tested at 78°K.

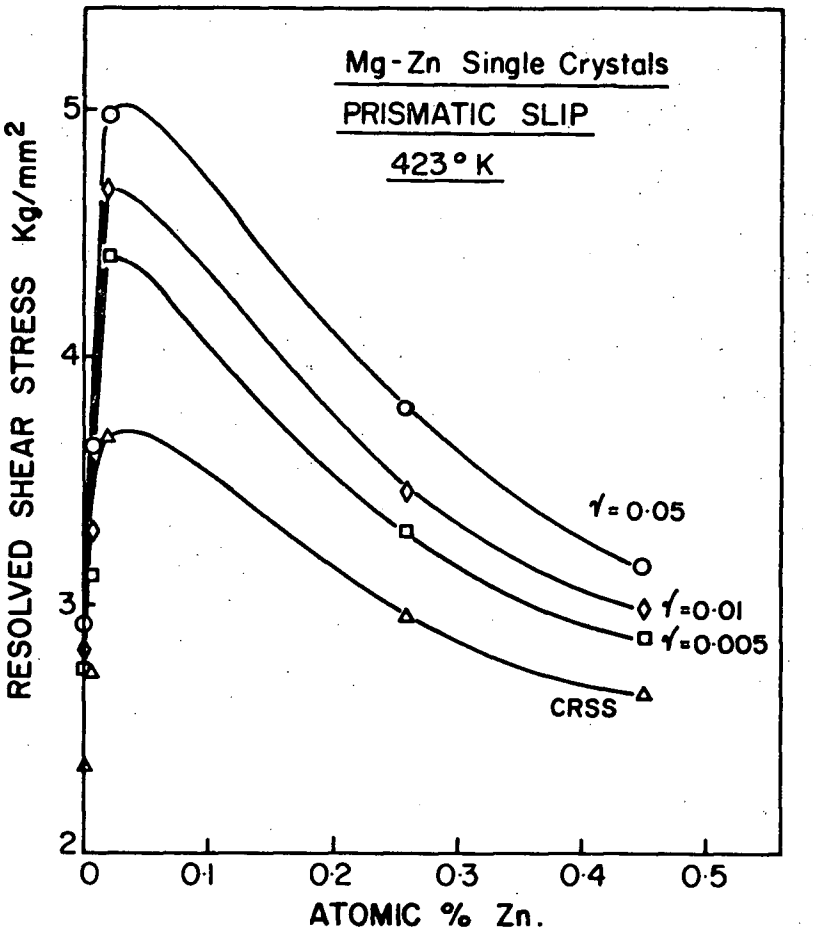

Fig. 96. Flow stress vs. concentration for Mg-Zn single crystals tested at 423°K.

2.4.5.3. Discussions:

An understanding of the dislocation mechanisms for slip in the pure metal is often helpful in analyzing the nature of the solute-dislocation interaction. With this view in mind the dislocation mechanisms responsible for prismatic slip in magnesium will be discussed followed by a discussion of the effect of solute.

2.4.5.3.1. The Dislocation Mechanism for Prismatic Slip:

Attempts have been made earlier to explain the dislocation mechanisms for prismatic slip in pure magnesium[52,143]. It has been the conclusion of Ward-Flynn, Mote and Dorn[143] that the rate controlling mechanism in prismatic slip above 450°K is the thermally activated cross slipping of screw dislocations extended in the basal plane as proposed by Friedel[104].

The low temperature rate controlling mechanism has never been systematically investigated in the pure metal. However, from the trend of the τ-T curve, Dorn suggests[73] that Peierls mechanism must be controlling below room temperature.

In the present work a limited number of strain rate change tests were conducted to test Dorns prediction of the mechanism of low temperature prismatic slip. The activation volumes were measured by changing the strain rate by a factor of ten. However, since Mg shows rather limited ductility at low temperatures it was difficult to conduct differential strain rate tests. This difficulty was overcome by deforming crystals of identical orientations to fracture using two different strain rates. The difference in yield stress was then used for calculating V^*.

Such a procedure has been used in the past on Mg-Li alloy single crystals[73]. The results of such tests on Mg, as well as a series of Mg-Zn alloys are shown in fig. (97). It is seen that in Mg as well as its alloys the activation volumes remain below 80 b^3 at temperatures up to 295°K. This is consistent with the idea of Peierls mechanism as the rate controlling step. It is important to point out at this juncture that the activation volume associated with the cross slip process is $> 100\ b^3$. In the alloy containing 0.006 at.% Zn, the activation volume was found to be 205 b^3 at room temperature which is higher than that associated with Peierls mechanism. No explanation, however, could be afforded for this exception.

A quantitative verification of the Peierls mechanism cannot be made here since magnesium does not show a distinct transition temperature from the thermally activated to an athermal mechanism. It is interesting to note that in the case of magnesium an athermal region does not exist i.e. The Friedel cross slip mechanism, which is a thermally activated process, takes over the low temperature Peierls mechanism, which again is thermally activated.

2.4.5.3.2. The Effect of Solute:

The effect of solute on the strength of crystalline solids in general is best understood if the contribution of the solute to the athermal and the thermally activated components of the flow stress are considered separately.

The experimental results on solid solutions available to date indicate that the athermal flow stress never decreases with the addition of solute, although τ^* increases or decreases depending on the rate

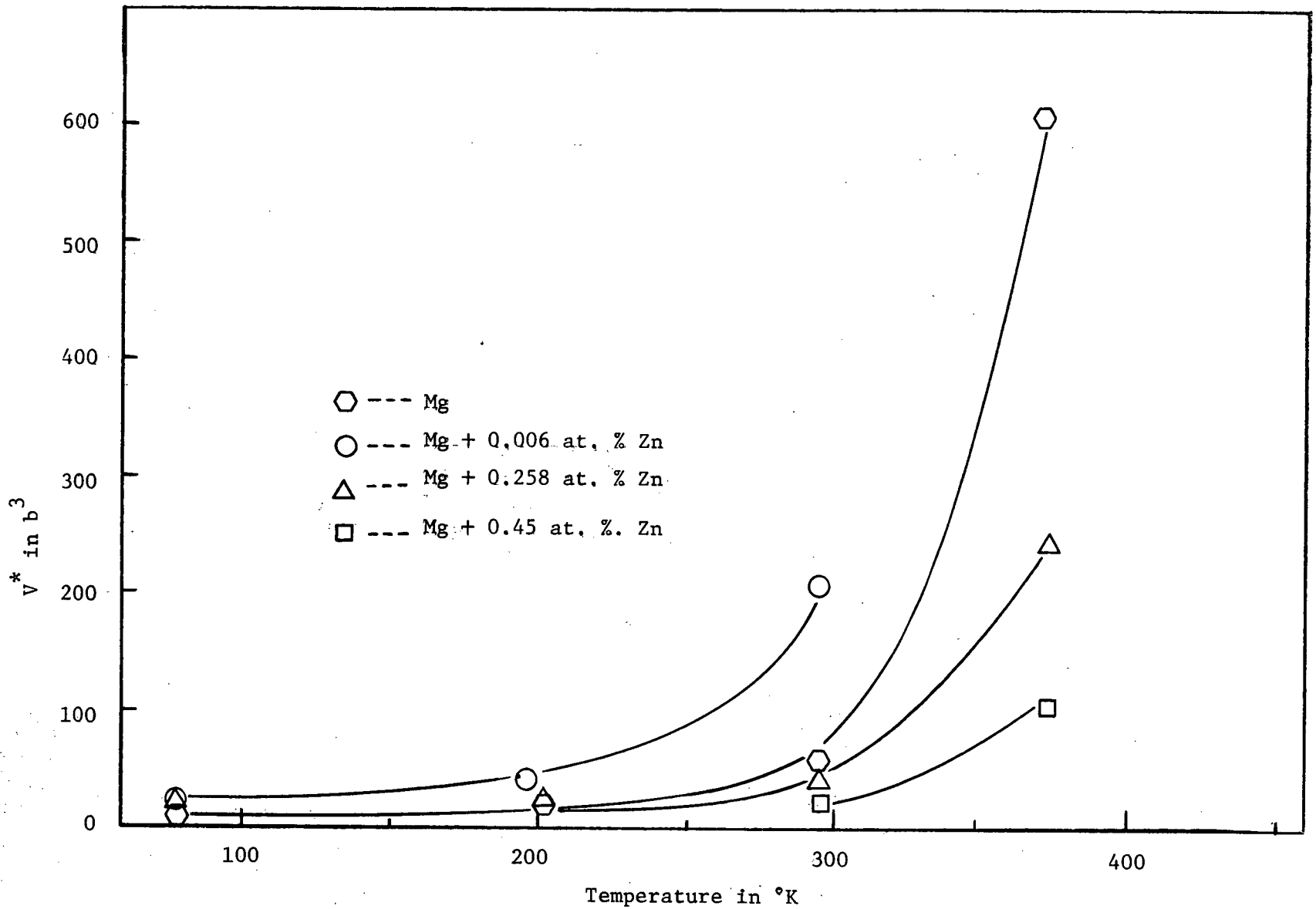

Fig. 97. Activation volume at yield vs. temperature for Mg-Zn single crystals deformed in prism slip orientation.

controlling mechanism operative in the alloy. From the results of the experiments by Ahmadieh and Dorn[73] on Mg-Li alloys it is seen that at sufficiently high concentrations of lithium the athermal stress level becomes apparent and that it increases with increasing solute content, as would be expected of the athermal stress in relation to solute. The appearance of the athermal stress level deserves a critical examination. For the time being the experimental observation that the Peierls stress decreases with increasing Li content will be taken for granted. Since the athermal stress increases and the τ^* term decreases with increasing lithium addition, T_c (from Peierls to athermal) is expected to decrease also with lithium concentration as is observed (fig. 98). The consequence of such a decrease in T_c is that the thermal energy available at T_c is not high enough for cross slip to occur, therefore, the dislocations have to move under the long range stress field (athermal).

].4.5.3.3. The Results of the Present Work:

The results of the Mg-Zn alloys can be explained in terms of an increasing τ_G and a decreasing τ^*. Note that in the case of Mg-Zn alloys the increase in τ_G and the decrease in τ^* are not sufficient to make the athermal stress level appear in the τ -T curve. At lower temperatures, where the τ^* term is dominant over τ_G, the increase in τ_G is of little importance and therefore the CRSS decreases continuously with Zn concentration.

At higher temperatures, however, a peak in the CRSS-concentration curve appears. This can be explained better with the help of a sketch. Fig. (99) illustrates the situation schematically. We will assume for the sake of argument that τ_G in the alloys arises due to a friction stress

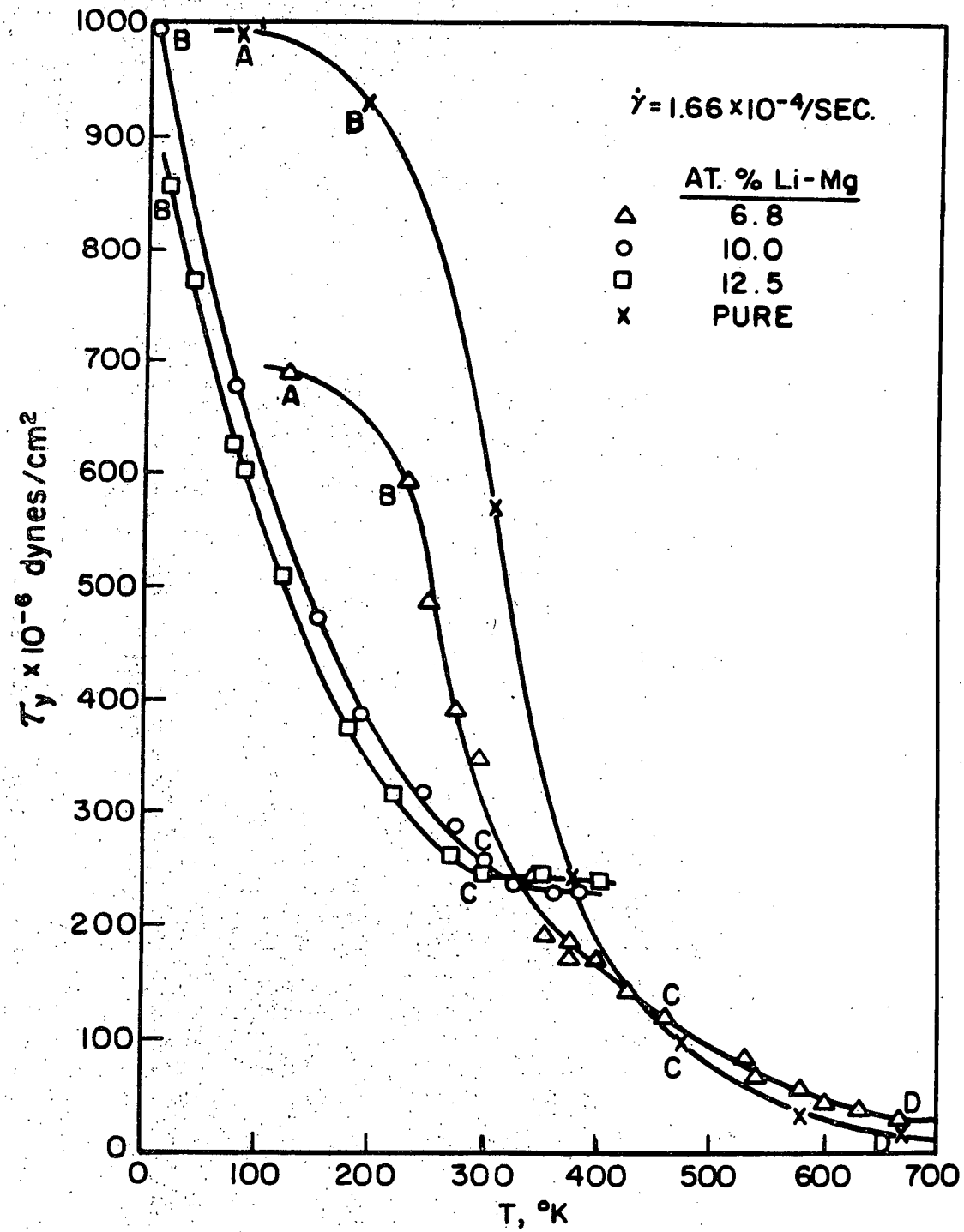

Fig. 98. CRSS for prismatic slip vs. temperature for Mg-Li alloy single crystals (after Ahmadieh and Dorn[73]).

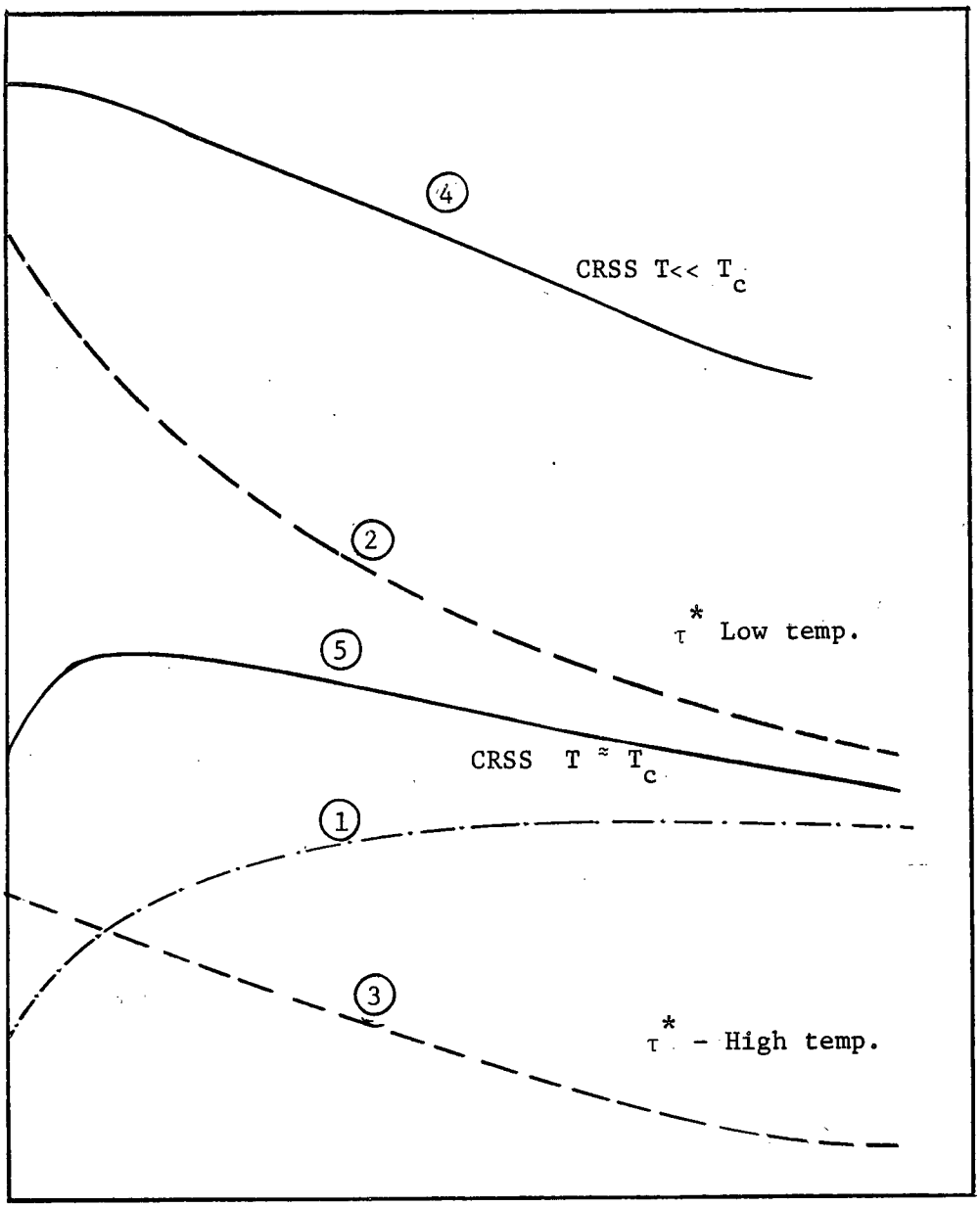

Fig. 99. Schematic representation of the effect of solute on the various components of flow stress in prismatic slip.

mechanism involving size and modulus effect. This would lead to a $C^{\frac{1}{2}}$ dependence of τ_G. This is shown as curve (1). Since τ_G changes only slightly (through a change in shear modulus) with temperature curve (1) should be valid to a first approximation at all temperatures. On the contrary the variation of τ^* with concentration is a strongly temperature dependent function. Curves (2) and (3) represent the effect of solute on τ^* at a low temperature ($T << Tc$) and at a high temperature ($T \approx Tc$) respectively. The combination of (1) and (2) and (1) and (3) are shown as curves (4) and (5). Curves (4) and (5) are qualitatively in good agreement with the observed concentration dependence of CRSS at low and high temperatures respectively. A quantitative varification of such a proposition, however, is not possible at the present, because τ^* cannot be separated from τ_G in the absence of a well defined T_c.

The anomalous CRSS-concentration relationships in bcc Ta-base alloys have also been explained by Mitchell and Raffo[144] in a similar manner.

2.4.5.3.4. The Origin of τ_G and τ^*:

In the above explanation there has been no mention of the origin of τ_G and τ^* and their variation with solute concentration. This will be done in the following pages.

2.4.5.3.4.1. The Athermal Stress:

The observed athermal stress in the Mg-Li alloys was attributed by Dorn to the short range ordering in these alloys[73]. However, a determination of the short range order parameter by Averbach and Herbstein[145] in these alloys indicates that short range ordering cannot account for

the observed athermal stress. A friction stress mechanism similar to the one in basal slip of Mg-Zn alloys could be controlling, however, such a guess would be premature in the absence of sufficient experimental data on prismatic slip.

2.4.5.3.4.2. The Variation of τ^* With Alloying:

From the results of the polycrystalline Mg-Li alloys Hauser, Landon and Dorn[14] proposed that the CRSS for prismatic slip in these alloys decreases with increasing solute and that this decrease is a result of the decreasing axial ratio (c/a) with alloying. Subsequently the rate controlling mechanism was identified in single crystals oriented for prismatic slip by Ahmadieh, Mitchell and Dorn[73] to be one of Peierls stress. However, no explanation was given as to why the Peierls stress decreases with lithium alloying. Recently Dorn has modified his explanation further to explain the observed lowering of CRSS[127]. This is the so called "Pseudo-Peierls mechanism", which is an intermediate situation between Peierls stress and the Friedel cross slip mechanisms. Dorn argues that Friedel's derivations do not hold good for cases where the stacking fault energy is so high that the distance between the partials is 0.5 - 2b as is the case with Mg. In such situations the stacking fault energy must be taken into account. These considerations led Dorn to the conclusion that the stacking fault energy of magnesium increases with the addition of solute[127].

It is not very clear from his theory as to whether it is meaningful to talk about a higher stacking fault energy when the distance between the partials is already of the order of 0.5 - 2b, especially when the present knowledge of the interatomic forces is so limited. Even if the

theory is taken for granted, certain other inconsistencies are encountered. The increase in the stacking fault energy with lithium alloying is considered by Dorn to be a result of the decreasing electron to atom ratio (e/a). Therefore, in the case of Zn solute where e/a remains constant and Al where e/a increases, there should not be lowering of CRSS with solute. The present results do not conform to these conclusions.

Also if we take the c/a to be the criterion as was proposed earlier by Hauser and Dorn[14] then also the results of Mg-Zn alloys in which the c/a ratio remains constant and the Mg-Al alloys where c/a increases cannot be accounted for.

Lately, however, it has been suggested by Mitchell and Raffo[144] that the nucleation of a pair of kinks becomes easier in the presence of small amounts of (up to 4% Re in Ta) solute thus lowering the Peierls stress. The effect of solute can alternatively be visualized as being perturbation of the periodicity of the Peierls hill, thus lowering the effective value of the height of the barrier. The acceptance or rejection of this idea will probably depend on whether all solutes decrease τ^* at all concentrations of solute or not. Sufficient experimental data are not available at the present to take such a decision. It should be borne in mind here that even if the CRSS data are available, there must be a method of obtaining τ^* from the experimentally measured CRSS.

From the results on Mg-solid solutions oriented for prismatic slip it appears that the decrease in Peierls stress with increasing solute concentration is not necessarily associated with a decreasing c/a ratio or with the valency of the solute. The results of the polycrystalline solid solutions in the present work in fact suggest this to be a general solution effect in Mg.

3. Summary and Conclusions:

1) In binary alloy polycrystals of Mg containing Zn, Al, Pb, Cd or In as solute, solution hardening occurs in a two or three stage fashion. In stage I at the lowest solute concentrations, the hardening is very high and linear. Beyond a transition concentration, the hardening is very much reduced.

2) A third stage characterized by a "solution softening" effect was observed in the case of Zn and Al solutes.

3) The strengthening observed is in the order listed, and this is also the order of size mismatch with Zn being the greatest. The ductility decreases for solute additions upto C_T and then increases.

4) The transition concentration C_T is a function of the size difference between the solvent and the solute, being smaller for larger Δr.

5) The predominant factor during stage I hardening is the increase in the CRSS for prismatic slip. During stage II, the CRSS for prismatic slip decreases with increasing solute additions.

6) The discontinuities observed in the ductility temperature plot of the Mg-Al alloys arise due to a combined effect of recrystallization and grain boundary cavitation, the former being related to the CRSS for prismatic slip in the alloy.

7) The experiments on the ternary Mg-In-Zn alloys suggest that stage I hardening results from a type of solute atom dislocation interaction, with preference for prism plane dislocations and large size difference solutes to be involved.

8) In single crystals of magnesium-Zn alloys oriented for basal slip, the athermal component of the CRSS is independent of Zn concentration upto 0.025 at.% beyond which a $C^{\frac{1}{2}}$ dependence is obeyed.

9) Transmission electron microscopy of thin foils of Mg-Al crystals shows that the grown in basal dislocation density increases in a parabolic manner with increasing solute content. This increase, however, cannot account for the observed variation of τ_G with solute concentration.

10) The athermal component of the CRSS in Mg solid solutions arises due to an increase in the friction stress with increasing solute concentration.

11) An etch pit technique for revealing the forest dislocations in Mg has been developed and used to evaluate the increase in the forest density with solute concentration. The results show that the increase is high and linear upto 0.04 at.% Zn, beyond which the change is rather small.

12) The low temperature solution hardening occurs in two stages, the two stages being linear functions of $C^{\frac{1}{2}}$ having different slopes, with the transition at 0.025 at.% Zn.

13) Stage I hardening arises due to an increase in the forest dislocation density with solute concentration whereas in stage II a change in the thermally activated mechanism occurs from intersection to the single solute atom dislocation pinning mechanism.

14) The effects of Zn on the work hardening parameters of Mg single crystals in basal slip are to increase the stage A and stage B slopes and to decrease the extent of easy glide.

15) Tensile tests conducted on oriented single crystals to suppress basal slip and $\{10\bar{1}2\}$ twinning and to induce prismatic slip show that for Zn and Al solutes at low temperatures the CRSS for prismatic slip decreases with increasing solute addition. At high temperatures, however, the CRSS first increases with solute concentration followed by a decrease.

16) The low temperature rate controlling mechanism in prismatic slip is the overcoming of the Peierls stress barrier.

17) The observed concentration dependence of the CRSS in prismatic slip can be accounted for in terms of a decreasing Peierls stress with increasing solute concentration.

18) The decrease in the Peierls stress of magnesium with increasing solute addition is not necessarily associated with either a reduction of the axial ratio or the relative valency of the solute.

4. SUGGESTIONS FOR FUTURE WORK:

The present study can lead to several lines of investigation. The ones that deserve immediate attention include:

1. An extension of the study of the effect of solute on the ease of prismatic slip to include other solute elements and testing temperatures down to 4.2°K, in order to determine the nature of the athermal and the thermally activated components of the flow stress.

2. A thorough study of the dilute ternary alloy single crystals in order to gather more information on the preferential nature of solute-dislocation interaction on the prism planes and to determine the significance of C_T.

3. An investigation of the dependence of the forest dislocation. Spacing on pre-strain, using the etch pitting technique developed in the present work can lead to a better understanding of the work hardening behaviour of magnesium.

4. A systematic study of the yield points and the serrated yielding phenomenon in the Mg-Zn alloys.

5. An investigation of solution strengthening in basal slip at higher solute concentrations and lower temperatures (up to 4.2°K) in order to supplement the present data and to determine the nature of the solute dislocation interaction.

6. An experimental study of the effect of a variety of solutes on the work hardening parameters of Mg coupled with a thorough slip line study and transmission electron microscopy of thin foils to determine the microstructural aspects of work-hardening in the alloys.

APPENDIX - A

DETERMINATION OF SOLUTE CONCENTRATION IN THE ALLOYS:

Much of the present work has been carried out on materials containing small amounts of alloying elements. Atomic absorption spectrophotometry has been used to determine the concentration of solute. The attributes which made atomic absorption attractive are the relatively few analytical interferences and the high precision of the technique.

PRINCIPLE OF THE METHOD:

In principle the sample is dissociated from its chemical bonds (in solution) and placed into an unexcited, unionized ground state. It is then capable of absorbing radiation at discrete frequencies of narrow band width.

Dissociation is achieved by burning the sample in a flame. An effective burner for atomic absorption is designed with a "premix" system, in which fuel, oxidant and the sample are combined in a mixing chamber before being burned. A combination of air and acetylene was used for Cd, Zn and Pb. In the case of Al solute, however, a special nitrous-oxide acetylene flame was used, since the air-acetylene mixture does not give a flame hot enough to dissociate aluminum compounds[149].

The radiation to be absorbed by the sample is provided by a hollow cathode lamp, which emits only the spectrum of the desired element, together with that of the filler gas. In order to screen out the undesired emission, the radiation is passed through a filter or monochromator which is tuned to pass the line of interest but screens out others.

INTERFERENCE:

For a given design of the burner, optical system and the fuel-oxidant combination, the two most serious errors in making a quantitative estimate of elements by atomic absorption are brought about by the presence of another interfering element in solution and due to a difference in the viscosity of the solutions under examination.

The viscosity effect otherwise known as the Bulk or Matrix effect arises due to the variation in the amount of dissolved material in solution. In order to minimize the error due to viscosity effect, the concentration of the anion (NO_3^- in the present case) and the Mg^{++} ion were kept constant in all the solutions of each set of unknowns and the corresponding standards. Since the alloys under examination contained only small amounts of alloying elements, the change in the viscosity arising due to the difference in the amount of the solute element present in the samples was considered negligible.

Another type of interference known as the chemical interference arises when the presence of a second ion in solution either depresses or enhances absorption due to the ion under examination. Earlier work by Bell[150] has indicated that the presence of magnesium does not interfere in the analysis of Zn and Cd. In the presence of aluminum, however, the analysis of Mg is difficult. Although in the present case Al was analysed in Mg matrix, it was considered safe to keep the Mg^{++} concentration in the sample very nearly constant. Such matching techniques have been used by earlier workers in order to overcome chemical interference[150].

PROCEDURE:

Preweighed samples were dissolved in 10% HNO_3. The concentration of NO_3^- ion and Mg^{++} were adjusted to a constant value and absorption tests were carried out at the following wavelengths[151].

Metal	Wavelength A°
Al	3093
Cd	2288
Pb	2170
Zn	2138

A typical concentration absorbance plot for Mg-Zn alloys is shown in fig. (100). It is seen that absorption is a linear function of the Zn concentration up to approximately 10 ppm. The linear part of the curve was used for determining the composition of the unknown.

RESULTS AND LIMITATIONS:

Atomic absorption was found to be most sensitive in the case of Zn and Cd where 1 ppm of the element in solution could be detected easily. In the case of aluminum, however, the sensitivity was about an order of magnitude lower, which necessitated upgrading of the solutions.

The compositions determined using atomic absorption were found to be lower by up to 20% of the nominal composition in the case of Zn and Cd solutes. This is to be expected since the vapour pressure of these solutes is rather high at the melting temperature of the alloy. In the case of Pb and Al solutes, the determined compositions were within $\pm$ 10% of the nominal compositions.

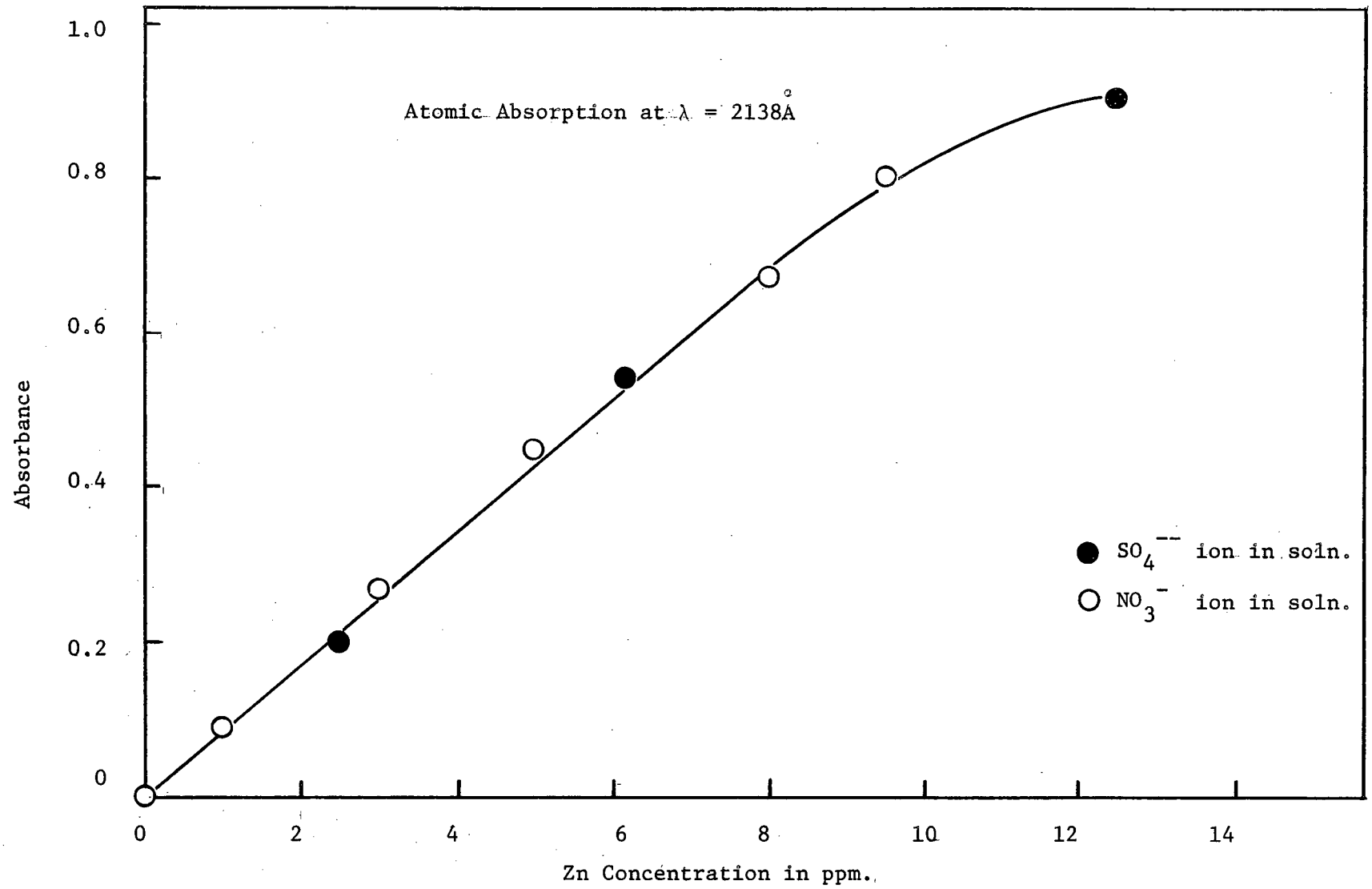

Fig. 100. Absorbance vs. Zn concentration.

APPENDIX - B

THE PREFERENTIAL NATURE OF THE SOLUTE-DISLOCATION INTERACTION:

A ternary Mg alloy containing 0.07 at.% Zn and 1 at.% In was tested in tension at room temperature. The yield stress-composition curves for the binary Mg-Zn and Mg-In alloys are shown together in fig. (101). It is apparent that the concentration of each solute in the ternary is higher than C_T for the corresponding binary system. The yield stress of pure Mg is 8,500 psi. From the figure σ_{YP} for Mg-0.07 at.% Zn alloy is 12,580 psi and that for Mg-1 at.% In is equal to 11,430 psi. Assuming that the strength of a multi-component solid solution can be obtained by adding up the strengthening effects of the corresponding binary solutions, the strength of the Mg-Zn-In binary alloy examined should equal 15,510 psi. Experimentally, however σ_{YP} for the ternary alloy is observed to be $12,800 \pm 200$ psi, suggesting that the strengthening effect of the various solute species present simultaneously in Mg is non-additive.

An alternative possibility is the preferential interaction of one solute species with dislocations giving rise to hardening which is equivalent to that in stage I in the corresponding binary system. The excess of the preferred solute above C_T (in the binary) as well as the total amount of each of the other solute species present in the ternary will have additive strengthening contributions equivalent to those in stage II of their corresponding binary systems.

In the case of Mg-Zn-In ternary alloy whether In or Zn is the preferred species can be decided as follows. Assuming that In atoms are participating in the stage I interaction;

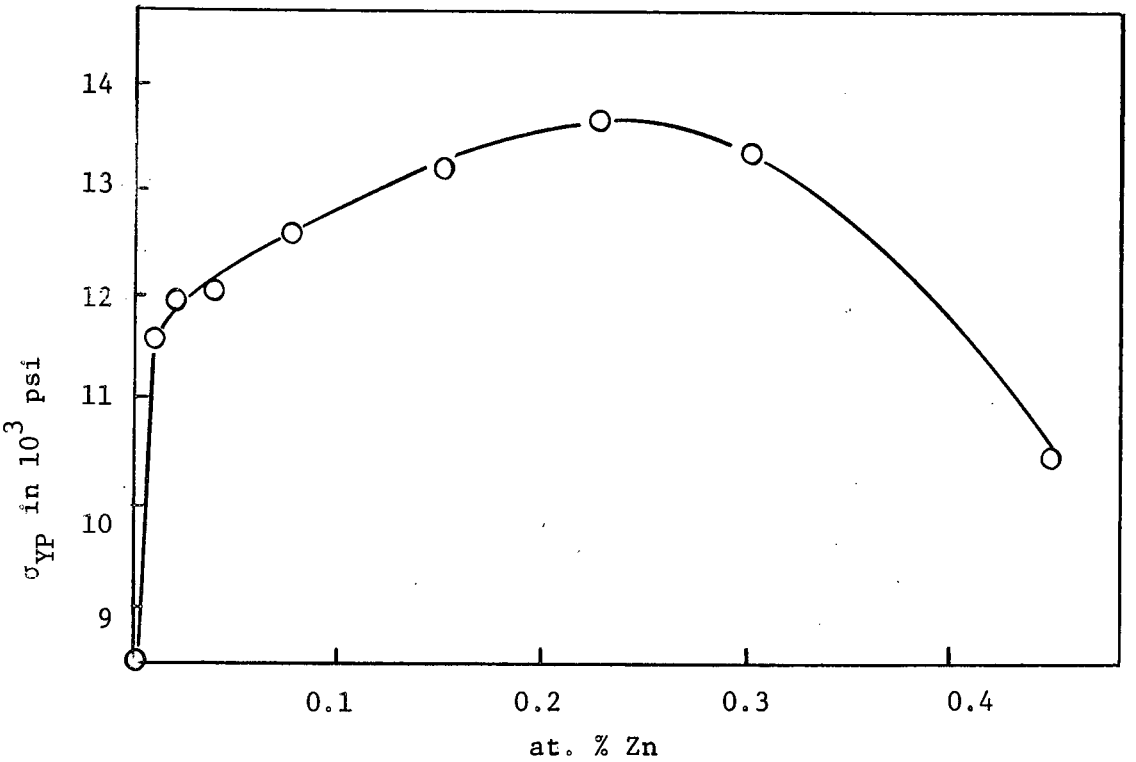

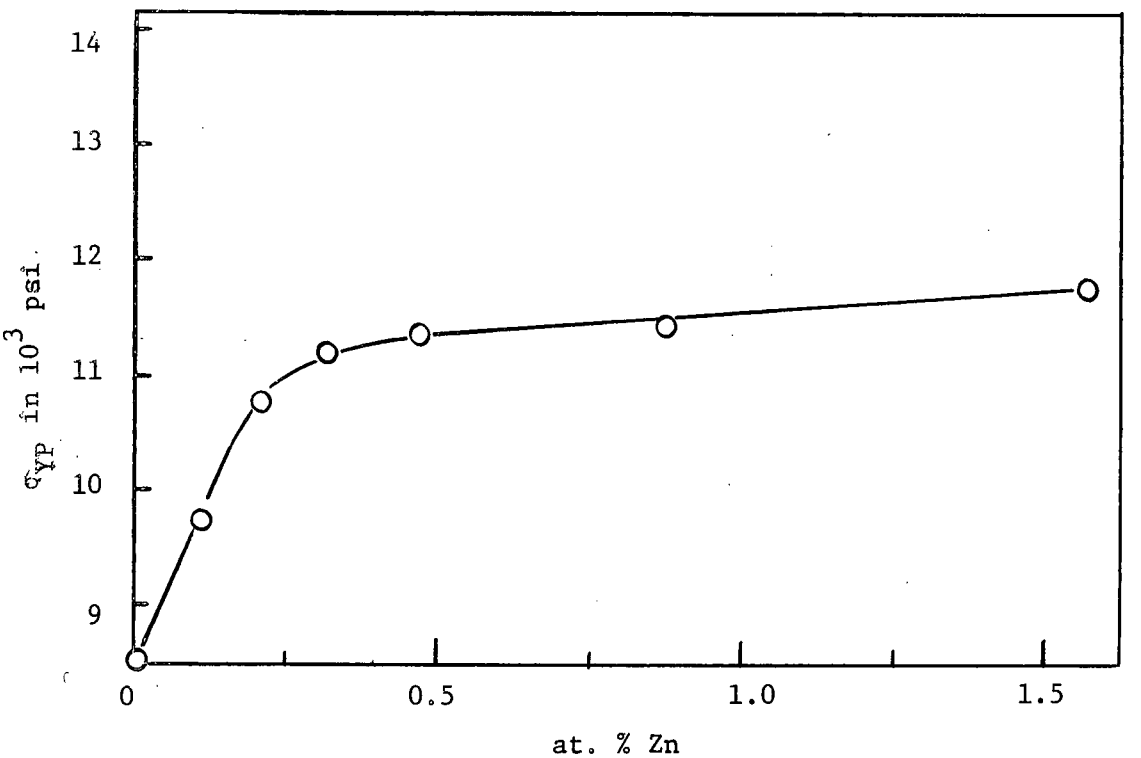

Fig. 101. Solution hardening curves for Mg-Zn and Mg-In binary systems.

Strength due to In present in an amount equal to C_T (0.25 at.%) = 11,250 psi (A)

0.75 at.% In will participate in stage II interaction giving rise to another 187 psi (B)

0.07 at.% Zn will also contribute an equivalent of stage II of Mg-Zn binary which is 630 psi (C)

∴ The strength of the ternary alloy with In as the preferred species would then be = (A) + (B) + (C)

= 11,250 + 187 + 630 psi

= 12,067 psi

A similar calculation taking Zn to be the preferred species yields 12,750 psi to be the strength of the ternary alloy.

Keeping in mind that the reproducibility of the present results are within $\pm$ 250 psi, a comparison of the calculated strength values with the experimental result suggests Zn to be the preferred species in stage I interaction. This conclusion is further substantiated by the experiments on a series of ternary alloys.

It should, however, be noted here that the additive effect of solute at concentrations above C_T is not strictly valid, because at sufficiently high Zn concentrations solution softening is to be expected rather than strengthening. Whether or not the limiting concentration above which softening occurs would be affected by the presence of In cannot be decided until further experiments are performed.

APPENDIX - C

THE DETERMINATION OF $\Delta\tau^*$ FROM STRAIN RATE CHANGE TESTS:

The most convenient method of determing the variation of $\Delta\tau^*$ with strain rate is through instantaneous changes in strain rate during the tensile test. It is, however, important to remember that the flow stress difference accompanying a change in strain rate can be equated to $\Delta\tau^*$ only if it is assumed that the dislocation structure remains constant during the instant of change.

In the present work the strain rate was changed by a factor of 10^2 (from a cross head speed of 0.002 to 0.2 ipm) during the tensile test using a push button speed selector. In principle both stress increments and decrements may be taken as $\Delta\tau^*$. However, a considerable delay was observed to be associated with the change from high to low strain rate. For this reason, it was decided that the error arising from yield point phenomenon (in the alloys) would be less than that resulting from the time delay during the decrease in strain rate. Therefore, all $\Delta\tau^*$ values were obtained during an increase in strain rate.

Much of the strain rate change tests were conducted at 78°K. Fig. (102) illustrates schematically the flow curves during strain rate change tests. Because of the abrupt nature of yield after a change in strain rate, it was relatively easy to obtain $\Delta\tau^*$ in the case of Mg. However, yield points became apparent as the solute content was increased. In the presence of yield points, $\Delta\tau^*$ was evaluated as shown in figure (102).

At temperatures near and above 295°K considerable difficulty was encountered in obtaining reliable values of $\Delta\tau^*$. In the case of Mg, the flow curve became parabolic in nature, thereby making it difficult to extrapolate the two linear stages to obtain $\Delta\tau^*$. In Mg-Zn alloys on the other hand the multiple yield-point effect made the evaluation of the reversible change in flow stress difficult.

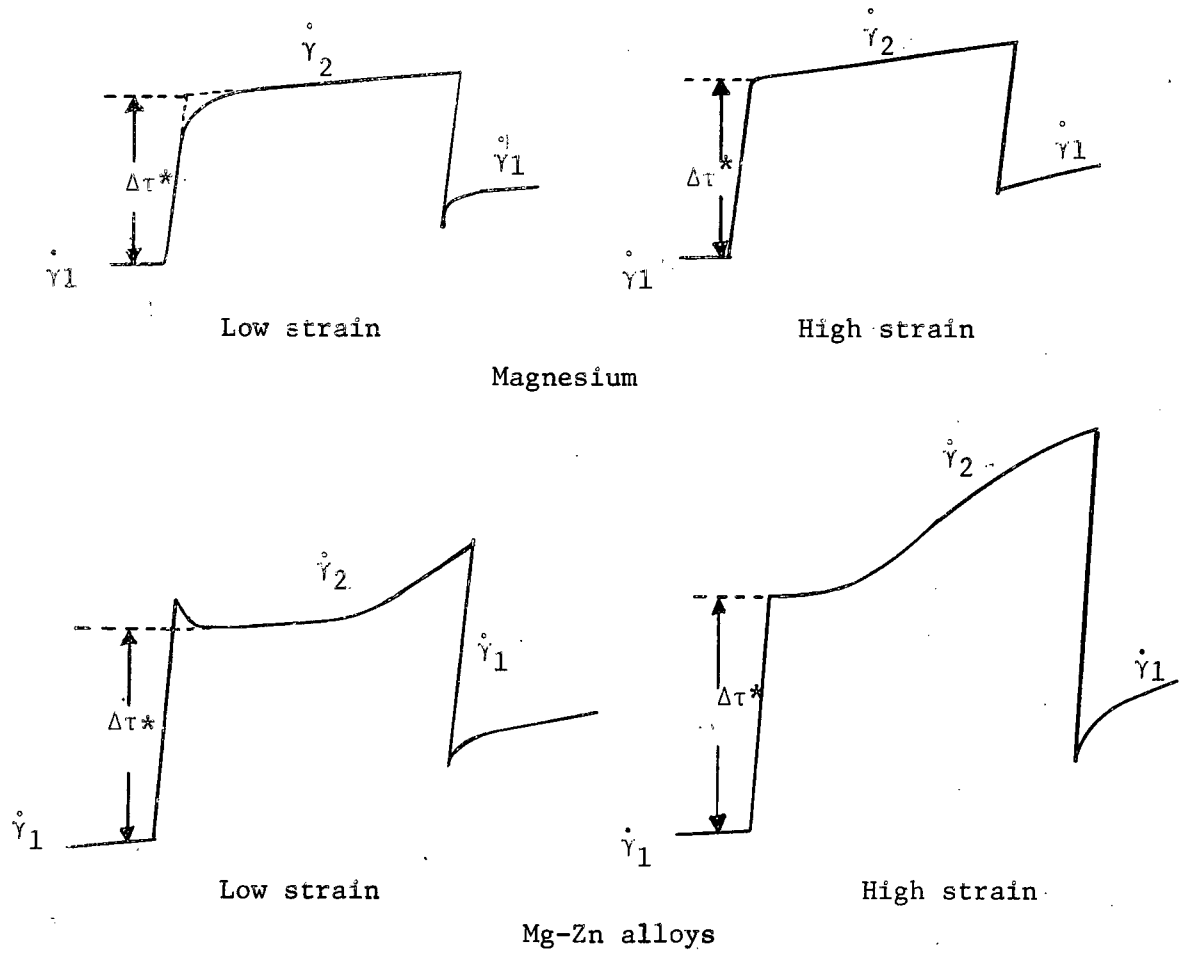

Fig. 102. The nature of the flow stress observed during strain rate change tests in Mg-Zn single crystals. (oriented for basal slip).

BIBLIOGRAPHY

1) R.L. Fleischer and W. R. Hibbard, Jr.; NPL Symposium No. 15, The Relation between the structure and mechanical properties of metals, 262, (1963).

2) P. Haasen; Structural defects, Alloying behaviour and effects in concentrated solid solutions, Edited by T.B.Massalski, page 270, (1965).

3) Z. S. Basinski; Aust. J. Physics, 13, 284, (1960).

4) H. Conrad, R. Armstrong, H. Wiedersich and G. Schoeck; Phil. Mag. 6, 177, (1961).

5) H. Conrad, L. Hays, G. Schoeck and H. Wiedersich; Acta Met., 9, 367, (1961).

6) H. Conrad, and W.D. Robertson; Trans. AIME, 209, 503, (1957).

7) H. Conrad; Trans. AIME, 215, 58, (1959).

8) H. Conrad and W.D. Robertson; Trans. AIME, 212, 536, (1958).

9) P. Ward-Flynn, J.D. Mote and J.E. Dorn; Trans. AIME, 221, 1148, (1961).

10) J.D. Mote and J.E. Dorn; Trans. AIME, 218, 491, (1960).

11) F.E. Hauser, C.D. Starr, L. Tietz and J.E. Dorn; Trans. ASM, 47, 102, (1955).

12) F. E. Hauser, P. R. Landon and J. E. Dorn; Trans. ASM, 48, 986, (1956).

13) W. F. Sheely and R.R. Nash; Trans. AIME, 218, 416, (1960).

14) F.E. Hauser, P.R. Landon, and J.E. Dorn; Trans. ASM, 50, 856, (1958).

15) R. M. Quimby, J.D. Mote and J.E. Dorn; Trans. ASM, 55, 149, (1962).

16) H. Yoshinaga and R. Horiuchi; Trans. Japan Inst. Met., 4, 134, (1963).

17) R.S. Busk; J. Metals, 188, 1460, (1950).

18) D. Hardie and R.N. Parkins; J. Inst. Met., 85, 449, (1957).

19) R. von Mises; Z. Angew. Math. Mech., 8, 161, (1928).

20) G. W. Groves and A. Kelly; Phil. Mag., 8, 877, (1963).

21) U. F. Kocks; Phil. Mag., 10, 187, (1964).

22) G. I. Taylor; J. Inst. Met., 62, 307, (1938).

23) L. E. Samuels; J. Inst. Met., 91, 191, (1962).

24) B. Sestak and S. Libovický; Czech. J. Phys., 10, 759, (1960).

25) J. W. Steeds; Inst. of Physics, Conf. on Electron Microscopy, Cambridge, (1963).

26) L. S. Platnik et al; Soviet Phys.-Cryst., 6, 472, (1961).

27) P. M. Hazzledine; See reference 29.

28) A. P. L. Turner et al; Materials Science and Engineering, 1, No. 1, 70, (1966).

29) P. B. Hirsch and J. S. Lally; Phil. Mag., 12, 595, (1965).

30) F. E. Huaser, P. R. Landon, and J. E. Dorn; Trans. AIME, 206, 589, (1956).

31) D. Hardie and R. N. Parkins; Phil. Mag., 4, 815, (1959).

32) F. W. von Batchelder and R. F. Raeuchle; Phys. Rev., 105, 59, (1957).

33) H. W. King; Journal of Mat. Sc., 1, 79, (1966).

34) L. H. Van Vlack, Elements of Materials Science, page 464, Addison Wesley, (1960).

35) J. N. Greenwood, D. R. Miller and J. W. Suiter; Acta. Met., 2, 250, (1954).

36) R. D. Stacey; Metallurgia, 58, 125, (1958).

37) J. J. Hauser and B. Chalmers; Acta Met., 9, 802, (1961).

38) W. T. Read, Jr.; Dislocations in crystals, McGraw Hill, New York, Chapter 7 (1953).

39) A. Seeger; Report of the Conference on the defects in crystalline solids. The Physical Society, London, (1955).

40) N. S. Stoloff and M. Gensamer; Trans. AIME, 227, 70, (1963).

41) W. J. McG. Tegart; Phil. Mag. 9, 339, (1964).

42) R. L. Bell and R. W. Cahn; Proc. Roy. Soc. (London) Ser. A., 239, 494, (1957).

43) D. Beasley and A. Moore; Beryllium Technology, Gordon and Breach, AIME, (1966).

44) A. Seeger; Phil. Mag., 46, 1194, (1955).

45) N. S. Stoloff and R. G. Davies; J. Inst. Met. 93, 127, (1965).

46) J. L. Martin and R. E. Reed-Hill; Trans. AIME, 226, 216, (1964).

47) A. P. Green and J. Sawkill; J. Nucl. Materials, 3, 101, (1961).

48) E. Schmid; Z. Electrochem., 37, 447, (1931).

49) P. W. Bakarian and C. H. Mathewson; Trans. AIME, 152, 226, (1943).

50) E. C. Burke and W. R. Hibbard Jr.; Trans. AIME, 194, 295, (1952).

51) R. E. Reed-Hill and W. D. Robertson; Trans. AIME, 209, 496, (1957).

52) H. Yoshinaga and R. Horiuchi; Trans. Jap. Inst. Met., 5, 14, (1963).

53) R. E. Reed-Hill and W. D. Robertson; Trans. AIME, 212, 256, (1958).

54) A. R. Chaudhuri, N. J. Grant and J. T. Norton; Trans. AIME, 197, 712, (1953).

55) A. R. Chaudhuri, H. C. Chang and N. J. Grant; Trans. AIME, 203, 682, (1955).

56) J. E. Dorn and J. B. Mitchell;"Proceedings of the International Symposium on Materials", Berkeley, (1964).

57) R. A. Jeffry and E. Smith; Phil. Mag. 13, 1163, (1966).

58) A. T. Churchman; Proc. Roy. Soc. (London), Ser. A., 226, 216, (1954).

59) D. G. Westlake; Unpublished results, Argonne National Lab., Argonne, Ill, USA, See ref. (60).

60) U.F. Kocks and D. G. Westlake; Trans. AIME, 239, 1107 (1967).

61) C. S. Roberts; Wright Air Development Centre Tech. Rept. No. 55-241, (1955).

62) S. L. Couling and C. S. Roberts; Acta. Cryst., 9, 972, (1956).

63) R. E. Reed-Hill and W. D. Robertson; Acta. Met. 5, 717, (1957).

64) W. H. Hartt and R. E. Reed-Hill; Trans. AIME, 239, 1511, (1967).

65) B. C. Wonsiewicz and W. A. Backofen; Trans. AIME, 239, 1422, (1967).

66) E. W. Kelley and W. F. Hosford, Jr., 242, 5, (1968).

67) Magnesium and its alloys; Edited by C. S. Roberts, John Wiley and Sons, page 94, (1960).

68) S. L. Couling and C. S. Roberts; Trans. AIME, 209, 1252, (1957).

69) M. W. Toaz and E. J. Ripling; Trans. AIME, 206, 936, (1956).

70) J. W. Suiter and W. A. Wood; J. Inst. Met. 81, 181, (1952).

71) N. J. Petch; J. Iron Steel Inst. (London), 173, 25, (1953).
E. O. Hall, Proc. Phys. Soc (London), 64(B), 747, (1951).

72) N. R. Risebrough; Ph.D. Thesis, University of British Columbia, (1965).

73) A. Ahmadieh, J. Mitchell, and J. E. Dorn; Trans. AIME, 233, 1130, (1965).

74) E. S. Levine, W. F. Sheely and R. R. Nash; Trans. AIME, 215, 521, (1959).

75) A. Seeger; Dislocations and Mechanical Properties of Crystals, edited by J. C. Fisher et al, p. 243, John Wiley, New York, (1957).

76) F. R.N. Nabarro, Z.S. Basinski and D. B. Holt; Advanc. Phys., 13, 193, (1964).

77) T. E. Mitchell; Progress in materials research. (1964).

78) R. W. Davidge and P.L. Pratt, Phys. Stat. Sol., 6, 759, (1964).

79) E. M. Schulson, Ph.D. Thesis, University of British Columbia, (1968).

80) T.E. Mitchell, R.A. Foxall and P.B. Hirsch; Phil. Mag., 8, 1895, (1963).

81) H. Alexander and P. Haasen; Acta Met., 9, 1001, (1961).

82) A. Seeger, H. Kronmüller, O. Boser and M. Rapp; Phys. Stat. Sol. 3, 1107, (1963).

83) M. Boček; Phys. Stat. Sol., 3, 2169, (1963).

84) A. Seeger and H. Träuble; Z. Metallkunde 51, 441, (1960).

85) R. H. Hammar, W.C.T. Yeh, T.G. Oakwood and A.A. Hendrickson; Trans. AIME, 239, 1692, (1967).

86) L. J. Slutsky and C.W. Garland; Phys. Rev., 107, 972, (1957).

87) W. Köster; Z. Metallkunde, 39, 4, (1948).

88) E. Schmid and W. Boas; Plasticity of Crystals, Translated by F. A. Hughes and Co., London, (1950).

89) M. Boček, G. Hŏtzsch and B. Simmen; Phys. Stat. Sol., 7, 833, (1964).

90) W. A. Tiller; J. Appl. Phys., 29, 611, (1958).

91) A. I. Goss, K.F. Benson and W.G. Pfann; Acta Met., 4, 332, (1956).

92) A. Seeger; "The Relation between the structure and mechanical properties of metals", NPL Symposium, Teddington, H.M.S.O., (1963).

93) P.B. Hirsch and T.E. Mitchell; Can. J. Phys., 45, 663, (1967).

94) P.B. Hirsch; "The relation between the structure and mechanical properties of metals", NPL Symposium, Teddington, page 40, H.M.S.O., (1963).

95) R.K. Ham; Phil. Mag., 1, 651, (1956).

96) R.T.C. Tsui; Acta Met., 15, 1723, (1967).

97) R.K. Ham; Phil. Mag., 6, 1183, (1961).

98) R.K. Ham; Phil. Mag., 7, 1617, (1962).

99) J. Friedel; Phil. Mag., 46, 1169, (1955).

100) A.H. Cottrell; "Relations of properties to microstructure", ASM, (1954).

101) H. Suzuki; "Dislocations and Mechanical properties of crystals", John Wiley and Sons, New York, p. 361, (1957).

102) A. H. Cottrell; "Dislocations and Plastic flow in crystals", Oxford, New York, (1953).

103) B.A. Bilby; Proc. Roy. Soc., A63, 191, (1950).

104) J. Friedel; "Les dislocations", Ganthier-Villars, Paris, (1956).

105) J. Spreadborough; Phil. Mag., 3, 1167, (1958).

106) H. Suzuki; Sc. Rep. Res. Inst., Tohoku Univ., Series A, 4, 455, (1952).

107) R. W. Guard and M.E. Fine; Trans. AIME, 233, 1383, (1965).

108) P.A. Flinn; Strengthening mechanisms in solids, ASM, (1960).

109) J.C. Fisher; Acta. Met., 2, 9, (1954).

110) P.A. Flinn; Acta Met., 6, 631, (1958).

111) T.J. Koppenaal; Acta. Met., 12, 487, (1964).

112) N.F. Mott and F.R.N. Nabarro; "Report of Conference on Strength of Solids", Phys. Soc. London, (1948).

113) R.L. Fleischer; Acta Met., 9, 996, (1961).

114) J.E. Dorn; P. Pietrokowsky and T.E. Tietz; Trans. AIME, 188, 933, (1950).

115) W.R. Hibbard Jr.,; Trans. AIME, 212, 1, (1958).

116) R.L. Fleischer; Acta. Met., 11, 203, (1963).

117) I. Saxl; Czech. J. Phys. B14, 381, (1964).

118) K.H. Adams, T. Vreeland, Jr., and D.S. Wood, Trans. AIME, 242, 132, (1968).

119) The Dow Chem. Co. Labs.

120) T.R. Long and C.S. Smith; Acta. Met., 5, 200, (1957).

121) P. Haasen; Z. Metallkde, 55, 55, (1964).

122) N.P. Allen, T.H. Schofield and A.E.L. Tate; Nature, Lond., 168, 378, (1951).

123) G. Schoeck; Phys. Stat. Sol., 8, 499, (1965).

124) J.E. Dorn; Symposium, University of Denver, (1962).

125) H. Conrad; J. of Metals, 16, 582, (1964).

126) P. Guyot and J.E. Dorn; Can. J. Physics, 45, 983, (1967).

127) J.E. Dorn; Low temperature dislocation dynamics, p. 28, Battelle Colloquium on dislocation dynamics, Seattle, (1967).

128) A.A. Hendrickson and M.E. Fine; Trans. AIME, 221, 967, (1961).

129) A.J.E. Foreman and M.J. Makin; Can. J. Phys. 45, 511, (1967).

130) U.F. Kocks; Can. J. Phys. 45, 737, (1967).

131) J. Diehl; Z. Met, 47, 331, (1956).

132) L.M. Clarebrough and M.E. Hargreaves; Progress in Metal Physics, 8, 1, (1959).

133) S.K. Mitra and J.E. Dorn; Trans. AIME, 227, 1015, (1963).

134) E. Macherauch; Z. Metallkunde, 55, 91 (1964).

135) B. Russell and D. Jaffrey; Acta. Met., 13, 1, (1965).

136) N.F. Mott; Phil. Mag. 45, 742, (1952).
Nature, 175, 365, (1955).

137) A. Seeger, H. Kronmüller, S. Mader, H. Träuble; Phil. Mag. 6, 639, (1961).

138) P.M. Hazzledine, Can. J. Phys., 45, 765, (1967).

139) A. Seeger; Handbuch der Physic, 7, No. 2, Kristallphysik 2, Springer, (1958).

140) R.W.K. Honeycombe; Progress in Materials Science, 9, 95, (1961).

141) P. Haasen; Phil. Mag., 3, 384, (1958).

142) A. Seeger, R. Berner and H. Wolf; Z. Physik, 155, 247, (1959).

143) P. Ward-Flynn; J. Mote and J.E. Dorn; Trans. AIME, 221, 1148, (1961).

144) T.E. Mitchell and P.L. Raffo; Can. J. Phys., 45, 1047, (1967).

145) F.H. Herbstein and B.L. Averbach; Acta. Met., 4, 414, (1956).

146) J.W. Christian and P.R. Swann; "Alloying behaviour and effects in concentrated solid solutions" Edited by T.B. Massalski, Gordon and Breach, (1965).

147) M. Boček and P. Lukáč, Phys. Stat. Sol., 2, 439, (1962).

148) A. Seeger; Phil. Mag. 46, 1194, (1955).

149) J.B. Willis; Nature, 207, 715, (1965).

150) G.F. Bell; Atomic absorption newsletter, 5, 73, (1966).

151) H.L. Kahn; J. of Met. 1102, (1966).